ELUCIDATION OF ESSENTIAL METABOLIC PATHWAYS IN THE APICOPLAST ORGANELLE OF *PLASMODIUM FALCIPARUM*

by
Russell P. Swift

A dissertation submitted to Johns Hopkins University in conformity with the requirements for the degree of Doctor of Philosophy

Baltimore, Maryland
April, 2019

ABSTRACT

The apicoplast within *Plasmodium falciparum* has been thought of as an attractive source of potential drug targets since its discovery. While the apicoplast is essential throughout the parasite lifecycle it has been demonstrated that the organelle is dispensable in the asexual blood-stage of the parasite as long as the isoprenoid precursor isopentenyl pyrophosphate (IPP) is supplemented. IPP supplementation thus provides a bypass system which allows for the investigation and deletion of essential apicoplast specific proteins that would otherwise be impossible. Building on this work, we were successful in optimizing this system though the creation of a parasite line containing a genetically encoded alternative bypass we are calling PfMev. We have validated the functionality of the PfMev line and have established it as a new user-friendly platform that more easily allows for the investigation of essential apicoplast processes.

Using PfMev line we elucidated the essentiality of numerous proteins and pathways within the apicoplast including multiple components of the SUF iron-sulfur cluster biosynthetic pathway and the proteins within the organelle that are reliant on these cofactors, the various proteins involved in carbon metabolism and the production of energy and reducing power within the organelle, in addition to the proteins involved in the generation and utilization of CoA within the apicoplast, among others. Not only were we able to determine which components of these pathways are essential for blood stage parasite survival, we also were able to determine which are required for the maintenance of the apicoplast organelle. Additionally, we made considerable progress in uncovering the functions of these proteins, and determining the ultimate roles that these various proteins play in the maintenance of the organelle.

Advisor: Dr. Sean T. Prigge
Thesis readers: Dr. Michael Matunis, Anna Durbin, MD, and David Sullivan, MD.

ACKNOWLEDGMENTS

I would like to thank my PhD thesis advisor Dr. Sean Prigge for the resources, mentoring, and collaboration that have made this work possible. I would also like to thank current and former members of the Prigge lab, and would like to recognize their contributions to this work, in addition to the role that they played in mentoring and my development as a scientist. I would also like to thank the members of my thesis advisory committee, and am deeply appreciative of the feedback and guidance that they have offered throughout the course of my research endeavors. I would also like to thank my family and friends for all of the support that they have offered over the years spent in pursuit of this research.

TABLE OF CONTENTS

Title ……...……...……...……. i

Abstract ….…….…….……..……. ii

Acknowledgements ...…...……..……..……..……..…… iii

List of Tables ……..……...……...… viii

List of Figures ……..……..……...…..… xi

List of Abbreviations ……..……...……..……...…….. xvi

CHAPTER 1: Introduction to malaria

Plasmodium falciparum Malaria ……...…… 2

The Apicoplast Organelle …...…… 4

Apicoplast Metabolic Bypass …..……..…….... 6

Iron Sulfur Cluster Biosynthesis in the Apicoplast Organelle …….……. 8

Carbon Metabolism in the Apicoplast Organelle ..…….... 9

CoA Generation in *P. falciparum* …..……...… 10

Thesis Rationale……...……...…...… 11

Figures ……..…….. 15

References ……. 20

Chapter 2: Generation of an Alternative Genetically-Encoded Apicoplast Metabolic Bypass System

Abstract 30

Introduction 30

Results 34

Conclusions and Discussion 38

Methods 43

Figures 57

References 73

Chapter 3: The Essentiality and Role of the SUF Iron Sulfur Cluster Biosynthetic Pathway in the Apicoplast of *P. falciparum* Parasites

Abstract 79

Introduction 80

Results 85

Conclusions and Discussion 96

Methods 107

Figures 116

References 146

Chapter 4: The Role of Carbon Metabolism in the Apicoplast of *P. falciparum* Parasites

Abstract 159

Introduction 160

Results 166

Conclusions and Discussion 176

Methods 181

Figures 198

References 219

Chapter 5: CoA Biosynthesis in *P. falciparum* Parasites

Abstract 227

Introduction 228

Results 231

Conclusions and Discussion 241

Methods 248

Figures 263

References 288

Chapter 6: Conclusions and Future Directions

Future Applications of the PfMev line ……..……..... 294

Iron Sulfur Cluster Biosynthesis, Sulfur Utilization, and tRNA Modification within the Apicoplast ……..... 296

Carbon Metabolism, Energy, Reducing Power, and NTP/dNTP Generation within the Apicoplast 300

The Role of the Apicoplast in CoA Generation and Utilization ……..…….. 303

Final Remarks 305

Figures 307

References 309

Appendix I: Introduction of Exogenous Non-Homologous End Joining Machinery in *P. falciparum*

Abstract 316

Introduction 316

Results 319

Conclusions and Discussion 322

Methods 325

Figures 329

References 335

Appendix II: *P. falciparum* Allelic Exchange for *P. vivax* CSP

Abstract 340

Introduction 340

Results 343

Conclusions and Discussion 345

Methods 346

Figures 349

References 354

Appendix III: Quantifying the Effect of Fumarate on Central Carbon Metabolism in *Plasmodium falciparum* (adapted)

Abstract 360

Introduction 361

Results 364

Conclusions and Discussion 367

Methods 373

Figures 387

References 398

Curriculum Vitae 405

List of Tables

Table 2-1 Primer sequences used for amplifying DXPR homology arms

Table 2-2 Guide RNA (gRNA) oligo sequences

Table 2-3 Primer sequences used for DXPR KO confirmation

Table 2-4 Primer sequences used for determining apicoplast presence

Table 2-5 Mycoplasma detection primers

Table 3-1 List of potential iron sulfur cluster binding proteins in *P. falciparum* 3D7

Table 3-2 Resulting apicoplast-specific gene deletion phenotypes

Table 3-3 Primer sequences used to amplify homology arms for genetic knock outs

Table 3-4 Oligonucleotides designed for In-Fusion insertion of gRNA sequences

Table 3-5 Primer sequences used for confirmation of gene deletions

Table 3-6 Primer sequences used to detect genes from the nuclear and organellar genomes

Table 3-7 Primer sequences used to generate the pRSng SufA (BSD) plasmid

Table 4-1 oTPT deletion transfection attempts

Table 4-2 Enzyme kinetics of pure recombinant PyrKII as compared to *T. gondii* PyrKII

Table 4-3 Primer sequences used to amplify homology arms for genetic knock outs

Table 4-4 Oligonucleotides designed for In-Fusion insertion of gRNA sequences

Table 4-5 Primer sequences used for confirmation of gene deletions

Table 4-6 Primer sequences used to detect genes from the nuclear and organellar genomes

Table 4-7 Primer sequences used to amplify harmonized PyrKII for In-Fusion insertion into the pMAL-cHT expression plasmid

Table 4-8 Primer sequences used for generation of the PyrKII-TetR-DOZI line

Table 4-9 Primer sequences used for generation of the PyrKII-CLD line

Table 4-10 Insertion validation primers for the PfPyrKII-CLD line

Table 5-1 Predicted essentiality of genes via forward genetic screens

Table 5-2 DPCK transfection attempts

Table 5-3 Primers for the generation of the *P. falciparum* DPCK localization plasmid

Table 5-4 Primer used for detecting the nuclear and organellar genomes

Table 5-5 Primers for the generation of the *E. coli* complementation plasmids

Table 5-6 Primer sequences used for amplifying homology arms

Table 5-7 Guide RNA oligo sequences

Table 5-8 Primer sequences used for confirmation of gene deletions

Table 5-9 Primers used for the generation of the PfMev CLD-EcDPCK-mCherry-apt line

Table 6-1 Resulting apicoplast-specific gene deletion phenotypes

Table ApI-1 Oligonucleotides designed for In-Fusion insertion of gRNA sequences

Table ApI-2 Primer sequences used for amplifying potential indel regions

Table ApII-1 Oligonucleotides designed for In-Fusion insertion of gRNA sequences

Table ApII-2 Primer sequences used for allelic exchange confirmation

Table ApIII-1 Erythrocyte metabolic reactions altered by parasite invasion

Table ApIII-2 Average estimated deviation in *P. falciparum* enzymatic fluxes expressed relative to a 10% increase in fumarate

Table ApIII-3 Metabolites and reactions added to the models based on intracellular metabolomic data

Table ApIII-4 Average rates of uptake/secretion of 10 nutrient by uninfected and infected erythrocytes during the IDC

Table ApIII-5 Gene transcription delays for DNA and lipid synthesis genes

List of Figures

Figure 1-1 The lifecycle of *Plasmodium falciparum* parasites

Figure 1-2 The endogenous (MEP) and engineered (Mev) isoprenoid pathways

Figure 1-3 Iron-sulfur cluster assembly and transfer in the apicoplast

Figure 1-4 Carbon metabolism in the apicoplast

Figure 1-5 Generation of CoA and utilization in the apicoplast

Figure 2-1 Plasmid pMPC-aSFG used to generate the PfMev parasite line

Figure 2-2 Diagram of the endogenous (MEP) and engineered (Mev) isoprenoid pathways

Figure 2-3 Growth of PfMev parasites treated with fosmidomycin and mevalonate

Figure 2-4 Fluorescent labeling of the apicoplast organelle in PfMev parasites and confirmation via co-localization

Figure 2-5 Generation and characterization of an apicoplast-minus PfMev parasite line

Figure 2-6 Mevalonate titration of apicoplast minus PfMev parasites

Figure 2-7 Metabolic labeling of PfMev parasites with [2-^{13}C]-mevalonate

Figure 2-8 Deletion of an apicoplast essential gene using Cas9 mediated gene editing

Figure 3-1 Iron-sulfur cluster assembly and transfer in the apicoplast

Figure 3-2 Characterization of the PfMev ΔLipA parasite line

Figure 3-3 Characterization of the PfMev ΔMiaB parasite line

Figure 3-4 Characterization of the PfMev ΔIspG parasite line

Figure 3-5 Characterization of the PfMev ΔIspH parasite line

Figure 3-6 Characterization of the PfMev ΔFd parasite line

Figure 3-7 Characterization of the PfMev ΔFNR parasite line

Figure 3-8 Characterization of the PfMev ΔSufA parasite line

Figure 3-9 Characterization of the PfMev ΔNifU parasite line

Figure 3-10 Characterization of the PfMev ΔSufA/NifU parasite line

Figure 3-11 Characterization of the PfMev ΔSufD parasite line

Figure 3-12 Characterization of the PfMev ΔSufC parasite line

Figure 3-13 Characterization of the PfMev ΔSufC/SufD parasite line

Figure 3-14 Characterization of the PfMev ΔSufE parasite line

Figure 3-15 Characterization of the PfMev ΔSufS parasite line

Figure 3-16 Characterization of the PfMev ΔMnmA parasite line

Figure 4-1 Carbon metabolism in the apicoplast

Figure 4-2 Characterization of the PfMev ΔTPI parasite line

Figure 4-3 Characterization of the PfMev ΔPyrKII parasite line

Figure 4-4 Characterization of the PfMev ΔiTPT parasite line

Figure 4-5 Characterization of the PfMev ΔPDH E2 parasite line

Figure 4-6 Characterization of the PfMev ΔDXS parasite line

Figure 4-7 Growth of the PfMev PyrKII TetR-DOZI line under permissive and non-permissive knockdown conditions

Figure 4-8 Growth of the PfMev PyrKII-CLD line under permissive and non-permissive conditional localization conditions

Figure 4-9 Tracking apicoplast disruption in PyrKII-CLD parasites via live epifluorescent microscopy

Figure 4-10 Quantifying apicoplast disruption in PyrKII-CLD parasites via live epifluorescent microscopy

Figure 4-11 Measuring apicoplast transcript levels in Shield1-treated PyrKII-CLD parasites

Figure 5-1 Generation of CoA and utilization in the apicoplast

Figure 5-2 Co-localization of DPCK-mCherry with apicoplast marker api-SFG

Figure 5-3 *E. coli* DPCK complementation in the apicoplast and deletion of DPCK

Figure 5-4 Azithromycin treatment of PfMev-asfg Api-*Ec*-DPCK-mCherry ΔDPCK parasites

Figure 5-5 *E. coli* DPCK complementation in the cytosol and deletion of DPCK

Figure 5-6 Generation of the PfMev CLD-*Ec*DPCK-mCherry-aptamer line and deletion of DPCK

Figure 5-7 Testing protein knockdown and mislocalization in the PfMev CLD-*Ec*DPCK-mCherry-apt parasite line

Figure 5-8 Growth of the PfMev CLD-*Ec*DPCK-mCherry-apt ΔDPCK parasite line under permissive and non-permissive conditions

Figure 5-9 Titration of pantothenate affecting the growth of the PfMev parasite line

Figure 5-10 Titration of pantothenate affecting the growth of the PfMev CLD-*Ec*DPCK-mCherry-apt ΔDPCK parasite line under permissive and non-permissive conditions

Figure 5-11 Growth curve of PfMev CLD-*Ec*DPCK-mCherry-apt ΔDPCK parasite line under permissive and non-permissive conditions at 50nM pantothenate

Figure 5-12 Azithromycin treatment of PfMev CLD-*Ec*DPCK-mCherry-apt ΔDPCK parasite line

Figure 5-13 Growth curve of the azithromycin-treated PfMev CLD-*Ec*DPCK-mCherry-aptamer ΔDPCK parasite line under permissive and non-permissive conditions at 50nM pantothenate

Figure 5-14 Characterization of the PfMev ΔACP parasite line

Figure 5-15 Characterization of the PfMev ΔACP-S parasite line

Figure 5-16 Characterization of the PfMev ΔFabD parasite line

Figure 6-1 Apicoplast metabolic map showing which genes are essential for dispensable, essential, or required for apicoplast maintenance in blood-stage parasites

Figure ApI-1 Schematic representation of the Pf-NHEJ construct

Figure ApI-2 Fluorescence microscopy of the NHEJ lines

Figure ApI-3 Comparison of the wild type and potential repair products for SFG

Figure ApI-4 Comparison of the wild type and potential repair products for FabD

Figure ApII-1 *P. falciparum*/*P. vivax* allelic exchange construct

Figure ApII-2 Pf/Pv-CSP-allelic exchange PCR confirmation

Figure ApII-3 Pf/Pv-CSP allelic exchange mosquito passage and sporozoite formation

Figure ApIII-1 Schematic of our computational approach for predicting *P. falciparum* metabolic fluxes during the intraerythrocytic developmental cycle (IDC)

Figure ApIII-2 Model predictions of DNA, RNA, and lipid synthesis during the intraerythrocytic developmental cycle (IDC)

Figure ApIII-3 Fate of fumarate based on perturbation analysis

Figure ApIII-4 Proposed mechanism responsible for an increase in oxidative pentose phosphate pathway (PPP) enzyme fluxes in response to an increase in cytosolic fumarate (FUM)

List of Abbreviations

1,3-DPGA = 1,3-diphosphoglycerate

3PGA = 3-Phosphoglyceric acid

6pgd = 6-phosphogluconate dehydrogenase

ACC = acetyl-CoA carboxylase

Acetyl-CoA = acetyl-coenzyme A

ACP = acyl carrier protein

ACP-S = acyl carrier protein synthase

ACT = artemisinin-based combination therapies

ADP = adenosine diphosphate

AKG = alpha-ketoglutatare

Api-SFG = super folder green tagged on the N-terminus with the first 55 amino acids from the acyl-carrier protein

ASP = aspartate

Aspta = aspartate aminotransferase

aTc = anhydrotetracycline

ATP = adenosine triphosphate

AUC = area under the curve

Azith = azithromycin

BCDH = branched-chain alpha-ketoacid dehydrogenase

BCKDK = 3-methyl-2-oxobutanoate dehydrogenase

BioB = biotin synthase

BSA = bovine serum albumin

Bp = base pairs

BSD = blasticidin S-deaminase

Cam = calmodulin

Cas9 = CRISPR-associated protein 9

CDP = cytidine diphosphate

CDP-ME = 4-diphosphocytidyl-2-C-methylerythritol

CDP-ME kinase = 4-diphosphocytidyl-2-C-methyl-D-erythritol kinase

CDP-ME Synthase = 2-C-methyl-D-erythritol 4-phosphate cytidylyltransferase

CDP-MEP = 4-diphosphocytidyl-2-C-methyl-D-erythritol 2-phosphate

CHMI = controlled human malaria infection

CIA = cytosolic iron-sulfur protein assembly

CLD = conditional localization domain

ClpC = caseinolytic protease C

CMA = Complete Medium with AlbuMAX

CoA = coenzyme A

Cox1 = cyclooxygenase 1

CSP = circumsporozoite protein

CRISPR = clustered regularly interspaced short palindromic repeats

DAPI = 4', 6-diamidino-2-phenylindole

dADP = deoxyadenosine diphosphate

dATP = deoxyadenosine triphosphate

dCDP = deoxycytidine diphosphate

dCTP = deoxycytidine triphosphate

dGDP = deoxyguanosine diphosphate

dGTP = deoxyguanosine triphosphate

DHAP = dihydroxyacetone phosphate

DHFR = dihydrofolate reductase

DMAPP = dimethylallyl pyrophosphate

DMSO = dimethyl sulfoxide

DNA = deoxyribonucleic acid

dNDP = deoxynucleoside diphosphate

dNTP = deoxynucleoside triphosphate

DOXP = 1-Deoxy-D-xylulose 5-phosphate

DOZI = development of zygote inhibited

DPCK = dephospho-CoA kinase

DSB = double strand break

dTDP = deoxythymidine diphosphate

DXPR = 1-deoxy-D-xylulose 5-phosphate (DOXP) reductoisomerase

DXS = 1-deoxy-D-xylulose-5-phosphate (DOXP) synthase

EDTA = ethylenediaminetetraacetic acid

E. coli = *Escherichia coli*

ER = endoplasmic reticulum

ESI = electrospray ionization

ETC = electron transport chain

F = forward primer

FASII = type 2 fatty acid synthesis

Fd = ferredoxin

Fh = fumarate hydratase

FNR = ferredoxin $NADP^+$ reductase

Fos = fosmidomycin

FPP = farnesyl pyrophosphate

FUM = fumarate

G = gravities

G3P = glycerol-3-phosphate

g6pd = glucose-6-phosphate dehydrogenase

GA3P = glyceraldehyde 3-phosphate

GAPDH = glyceraldehyde 3-phosphate dehydrogenase

GDP = guanosine diphosphate

gDW = dry weight

GFP = green fluorescent protein

Gln = glutamine

Glu = glutamic acid

GpdA = glycerol phosphate dehydrogenase

gRNA = guide RNA

GTP = guanosine triphosphate

HA = homology arm

HCl = hydrogen chloride

hDHFR = human dihydrofolate reductase

HEPES = 4-(2-hydroxyethyl)-1-piperazineethanesulfonic acid

HILIC = hydrophilic-interaction chromatography

HMB-PP = (E)-4-Hydroxy-3-methyl-but-2-enyl pyrophosphate

HMP = hydroxymethylpyrimidine

HMP-PP = 4-amino-2-methyl-5-hydroxymethylpyrimidine pyrophosphate

HR = homology directed repair

i^6A = isopentenylation of adenine at position 6

i^6A37 = isopentenylation of adenine at position 6 at the adenine base 37

IC_{50} = half maximal inhibitory concentration

IDC = intraerythrocytic developmental cycle

Idi = isopentenyl diphosphate isomerase

IFA = immunofluorescence assay

IPP = isopentenyl pyrophosphate

IPTG = isopropyl β-thiogalactoside

iRBC = infected RBC

ISC = iron-sulfur cluster formation pathway

IspD = 4-diphosphocytidyl-2*C*-methyl-D-erythritol synthetase

IspE = 4-diphosphocytidyl-2*C*-methyl-D-erythritol kinase

IspF = 2*C*-methyl-D-erythritol 2,4-cyclodiphosphate synthase

IspG = (*E*)-4-hydroxy-3-methyl-but-2-enyl diphosphate synthase

IspH = (*E*)-4-hydroxy-3-methyl-but-2-enyl diphosphate reductase

iTPT = inner triose phosphate transporter

kb = kilobase

KDH = alpha-ketoglutarate dehydrogenase

KO = knock out

LC-MS = liquid chromatography mass spectrometry

LDH = lactate dehydrogenase

LipA = lipoic acid synthase

LipB = lipoate ligase

Lys = lysine

mAB = monoclonal antibody

MAL = malate

Malonyl-CoA = malonyl-coenzyme A

MBP = maltose binding protein

Mdh = malate dehydrogenase

MEc-PP = 2-C-methyl-D-erythritol 2,4-cyclodiphosphate (methylerythritol cyclic diphosphate)

MEc-PP Synthase = 2-C-methyl-D-erythritol 2,4-cyclodiphosphate synthase

MEP = 2-C-methyl-D-erythritol 4-phosphate (methylerythritol)

Mev = mevalonate

MevK = mevalonate kinase

MiaB = tRNA methylthiotransferase

Min = minutes

MMEJ = microhomology-mediated end joining

Mnm = methylaminomethyl

MnmA = 5-methylaminomethyl-2-thiouridylate methyltransferase

MnmE = tRNA modification GTPase

MnmG = tRNA uridine 5-carboxymethylaminomethyl modification enzyme

Mqo = malate:quinone oxidoreductase

mRNA = messenger RNA

ms^2i^6A = 2-methylthio-*N*^{6}-isopentenyl-adenosine

MS/MS = tandem mass spectrometry

MVA = mevalonate pathway

MVA kinase = mevalonate kinase

MVA-P = mevalonate-5-kinase

MVA-P kinase = phosphomevalonate kinase

MVA-PP = mevalonate-5-pyrophosphate

MVA-PP decarboxylase = mevalonate-5-pyrophosphate decarboxylase

MVD = mevalonate 5-diphosphate decarboxylase

m/z = mass-to-charge ratio

$NaBH_4$ = sodium borohydride

NADH = nicotinamide adenine dinucleotide

NADPH = nicotinamide adenine dinucleotide phosphate

NDP = nucleoside diphosphate

NHEJ = non-homologous end joining

NLS = nuclear localization signal

NMP = nucleoside monophosphate

NPP = new permeability pathway

NTP = nucleoside triphosphate

OAA = oxaloacetate

Oaat = oxaloacetate transporter

OD = optical density

oTPT = outer triose phosphate transporter

OxoDH = 2-oxoglutarate dehydrogenase

pAB = polyclonal antibody

PanK = pantothenate kinase

PAT = pantothenate transporter

PBS = phosphate-buffered saline

PCR = polymerase chain reaction

PDH = pyruvate dehydrogenase

PEP = phosphoenolpyruvate

Pf = *Plasmodium falciparum*

Pi = inorganic phosphate

PMevK = phosphomevalonate kinase

PMSF = phenylmethane sulfonyl fluoride

Pnt = pyridine nucleotide transhydrogenase

PPAT = phosphopantetheine adenylyltransferase

Ppc = phosphoenolpyruvate carboxylase

PPCDC = phosphopantothenoylcysteine decarboxylase

Ppck = phosphoenolpyruvate carboxykinase

PPCS = phosphopantothenoylcysteine synthase

PPP = pentose phosphate pathway

PPT = inner triose phosphate isomerase

Pv = *Plasmodium vivax*

PV = parasitophorous vacuole

PyrK = pyruvate kinase I

PyrKII = pyruvate kinase II

Q8 = ubiquinone

Q8h2 = ubiquinol

QC = quality check

QQQ = triple stage quadrupole

r = correlation coefficient

R = reverse primer

RBC = red blood cell

Redox = reduction oxidation

RI = retention index

RL2 = ribosomal L2

RNA = ribonucleic acid

RP = reverse phase

RPM = rotations per minute

RPMI = Roswell Park Memorial Institute 1640 culture medium

RPO = DNA-directed RNA polymerase

rRNA = ribosomal RNA

rSAP = recombinant shrimp alkaline phosphatase

RU5P = ribulose-5-phosphate

RT = room temperature

s^2U34 = 2-thiolation of uridine at position 34

s4U = 4-thiouridine

SEM = standard error of the mean

SFG = super folder green

Spp. = species

Spz = sporozoite

SRM = selected reaction monitoring

SUF = sulfur utilization factor pathway

TCA = tricarboxylic acid cycle

TDP = thymidine diphosphate

TetR = tetracycline repressor

TEV = Tobacco Etch Virus

ThiG = thiazole synthase

ThiL = thiamine-monophosphate kinase

ThiM = hydroxyethylthiazole kinase

THZ = 5-(2-hydroxyethyl)-4-methylthiazole

TPI = Triose phosphate isomerase

TPK = thiamine phosphate kinase

TPP = thiamine pyrophosphate

tRNA = transfer RNA

TPT = outer triose phosphate transporter

TTP = thymidine triphosphate

U34 = uridine at position 34 of a tRNA

UDP = uridine diphosphate

UMP = uridine monophosphate

UTR = untranslated region

uHPLC = ultra high-performance liquid chromatography

UTP = uridine triphosphate

Vnut = nutrient uptake/secretion rate

WT = wild type

WBC = white blood cell

yDHOD = yeast dihydroorotate dehydrogenase

Chapter 1

Introduction

Plasmodium falciparum Malaria

Malaria is a disease caused by a parasitic infection from *Plasmodium* spp. and represents a significant public health burden throughout the world. In 2017 alone there were an estimated 219 million cases, and 435,000 deaths (1). Of the five species of *Plasmodium* that infect humans, *P. falciparum* causes the largest majority of malaria-related deaths, responsible for 99.7% of malaria cases in the African region, with 93% of all malaria deaths occurring within that region (1). While individuals infected with *P. falciparum* can be non-symptomatic, those with mild or uncomplicated malaria can present clinically with fever, sweating, chills, diarrhea, and swelling of the spleen (2). However, infection can also result in severe or complicated malaria, in which individuals can present clinically with severe anemia, metabolic acidosis, coma, convulsions, pulmonary edema, or hemoglobinuria, with infection also potentially resulting in death (2).

P. falciparum parasites have a complex lifecycle that requires a human host in addition to requiring a female *Anopheles* mosquito vector as well (**Figure 1-1**) (3). Within the human host, during the disease causing asexual stage of the lifecycle, parasites invade and replicate within red blood cells (RBCs) in a cycle that takes ~48 hours (4). This asexual cycle begins when parasites in the merozoite stage invade RBCs, and develop into ring-stage parasites, progressing further into the trophozoite stage of the parasite, before forming the schizont stage of the parasite, in which parasites have undergone division and formed ~16-32 daughter merozoites, which are released and invade other RBCs (5). A subpopulation of blood-stage parasites (~0.8-1%) can undergo differentiation into the sexual forms of the parasite, forming male and female gametocytes (6, 7). These sexual forms of the parasite are then taken up by a female *Anopheles* mosquito during a blood meal (8). Once the gametocytes reach the midgut of the mosquito they are activated, forming fertile male microgametes and

female macrogametes (9). The gametes then egress out of the RBCs and the microgamete and macrogamete can fuse, forming a zygote (9). The zygote then develops into the motile ookinete form and traverses through the midgut of the mosquito (10). On the opposite side of the midgut wall, the parasites form a cyst-like structure called an oocyst in which serves as a protective structure for the formation of thousands of sporozoites. The sporozoites are a motile form of the parasite and, after release from the oocyst, they migrate to the salivary gland of the mosquito (11). The now infectious mosquito then takes another bloodmeal, and is capable of transmitting the sporozoites into the dermis of the human (12). The sporozoites then enter into the bloodstream, eventually reaching the liver where they invade and replicate inside of liver hepatocyte cells (13, 14). Within the liver, infectious merozoites are ultimately formed and released into the bloodstream; these parasites specifically infect RBCs within the human host, beginning the lifecycle anew (12).

The current recommendation for the treatment of uncomplicated infection with *P. falciparum* are artemisinin-based combination therapies (ACTs) (15). Prior treatments relied on drugs such as chloroquine, sulfadoxine–pyrimethamine, mefloquine, quinine and lumefantrine (16, 17). Due to treatment failures and resistance to these previously used therapies, ACTs are now the frontline therapy (18–22). The introduction and widespread utilization of ACTs is believed to have significantly attributed to the 18% reduction in malaria cases between 2010 and 2016 (23). However, parasite recrudescence, delayed parasite clearance, and treatment failures are now being seen with ACTs in certain regions of the world (24–26). Treatment failures observed after standard artemisinin treatment regimens have been attributed to mutations within the Kelch-13 protein of the parasite (27, 28). Selection of this mutation is believed to have arisen in Southeast Asia, and appears to be spreading, fueling concerns that this may threaten the goals of malaria control and

elimination (29, 30).

Due to resistance being seen to current frontline antimalarial treatments, there is a critical need to develop new antimalarial drugs with novel mechanisms of action. In order to develop new drugs to treat infection, the apicoplast organelle within the parasite has been thought of as a source of additional drug targets since its initial discovery and characterization (31, 32). This is largely due to the unique evolutionary lineage of the organelle, which contains biochemical pathways that are highly dissimilar from that of the human host (33).

The Apicoplast Organelle

Plasmodium falciparum parasites are a member of the Apicomplexa phylum, with many of the species within this phylum, including *P. falciparum*, possessing a non-photosynthetic plastid organelle, called an apicoplast (34). The apicoplast is an organelle surrounded by four membranes, a result of its evolutionary origin resulting from a secondary endosymbiotic process. In the first endosymbiotic event, the chloroplast of an algal cell was formed from an engulfed cyanobacterium. The algal cell was then phagocytosed, and lost all of its cellular contents except for its chloroplast organelle (35). The two inner membranes of the apicoplast are believed to correspond to the algal chloroplast membranes, while the third membrane corresponds to the algal plasma membrane, and the fourth membrane derives from the phagocytic membrane that originally engulfed the endosymbiont (36).

Over the course of endosymbiosis, the apicoplast has become extremely reduced in terms of the biochemical processes and genetic material that it possesses. The genetic material that continues to be retained within the apicoplast exists as a small circular 35kb organellar genome in *P. falciparum* (37), which encodes a full complement of tRNAs, RNA

polymerase subunits, a translation elongation factor, small and large subunit ribosomal RNAs, ribosomal proteins, a caseinolytic protease C (ClpC), and SufB of the iron-sulfur cluster biosynthetic pathway (37, 38). The remainder, and vast majority of apicoplast-specific proteins are now encoded by the nuclear genome, likely due to multiple gene transfer events that occurred over time (39–41). The trafficking of these apicoplast-specific proteins is mediated by an N-terminal signal and transit peptide (42), with these proteins being packaged into vesicles and then trafficked to the organelle via the secretory system (43–45). There are an estimated ~400 proteins trafficked to the organelle, representing ~7% of the parasite genome [36]–[39].

Each parasite cell contains only one apicoplast organelle, but it is essential for the survival of blood-stage *P. falciparum* parasites. This essentiality has been demonstrated through the administration of antibiotics such as chloramphenicol, clindamycin, or doxycycline. These antibiotics are effective in inhibiting translation within prokaryotic organisms, and due to the prokaryotic origin of the apicoplast, are also effective at specifically inhibiting translation within the apicoplast (51, 52). The requirement for the apicoplast is driven by the metabolism that takes place inside the organelle, with the apicoplast being home to biochemical pathways involved in the biosynthesis of heme, fatty acids, isoprenoid precursors, and iron-sulfur cluster cofactors (46). While the FasII fatty acid biosynthetic pathway was initially thought to be an attractive drug target, it was ultimately proven to be dispensable for blood-stage *P. falciparum* parasites (53, 54). It has also been demonstrated that the heme biosynthetic pathway that is shared between the apicoplast and mitochondrion is dispensable for *P. falciparum* blood-stage survival as well (55, 56). The methylerythritol phosphate (MEP) pathway, which generates the isoprenoid precursors isopentenyl pyrophosphate (IPP) and dimethylallyl pyrophosphate (DMAPP), is responsible

for generating the seemingly only essential product of the apicoplast required for the survival of blood-stage *P. falciparum* parasites (57). This was demonstrated through the treatment of blood-stage parasites with the above-mentioned antibiotics, which typically results in parasite death (58, 59). However, the lethality of these drugs can be bypassed if the parasites are supplemented with a sufficient concentration of IPP (57). But due to the action of the antibiotic, inhibiting protein expression within the organelle, the apicoplast becomes disrupted and lost (57). However, these 'apicoplast-negative' parasites can continue to survive and replicate, seemingly in perpetuity, as long as IPP is provided, demonstrating that the entire organelle is dispensable as long the isoprenoid precursor production functionality of the organelle is compensated through the direct supplementation of IPP (57). The resulting apicoplast disruption phenotype has been analyzed and results in the loss of the 35kb apicoplast organelle genome, in addition to loss of the typically intact structure of the apicoplast, replaced by the accumulation of multiple vesicles throughout the cell, presumably containing proteins destined for the apicoplast (57, 60).

Apicoplast Metabolic Bypass

The above-mentioned work demonstrating that the apicoplast is dispensable in blood-stage *P. falciparum* parasites under IPP supplementation helped to establish a powerful tool in the form of a chemical bypass system, useful for the investigation of essential apicoplast-specific proteins and pathways (57). This chemical bypass system allows for the interrogation of the apicoplast in ways that would have previously been impossible, including investigating the essentiality of genes encoding apicoplast-specific proteins (61–65), in addition to having the ability to determine if drugs are apicoplast-specific by looking for differential drug sensitivity in the presence of IPP (66).

While the establishment of the IPP chemical bypass system has been invaluable, there are certain drawbacks to the system that make longer-term and larger-scale experimentation untenable, potentially explaining why there have been no published genetic knockouts of essential apicoplast-specific genes since its establishment in 2011 (57). Drawbacks include the incomplete rescue of apicoplast-negative parasites to wild-type growth levels, the inability of IPP-dependent parasites to survive cryopreservation, and the expense of the chemical at ~$22,500/g (Sigma-Aldrich) with the large amounts (200μM) required to rescue parasite growth, in addition to the chemical being labile and requiring frequent media exchange (60).

As detailed in chapter 2 of this thesis, in order to overcome these issues we have developed an alternative genetically-encoded bypass system by engineering parasites to express enzymes from the mevalonate (MVA) isoprenoid precursor pathway, creating a separate controllable pathway reliant on supplementation with the biomolecule mevalonate (67). The mevalonate pathway is an alternative pathway used to generate isoprenoid precursors that is common to most other eukaryotes and uses an entirely different set of enzymes than the endogenous MEP isoprenoid precursor pathway found within the apicoplast organelle of the parasite (67, 68). This line, that we are calling PfMev, converts exogenously supplied mevalonate into IPP and DMAPP (**Figure 1-2**). This alternative bypass system addresses many of the problems seen in the chemical bypass, namely, mevalonate supplementation in parasites lacking an apicoplast restores growth to wild-type levels and only requires 10μM mevalonate. Mevalonate-dependent parasites can be successfully cryopreserved, the compound is stable reducing the need for frequent media exchanges, and the compound is affordable at $142/g (Sigma Aldrich). These aspects make the mevalonate bypass an attractive alternative to the chemical bypass, and should allow for

larger-scale and longer-term experimentation, which would be not be feasible without it. The PfMev line also contains a fluorescently labeled apicoplast, easily allowing for the determination of the resulting phenotype of the organelle from any potential perturbations (69). Using this system, we have been able to elucidate the essentiality of numerous proteins and pathways within the apicoplast including the SUF iron-sulfur cluster biosynthetic pathway, carbon metabolism, and the generation of CoA among others. Investigations into these pathways form three of the data chapters of this thesis.

Iron-Sulfur Cluster Biosynthesis in the Apicoplast Organelle

Within the apicoplast, iron-sulfur clusters are believed to be generated by the SUF iron-sulfur cluster biosynthetic pathway and utilized as cofactors in multiple pathways throughout the organelle (64, 70, 71). The generation of iron-sulfur clusters by the SUF pathway begins with sulfur acquisition, in which the cysteine desulfurase SufS liberates sulfur from L-cysteine (72, 73). A non-enzymatic effector protein, SufE, transfers the sulfur to the SufBCD iron-sulfur cluster assembly complex (74), which joins the sulfur with iron to form the iron-sulfur cluster (**Figure 1-3**) (75, 76). The iron-sulfur clusters are then handed off to the iron-sulfur cluster transfer proteins SufA and NifU (SufU) (77, 78), which deliver the iron-sulfur cluster cofactors to the terminal acceptors within the apicoplast (79–81). These iron-sulfur cluster dependent proteins are predicted to include lipoic acid synthase (LipA) involved the lipoylation of pyruvate dehydrogenase (PDH) (82), MiaB believed to be involved in tRNA modification (46, 83), ferredoxin (Fd) which delivers reducing power throughout the organelle (46, 84–86), and IspG and IspH of the MEP pathway, which are involved in isoprenoid precursor generation (46, 87). Previous work has suggested that the SUF pathway is likely essential for parasite survival, as multiple genes involved in this

pathway are refractory to deletion (78). Additional experimentation involving the generation of a SufC (K140A) dominant-negative mutant resulted in the disruption of the organelle (64), suggesting that iron-sulfur cluster formation is essential for parasite survival, as well as maintenance of the apicoplast. However, the ultimate mechanism by which iron-sulfur cluster generation is potentially responsible for organelle maintenance has remained unclear. Although, it is hypothesized to potentially occur due to the dysfunction of one of the downstream proteins that are reliant on these cofactors for their activity (64). In chapter 3 of this thesis we investigate which iron-sulfur cluster dependent proteins and components of the SUF pathway are required for blood-stage parasite survival and apicoplast maintenance.

Carbon Metabolism in the Apicoplast Organelle

In order to fuel any anabolic pathway within the apicoplast there needs to be a source of energy, reducing power, and carbon backbones. These requirements are believed to be met from the import and utilization of glycolytic products from the parasite in the form of the triose phosphate compounds phosphoenolpyruvate (PEP) and dihydroxyacetone phosphate (DHAP), which are imported by the triose phosphate transporters on the inner (iTPT) and outer (oTPT) membranes (**Figure 1-4**) (46, 88). Within the apicoplast, DHAP is believed to be utilized as a substrate by triose phosphate isomerase (TPI), generating glyceraldehyde-3-phosphate (GA3P) (46), which is fed into the MEP pathway, to generate IPP and DMAPP (89). DHAP is also believed to be utilized for phospholipid biosynthesis (46, 90), and to potentially be an important source of reducing power within the apicoplast (89, 91). Once PEP is imported it is believed to be used as a substrate, along with ADP, by pyruvate kinase II (PyrKII) to generate pyruvate and ATP (40, 92, 93), with PyrKII being the only predicted source of both ATP and pyruvate within

the apicoplast (94). The ATP generated presumably powers all energy requiring reactions within the organelle (46). The pyruvate generated is fed into the MEP pathway along with DHAP for the generation of isoprenoid precursors (89), in addition to being utilized by the pyruvate dehydrogenase (PDH) complex, to generate NADH and acetyl-CoA (95). The acetyl-CoA is then presumably fed into the FasII pathway for fatty acid biosynthesis, and the NADH generated is believed to provide an important source of reducing power in the apicoplast, if not providing the only source (46, 96, 97). Additionally, while PyrKII is purportedly the only source of ATP and pyruvate within the apicoplast, it may also be required for the generation of all NTPs and dNTPs within the apicoplast, as there is no other known source for the generation or import of these biomolecules (46). Pyruvate kinase enzymes can be active against different NDPs and often don't exclusively use ADP as a substrate (98–101). In other systems pyruvate kinase enzymes are believed to play an import role in the generation of nucleoside triphosphates, and may function as a competent substitute for nucleoside diphosphate kinase (99). In chapter 4 of this thesis we investigate carbon metabolism within the apicoplast, and attempt to determine the importance and role that the proteins within this pathway play in blood-stage parasite survival and apicoplast maintenance.

CoA Generation in *P. falciparum*

In addition to the pathways and proteins previously mentioned, the last step of Coenzyme A (CoA) generation within the parasite is believed to occur within the apicoplast (46), being mediated by dephospho-CoA kinase (DPCK) (**Figure 1-5**). *P. falciparum* parasites are reliant on an exogenous source of pantothenate (vitamin B5) (102, 103), which is used for the *de novo* synthesis of CoA (104). CoA functions as a cofactor and metabolite within

parasites (105) and is required for several key processes including fatty acid biosynthesis and modification, cellular oxidation and metabolism, and gene expression (106). The CoA biosynthetic pathway is essential for parasite survival, with pantothenate analogs inhibiting this pathway, and are effective against the asexual blood-stage of the parasite (107–109). However, while DPCK is predicted to be localized to the apicoplast and be essential for parasite survival, previous work has demonstrated that the entire apicoplast organelle is dispensable in blood-stage *P. falciparum* parasites if supplemented with a sufficient concentration of IPP (57). This has been interpreted as IPP being the only essential product of the apicoplast, but due to the proposed essential activity and putative localization of DPCK, the requirement for this enzyme should not be bypassable with IPP supplementation (46, 110). The phenotype of parasites containing a disrupted organelle has been characterized, with the typically intact structure of the organelle being lost, replaced by the accumulation of vesicles throughout the cell, in addition to the ~35kb apicoplast genome being lost as well (57, 64). However, these vesicles are predicted to contain proteins that would typically be trafficked to the apicoplast organelle (43). Thus, it is possible these vesicles potentially containing apicoplast-specific proteins are still biochemically active, with DPCK possibly being present and active within these vesicles, fulfilling its essential function required for parasite survival. In chapter 5 of this thesis we investigate DPCK, and the importance of this protein for parasite survival, and the localization and function of DPCK activity when the apicoplast is intact or disrupted.

Thesis Rationale

The impetus for this work began with research conducted previously in our lab demonstrating that the generation of a SufC (K140A) dominant-negative mutant resulted in

disruption of the apicoplast organelle when expressed in the presence of IPP supplementation (64). While the ultimate mechanism was not elucidated in that work, it was speculated that the loss of the organelle was likely due to the loss of function of one of the downstream iron-sulfur cluster dependent proteins being deprived of its essential iron-sulfur cluster cofactor. We wanted to follow up on this, and determine which of these iron-sulfur cluster dependent proteins may replicate the previously observed phenotype. However, further exploration of essential apicoplast-specific proteins would likely require the generation of genetic knockouts, and since its establishment in 2011 (57), there have been no published deletions of genes encoding essential apicoplast-specific proteins, likely due to the cost and inherent difficulty associated with the IPP chemical bypass system. Thus, in order to follow up on this work, and potentially identify other apicoplast-specific proteins in other pathways that are essential for parasite survival and apicoplast maintenance, our lab produced the PfMev apicoplast metabolic bypass line.

As outlined in this thesis, our lab was successful in generating a genetic-based apicoplast bypass system, reliant on the supplementation of mevalonate, which is converted into IPP by the parasite through the expression of four exogenous enzymes from the alternative mevalonate pathway. We were able to characterize this line and validate it as a useful platform that could be used to interrogate essential apicoplast proteins and pathways. Perhaps most importantly, we were able to demonstrate the facile deletion of a gene encoding an essential apicoplast-specific protein using the PfMev line through CRISPR-Cas9 mediated genome editing. This set the stage for the rest of the work outlined in this thesis. Having this tool allowed us to follow up on which, if any iron-sulfur cluster dependent proteins were essential for parasite survival and organelle maintenance through their deletion in this line under mevalonate supplementation. We were also able to explore which other

proteins and pathways within the apicoplast may also be required for parasite survival and apicoplast maintenance as well.

In an attempt to uncover the ultimate mechanism by which iron-sulfur cluster generation is required for organelle maintenance and parasite survival we made use of the PfMev line by generating a series of genetic knockouts. Through this work we were able to determine which iron-sulfur cluster dependent proteins, in addition to which proteins involved in the apicoplast SUF iron-sulfur cluster biosynthetic pathway are essential for parasite survival and apicoplast maintenance. The results obtained were surprising and unexpected, and demonstrated that while iron-sulfur cluster generation is not required for the maintenance of the organelle, the generation and utilization of sulfur by a tRNA modifying enzyme likely is.

We went on to use this tool to explore, and potentially solve additional unanswered questions in the field relating to *P. falciparum* apicoplast metabolism. For example, it is not entirely clear how the apicoplast generates energy and reducing equivalents needed to supply the various metabolic pathways within the organelle (46), and which if any of the anabolic pathways within the apicoplast are required for the maintenance of the organelle. Thus, we attempted to determine this through a series of genetic knockouts in the pathways involved in apicoplast carbon metabolism, using our PfMev line under mevalonate supplementation, in addition to using other techniques as well.

It has also been shown that the apicoplast can be disrupted as long as IPP is provided (57). However, it appears as if apicoplast-specific proteins are still being transcribed, translated, packaged, and sent out into the cell within vesicles (43). It is not clear if all apicoplast-specific proteins are functionally null due to the loss of the intact organelle, or if they are present and active within the disrupted vesicles. Central to this question is

dephospho-CoA kinase (DPCK), which is predicted to be apicoplast localized, but whose activity should be essential for parasite survival, and not be able to be bypassed through IPP supplementation (106, 110). Additionally, it is not clear why DPCK would be localized to the extremely reduced apicoplast, and if its activity is required within the apicoplast organelle. Thus, we also utilized the PfMev line in an attempt to answer these questions through a series of genetic deletions, complementation experiments, and other functional studies.

FIGURES

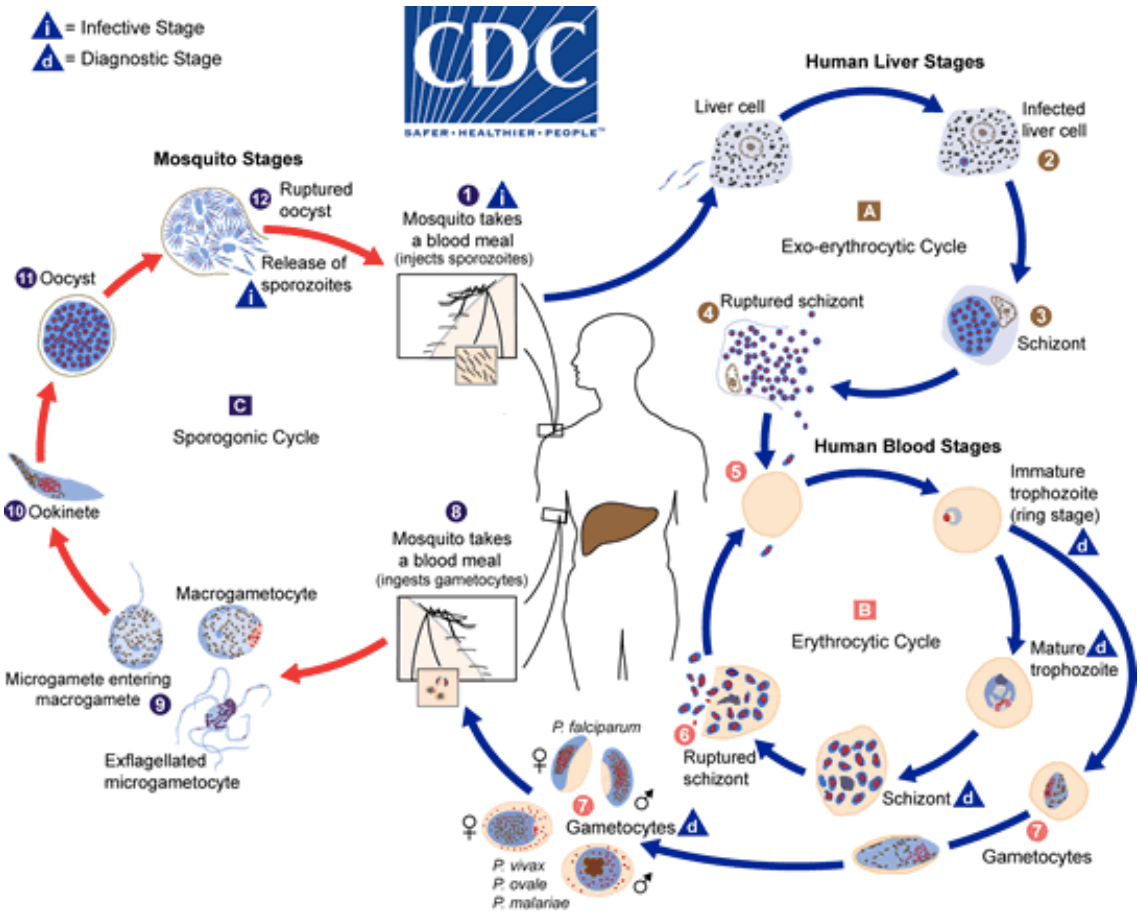

Figure 1-1 The lifecycle of *Plasmodium falciparum* parasites

P. falciparum parasites complete their lifecycle by replicating within the human host in addition to an *Anopheles* mosquito vector. The asexual stage of the parasite within the human host cyclically infects RBCs, progressing through the ring, trophozoite and schizont stages before releasing merozoites, which invade RBCs. A subpopulation of these parasites undergo sexual differentiation, forming male and female gametocytes. These gametocytes are taken up by an *Anopheles* mosquito, eventually fusing and forming a zygote, before forming infectious sporozoites that localize to the salivary gland of the mosquito and are later released into a human host. These parasites then invade hepatocyte liver cells, and undergo multiple cycles of replication before releasing merozoites and beginning the cycle anew.

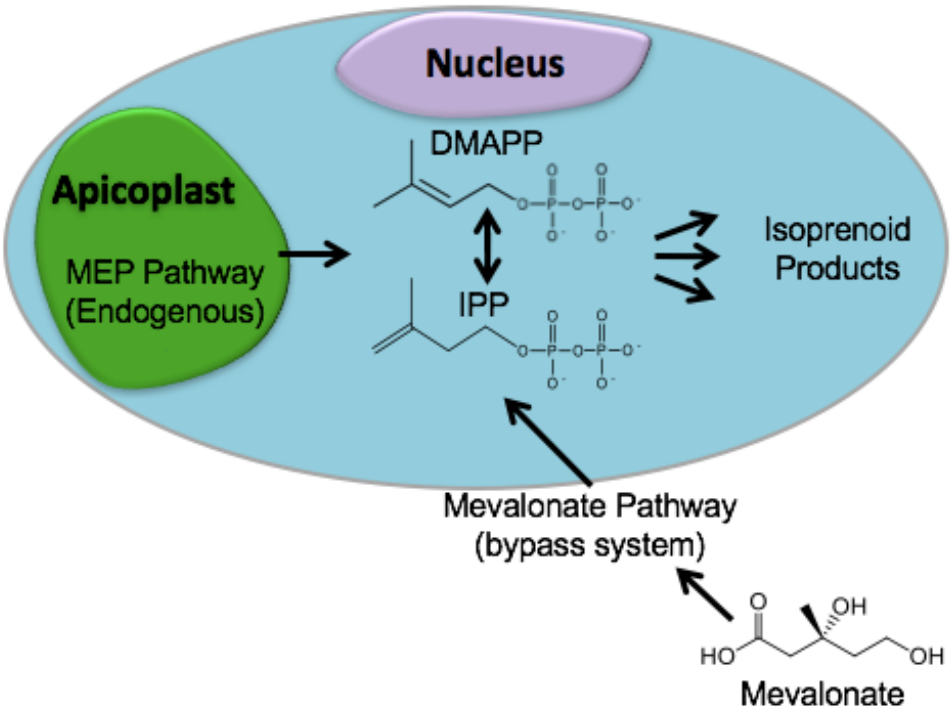

Figure 1-2 The endogenous (MEP) and engineered (MVA) isoprenoid pathways

Plasmodium parasites contain the endogenous MEP isoprenoid precursor pathway within the apicoplast organelle of the parasite. PfMev parasites were engineered to convert exogenously supplied mevalonate into IPP and DMAPP through the expression of four enzymes from the mevalonate pathway, which are expressed in the cytosol of the parasite.

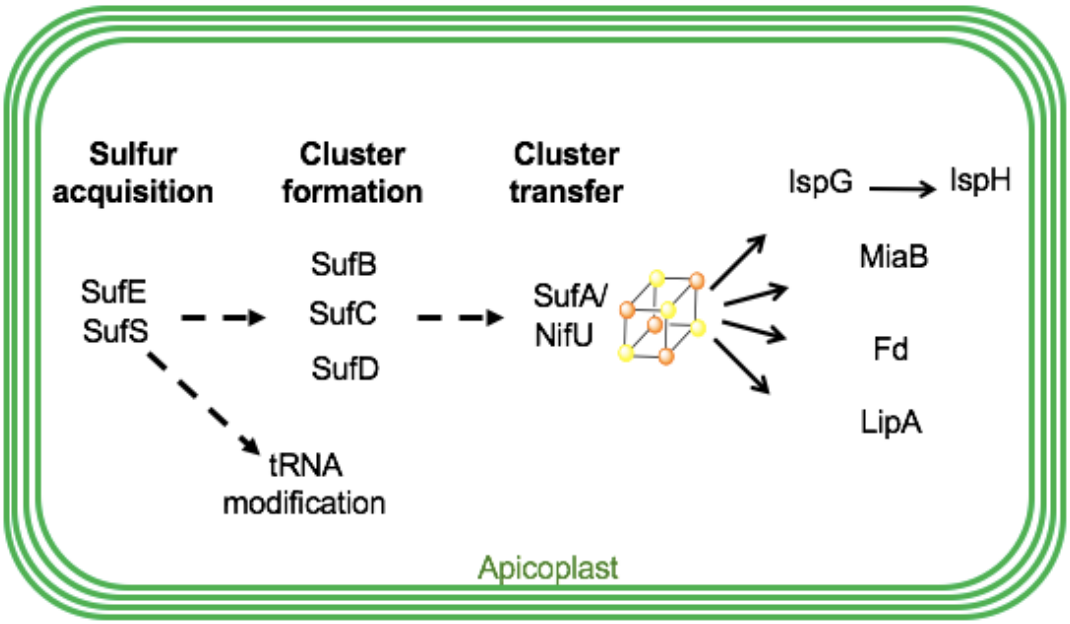

Figure 1-3 Iron-sulfur cluster assembly and transfer in the apicoplast

Iron-sulfur cluster assembly takes place in three steps: sulfur acquisition – mediated by the cysteine desulfurase SufS along with SufE. Sulfur is transferred by SufE to the SufBCD cluster assembly complex. Fe-S clusters are handed off to SufA or NifU, which deliver the Fe-S clusters to the terminal acceptors within the apicoplast: MiaB, LipA, IspG, IspH, and Fd.

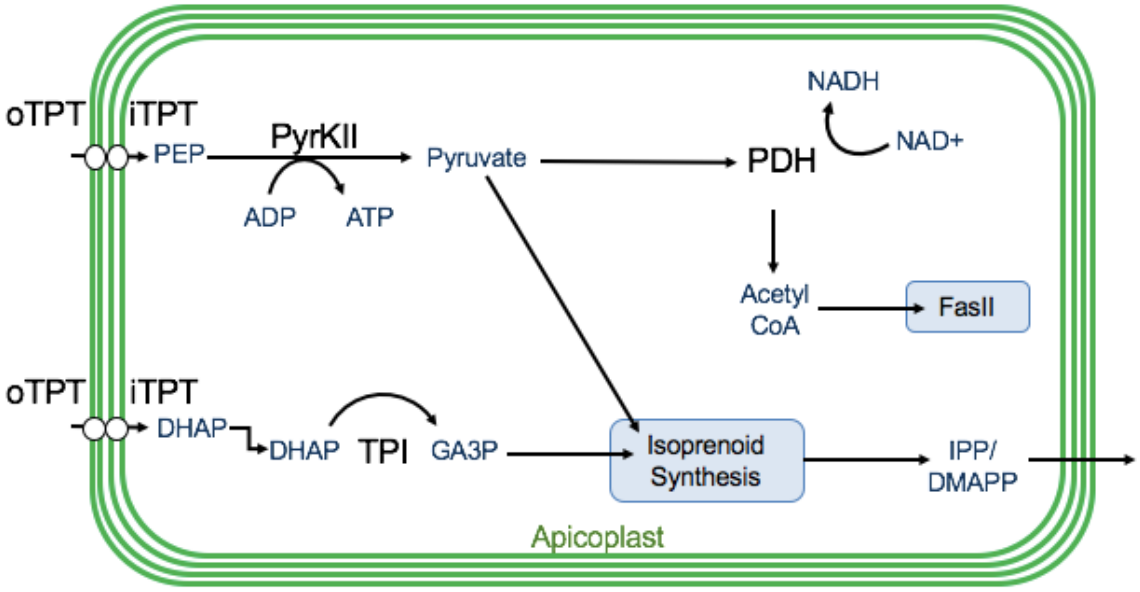

Figure 1-4 Carbon metabolism in the apicoplast

Carbon backbones are imported into the apicoplast organelle in the form of 3-carbon phosphates by the apicoplast membrane outer triose phosphate transporter (oTPT) and inner triose phosphate transporter (iTPT). Phosphoenolpyruvate (PEP) along with adenosine diphosphate (ADP) are converted into pyruvate as well as adenosine triphosphate (ATP). Pyruvate is utilized by the FasII fatty acid pathway as well as the isoprenoid precursor pathway. Dihydroxyacetone phosphate (DHAP) is also imported and converted to glyceraldehyde-3-phosphate (GA3P) by triose phosphate isomerase (TPI), which is also utilized by the isoprenoid precursor pathway.

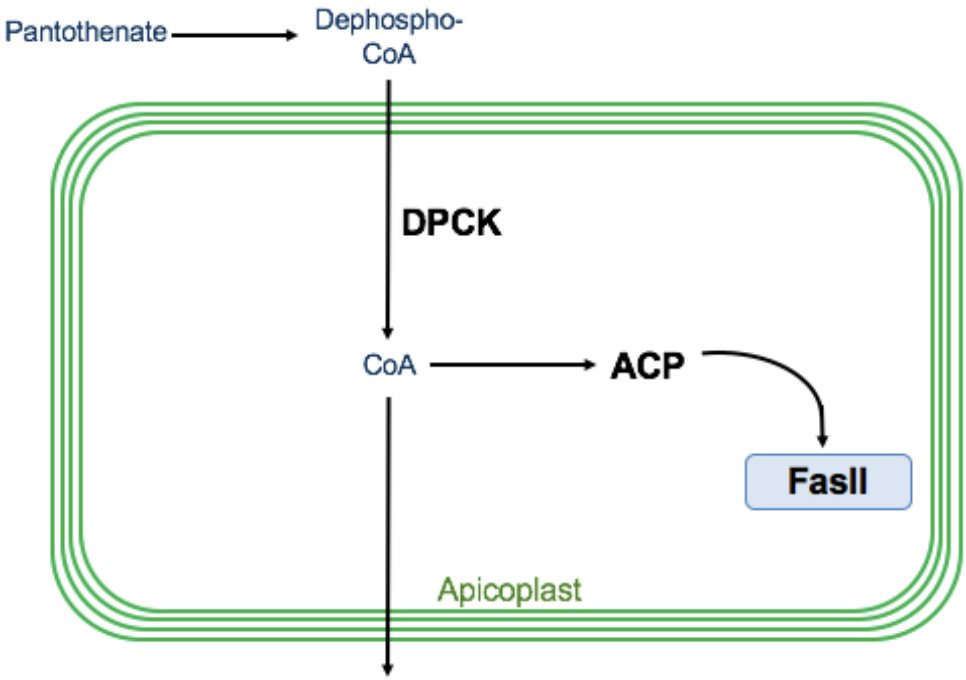

Figure 1-5 Generation of CoA and utilization in the apicoplast

Parasites are reliant on scavenged pantothenate, which is used to generate CoA through a series of enzymes within the cytosol. The final step involving the conversion of dephospho-CoA to CoA by DPCK is believed to occur within the apicoplast. CoA is presumably exported, as well as used within the organelle by ACP, which is involved in the FasII pathway.

REFERENCES

1. Health Organization W. WORLD MALARIA REPORT 2018 ISBN 978 92 4 156565 3.

2. 2000. Severe *falciparum* malaria. World Health Organization, Communicable Diseases Cluster. Trans R Soc Trop Med Hyg 94 Suppl 1:S1-90.

3. Cowman AF, Healer J, Marapana D, Marsh K. 2016. Malaria: Biology and Disease. Cell 167:610–624.

4. Hawking F, Worms MJ, Gammage K. 1968. 24- and 48-hour cycles of malaria parasites in the blood; their purpose, production and control. Trans R Soc Trop Med Hyg 62:731–65.

5. Bannister LH, Hopkins JM, Fowler RE, Krishna S, Mitchell GH. 2000. A brief illustrated guide to the ultrastructure of *Plasmodium falciparum* asexual blood stages. Parasitol Today 16:427–33.

6. Bruce MC, Alano P, Duthie S, Carter R. 1990. Commitment of the malaria parasite *Plasmodium falciparum* to sexual and asexual development. Parasitology 100 Pt 2:191–200.

7. Sinden RE. 1983. Sexual Development of Malarial Parasites. Adv Parasitol 22:153–216.

8. Molina-Cruz A, Zilversmit MM, Neafsey DE, Hartl DL, Barillas-Mury C. 2016. Mosquito Vectors and the Globalization of *Plasmodium falciparum* Malaria. Annu Rev Genet 50:447–465.

9. Bennink S, Kiesow MJ, Pradel G. 2016. The development of malaria parasites in the mosquito midgut. Cell Microbiol 18:905–18.

10. Aly ASI, Vaughan AM, Kappe SHI. 2009. Malaria Parasite Development in the Mosquito and Infection of the Mammalian Host. Annu Rev Microbiol 63:195–221.

11. Ghosh AK, Jacobs-Lorena M. 2009. *Plasmodium* sporozoite invasion of the mosquito salivary gland. Curr Opin Microbiol 12:394–400.

12. Ménard R, Tavares J, Cockburn I, Markus M, Zavala F, Amino R. 2013. Looking under the skin: the first steps in malarial infection and immunity. Nat Rev Microbiol 11:701–712.

13. Vaughan AM, Aly ASI, Kappe SHI. 2008. Malaria parasite pre-erythrocytic stage infection: gliding and hiding. Cell Host Microbe 4:209–18.

14. Yuda M, Ishino T. 2004. Liver invasion by malarial parasites - how do malarial parasites break through the host barrier? Cell Microbiol 6:1119–1125.

15. 2018. WHO | Responding to antimalarial drug resistance. WHO.

16. Jong EC, Nothdurft HD. 2001. Current drugs for antimalarial chemoprophylaxis: a review of efficacy and safety. J Travel Med 8:S48-56.

17. Jensen M, Mehlhorn H. 2009. Seventy-five years of Resochin® in the fight against malaria. Parasitol Res 105:609–627.

18. Gatton ML, Martin LB, Cheng Q. 2004. Evolution of resistance to sulfadoxine-pyrimethamine in *Plasmodium falciparum*. Antimicrob Agents Chemother 48:2116–23.

19. Price RN, Uhlemann A-C, Brockman A, McGready R, Ashley E, Phaipun L, Patel R, Laing K, Looareesuwan S, White NJ, Nosten F, Krishna S. 2004. Mefloquine resistance in *Plasmodium falciparum* and increased pfmdr1 gene copy number. Lancet (London, England) 364:438–447.

20. Jelinek T, Schelbert P, Löscher T, Eichenlaub D. 1995. Quinine resistant *falciparum* malaria acquired in east Africa. Trop Med Parasitol 46:38–40.

21. Cui L, Mharakurwa S, Ndiaye D, Rathod PK, Rosenthal PJ. 2015. Antimalarial Drug Resistance: Literature Review and Activities and Findings of the ICEMR Network. Am J Trop Med Hyg 93:57–68.

22. Ljolje D, Dimbu PR, Kelley J, Goldman I, Nace D, Macaia A, Halsey ES, Ringwald P, Fortes F, Udhayakumar V, Talundzic E, Lucchi NW, Plucinski MM. 2018. Prevalence of molecular markers of artemisinin and lumefantrine resistance among patients with uncomplicated *Plasmodium falciparum* malaria in three provinces in Angola, 2015. Malar J 17:84.

23. Ouji M, Augereau J-M, Paloque L, Benoit-Vical F. 2018. *Plasmodium falciparum* resistance to artemisinin-based combination therapies: A sword of Damocles in the path toward malaria elimination. Parasite 25:24.

24. Health Organization W. Artemisinin resistance and artemisinin-based combination therapy efficacy (Status report -- August 2018).

25. Huang F, Takala-Harrison S, Jacob CG, Liu H, Sun X, Yang H, Nyunt MM, Adams M, Zhou S, Xia Z, Ringwald P, Bustos MD, Tang L, Plowe C V. 2015. A Single Mutation in K13 Predominates in Southern China and Is Associated With Delayed Clearance of *Plasmodium falciparum* Following Artemisinin Treatment. J Infect Dis 212:1629–1635.

26. Cheng Q, Kyle DE, Gatton ML. 2012. Artemisinin resistance in *Plasmodium falciparum*: A process linked to dormancy? Int J Parasitol Drugs drug Resist 2:249–255.

27. Tilley L, Straimer J, Gnädig NF, Ralph SA, Fidock DA. 2016. Artemisinin Action and Resistance in *Plasmodium falciparum*. Trends Parasitol 32:682–696.

28. Suresh N, Haldar K. 2018. Mechanisms of artemisinin resistance in *Plasmodium*

falciparum malaria. Curr Opin Pharmacol 42:46–54.

29. Ashley EA, Dhorda M, Fairhurst RM, Amaratunga C, Lim P, Suon S, Sreng S, Anderson JM, Mao S, Sam B, Sopha C, Chuor CM, Nguon C, Sovannaroth S, Pukrittayakamee S, Jittamala P, Chotivanich K, Chutasmit K, Suchatsoonthorn C, Runcharoen R, Hien TT, Thuy-Nhien NT, Thanh NV, Phu NH, Htut Y, Han K-T, Aye KH, Mokuolu OA, Olaosebikan RR, Folaranmi OO, Mayxay M, Khanthavong M, Hongvanthong B, Newton PN, Onyamboko MA, Fanello CI, Tshefu AK, Mishra N, Valecha N, Phyo AP, Nosten F, Yi P, Tripura R, Borrmann S, Bashraheil M, Peshu J, Faiz MA, Ghose A, Hossain MA, Samad R, Rahman MR, Hasan MM, Islam A, Miotto O, Amato R, MacInnis B, Stalker J, Kwiatkowski DP, Bozdech Z, Jeeyapant A, Cheah PY, Sakulthaew T, Chalk J, Intharabut B, Silamut K, Lee SJ, Vihokhern B, Kunasol C, Imwong M, Tarning J, Taylor WJ, Yeung S, Woodrow CJ, Flegg JA, Das D, Smith J, Venkatesan M, Plowe C V., Stepniewska K, Guerin PJ, Dondorp AM, Day NP, White NJ, Tracking Resistance to Artemisinin Collaboration (TRAC). 2014. Spread of Artemisinin Resistance in *Plasmodium falciparum* Malaria. N Engl J Med 371:411–423.

30. Hemming-Schroeder E, Lo E. 2017. Evidence of a hard selective sweep for artemisinin resistant *Plasmodium falciparum*. Lancet Infect Dis 17:462–463.

31. McFadden GI, Reith ME, Munholland J, Lang-Unnasch N. 1996. Plastid in human parasites. Nature 381:482–482.

32. Köhler S, Delwiche CF, Denny PW, Tilney LG, Webster P, Wilson RJ, Palmer JD, Roos DS. 1997. A plastid of probable green algal origin in Apicomplexan parasites. Science 275:1485–9.

33. Mukherjee A, Sadhukhan CG. 2016. Anti-malarial Drug Design by Targeting Apicoplasts: New Perspectives. J pharmacopuncture 19:7–15.

34. Janouskovec J, Horák A, Oborník M, Lukes J, Keeling PJ. 2010. A common red algal origin of the apicomplexan, dinoflagellate, and heterokont plastids. Proc Natl Acad Sci U S A 107:10949–54.

35. Gould SB, Waller RF, McFadden GI. 2008. Plastid Evolution. Annu Rev Plant Biol 59:491–517.

36. Gould SB, Maier U-G, Martin WF. 2015. Protein Import and the Origin of Red Complex Plastids. Curr Biol 25:R515–R521.

37. Arisue N, Hashimoto T, Mitsui H, Palacpac QNM, Kaneko A, Kawai S, Hasegawa M, Tanabe K, Horii T. 2012. The *Plasmodium* apicoplast genome: conserved structure and close relationship of P. ovale to rodent malaria parasites. Mol Biol Evol 29:2095–2099.

38. Wilson RJ, Denny PW, Preiser PR, Rangachari K, Roberts K, Roy A, Whyte A, Strath M, Moore DJ, Moore PW, Williamson DH. 1996. Complete gene map of the plastid-

like DNA of the malaria parasite *Plasmodium falciparum*. J Mol Biol 261:155–72.

39. McFadden GI. 2000. Mergers and acquisitions: malaria and the great chloroplast heist. Genome Biol 1:reviews1026.1.

40. Lim L, McFadden GI. 2010. The evolution, metabolism and functions of the apicoplast. Philos Trans R Soc Lond B Biol Sci 365:749–63.

41. Martin W. 2003. Gene transfer from organelles to the nucleus: Frequent and in big chunks. Proc Natl Acad Sci 100:8612–8614.

42. Gallagher JR, Matthews KA, Prigge ST. 2011. *Plasmodium falciparum* apicoplast transit peptides are unstructured in vitro and during apicoplast import. Traffic 12:1124–38.

43. Bouchut A, Geiger JA, DeRocher AE, Parsons M. 2014. Vesicles Bearing *Toxoplasma* Apicoplast Membrane Proteins Persist Following Loss of the Relict Plastid or Golgi Body Disruption. PLoS One 9:e112096.

44. Parsons M, Karnataki A, Feagin JE, DeRocher A. 2007. Protein trafficking to the apicoplast: deciphering the apicomplexan solution to secondary endosymbiosis. Eukaryot Cell 6:1081–8.

45. Chaudhari R, Dey V, Narayan A, Sharma S, Patankar S. 2017. Membrane and luminal proteins reach the apicoplast by different trafficking pathways in the malaria parasite *Plasmodium falciparum*. PeerJ 5:e3128.

46. Ralph SA, van Dooren GG, Waller RF, Crawford MJ, Fraunholz MJ, Foth BJ, Tonkin CJ, Roos DS, McFadden GI. 2004. Tropical infectious diseases: metabolic maps and functions of the *Plasmodium falciparum* apicoplast. Nat Rev Microbiol 2:203–16.

47. Foth JB, Ralph AS, Tonkin JC, Struck SN, Fraunholz M, Roos SD, Cowman FA, McFadden IG. 2003. Dissecting apicoplast targeting in the malaria parasite *Plasmodium falciparum*. Science 299:705–708.

48. Zuegge J, Ralph S, Schmuker M, McFadden GI, Schneider G. 2001. Deciphering apicoplast targeting signals – feature extraction from nuclear-encoded precursors of *Plasmodium falciparum* apicoplast proteins. Gene 280:19–26.

49. Cilingir G, Lau AOT, Broschat SL. 2013. ApicoAMP: The first computational model for identifying apicoplast-targeted transmembrane proteins in Apicomplexa. J Microbiol Methods 95:313–319.

50. Cilingir G, Broschat SL, Lau AOT. 2012. ApicoAP: The First Computational Model for Identifying Apicoplast-Targeted Proteins in Multiple Species of Apicomplexa. PLoS One 7:e36598.

51. Fichera ME, Roos DS. 1997. A plastid organelle as a drug target in apicomplexan parasites. Nature 390:407–409.

52. Ramya TNC, Mishra S, Karmodiya K, Surolia N, Surolia A. 2007. Inhibitors of nonhousekeeping functions of the apicoplast defy delayed death in *Plasmodium falciparum*. Antimicrob Agents Chemother 51:307–16.

53. Yu M, Kumar STR, Nkrumah JL, Coppi A, Retzlaff S, Li DC, Kelly JB, Moura AP, Lakshmanan V, Freundlich SJ, Valderramos J-C, Vilcheze C, Siedner M, Tsai H-CJ, Falkard B, Sidhu SAB, Purcell AL, Gratraud P, Kremer L, Waters PA, Schiehser G, Jacobus PD, Janse JC, Ager A, Jacobs RW, Sacchettini CJ, Heussler V, Sinnis P, Fidock AD. 2008. The fatty acid biosynthesis enzyme FabI plays a key role in the development of liver-stage malarial parasites. Cell Host Microbe 4:567–578.

54. Vaughan MA, O'Neill TM, Tarun SA, Camargo N, Phuong MT, Aly IAS, Cowman FA, Kappe ISH. 2009. Type II fatty acid synthesis is essential only for malaria parasite late liver stage development. Cell Microbiol 11:506–520.

55. Nagaraj VA, Sundaram B, Varadarajan NM, Subramani PA, Kalappa DM, Ghosh SK, Padmanaban G. 2013. Malaria Parasite-Synthesized Heme Is Essential in the Mosquito and Liver Stages and Complements Host Heme in the Blood stages of Infection. PLoS Pathog 9:e1003522.

56. Ke H, Sigala PA, Miura K, Morrisey JM, Mather MW, Crowley JR, Henderson JP, Goldberg DE, Long CA, Vaidya AB. 2014. The Heme Biosynthesis Pathway Is Essential for *Plasmodium falciparum* Development in Mosquito Stage but Not in Blood stages. J Biol Chem 289:34827–34837.

57. Yeh E, DeRisi LJ. 2011. Chemical rescue of malaria parasites lacking an apicoplast defines organelle function in blood-stage *Plasmodium falciparum*. PLoS Biol 9.

58. Dahl LE, Shock LJ, Shenai RB, Gut J, DeRisi LJ, Rosenthal JP. 2006. Tetracyclines specifically target the apicoplast of the malaria parasite *Plasmodium falciparum*. Antimicrob Agents Chemother 50:3124–3131.

59. Dahl LE, Rosenthal JP. 2007. Multiple antibiotics exert delayed effects against the *Plasmodium falciparum* apicoplast. Antimicrob Agents Chemother 51:3485–3490.

60. Gisselberg JE, Dellibovi-Ragheb T a., Matthews K a., Bosch G, Prigge ST. 2013. The Suf Iron-Sulfur Cluster Synthesis Pathway Is Required for Apicoplast Maintenance in Malaria Parasites. PLoS Pathog 9.

61. Amberg-Johnson K, Hari BS, Ganesan MS, Lorenzi AH, Sauer TR, Niles CJ, Yeh E. 2017. Small molecule inhibition of apicomplexan FtsH1 disrupts plastid biogenesis in human pathogens. Elife 6.

62. Pasaje ACF, Cheung V, Kennedy K, Lim EE, Baell BJ, Griffin WMD, Ralph AS. 2016. Selective inhibition of apicoplast tryptophanyl-tRNA synthetase causes delayed death in *Plasmodium falciparum*. Sci Rep 6.

63. Florentin A, Cobb DW, Fishburn JD, Fierro MA, Striepen B, Correspondence VM.

2017. PfClpC Is an Essential Clp Chaperone Required for Plastid Integrity and Clp Protease Stability in *Plasmodium falciparum*. Cell Rep 21.

64. Gisselberg EJ, Dellibovi-Ragheb AT, Matthews AK, Bosch G, Prigge TS. 2013. The suf iron-sulfur cluster synthesis pathway is required for apicoplast maintenance in malaria parasites. PLoS Pathog 9.

65. Walczak M, Ganesan SM, Niles JC, Yeh E. 2018. ATG8 Is Essential Specifically for an Autophagy-Independent Function in Apicoplast Biogenesis in Blood-Stage Malaria Parasites. MBio 9:e02021-17.

66. Wu W, Herrera Z, Ebert D, Baska K, Cho HS, DeRisi LJ, Yeh E. 2015. A chemical rescue screen identifies a *Plasmodium falciparum* apicoplast inhibitor targeting MEP isoprenoid precursor biosynthesis. Antimicrob Agents Chemother 59:356–364.

67. Kuzuyama T, Seto H. 2012. Two distinct pathways for essential metabolic precursors for isoprenoid biosynthesis. Proc Jpn Acad Ser B Phys Biol Sci 88:41–52.

68. Guggisberg MA, Amthor ER, Odom RA. 2014. Isoprenoid biosynthesis in *Plasmodium falciparum*. Eukaryot Cell 13:1348–1359.

69. Stanway RR, Witt T, Zobiak B, Aepfelbacher M, Heussler VT. 2009. GFP-targeting allows visualization of the apicoplast throughout the life cycle of live malaria parasites. Biol Cell 101:415–435.

70. Ellis EK, Clough B, Saldanha WJ, Wilson JR. 2001. Nifs and Sufs in malaria. Mol Microbiol 41:973–981.

71. Charan M, Singh N, Kumar B, Srivastava K, Siddiqi IM, Habib S. 2014. Sulfur mobilization for Fe-S cluster assembly by the essential SUF pathway in the *Plasmodium falciparum* apicoplast and its inhibition. Antimicrob Agents Chemother 58:3389–3398.

72. Loiseau L, Ollagnier-de-Choudens S, Nachin L, Fontecave M, Barras F. 2003. Biogenesis of Fe-S cluster by the bacterial Suf system: SufS and SufE form a new type of cysteine desulfurase. J Biol Chem 278:38352–38359.

73. Outten FW, Wood MJ, Munoz FM, Storz G. 2003. The SufE protein and the SufBCD complex enhance SufS cysteine desulfurase activity as part of a sulfur transfer pathway for Fe-S cluster assembly in *Escherichia coli*. J Biol Chem 278:45713–9.

74. Layer G, Gaddam AS, Ayala-Castro NC, Ollagnier-de Choudens S, Lascoux D, Fontecave M, Outten WF. 2007. SufE transfers sulfur from SufS to SufB for iron-sulfur cluster assembly. J Biol Chem 282:13342–13350.

75. Saini A, Mapolelo TD, Chahal KH, Johnson KM, Outten WF. 2010. SufD and SufC ATPase activity are required for iron acquisition during in vivo Fe-S cluster formation on SufB. Biochemistry 49:9402–9412.

76. Hirabayashi K, Yuda E, Tanaka N, Katayama S, Iwasaki K, Matsumoto T, Kurisu G, Outten FW, Fukuyama K, Takahashi Y, Wada K. 2015. Functional Dynamics Revealed by the Structure of the SufBCD Complex, a Novel ATP-binding Cassette (ABC) Protein That Serves as a Scaffold for Iron-Sulfur Cluster Biogenesis. J Biol Chem 290:29717–31.

77. Haussig MJ, Matuschewski K, Kooij ATW. 2013. Experimental Genetics of *Plasmodium berghei* NFU in the Apicoplast Iron-Sulfur Cluster Biogenesis Pathway. PLoS One 8.

78. Haussig MJ, Matuschewski K, Kooij ATW. 2014. Identification of vital and dispensable sulfur utilization factors in the *Plasmodium* apicoplast. PLoS One 9.

79. Gupta V, Sendra M, Naik GS, Chahal KH, Huynh HB, Outten WF, Fontecave M, de Choudens S. 2009. Native *Escherichia coli* SufA, coexpressed with SufBCDSE, purifies as a [2Fe-2S] protein and acts as an Fe-S transporter to Fe-S target enzymes. J Am Chem Soc 131:6149–6153.

80. Py B, Gerez C, Angelini S, Planel R, Vinella D, Loiseau L, Talla E, Brochier-Armanet C, Garcia Serres R, Latour J-M, Ollagnier-de Choudens S, Fontecave M, Barras F. 2012. Molecular organization, biochemical function, cellular role and evolution of NfuA, an atypical Fe-S carrier. Mol Microbiol 86:155–171.

81. Chahal KH, Dai Y, Saini A, Ayala-Castro C, Outten WF. 2009. The SufBCD Fe-S scaffold complex interacts with SufA for Fe-S cluster transfer. Biochemistry 48:10644–10653.

82. Wrenger C, Müller S. 2004. The human malaria parasite *Plasmodium falciparum* has distinct organelle-specific lipoylation pathways. Mol Microbiol 53:103–113.

83. Esberg B, Leung HC, Tsui HC, Björk GR, Winkler ME. 1999. Identification of the miaB gene, involved in methylthiolation of isopentenylated A37 derivatives in the tRNA of *Salmonella typhimurium* and *Escherichia coli*. J Bacteriol 181:7256–65.

84. Seeber F, Soldati-Favre D. 2010. Metabolic Pathways in the Apicoplast of Apicomplexa. Int Rev Cell Mol Biol 281:161–228.

85. Seeber F, Aliverti A, Zanetti G. 2005. The plant-type ferredoxin-NADP+ reductase/ferredoxin redox system as a possible drug target against apicomplexan human parasites. Curr Pharm Des 11:3159–72.

86. Röhrich CR, Englert N, Troschke K, Reichenberg A, Hintz M, Seeber F, Balconi E, Aliverti A, Zanetti G, Köhler U, Pfeiffer M, Beck E, Jomaa H, Wiesner J. 2005. Reconstitution of an apicoplast-localised electron transfer pathway involved in the isoprenoid biosynthesis of *Plasmodium falciparum*. FEBS Lett 579:6433–6438.

87. Saggu SG, Garg S, Pala RZ, Yadav KS, Kochar KS, Kochar KD, Saxena V. 2017. Characterization of 4-hydroxy-3-methylbut-2-en-1-yl diphosphate synthase (IspG)

from *Plasmodium vivax* and it's potential as an antimalarial drug target. Int J Biol Macromol 96:466–473.

88. Lim L, Linka M, Mullin KA, Weber APM, McFadden GI. 2010. The carbon and energy sources of the non-photosynthetic plastid in the malaria parasite. FEBS Lett 584:549–554.

89. Lim L, McFadden GI. 2010. The evolution, metabolism and functions of the apicoplast. Philos Trans R Soc Lond B Biol Sci 365:749–63.

90. Lindner SE, Sartain MJ, Hayes K, Harupa A, Moritz RL, Kappe SHI, Vaughan AM. 2014. Enzymes involved in plastid-targeted phosphatidic acid synthesis are essential for *P lasmodium yoelii* liver-stage development. Mol Microbiol 91:679–693.

91. Fleige T, Fischer K, Ferguson DJP, Gross U, Bohne W. 2007. Carbohydrate metabolism in the *Toxoplasma gondii* apicoplast: localization of three glycolytic isoenzymes, the single pyruvate dehydrogenase complex, and a plastid phosphate translocator. Eukaryot Cell 6:984–96.

92. Saito T, Nishi M, Lim IM, Wu B, Maeda T, Hashimoto H, Takeuchi T, Roos SD, Asai T. 2008. A novel GDP-dependent pyruvate kinase isozyme from *Toxoplasma gondii* localizes to both the apicoplast and the mitochondrion. J Biol Chem 283:14041–14052.

93. Israelsen JW, Vander Heiden GM. 2015. Pyruvate kinase: function, regulation and role in cancer. Semin Cell Dev Biol 43:43–51.

94. Lim L, Linka M, Mullin KA, Weber APM, McFadden GI. 2010. The carbon and energy sources of the non-photosynthetic plastid in the malaria parasite. FEBS Lett 584:549–554.

95. Foth JB, Stimmler ML, Handman E, Crabb SB, Hodder NA, McFadden IG. 2005. The malaria parasite *Plasmodium falciparum* has only one pyruvate dehydrogenase complex, which is located in the apicoplast. Mol Microbiol 55:39–53.

96. Foth JB, Stimmler ML, Handman E, Crabb SB, Hodder NA, McFadden IG. 2004. The malaria parasite *Plasmodium falciparum* has only one pyruvate dehydrogenase complex, which is located in the apicoplast: The single, plastidic PDH of *Plasmodium falciparum*. Mol Microbiol 55.

97. Laine LM, Biddau M, Byron O, Müller S. 2015. Biochemical and structural characterization of the apicoplast dihydrolipoamide dehydrogenase of *Plasmodium falciparum*. Biosci Rep 35.

98. Boehme C, Bieber F, Linnemann J, Breitling R, Lorkowski S, Reissmann S. 2013. Chemical and enzymatic characterization of recombinant rabbit muscle pyruvate kinase. Biol Chem 394:695–701.

99. Saeki T, Hori M, Umezawa H. 1974. Pyruvate kinase of *Escherichia coli*. Its role in supplying nucleoside triphosphates in cells under anaerobic conditions. J Biochem 76:631–7.

100. Knowles VL, Smith CS, Smith CR, Plaxton WC. 2001. Structural and Regulatory Properties of Pyruvate Kinase from the Cyanobacterium *Synechococcus* PCC 6301 . J Biol Chem 276:20966–20972.

101. Abbe K, Yamada T. 1982. Purification and properties of pyruvate kinase from *Streptococcus mutans*. J Bacteriol 149:299–305.

102. Geary GT, Divo AA, Bonanni CL, Jensen BJ. 1985. Nutritional requirements of *Plasmodium falciparum* in culture. III. Further observations on essential nutrients and antimetabolites. J Protozool 32:608–613.

103. Saliba KJ, Ferru I, Kirk K. 2005. Provitamin B5 (pantothenol) inhibits growth of the intraerythrocytic malaria parasite. Antimicrob Agents Chemother 49:632–7.

104. Spry C, Saliba JK. 2009. The human malaria parasite *Plasmodium falciparum* is not dependent on host coenzyme A biosynthesis. J Biol Chem 284:24904–24913.

105. Spry C, Kirk K, Saliba JK. 2008. Coenzyme A biosynthesis: an antimicrobial drug target. FEMS Microbiol Rev 32:56–106.

106. Spry C, van Schalkwyk DA, Strauss E, Saliba KJ. 2010. Pantothenate utilization by *Plasmodium* as a target for antimalarial chemotherapy. Infect Disord Drug Targets 10:200–16.

107. Spry C, Chai LCL, Kirk K, Saliba JK. 2005. A class of pantothenic acid analogs inhibits *Plasmodium falciparum* pantothenate kinase and represses the proliferation of malaria parasites. Antimicrob Agents Chemother 49:4649–4657.

108. Spry C, Macuamule C, Lin Z, Virga KG, Lee RE, Strauss E, Saliba KJ. 2013. Pantothenamides Are Potent, On-Target Inhibitors of *Plasmodium falciparum* Growth When Serum Pantetheinase Is Inactivated. PLoS One 8:e54974.

109. Macuamule CJ, Tjhin ET, Jana CE, Barnard L, Koekemoer L, de Villiers M, Saliba KJ, Strauss E. 2015. A Pantetheinase-Resistant Pantothenamide with Potent, On-Target, and Selective Antiplasmodial Activity. Antimicrob Agents Chemother 59:3666–3668.

110. Hart JR, Abraham A, Aly IAS. 2017. Genetic Characterization of Coenzyme A Biosynthesis Reveals Essential Distinctive Functions during Malaria Parasite Development in Blood and Mosquito. Front Cell Infect Microbiol 7.

Chapter 2

Generation of an Alternative Genetically-Encoded Apicoplast Metabolic Bypass System

Attributions:

- The generation of the pMPC-aSFG plasmid was a collaborative effort between Dr. Sean Prigge, Dr. Hugo Jhun, Dr. Aleah Roberts, and Dr. Krista Matthews.
- The Figure 2-4 IFA was generated by Dr. Aleah Roberts
- The Figure 2-5 IFA was generated by Dr. Krithika Rajaram
- The growth curves on Figures 2-3, 2-6, and 2-8 were generated by Hans Liu

ABSTRACT

The apicoplast plays an essential role in the survival of *Plasmodium falciparum* parasites. However, the entire organelle is dispensable in blood-stage parasites as long as the isoprenoid precursor isopentenyl pyrophosphate (IPP) is added to the culture medium. Previous research established a chemical bypass system, allowing for the rescue of parasites missing the apicoplast organelle through the direct supplementation of IPP. While this tool has been invaluable to the field, the system has drawbacks that make larger-scale and longer-term experiments unfeasible. In order to overcome these issues, we have developed an alternative genetically-encoded bypass system by engineering parasites to express enzymes from an exogenous mevalonate isoprenoid precursor pathway. This parasite line, that we are calling PfMev, contains an IPP production pathway that is controllable through the supplementation of the biomolecule mevalonate.

INTRODUCTION

Work to eliminate or control the spread of the malarial infections span a century or more but have been hindered by the rise and spread of resistance to the antimalarial drugs (1–7). In order to continue the progress that has been made in reducing malarial infections and deaths attributed to the disease there is a critical need for new drugs with novel mechanisms of action (8). In efforts to identify new drug targets, the apicoplast organelle within the parasite has often been considered due to the organelle possessing evolutionarily distinct biochemical pathways that are not present in the human host (9), in addition to the organelle being essential for parasite survival, features which make it an attractive source of potential drug targets (10, 11).

The apicoplast is home to a number of biochemical pathways including the FasII fatty acid biosynthetic pathway, the methylerythritol phosphate (MEP) pathway responsible for the generation of the isoprenoid precursors isopentenyl pyrophosphate (IPP) and dimethylallyl pyrophosphate (DMAPP), the heme biosynthetic pathway shared with the mitochondrion, and the SUF pathway that generates iron-sulfur cluster cofactors for usage within the organelle (12). Additionally, there are an estimated ~400 proteins trafficked to the apicoplast, representing ~7% of the parasite genome [36]–[39]. However, of all the proteins and processes present within this organelle it has appeared that the isoprenoid precursors generated by the MEP pathway are the only essential products produced by the apicoplast that are required in other compartments of the cell during the asexual blood-stage of the parasite (17). Previous work by Yeh *et al.* in 2011 established a chemical bypass system, demonstrating that parasites can continue to survive and replicate without an intact apicoplast organelle as long as IPP is supplemented in sufficient quantities (17).

This chemical bypass system established by Yeh *et al.* has proven to be invaluable to the study of the apicoplast in malaria parasites, with previous research utilizing this bypass to interrogate the essentiality of apicoplast-specific genes (18–22), and test differential drug sensitivity to better determine the specificity and mechanism of action of certain drugs (18, 23). However, this system has some drawbacks that make certain longer-term and larger-scale experiments difficult to accomplish, including the expense of the chemical at ~$25,800/g (Sigma-Aldrich) with the large amounts (200μM) required to rescue parasite growth (17), in addition to the chemical being labile and requiring frequent media exchange. In our hands, we have also experienced incomplete rescue of apicoplast-negative parasites to wild-type growth levels under IPP supplementation, and have found IPP-dependent parasites to be unable to survive cryopreservation, failing to detect parasites via Giemsa stain

after 30-days of culturing. For these reasons, the chemical bypass system is not easily amenable to longer-term experimentation, such as the generation of nuclear-encoded apicoplast-specific genetic knockouts, which is likely why none have been published since the discovery of the IPP chemical bypass in 2011. However, it should be noted that there have been multiple published reports of transcripts encoding essential apicoplast-specific proteins being knocked-down using conditional systems and rescued through IPP supplementation (18–20, 22), in addition to IPP rescuing the expression of a dominant-negative mutant (21).

In order to address these issues we have developed an alternative method of IPP supplementation through the cytosolic expression of four enzymes from the mevalonate-dependent (MVA) isoprenoid precursor pathway (24), encoded by a single plasmid that has been integrated into the parasite genome (**Figure 2-1**). The MVA pathway is an alternative pathway used to generate isoprenoid precursors that is common to gram-positive bacteria and most eukaryotes (25). This pathway uses an entirely different set of enzymes and intermediates than the endogenous MEP isoprenoid precursor pathway within the apicoplast organelle of the parasite (25, 26). This newly established line, that we are calling PfMev, converts exogenously supplied mevalonate into IPP and DMAPP. We have found that this alternative bypass system addresses many of the problems seen in the chemical bypass, namely, mevalonate supplementation in PfMev parasites lacking an apicoplast restores growth to wild-type levels and requires as little as 10μM mevalonate. Additionally, mevalonate-dependent PfMev parasites can be easily cryopreserved and thawed, mevalonate is stable, abrogating the need of frequent media exchange, and the compound is affordable at $142/g (Sigma-Aldrich). These aspects make the mevalonate bypass an attractive

alternative to the chemical bypass system, and should allow for larger-scale and longer-term experimentation that would be unfeasible without it.

We also engineered the PfMev parasite line to express a stable green fluorescent protein called super-folder green (SFG) in the apicoplast organelle. SFG has improved folding kinetics and is less likely to misfold when expressed with other proteins (27), particularly in higher redox potential environments like the secretory system (28). Since proteins traffic through the secretory pathway en route to the apicoplast, this final property is highly desirable. We appended the first 55 amino acids of the *P. falciparum* acyl-carrier protein to the N-terminus of SFG (api-SFG), resulting in its trafficking to the apicoplast, fluorescently labeling the organelle (29). Fluorescent labeling makes it easy to assess the morphology of the apicoplast after drug treatments or genetic perturbations that can result in disruption of the organelle (17, 30). Another useful feature of the PfMev line is that the cassette encoding the enzymes from the MVA pathway serves as its own genetic selection marker, and can be selected for with the drug fosmidomycin in the presence of mevalonate. This leaves any previously established drug resistance markers available for future genetic manipulations.

Through the work outlined here we have validated and characterized the PfMev line, showing that mevalonate supplementation provides an effective, and arguably superior apicoplast bypass system. We demonstrated that mevalonate can bypass the toxic effect of drugs that target proteins within the organelle, in addition to enabling the survival of parasites containing a disrupted apicoplast with as little as 10μM mevalonate. We also demonstrate the utility of this line in determining apicoplast morphology using live epifluorescent microscopy, by examining parasites with intact and disrupted organelles. We also tracked the incorporation of labeled carbons from mevalonate into isoprenoid products,

demonstrating the functionality of the mevalonate pathway. Additionally, we were able to establish that genetic deletions of essential apicoplast-specific genes can be generated in PfMev parasites using Cas9-mediated genome editing.

RESULTS

Mevalonate Rescue of Fosmidomycin Treated PfMev Parasites

Previous work attempting to circumvent the necessity of essential apicoplast-specific genes or bypass the toxicity of apicoplast-specific drugs have relied on direct supplementation of IPP (17–22, 31). However, the IPP chemical bypass system has some inherent downsides as outlined above. To overcome these issues, we engineered an alternative genetically encoded bypass in *P. falciparum* that can generate the isoprenoid precursors IPP and DMAPP using enzymes from the mevalonate (MVA) pathway, which are distinct from the enzymes that comprise the endogenous MEP pathway (**Figure 2-2a**). This parasite line that we are calling PfMev contains three enzymes from the MVA pathway capable of forming IPP from mevalonate (24) and a fourth enzyme (IPP Isomerase) that catalyzes the interconversion of IPP and its regioisomer DMAPP (32). All four enzymes were integrated into parasite genome and are expressed within the cytosol (**Figure 2-2b**).

In order to validate the PfMev line, we wanted to test whether the parasites could rely on the introduced MVA pathway for isoprenoid production. Therefore, we treated PfMev parasites with 25μM fosmidomycin (50x IC_{50}), which inhibits the activity of the DOXP-reductoisomerase (DXPR) enzyme of the endogenous MEP pathway within the apicoplast organelle (33), and supplemented the parasites with mevalonate at concentrations of either 0μM, 2.5μM, 10μM, 50μM, or 100μM. Parasites not treated with fosmidomycin or

supplemented with mevalonate served as controls. Parasitemia was quantified daily using SYBR green staining and flow-cytometry. As shown in **Figure 2-3**, mevalonate concentrations of 10μM or more successfully bypassed the lethal effect of fosmidomycin (30). These data also show that the ability to bypass the toxicity of the drug is reliant on mevalonate, consistent with reliance on the engineered mevalonate pathway for the generation of essential isoprenoid precursors.

Apicoplast Labeling for Determination of Organelle Phenotype

In addition to the MVA pathway enzymes, the PfMev parasite line also expresses the super-folder green protein (34) with the signal and transit peptide of the *P. falciparum* acyl-carrier protein (ACP) appended to the N-terminus of the protein. This results in SFG being trafficked to the apicoplast and fluorescently labeling the organelle (api-SFG) (29). Previous work demonstrated that under IPP supplementation, certain drug treatments or genetic perturbations can result in disruption of the apicoplast, and the fluorescent labeling of the organelle allows for a phenotypic readout (17, 30). Using live epifluorescent microscopy we were able to confirm that SFG is trafficked to a subcellular compartment consistent with the elongated morphology of the apicoplast organelle (**Figure 2-4a**). Trafficking of api-SFG to the apicoplast was confirmed using immunofluorescence (IFA) by co-localizing api-SFG with the Acyl Carrier Protein (ACP), a known apicoplast marker (29) (**Figure 2-4b**).

Titration of Mevalonate in Apicoplast Negative PfMev Parasites

Having established that the PfMev parasites can use the alternate bypass system, we wanted to determine how much mevalonate is required for the rescue of parasites lacking the apicoplast organelle. To accomplish this, we generated apicoplast negative parasites by

treating PfMev parasites with 100nM azithromycin (1x 96 hr IC_{50}) supplemented with 50μM mevalonate for one week. These parasites were permanently dependent on mevalonate for survival, indicating that azithromycin disrupted the apicoplast organelle, as previously described (30). Consistent with this result, we were unable to PCR amplify a gene from the apicoplast organellar genome while being able to amplify other genes from the nuclear and mitochondrial genomes (21) (**Figure 2-5a**). We were able to confirm loss of the apicoplast through live epifluorescent microscopy, and were unable to locate parasites with intact organelles, but instead observed the presence of multiple discrete vesicles, indicative of organelle loss (17) (**Figure 2-5b**). IFA co-localization experiments showed that ACP is also found in these api-SFG vesicles providing further evidence that the apicoplast organelle is disrupted (**Figure 2-5c**). Once parasites lacking an apicoplast were obtained, apicoplast negative parasites were grown in the presence of 0μM, 2.5μM, 10μM, 50μM, or 100μM mevalonate and compared with the growth of apicoplast intact PfMev parasites grown in the presence of 0μM or 50μM mevalonate. Parasitemia was counted via SYBR green staining and flow-cytometry. We found that supplementation with as little as 10μM mevalonate restored the growth of apicoplast-negative parasites to near wild-type levels (**Figure 2-6**).

Metabolic Labeling of PfMev Parasites with [2-^{13}C]-mevalonate

We also conducted metabolic labeling of PfMev parasites to demonstrate that exogenously supplemented mevalonate was being used by the MVA enzymes introduced into the parasite to form IPP and downstream isoprenoids. To show this, we generated parallel PfMev parasite cultures, both treated with 25μM fosmidomycin (50x IC_{50}) and supplemented with either 50μM [^{12}C]-mevalonate or [2-^{13}C]-mevalonate. After 48 hours of growth, metabolites were extracted and analyzed via targeted liquid-chromatography mass

spectrometry mass spectrometry (LC-MS/MS) using selected reaction monitoring (SRM) (35). Using this method, we were able to detect the isoprenoid precursor IPP (and/or the isobaric isomer DMAPP) (**Figure 2-7a**) in addition to the downstream isoprenoid product farnesyl pyrophosphate (FPP) (**Figure 2-7b**). We observed clear mass shifts of these metabolites between unlabeled and labeled parasite samples (36, 37), demonstrating incorporation of [^{13}C] carbon in the labeled samples. Furthermore, we were able to show that we were successful in inhibiting the endogenous MEP pathway, with an increased level of labeled metabolite to unlabeled metabolite in the labeled sample. These data clearly indicate usage of mevalonate by the MVA pathway enzymes to generate IPP/DMAPP and the downstream isoprenoid FPP.

Deletion of an Apicoplast Essential Gene using Cas9-mediated Genome Editing

Supplementation of PfMev parasites with mevalonate allows us to disrupt the apicoplast organelle, and thus should also allow for the deletion of essential apicoplast-specific genes. In order to test this, we chose to delete the target of fosmidomycin, DXPR (PF3D7_1467300; 1-deoxy-D-xylulose 5-phosphate reductoisomerase) (33). Genetic deletions were obtained utilizing Cas9-mediated editing, as previously described (38), but under continuous supplementation with 50μM mevalonate. The DXPR deletion was confirmed via PCR, showing the expected 5' and 3' integration of the hDHFR selection cassette. Parasites were also screened for the original locus to detect if there were any residual wild-type parasites (**Figure 2-8a**). The phenotype of the apicoplast was then ascertained in order to determine if DXPR deletion had any effect on the organelle. Previous experiments showed that drug treatment or genetic disruptions can result in the loss of the organelle, and that when the apicoplast is lost under IPP supplementation there is a distinct

resulting phenotype (17, 21). Namely, the 35kb organellar genome of the apicoplast is lost, and the organelle itself is no longer intact, with proteins normally sent to the apicoplast instead accumulating in multiple discrete vesicles throughout the cell (17, 21). However, the parasites containing the disrupted DXPR locus retained the apicoplast organelle as evidenced by PCR amplification of SufB, a gene encoded by the apicoplast organellar genome (**Figure 2-8b**), in addition to live epifluorescent microscopy showing the presence of a single intact organelle (**Figure 2-8c**). We were also able to determine the essentiality of this gene through the removal of mevalonate. ΔDXPR parasites are reliant on mevalonate supplementation for growth indicating that this gene is essential for the blood-stage survival of the parasite (**Figure 2-8d**). These results confirm that the activity of DXPR is essential for parasite survival, but also show that the activity of DXPR is not needed for maintaining the apicoplast organelle. These results are similar to what has been seen with fosmidomycin treatment. Even at doses of 25μM fosmidomycin (50x IC_{50}), supplementation with IPP allowed parasites to survive and retain an intact apicoplast organelle (21). This differed from treatment with 100nM azithromycin (1x IC_{50}) and IPP supplementation, which resulted in disruption of the organelle (21), likely due to the target of azithromycin (protein translation within the organelle) playing a key role in the maintenance and replication of the organelle (39).

CONCLUSIONS AND DISCUSSION

Through the generation of our PfMev line we have been able to overcome many of the issues associated with the apicoplast chemical bypass system reliant on the direct supplementation of IPP. Namely, parasites expressing the MVA metabolic bypass enzymes

can grow at wild-type levels, even when lacking the apicoplast, if supplemented with mevalonate, and can quickly resume growth post-cryopreservation. The ability to easily cryopreserve parasite lines makes longer-term experimental approaches that may take place over many months or years, or larger-scale experiments that generate tens or hundreds of parasite lines reliant on mevalonate more feasible by allowing for the storage and future analysis of the lines. Additionally, the system is vastly more affordable due to the drastically lower cost of mevalonate in comparison to IPP. There are also the added benefits that 20-fold lower concentrations of mevalonate are needed to support parasite growth, and that the chemical is more stable than IPP which has a half-life of ~4.5 hours at 37°C (40). PfMev parasites also contain a fluorescent reporter that is trafficked to and labels the apicoplast. This allows for the observation of the organellar phenotype via live epifluorescent microscopy and the ability to determine if a given treatment or manipulation has resulted in the disruption of the organelle.

We were able to successfully generate the PfMev line by selecting for transfectants with 25μM fosmidomycin supplemented with 50μM mevalonate. By doing so we were able to select for these parasites using a novel method, not reliant on any previously validated drug selectable markers. Selection of the line using this method is beneficial, as it allows for further genetic manipulation of this line by sparing the commonly used drug selectable markers in *P. falciparum*, such as human dihydrofolate reductase (hDHFR) (41), blasticidin *S* deaminase (BSD), neomycin phosphotransferase (NEO) (42), and yeast dihydroorotate dehydrogenase (yDHOD) (43). This should facilitate straightforward selection in the PfMev line using previously established genetic tools and plasmids. Additionally, this should allow for selection of multiple drug resistance markers, enabling the generation of double knockouts or other complex multi-step genetic manipulations.

Furthermore, we have been able to provide in-depth metabolic characterization of the PfMev line by tracking the utilization of the MVA pathway and detecting the breakdown of mevalonate into IPP/DMAPP and FPP through isotopic-labeling and LC-MS/MS. Seeing as how the generation of isoprenoid precursors for the production of downstream isoprenoids is the only presumed essential function of the intact apicoplast during the asexual blood-stage of the parasite (17), the importance of further investigation into this metabolic pathway is clear. While our motivation was to prove the activity of the introduced mevalonate-pathway enzymes, we believe that similar metabolic labeling techniques using the PfMev line may be useful in the identification of previously unknown isoprenoid products. Investigation and discovery of novel isoprenoid products is an active area of research, with the recent discovery of parasite produced volatile isoprenoid products that act as mosquito attractants (44).

Using CRISPR-Cas9 in PfMev parasites we were able to successfully delete DXPR, an essential apicoplast-specific protein, and maintain the knockout line in culture through mevalonate supplementation. This work represents the first published result of this kind, clearly demonstrating the utility of this system as a platform that can be used to investigate additional essential apicoplast-specific proteins and their roles in parasite survival. While the production of isoprenoid precursors has been proposed to be the only essential function of the apicoplast during the asexual blood-stage of the parasite, additional proteins with functions supporting the MEP pathway also represent an important area of potential research. Furthermore, it has previously been shown that certain genes are essential for the maintenance or replication of the apicoplast, with their disruption causing the loss of the organelle under IPP supplementation (21). There are likely to be numerous proteins required to maintain the apicoplast that are playing roles in transcription, translation, organelle

genome replication, trafficking of proteins to the organelle, import of substrates, export of products, and replication and division of the organelle, among others. Although the proteins involved in these processes probably number in the 100s, most of them have not been identified or studied. As mentioned above, there are a predicted ~400 proteins that are trafficked to the apicoplast, representing ~7% of the genes in the parasite genome [36]–[39]. However, approximately half of the proteins predicted to be apicoplast localized in PlasmoDB are annotated as having an unknown function (45), representing a significant gap in our basic understanding of apicoplast biology. The PfMev line provides a viable method to interrogate genes essential to apicoplast maintenance and replication by utilizing the engineered metabolic bypass, in addition to allowing for phenotypic characterization of the organelle through the visualization of the SFG-labeled apicoplast, in order to determine whether a given genetic manipulation resulted in the loss of the organelle. Investigation of these genes may be especially attractive because drugs that inhibit proteins that result in apicoplast loss may help to prevent recrudesce and the subsequent development of drug resistance.

In order to uncover the importance of unannotated apicoplast-trafficked proteins, PfMev parasites could be used for forward genetic screens in order to determine which are essential for parasite survival, and which are required for the maintenance and replication of the organelle. Initial hits using this approach could help to prioritize which genes to follow up on to characterize the role and function of the gene product. Forward genetic screens using the PfMev line could take advantage of current chemical mutagenesis (46) or PiggyBac transposon insertional mutagenesis techniques used in *P. falciparum* (47). Furthermore, the PfMev line could be used for drug discovery efforts by screening compound libraries against PfMev parasites with or without mevalonate supplementation to test for the differential drug

sensitivity indicative of compounds that are apicoplast-specific. Finding drugs with such differential activity would be useful in helping to narrow down the list of potential targets, and help to inform the potential mechanism of action. Previous efforts using the IPP chemical bypass system have accomplished this for certain compound libraries (23). However, the reduced cost of mevalonate would make screening much larger compound libraries more feasible.

Ultimately, we hope that the work done using the PfMev line to identify and validate proteins that are essential for apicoplast maintenance and parasite survival will be translated to practical applications such as drug discovery efforts. The PfMev line is likely to be a useful tool in drug target identification as well as validation. Previous work on putative drug targets such as those within the FasII pathway led to vast amounts of wasted time, effort, resources, and millions of dollars, because the enzymes were not properly validated and were erroneously assumed to be essential (48, 49). This misspent effort could have been avoided by validating the essentiality of a given gene by deleting it in a bypass system such as the PfMev parasite line.

Overall, we believe that the generation of the PfMev line will be a valuable tool for the investigation of the apicoplast organelle and represents a significant improvement to the existing IPP chemical bypass system. To our knowledge, this is also the first time a metabolic pathway has been reconstituted in malaria parasites. The benefits of the PfMev line include the decreased expense of supplementation, the restoration of growth of apicoplast defective parasites to wild-type levels, and the relative ease of cryopreservation. The PfMev line should make longer-term experimentation such as the deletion of apicoplast-essential genes more feasible. We also envision this line being useful for larger-scale experimentation, such as forward genetic screens, or the screening of compound libraries against PfMev parasites with

or without mevalonate supplementation to test for the differential drug sensitivity of compounds that may be apicoplast-specific. Additionally, discoveries pertaining to basic apicoplast biology or the identification of essential apicoplast proteins that are potential drug targets in *P. falciparum* using the PfMev line may have a broader impact and assist in understanding basic plastid biology that may be applicable to other Apicomplexan species such as *T. gondii* or *Babesia* spp.

METHODS

P. falciparum culture and maintenance

Unless otherwise noted, blood-stage *P. falciparum* parasites were cultured in human erythrocytes collected under IRB protocol NA_00019050 at 1% hematocrit in a 10mL total volume of CMA (complete medium with Albumax) medium containing RPMI 1640 media with L-glutamine (USBiological Life Sciences), supplemented with 25mM HEPES, 0.2% sodium bicarbonate, 12.5µg/mL hypoxanthine, 5g/L Albumax II (Life Technologies) and 25µg/mL gentamicin. Cultures were maintained in gassed flasks (94% N_2, 3% O_2, 3% CO_2) and incubated in sealed 25cm^2 flasks at 37°C.

Construction of the pMPc-aSFG (PfMev) mevalonate bypass plasmid

Generation of the mevalonate bypass plasmid utilized a modified pACYC replicon, with a p15a origin and chloramphenicol resistance cassette. The sequence encoding the MVA pathway itself was developed through the generation of synthetic genes encoding *Streptococcus pneumoniae* mevalonate kinase (MevK), *Homo sapiens* phosphomevalonate kinase (PMevK), *S. pneumoniae* mevalonate 5-diphosphate decarboxylase (MVD), as well as the *E.*

coli isopentenyl diphosphate isomerase (Idi) gene. All genes were codon optimized for expression in *E. coli* and manually modified to avoid rare codons for expression in *P. falciparum*. The four genes are connected by nucleotides encoding seven amino acid flexible linkers.

To visualize apicoplast morphology another cassette was added to the plasmid expressing the first 55 amino acids of the *P. falciparum* Acyl Carrier Protein (ACP) fused to a N-terminus of a codon-optimized variant of GFP called Super Folder Green (SFG). The ACP leader peptide is known to traffic proteins to the apicoplast (50) and SFG is a fast folding version of GFP that minimizes the kinetic trap of disulfide formation in the oxidizing environment of the endoplasmic reticulum (28, 34). To drive expression of the apicoplast SFG (api-SFG) and MVA bypass pathway cassettes a strong bidirectional promoter (Pcam/Psti) was used (51, 52).

Generation of the PfMev bypass line

For generation of the PfMev line we transfected *P. falciparum* NF54attB parasites, generously provided by Dr. David Fidock (Columbia University), using methods previously described (53, 54). Briefly, 400µL of red blood cells were washed with 5mL of CytoMix and resuspended in 340µL of CytoMix and electroporated with 75µg each of the pmpc-asfg (expressing the MVA pathway enzymes and api-SFG) and pINT (encoding the mycobacteriophage Bxb1 integrase) plasmids (53). The electroporated RBCs were then mixed with ~2.5mL of a 10mL culture of NF54attB parasites synchronized as schizonts at 1% hematocrit and ~10% parasitemia, with an additional 10mL of CMA media added. After 48 hours, transfectants were selected for integration of the pMPc-aSFG plasmid into the attB site through selection with 25µM fosmidomycin (50x IC_{50}), supplemented with 50µM

mevalonate until parasites were observed. Infected red blood cells (iRBC) were first observed approximately 20-25 days after beginning drug selection. Once parasites were observed the culture was maintained on CMA medium.

Mevalonate rescue of fosmidomycin treated parasites growth curve

PfMev parasites were seeded in a 96-well flat bottom cell culture plate (Corning) at a starting parasitemia of 0.5% at 2% hematocrit, at a total volume of 250µL in quadruplicate. There was one parental control condition of PfMev parasites grown in CMA (positive control). For the rest of the conditions, parasites were grown in the presence of 25µM fosmidomycin (50x IC_{50}), and supplemented with mevalonate at concentrations of either 0µM (negative control), 2.5µM, 10µM, 50µM, or 100µM. Parasites were collected every 24 hours for four days, and the parasitemia was counted via SYBR green staining and flow-cytometry as outlined below.

Mevalonate titration of apicoplast negative parasites growth curve

Apicoplast negative parasites were generated by treating PfMev parasites with 100nM azithromycin (1x IC_{50}) supplemented with 50µM mevalonate for one week. Loss of the organelle was confirmed via PCR as outlined below, and additionally verified via live epifluorescent microscopy using methods described below. Parasites were seeded in a 96-well flat bottom cell culture plate (Corning) at a starting parasitemia of 0.5% at 2% hematocrit, at a total volume of 250µL in quadruplicate. To serve as a control, PfMev parasites with an intact apicoplast were cultured in either 0µM or 50µM mevalonate. The apicoplast negative PfMev parasites were grown with mevalonate at concentrations of either 0µM (negative control), 2.5µM, 10µM, 50µM, or 100µM. Parasites were collected every 24

hours for four days, and the parasitemia was counted via SYBR green staining and flow-cytometry as described below.

Testing mevalonate dependence in PfMev deletion mutants via growth curve

For each of the PfMev deletion lines, the parasitemia was determined via Gimesa stain, with the appropriate amount of the parental culture removed to seed quadruplicate samples with or without mevalonate. This volume was resuspended in a total of 10mL CMA and centrifuged at 1,600rcf at room temperature (~25°C) for 5 minutes, washed a second time with an additional 10mL CMA, and then resuspended in the appropriate volume of CMA, and then split equally into two tubes. To one of the tubes, the appropriate volume of a 10mM stock of mevalonate was added to bring to final concentration to 50μM mevalonate. Parasites were seeded in a 96-well plate at 0.5% starting parasitemia, 2% hematocrit, and at a total volume of 250μL per well in quadruplicate. Additionally, 150μL of the appropriate media was replaced in each well on days 1, 2, and 3. Parasite samples were collected every 24 hours for four days, and the parasitemia was counted via SYBR green staining and flow-cytometry as outlined below.

Flow cytometry for parasite growth curve determination

Growth curves were generated by staining parasites with SYBR Green and counting parasitemia via flow cytometry. In order to setup the growth curve, the parasitemia of the starting culture was determined via Giemsa stain. Based on the determined parasitemia the culture was used to seed a 96-well flat bottom cell culture plate (Corning) at a 0.5% starting parasitemia and 2% hematocrit, at a total volume of 250μL in quadruplicate. In order to minimize evaporation and edge effects, the surrounding wells were filled with 250μL of

1mM EDTA. Plates were incubated in chambers gassed with 94% N_2, 3% O_2, 3% CO_2 for 1 minute and 15 seconds, and incubated at 37°C.

Parasite samples were collected immediately after seeding and analyzed via flow cytometry to verify the starting parasitemia and then collected every 24 hours thereafter. Samples collected on days 1-3 were diluted 1:10 in phosphate-buffered saline (PBS) and stored in a 96-well plate (Corning) at 4°C. We have previously verified that storage under these conditions and subsequent staining with SYBR Green reflects accurate parasitemia values.

On day 4 parasites were stained with SYBR Green by transferring 1μL of parasite culture, or 10μL of the 1:10 dilutions (the day 1-3 samples), to a 96-well plate containing 100μL of 1x SYBR Green (Invitrogen) in PBS. The samples were then incubated for 30 minutes on a platform Titramax 101 shaker (Heidolph) at 950rpm while protected from light. Post-incubation, 150μL of PBS was added to each well to dilute unbound SYBR Green dye. A control consisting of uninfected RBCs was also prepared in parallel and treated in the same manner as listed above.

Samples were analyzed with an Attune Nxt Flow Cytometer (Thermo Fisher Scientific). With a 50μL acquisition volume, 250μL total sample volume, and a running speed of 25μL/minute with 10,000 total events were collected within the R2 gate.

For flow cytometer gating, the R1 gate used forward-scatter area by side-scatter area to identify total RBCs from the sample. The R2 gate used forward-scatter height to identify single cells, and the R3 gate was used to measure parasitemia using fluorescence from the SYBR Green staining of parasite DNA (ratio of SYBR Green positive cells to total cells).

Confirmation of apicoplast loss

The loss of the apicoplast was confirmed via PCR with primers specific for a gene within the nuclear (Lactate Dehydrogenase), apicoplast (SufB), and mitochondrial (Cox1) genomes (**Table 2-1**). Failure to amplify a gene from the apicoplast genome, while amplifying genes from the nuclear and mitochondrial genomes would indicate loss of the organelle (30). To collect samples for PCR, approximately 100μL of a resuspended parasite culture at ~5-10% parasitemia was placed in a 90°C heat block for 2 minutes, and then frozen at -20°C. For the PCR reaction, 1μL of the parasite sample was added to reactions with a 50μL total volume. Reactions were conducted using a Veriti 96 well thermal cycler (Applied Biosystems) and Phusion High-Fidelity DNA polymerase (Thermo Fisher Scientific). PCR products were separated by size on a 1.5% agarose gel stained with ethidium bromide. The parental PfMev line was always used as a positive control for apicoplast detection.

The PCR reaction volumes were as follows:

Water 34.5μL
5x Phusion HF buffer 10μL
Forward primer (10 μM)1.5μL
Reverse primer (10 μM) 1.5μL
dNTPs (10mM) 1μL
Phusion polymerase 0.5μL
parasite lysate 1μL
Total volume 50μL

The PCR program was as follows:

95°C 3.5 minutes
95°C 30 seconds
63°C 30 seconds
72°C 1 minute
72°C 4 minutes
4°C ∞

(steps 2-4 were repeated 35 times)

Live cell epifluorescent microscopy

For sample preparation, 100µL of parasite culture with a hematocrit of 1% and a parasitemia between 8-10% was obtained. Parasites were stained with 30nM mitoTracker CMX-Ros (Invitrogen) and 1µg/mL 4', 6-diamidino-2-phenylindole (DAPI), and incubated for 30 minutes at 37°C. Cells were then pelleted via mini-centrifuge (Fischer Scientific) for 10 seconds, and the media was aspirated and the cells were resuspended in 100µL of CMA media and incubated for 5 minutes at 37°C. This was done three times to wash the cells, with the cells being resuspended in 20µL of CMA and then pipetted onto slides and sealed with wax (2 parts paraffin, 1 part Vaseline) for observation on a Zeiss AxioImager M2 microscope. A series of images spanning 5µm were acquired with 0.2µm spacing and images were deconvolved with VOLOCITY software (PerkinElmer) to report a single combined z - stack image.

PfMev parasite immunofluorescence (IFA) microscopy

For analysis of PfMev parasites via IFA, slides were first prepared by creating 6 wells on a glass slide using a Super Pap Pen Liquid Blocker (Ted Pella, Inc.), followed by the addition of 30µL of 1:10 .1% poly-L-Lysine solution (Sigma-Aldrich) in water to each well, and allowed to dry for 30 minutes. Next, 500µL of the PfMev parasite line at a hematocrit of 2% and a parasitemia between ~5-10% was obtained and spun down at 500G for 1 minute, and resuspended in 300µL of a 1:1 solution of 4% PFA, .0075% GA, PBS to fix the cells. 40µL of the cells were then immediately pipetted into each well and incubated at room temperature for 30 minutes. Cells were permeabilized by aspirating the fixation solution and washing with 45µL 1x PBS. This solution was then aspirated and 1% Triton X-100 was

added, with the cells incubated at room temperature for 10 minutes. This solution was then aspirated and then cells were washed again with 45µL 1x PBS. This solution was aspirated, and then a solution of .1g/L $NaBH_4$ in 1x PBS was added to the cells, after which they were incubated at room temperature for 10 minutes to reduce the cells. This solution was then aspirated and the cells were washed with 45µL 1x PBS. This solution was then aspirated and then a solution of 3% (30g/L) BSA in 1x PBS was added as a blocking agent, and then allowed to incubate at room temperature for 2 hours. This solution was then aspirated, and the cells were washed with 45µL 1x PBS. That solution was aspirated and a 40µL solution containing the primary antibodies was added. This solution contained 500µL 3% BSA in 1x PBS with 1µL pAB anti-ACP (JHR72 rat, pool) and 1µL pAB anti-GFP (JH915 rabbit, 3g/L). Slides were then incubated at 4°C overnight (~14-16 hours). This solution was then aspirated and washed with 45µL 1x PBS 3 times, and then washed once with 3% (30g/L) BSA in 1x PBS. This solution was then aspirated and a 40µL solution containing the secondary antibodies was added. This solution contained 1mL 3% BSA in 1x PBS with 1µL anti-Rabbit Alexa 594 and 3µL anti-rat Alexa488. After this solution was added the slides were incubated at room temperature in the dark, protected from light for 2 hours. This solution was then aspirated, and the then washed with 45µL 1x PBS 3 times. Slides were then sealed with Gold DAPI antifade (Life Technologies) under a coverslip sealed with nail polish. Slides were then viewed using a Zeiss AxioImager M2 microscope. A series of images spanning 5µm were acquired with 0.2µm spacing and images were deconvolved with VOLOCITY software (PerkinElmer) to report a single combined z -stack image.

[2-^{13}C]-mevalonate parasite labeling and detection via LC-MS

A PfMev culture was synchronized through magnetic purification (55) and immediately used to seed two identical 20mL cultures at 2% hematocrit and ~2% parasitemia. Parasite cultures were cultured in media containing 25μM fosmidomycin (50x IC_{50}) and supplemented with either 50μM [^{12}C]-mevalonate (Sigma-Aldrich, cat. #M4667) or [2-^{13}C]-mevalonate (Sigma-Aldrich, cat. #486604), and incubated for 48 hours, equivalent to one parasite lifecycle, to allow for incorporation of the label. After 48 hours, the parasitemia had reached ~9% and the parasites were isolated via magnetic purification, resuspended in 12mL CMA, and quantified using a hemocytometer, with ~8x10^7 parasites purified from each culture.

Metabolite extraction was conducted following a previously established protocol (56). Briefly, the isolated parasites were pelleted via centrifugation using a Megafuge 1.0R (Heraeus) at 4,000rpm for 5 minutes at room temperature, followed by the aspiration of the supernatant. The parasite pellet was then snap frozen on dry ice, and stored at -80°C before extraction. For metabolite extraction, the pellet was thawed on ice and 600μL of 100% methanol cooled on dry ice was added, and then incubated on dry ice for 15 minutes with intermittent vortexing. Lysed parasites were then centrifuged in a Biofuge pico microcentrifuge (Heraeus) at 13,000rpm for 5 minutes at 4°C and the supernatant was transferred to a separate tube and stored on dry ice. To the original tube containing the pellet, 600μL of ice cold 80% methanol/20% H_2O was added, and the pellet was broken up by pipetting up and down with intermittent vortexing. The tube was then tip sonicated (Vibra-Cell, Sonics & Materials Inc.) on ice for 15 seconds with 0.5 second on/off cycles at 20% amplitude. This was done twice, with a 30 second pause between sonication cycles. Insoluble material was then pelleted by centrifugation at 13,000rpm for 5 minutes at 4°C. The resulting supernatant was then pooled with the 600uL 100% methanol extraction, mixed, and then

dried at room temperature under nitrogen gas until fully evaporated and stored at -80°C. On the day of analysis, dried samples were resuspended in 100µL of ice cold solvent A (2mM ammonium phosphate and 2mM hexylamine in H_2O) and then incubated on ice for ~1.5 hours with intermittent vortexing. The sample was then centrifuged at 13,000rpm for 5 minutes at 4°C, and the supernatant was transferred to a fresh tube for metabolite analysis.

Metabolites were detected using a Dionex Ultimate 3000 uHPLC system coupled to a TSQ Vantage Triple Stage Quadrupole (QQQ) mass spectrometer (Thermo Fisher Scientific) using a Hypersil-GOLD C18 column (3µm, 100mm x 1mm, Thermo Fischer Scientific) at a flow rate of 0.4mL/min. Solvent A was 2mM ammonium phosphate and 2mM hexylamine in H_2O and Solvent B was 100% acetonitrile. The following gradient was used: 0-2 minutes at 9% B, 2-15.5 minutes linearly increasing from 9% to 100% B, 15.6-17.6 minutes at 100% B, and 17.7-31.7 minutes at 9% B.

In order to optimize detection of IPP, we started by analyzing a chemical standard. For this we injected 10µL of 5µM IPP (Sigma) in 90% mobile phase A, and 10% mobile phase B (100% acetonitrile). The detection method relied on selected reaction monitoring (SRM) in negative ion mode to monitor the transition (m/z 244.9 → 79.0), in which the parent ion (244.9m/z) is selected for and fragmented, and the daughter ion fragment is detected (79.0m/z), indicative of the loss and detection of phosphate from IPP (36). The retention time of the IPP standard was found to be ~11.7 seconds. For sample analysis, 40µL of sample was injected. In order to detect IPP we monitored the above-mentioned transition (m/z 244.9 → 79.0). However, parasites supplemented with [^{13}C]-mevalonate should produce [^{13}C]-labeled IPP, shifting the molecular mass by one Dalton to (m/z) 245.9. Thus, for samples extracted from parasite cultures supplemented with [^{12}C]-mevalonate or [^{13}C]-mevalonate both transitions were monitored (m/z 244.9 → 79.0) and (m/z 245.9 →

79.0). The same SRM technique was used to look for downstream isoprenoid products, specifically farnesyl pyrophosphate (FPP). Using previously published methods, we monitored the transition (m/z 381.0 → 79) for unlabeled FPP (36). Since FPP is formed from three isoprenoid precursors, the mass of labeled FPP should be shifted by three Daltons to (m/z) 384.0. Thus, we also monitored both transitions (m/z 381.0 → 79) and (m/z 384.0 → 79) in the labeled and unlabeled samples.

Generation of the Cas9 gene deletion construct

Cas9 mediated gene deletion constructs were generated using modified versions of the pUF1-Cas9 and pL6-eGFP plasmids, which were generously provided by Dr. Jose-Juan Lopez-Rubio, approximately following methods previously described (38) [12]. The pL6-eGFP plasmid was modified to contain ligation independent cloning (LIC) sites. The 3' LIC was modified to contain a NgoMIV restriction site, while the 5' LIC was modified to contain a NotI restriction site. Additionally, the plasmid backbone was modified to remove a BsaI site within the AmpR *E. coli* drug resistance cassette, and the BtgZI restriction sites were replaced with BsaI sites. The resulting plasmid was renamed pL8. The pUF1-Cas9 plasmid was modified as well, to generate a plasmid that was are calling pCasG.

To generate the DXPR deletion construct, homology arms of ~300-600bp for DXPR were amplified using the homology arm (HA) 1 and 2 forward and reverse primers (**Table 2-1**) from blood-stage *P. falciparum* NF54-attb gDNA. HA1 and HA2 primers were designed to contain ~15bp overhangs for insertion into the cut pL8 plasmid using In-Fusion (Clontech) cloning methods. The pL8 plasmid containing the hDHFR drug resistance cassette for selection and contains flanking endonuclease sites for insertion of the homology arms. The pL8 plasmid was digested with NotI for insertion of HA1, and with NgoMIV for

HA2. Digests with either endonuclease were also treated with recombinant shrimp alkaline phosphatase (rSAP) and then ethanol precipitated before insertion of the homology arms. The pL8 plasmid also contains a guide RNA (gRNA) expression cassette. For insertion of the gRNA sequence the plasmid was digested with BsaI and also treated with rSAP, and then ethanol precipitated. Guide RNA sequences were synthesized as oligos (**Table 2-2**), annealed, and inserted into the pL8 via In-Fusion cloning.

P. falciparum transfections for gene deletion

Transfections were conducted as previously described (53, 54). Briefly, 400µL of red blood cells were washed with 5mL of CytoMix and resuspended in 400µL of CytoMix. The red blood cells were then electroporated with 75µg each of the pUF1-Cas9 and pL8-DXPR knock out plasmids (38). The electroporated RBCs were then mixed with ~2.5mL PfMev parasites synchronized as schizonts at 1% hematocrit and ~10% parasitemia and given 10mL CMA with 50µM mevalonate. After 48 hours, transfectants were selected with 0.75µM DSM1, 2.5nM WR99210, and 50µM mevalonate for seven days. After seven days, the parasites were switched to media containing only 50µM mevalonate. Infected red blood cells (iRBC) were first observed between 17 and 30 days after beginning drug selection. Once parasites were observed, the medium was switched to 2.5nM WR99210 and 50µM mevalonate.

Confirmation of knockout genotype

In order to screen for integration and successful gene knockout, in addition to the presence of any contaminating residual wild type parasites, a set of six primers were used: 5'F, 3'R, pL8 HA1 R, pL8 HA2F, 5' WT R and 3' WT F (**Table 2-1**). These primers were

designed to screen for integration and gene disruption at the 5' and 3' ends (Δ5' and Δ3') in addition to 5' and 3' regions of the WT gene (5' and 3'). The same reactions were also performed on the parental PfMev line concurrently as a control. Samples for PCR were collected when the parasitemia reached been 5-10%, as determined by Giemsa stain. Approximately 100μL of a resuspended parasite culture was placed in a heat block at 90°C for 2 minutes and stored at -20°C. For the PCR reaction, 1μL of the parasite sample was added to reactions with a 50μL total volume. Reactions were conducted using a Veriti 96 well thermal cycler (Applied Biosystems) and Phusion High-Fidelity DNA polymerase (Thermo Fisher Scientific). PCR products were separated on a 1.5% agarose gel stained with ethidium bromide for visualization.

The PCR reaction volumes were as follows:

Water 34.5μL
5x Phusion HF buffer 10μL
Forward primer (10 μM)1.5μL
Reverse primer (10 μM) 1.5μL
dNTPs (10mM) 1μL
Phusion polymerase 0.5μL
parasite lysate 1μL
Total volume 50μL

The PCR program was as follows:

95°C 3.5 minutes
95°C 30 seconds
62°C 1 minute
62°C 4 minutes
4°C ∞

(steps 2 and 3 were repeated 35 times)

A diagram of the primer combinations and DNA agarose gel used to screen for gene deletion are diagrammed below.

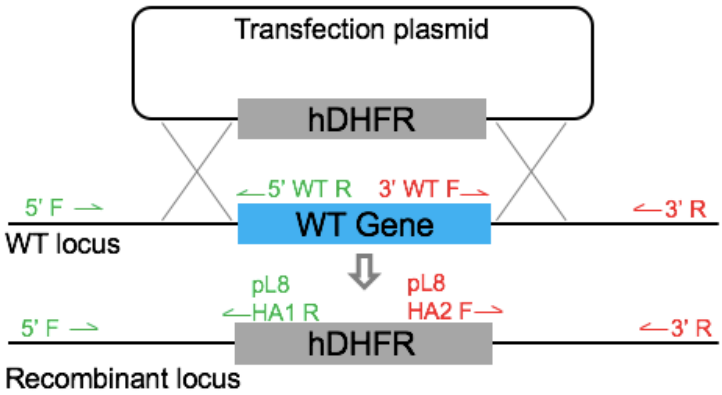

Lane	Primer Combination	Parasite Line
1. Δ5'	5'F, pL8 HA1R	Gene deletion line
2. Δ3'	pL8 HA2 F, 3'R	
3. 5' WT	5'F, 5' WT R	
4. 3' WT	3' WT F, 3'R	
5. Δ5'	5'F, pL8 HA1R	PfMev parental line
6. Δ3'	pL8 HA2 F, 3'R	
7. 5' WT	5'F, 5' WT R	
8. 3' WT	3' WT F, 3'R	

FIGURES

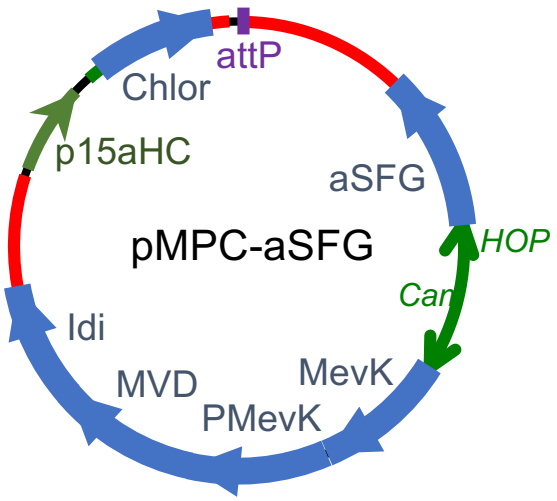

Figure 2-1 Plasmid pMPC-aSFG used to generate the PfMev parasite line

NF54-attb parasites were transfected with the pINT (integrase) and pMPC-aSFG plasmids, in order to integrate the pMPC-aSFG plasmid into the attb locus of the NF54 attb line. Parasites possessing the pMPC-aSFG plasmid were selected with fosmidomycin in the presence of mevalonate. Expression of the mevalonate pathway and apicoplast SFG (api-SFG) are driven by a bidirectional calmodulin promoter.

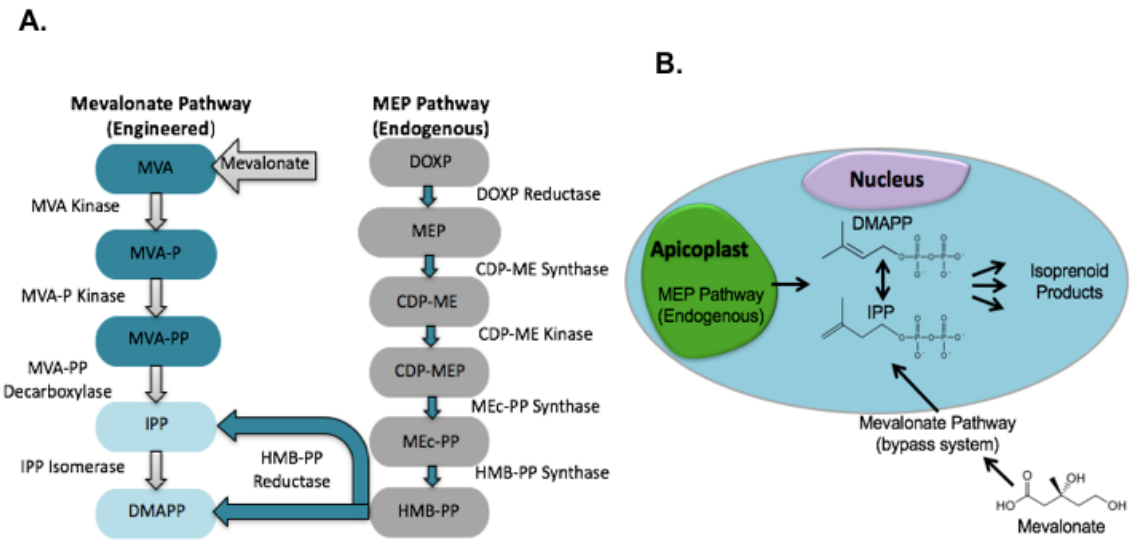

Figure 2-2 Diagram of the endogenous (MEP) and engineered (Mev) isoprenoid pathways

A.) *Plasmodium* parasites contain the endogenous MEP isoprenoid precursor pathway within the apicoplast. For the MEP pathway pyruvate and glyceraldehyde 3-phosphate (G3P) are joined together by DOXP synthase (DXS) to form 1-Deoxy-D-xylulose 5-phosphate (DOXP). DOXP is then converted by DOXP reductoisomerase (DXPR) to form 2-C-methylerythritol 4-phosphate (MEP), which is in turn converted by 2-C-methyl-D-erythritol 4-phosphate cytidylyltransferase (CDP-ME Synthase) to form 4-diphosphocytidyl-2-C-methylerythritol (CDP-ME). CDP-ME is then converted by 4-diphosphocytidyl-2-C-methyl-D-erythritol kinase (CDP-ME kinase) to form 4-diphosphocytidyl-2-C-methyl-D-erythritol 2-phosphate (CDP-MEP). CDP-MEP is converted by 2-C-methyl-D-erythritol 2,4-cyclodiphosphate synthase (MEc-PP Synthase) to form 2-C-methyl-D-erythritol 2,4-cyclodiphosphate (MEc-PP). MEc-PP is then converted by HMB-PP synthase to form (E)-4-Hydroxy-3-methyl-but-2-enyl pyrophosphate (HMB-PP). HMB-PP is then converted by

HMB-PP reductase to form Isopentenyl pyrophosphate (IPP) and Dimethylallyl pyrophosphate (DMAPP).

PfMev parasites were engineered to convert mevalonate into IPP/DMAPP through the expression of four enzymes from the mevalonate pathway. In this engineered pathway, mevalonate is converted by mevalonate kinase (MVA kinase) to form mevalonate-5-kinase (MVA-P). MVA-P is then converted by phosphomevalonate kinase (MVA-P kinase) to form mevalonate-5-pyrophosphate (MVA-PP). MVA-PP is then converted by mevalonate-5-pyrophosphate decarboxylase (MVA-PP decarboxylase) to form IPP, which can also be converted into DMAPP by isopentenyl pyrophosphate isomerase (IPP isomerase).

B.) Diagram of the parasite cell showing that the endogenous MEP pathway is localized with the apicoplast organelle of the parasite, with IPP and DMAPP presumably being exported out of the organelle. We engineered the PfMev parasites to express four enzymes from the MVA pathway, which are expressed in the cytosol of the parasite and metabolize exogenous mevalonate into IPP and DMAPP.

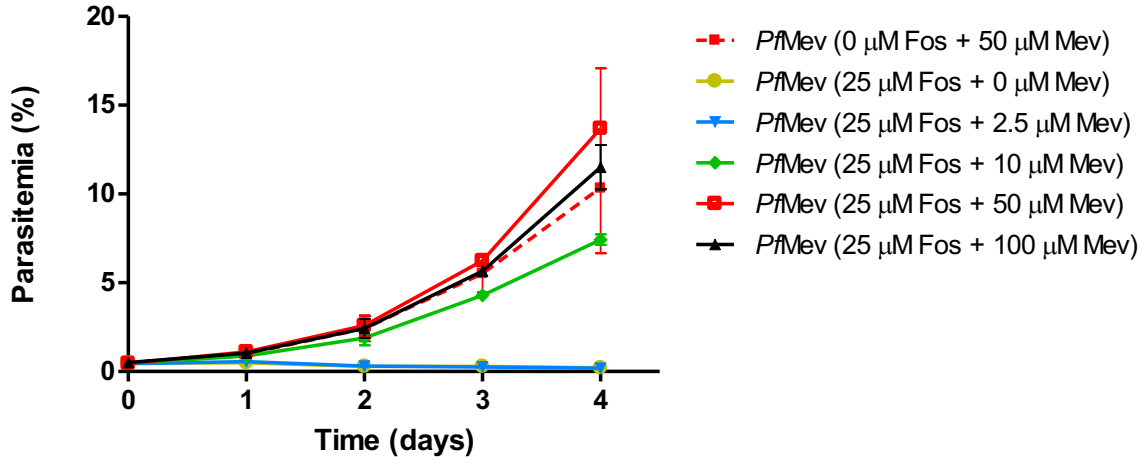

Figure 2-3 Growth of PfMev parasites treated with fosmidomycin and mevalonate

PfMev parasites were treated with 25μM fosmidomycin (50x IC_{50}), and supplemented with 100μM, 50μM, 25μM, 10μM, or 0μM mevalonate, with growth compared to an untreated control. PfMev parasites grew to wild-type levels in the presence of a typically lethal concentration of fosmidomycin with as little as 10μM mevalonate indicating usage of the engineered mevalonate pathway for the generation of essential isoprenoid precursors. PfMev parasites treated with 25μM fosmidomycin not supplemented with mevalonate failed to grow. Data from duplicate experiments conducted in quadruplicate are shown with error bars representing the standard error of the mean (SEM).

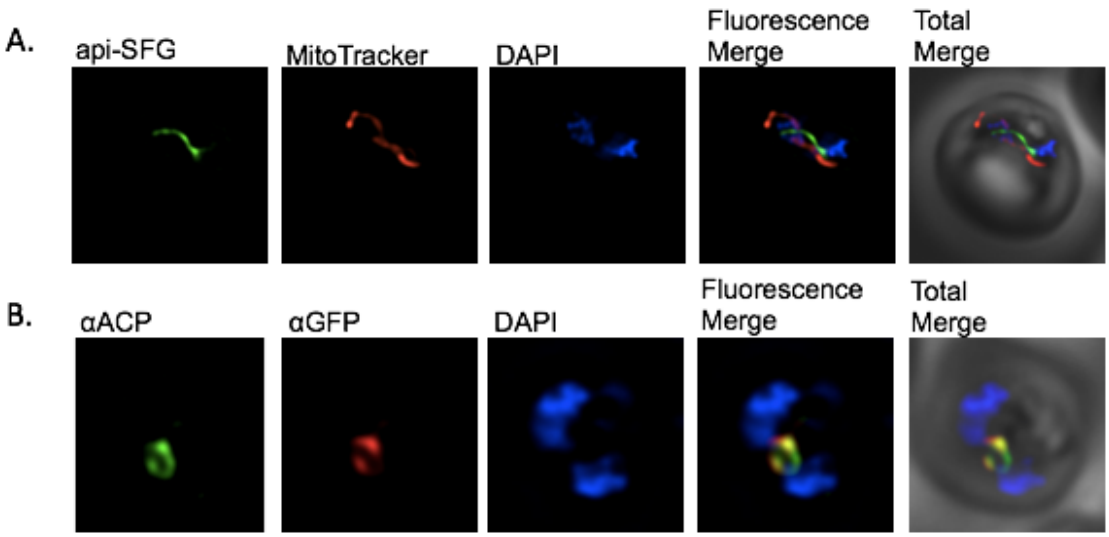

Figure 2-4 Fluorescent labeling of the apicoplast organelle in PfMev parasites and confirmation via co-localization

Figure 2-4 Fluorescent labeling of the apicoplast organelle **in PfMev parasites and confirmation via co-localization**

A.) Live fluorescence microscopy of the PfMev line expressing the signal sequence and transit peptide from ACP fused to SFG (api-SFG, green), the mitochondria was stained with MitoTracker (red), and nuclear DNA was stained with DAPI (blue).

B.) Immunofluorescence co-localization of api-SFG with the apicoplast marker ACP, with α-ACP (green), α-GFP (red), with nuclear DNA stained with DAPI (blue) in fixed PfMev parasites.

Images are 10 microns long by 10 microns wide.

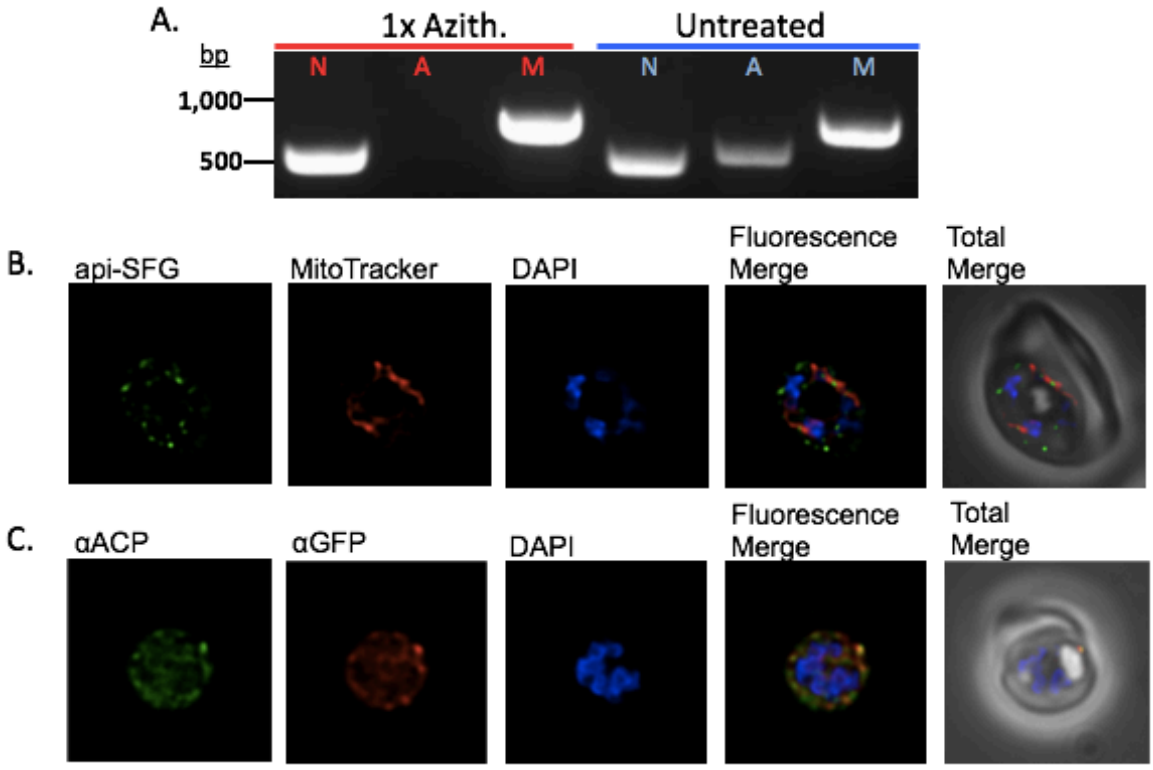

Figure 2-5 Generation and characterization of an apicoplast-minus PfMev parasite line

A.) Attempted detection of nuclear, mitochondrial, and apicoplast genomes via PCR amplification of LDH (nuclear), SufB (apicoplast), and Cox1 (mitochondrial) genes from PfMev parasites treated with 100nM azithromycin and 50μM mevalonate for one week (red), in addition to an untreated control (blue). Failure to amplify SufB in PfMev parasites treated with azithromycin/mevalonate indicates loss of the apicoplast organelle.

B.) Live fluorescence microscopy of PfMev parasites after treatment with 100nM azithromycin and 50μM mevalonate for one week, showing a disrupted organelle phenotype, with multiple discrete vesicles instead of a single intact organelle structure. The apicoplast is labeled with the api-SFG protein (green), the mitochondrion is stained with MitoTracker (red), and nuclear DNA is stained with DAPI (blue).

C.) Immunofluorescence co-localization of api-SFG with the apicoplast marker ACP, with α-GFP (red), α-ACP (green), with nuclear DNA stained with DAPI (blue) in fixed apicoplast minus PfMev parasites.

Images are 10 microns long by 10 microns wide.

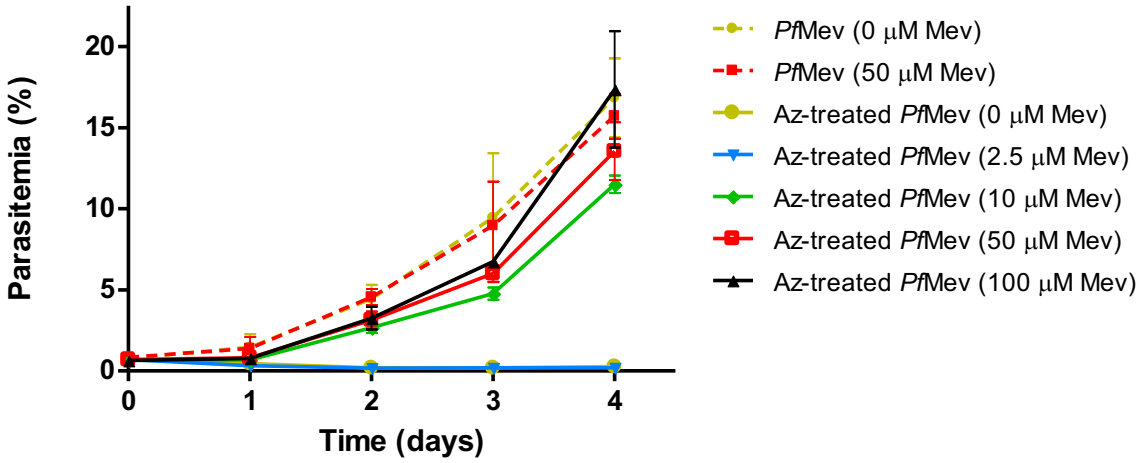

Figure 2-6 Mevalonate titration of apicoplast minus PfMev parasites

Growth curve of apicoplast minus PfMev parasites grown in the presence of 100μM, 50μM, 10μM, 2.5μM, and 0μM mevalonate. The growth of untreated (apicoplast positive) PfMev parasites was also measured in the presence of 50μM or 0μM mevalonate as a control. Supplementation with as little as 10μM mevalonate restored the growth of apicoplast negative parasites to near wild-type levels. Data from duplicate experiments conducted in quadruplicate are shown with error bars representing the standard error of the mean (SEM). Images are 10 microns long by 10 microns wide.

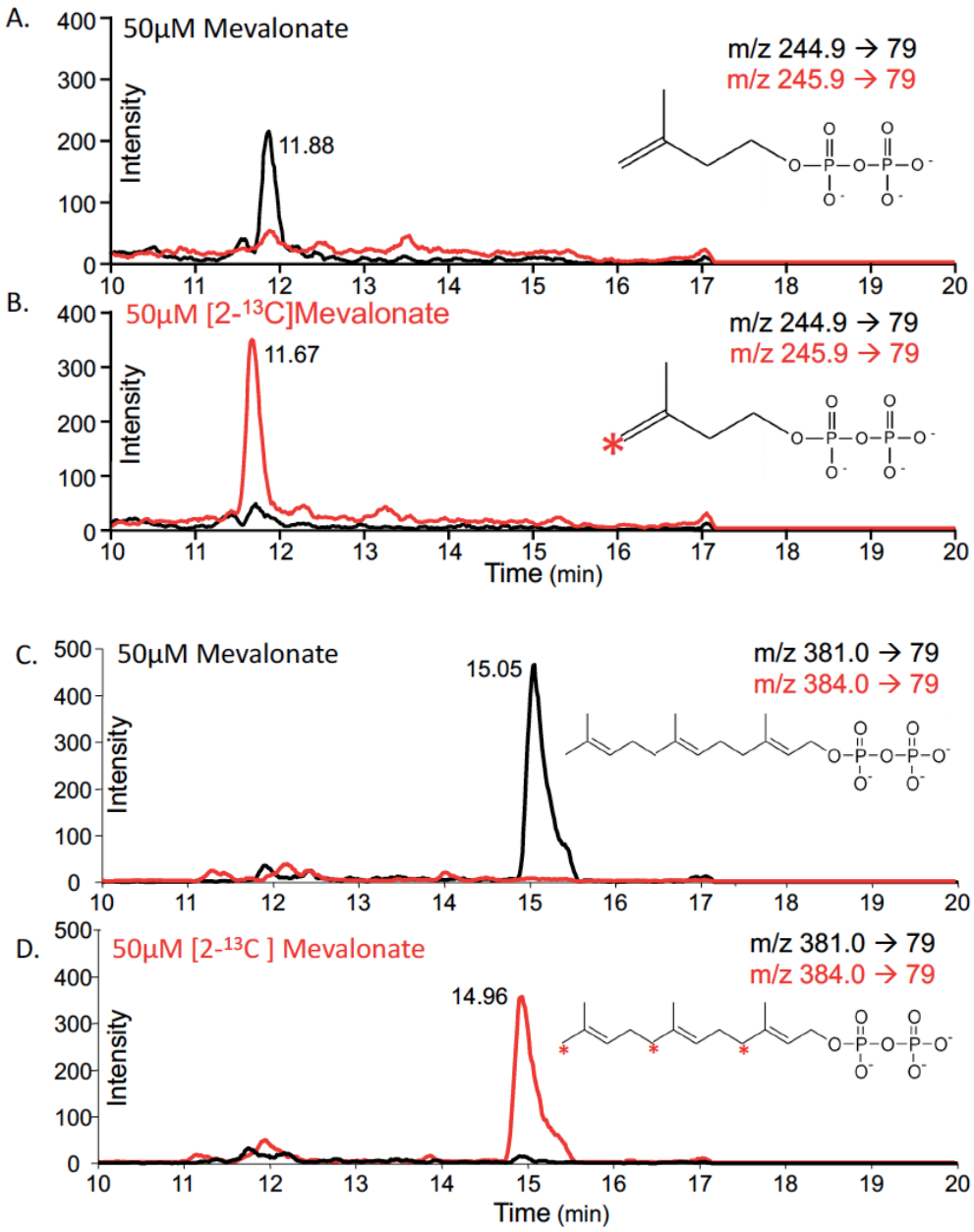

Figure 2-7 Metabolic labeling of PfMev parasites with [2-^{13}C]-mevalonate

PfMev parasite cultures were treated with 25µM fosmidomycin (50x IC_{50}) and supplemented with either 50µM [^{12}C]-mevalonate or [2-^{13}C]-mevalonate for 48 hours. Metabolites were extracted and analyzed via targeted liquid-chromatography mass spectrometry (LC-MS). The red asterisks on the biomolecules shown denotes the position of the labeled carbons.

A.) Detection of IPP/DMAPP (black) in parasites treated with 50μM mevalonate and 25μM fosmidomycin, with attempted detection of mass-shifted IPP/DMAPP (red).

B.) Detection of mass-shifted IPP/DMAPP (red) in parasites treated with 50μM [2-^{13}C]-mevalonate and 25μM fosmidomycin, with attempted detection of IPP/DMAPP (black).

C.) Detection of FPP (black) in parasites treated with 50μM mevalonate and 25μM fosmidomycin, with attempted detection of mass-shifted FPP (red).

D.) Detection of mass-shifted FPP (red) in parasites treated with 50μM [2-^{13}C]-mevalonate and 25μM fosmidomycin, with attempted detection of FPP (black).

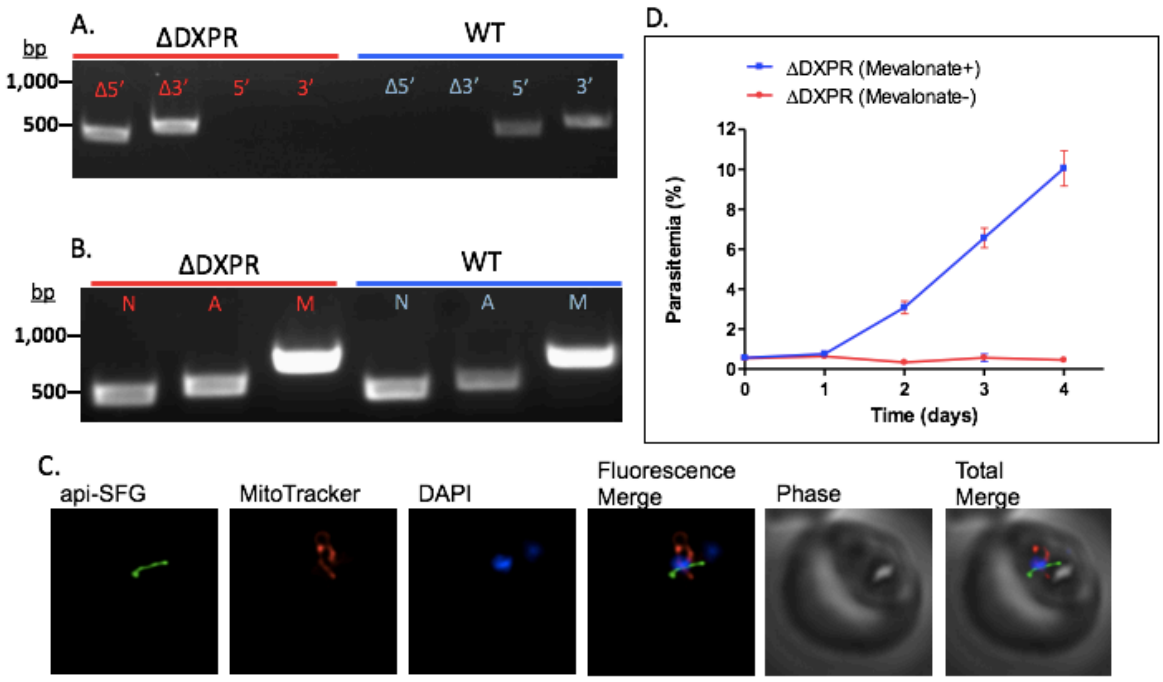

Figure 2-8 Deletion of an apicoplast essential gene using Cas9 mediated gene editing

A.) Confirmation of DXPR gene deletion via PCR showing the expected 5' and 3' integration of the selection cassette. Parasites were also screened for the unmodified 5' and 3' loci to detect if there were any residual wild-type parasites (red) and compared to a control (blue).

B.) PfMev ΔDXPR parasites were screened for the presence of the nuclear (LDH), apicoplast (SufB), and mitochondrial (Cox1) genomes via PCR (red), and compared to a control (blue). Both lines showed the presence of nuclear, apicoplast and mitochondrial genomes, indicating deletion of DXPR does not result in organelle loss.

C.) Live epifluorescent microscopy of the PfMev ΔDXPR parasites showing the presence of an intact organelle. This parasite line is expressing api-SFG (green), and is also stained with MitoTracker (red), and DAPI (blue). Images are 10 microns long by 10 microns wide.

D.) PfMev ΔDXPR parasites grown in the presence of 50μM mevalonate (blue) or no mevalonate (red). The reliance of PfMev ΔDXPR parasites on mevalonate for growth indicates that DXPR is essential for the blood-stage survival of the parasite.

Table 2-1 Primer sequences used for amplifying DXPR homology arms

Primer Name	Primer Sequence
DXPR HA1 F	GCCACGAGCGGCCTCCATTGAAAGAAGAAAAAATAACG
DXPR HA1 R	AAGCGCAGCGGCCCCTTCATCACCACACAATATTATAGG
DXPR HA2 F	CGACAGACGCCGGGGTTATAGAAACCCATTTTTTATTTGA
DXPR HA2 R	GGCCACCAGCCGGGTATATATCGGTAGCTTTATCTTTGGC

Table 2-2 Guide RNA (gRNA) oligo sequences

Oligo Name	Oligo Sequence
DXPR gRNA F	TAAGTATATAATATTTATGATGAATAAAGGTTTAGGTTTTAGAGCTAGAA
DXPR gRNA R	TTCTAGCTCTAAAACCTAAACCTTTATTCATCATAAATATTATATACTTA

Table 2-3 Primer sequences used for DXPR KO confirmation

Primer Name	Primer Sequence
pl8insHA1F	GCTATTTAGGTGACACTATAGAATACTCAAGC
pl8insHA2R	AATCTAGAATTCGACAGACGCCGG
DXPR 5' F	CTATTAATGATTTAGTAATAAATAATACATCAAAATGTG
DXPR 3'R	GTATTTTATTTTTTTTTGTACTATGAAGAATTATGTTTG
DXPR 5' WT R	CCTTGAAAAGAATCAATACCAATAACTATTTTATC
DXPR 3' WT F	GGAAAATGGGTAAGAAAATAACTATAGATTCTG

Table 2-4 Primer sequences used for determining apicoplast presence

Primer Name	Primer Sequence
Lactate Dehydrogenase (LDH) F	GGAGATGTAGTTTTGTTCGATATTG
Lactate Dehydrogenase (LDH) R	CTTGTAAAGGGATACCACCTACAG
SufB F	CATGTAGCTATAGTAGAAATAATAGTAAAAGATTATGG
SufB R	GACTCTGAAATACTTAAACCACGTTGC
Cox1 F	CTTCATCTTTAAGAATAATTGCACAAGAAAATGTAAATC
Cox1 R	GGAAGCTTAGTATGGGTACATCATATGTAC

REFERENCES

1. Gatton ML , Martin LB, Cheng Q. 2004. Evolution of resistance to sulfadoxine-pyrimethamine in *Plasmodium falciparum*. Antimicrob Agents Chemother 48:2116–23.

2. Price RN, Uhlemann A-C, Brockman A, McGready R, Ashley E, Phaipun L, Patel R, Laing K, Looareesuwan S, White NJ, Nosten F, Krishna S. 2004. Mefloquine resistance in *Plasmodium falciparum* and increased pfmdr1 gene copy number. Lancet (London, England) 364:438–447.

3. Jelinek T, Schelbert P, Löscher T, Eichenlaub D. 1995. Quinine resistant *falciparum* malaria acquired in east Africa. Trop Med Parasitol 46:38–40.

4. Cui L, Mharakurwa S, Ndiaye D, Rathod PK, Rosenthal PJ. 2015. Antimalarial Drug Resistance: Literature Review and Activities and Findings of the ICEMR Network. Am J Trop Med Hyg 93:57–68.

5. Ljolje D, Dimbu PR, Kelley J, Goldman I, Nace D, Macaia A, Halsey ES, Ringwald P, Fortes F, Udhayakumar V, Talundzic E, Lucchi NW, Plucinski MM. 2018. Prevalence of molecular markers of artemisinin and lumefantrine resistance among patients with uncomplicated *Plasmodium falciparum* malaria in three provinces in Angola, 2015. Malar J 17:84.

6. Huang F, Takala-Harrison S, Jacob CG, Liu H, Sun X, Yang H, Nyunt MM, Adams M, Zhou S, Xia Z, Ringwald P, Bustos MD, Tang L, Plowe C V. 2015. A Single Mutation in K13 Predominates in Southern China and Is Associated With Delayed Clearance of *Plasmodium falciparum* Following Artemisinin Treatment. J Infect Dis 212:1629–1635.

7. Cheng Q, Kyle DE, Gatton ML . 2012. Artemisinin resistance in *Plasmodium falciparum*: A process linked to dormancy? Int J Parasitol Drugs drug Resist 2:249–255.

8. Cibulskis RE, Alonso P, Aponte J, Aregawi M, Barrette A, Bergeron L, Fergus CA, Knox T, Lynch M, Patouillard E, Schwarte S, Stewart S, Williams R. 2016. Malaria: Global progress 2000 – 2015 and future challenges. Infect Dis Poverty 5:61.

9. Janouskovec J, Horák A, Oborník M, Lukes J, Keeling JP. 2010. A common red algal origin of the apicomplexan, dinoflagellate, and heterokont plastids. Proc Natl Acad Sci U S A 107:10949–10954.

10. Goodman CD, McFadden GI. 2013. Targeting apicoplasts in malaria parasites. Expert Opin Ther Targets 17:167–77.

11. Mukherjee A, Sadhukhan CG. 2016. Anti-malarial Drug Design by Targeting Apicoplasts: New Perspectives. J pharmacopuncture 19:7–15.

12. Ralph SA, van Dooren GG, Waller RF, Crawford MJ, Fraunholz MJ, Foth BJ, Tonkin CJ, Roos DS, McFadden GI. 2004. Tropical infectious diseases: metabolic

maps and functions of the *Plasmodium falciparum* apicoplast. Nat Rev Microbiol 2:203–16.

13. Foth JB, Ralph AS, Tonkin JC, Struck SN, Fraunholz M, Roos SD, Cowman FA, McFadden IG. 2003. Dissecting apicoplast targeting in the malaria parasite *Plasmodium falciparum*. Science 299:705–708.

14. Zuegge J, Ralph S, Schmuker M, McFadden GI, Schneider G. 2001. Deciphering apicoplast targeting signals – feature extraction from nuclear-encoded precursors of *Plasmodium falciparum* apicoplast proteins. Gene 280:19–26.

15. Cilingir G, Lau AOT, Broschat SL. 2013. ApicoAMP: The first computational model for identifying apicoplast-targeted transmembrane proteins in Apicomplexa. J Microbiol Methods 95:313–319.

16. Cilingir G, Broschat SL, Lau AOT. 2012. ApicoAP: The First Computational Model for Identifying Apicoplast-Targeted Proteins in Multiple Species of Apicomplexa. PLoS One 7:e36598.

17. Yeh E, DeRisi JL. 2011. Chemical rescue of malaria parasites lacking an apicoplast defines organelle function in blood-stage *Plasmodium falciparum*. PLoS Biol 9.

18. Amberg-Johnson K, Hari BS, Ganesan MS, Lorenzi AH, Sauer TR, Niles CJ, Yeh E. 2017. Small molecule inhibition of apicomplexan FtsH1 disrupts plastid biogenesis in human pathogens. Elife 6.

19. Pasaje ACF, Cheung V, Kennedy K, Lim EE, Baell BJ, Griffin WMD, Ralph AS. 2016. Selective inhibition of apicoplast tryptophanyl-tRNA synthetase causes delayed death in *Plasmodium falciparum*. Sci Rep 6.

20. Florentin A, Cobb DW, Fishburn JD, Fierro MA, Striepen B, Correspondence VM. 2017. PfClpC Is an Essential Clp Chaperone Required for Plastid Integrity and Clp Protease Stability in *Plasmodium falciparum*. Cell Rep 21.

21. Gisselberg EJ, Dellibovi-Ragheb AT, Matthews AK, Bosch G, Prigge TS. 2013. The suf iron-sulfur cluster synthesis pathway is required for apicoplast maintenance in malaria parasites. PLoS Pathog 9.

22. Walczak M, Ganesan SM, Niles JC, Yeh E. 2018. ATG8 Is Essential Specifically for an Autophagy-Independent Function in Apicoplast Biogenesis in Blood-Stage Malaria Parasites. MBio 9:e02021-17.

23. Wu W, Herrera Z, Ebert D, Baska K, Cho HS, DeRisi LJ, Yeh E. 2015. A chemical rescue screen identifies a *Plasmodium falciparum* apicoplast inhibitor targeting MEP isoprenoid precursor biosynthesis. Antimicrob Agents Chemother 59:356–364.

24. Martin JVJ, Pitera JD, Withers TS, Newman DJ, Keasling DJ. 2003. Engineering a mevalonate pathway in *Escherichia coli* for production of terpenoids. Nat Biotechnol

21:796–802.

25. Miziorko HM. 2011. Enzymes of the mevalonate pathway of isoprenoid biosynthesis. Arch Biochem Biophys 505:131–143.

26. Odom RA. 2011. Five questions about non-mevalonate isoprenoid biosynthesis. PLoS Pathog 7.

27. Pédelacq J-D, Cabantous S, Tran T, Terwilliger CT, Waldo SG. 2006. Engineering and characterization of a superfolder green fluorescent protein. Nat Biotechnol 24:79–88.

28. Aronson ED, Costantini ML , Snapp LE. 2011. Superfolder GFP is fluorescent in oxidizing environments when targeted via the Sec translocon. Traffic 12:543–548.

29. Waller FR, Reed BM, Cowman FA, McFadden IG. 2000. Protein trafficking to the plastid of *Plasmodium falciparum* is via the secretory pathway. EMBO J 19:1794–1802.

30. Gisselberg JE, Dellibovi-Ragheb T a., Matthews K a., Bosch G, Prigge ST. 2013. The Suf Iron-Sulfur Cluster Synthesis Pathway Is Required for Apicoplast Maintenance in Malaria Parasites. PLoS Pathog 9.

31. Wiley DJ, Merino FE, Krai MP, McLean JK, Tripathi KA, Vega-Rodríguez J, Jacobs-Lorena M, Klemba M, Cassera BM. 2015. Isoprenoid precursor biosynthesis is the essential metabolic role of the apicoplast during gametocytogenesis in *Plasmodium falciparum*. Eukaryot Cell 14:128–139.

32. Hahn FM, Hurlburt AP, Poulter CD. 1999. *Escherichia coli* open reading frame 696 is idi, a nonessential gene encoding isopentenyl diphosphate isomerase. J Bacteriol 181:4499–504.

33. Umeda T, Tanaka N, Kusakabe Y, Nakanishi M, Kitade Y, Nakamura KT. 2011. Molecular basis of fosmidomycin's action on the human malaria parasite *Plasmodium falciparum*. Sci Rep 1:9.

34. Pédelacq J-D, Cabantous S, Tran T, Terwilliger CT, Waldo SG. 2005. Engineering and characterization of a superfolder green fluorescent protein. Nat Biotechnol 24.

35. Zhou B, Xiao JF, Tuli L, Ressom HW. 2012. LC-MS-based metabolomics. Mol Biosyst 8:470–81.

36. Henneman L, van Cruchten GA, Denis WS, Amolins WM, Placzek TA, Gibbs AR, Kulik W, Waterham RH. 2008. Detection of nonsterol isoprenoids by HPLC-MS/MS. Anal Biochem 383:18–24.

37. Xiao JF, Zhou B, Ressom HW. 2012. Metabolite identification and quantitation in LC-MS/MS-based metabolomics. Trends Analyt Chem 32:1–14.

38. Ghorbal M, Gorman M, Macpherson CR, Martins RM, Scherf A, Lopez-Rubio J-J.

2014. Genome editing in the human malaria parasite *Plasmodium falciparum* using the CRISPR-Cas9 system. Nat Biotechnol 32:819–21.

39. Dahl LE, Rosenthal JP. 2007. Multiple antibiotics exert delayed effects against the *Plasmodium falciparum* apicoplast. Antimicrob Agents Chemother 51:3485–3490.

40. Logan DM. 1972. Thermal and pH stability of 2 -isopentenyl pyrophosphate. J Lipid Res 13:137–8.

41. Fidock DA, Wellems TE. 1997. Transformation with human dihydrofolate reductase renders malaria parasites insensitive to WR99210 but does not affect the intrinsic activity of proguanil. Proc Natl Acad Sci U S A 94:10931–6.

42. Mamoun CB, Gluzman IY, Goyard S, Beverley SM, Goldberg DE. 1999. A set of independent selectable markers for transfection of the human malaria parasite *Plasmodium falciparum*. Proc Natl Acad Sci U S A 96:8716–20.

43. Ganesan SM, Morrisey JM, Ke H, Painter HJ, Laroiya K, Phillips MA, Rathod PK, Mather MW, Vaidya AB. 2011. Yeast dihydroorotate dehydrogenase as a new selectable marker for *Plasmodium falciparum* transfection. Mol Biochem Parasitol 177:29–34.

44. Kelly M, Su C-Y, Schaber C, Crowley JR, Hsu F-F, Carlson JR, Odom AR. 2015. Malaria parasites produce volatile mosquito attractants. MBio 6:e00235-15-.

45. Aurrecoechea C, Brestelli J, Brunk BP, Dommer J, Fischer S, Gajria B, Gao X, Gingle A, Grant G, Harb OS, Heiges M, Innamorato F, Iodice J, Kissinger JC, Kraemer E, Li W, Miller JA, Nayak V, Pennington C, Pinney DF, Roos DS, Ross C, Stoeckert CJ, Treatman C, Wang H, Wang H. 2009. PlasmoDB: a functional genomic database for malaria parasites. Nucleic Acids Res 37:D539-43.

46. Tang Y, Meister TR, Walczak M, Pulkoski-Gross M, Hari SB, Sauer RT, Amberg-Johnson K, Yeh E. 2018. A mutagenesis screen for essential plastid biogenesis genes in human malaria parasites. bioRxiv 401570.

47. Zhang M, Wang C, Otto TD, Oberstaller J, Liao X, Adapa SR, Udenze K, Bronner IF, Casandra D, Mayho M, Brown J, Li S, Swanson J, Rayner JC, Jiang RHY, Adams JH. 2018. Uncovering the essential genes of the human malaria parasite *Plasmodium falciparum* by saturation mutagenesis. Science 360:eaap7847.

48. Yu M, Kumar STR, Nkrumah JL, Coppi A, Retzlaff S, Li DC, Kelly JB, Moura AP, Lakshmanan V, Freundlich SJ, Valderramos J-C, Vilcheze C, Siedner M, Tsai H-CJ, Falkard B, Sidhu SAB, Purcell AL, Gratraud P, Kremer L, Waters PA, Schiehser G, Jacobus PD, Janse JC, Ager A, Jacobs RW, Sacchettini CJ, Heussler V, Sinnis P, Fidock AD. 2008. The fatty acid biosynthesis enzyme FabI plays a key role in the development of liver-stage malarial parasites. Cell Host Microbe 4:567–578.

49. Vaughan MA, O'Neill TM, Tarun SA, Camargo N, Phuong MT, Aly IAS, Cowman

FA, Kappe ISH. 2009. Type II fatty acid synthesis is essential only for malaria parasite late liver stage development. Cell Microbiol 11:506–520.

50. Waller FR, Keeling JP, Donald GR, Striepen B, Handman E, Lang-Unnasch N, Cowman FA, Besra SG, Roos SD, McFadden IG. 1998. Nuclear-encoded proteins target to the plastid in *Toxoplasma gondii* and *Plasmodium falciparum*. Proc Natl Acad Sci U S A 95:12352–12357.

51. Crabb SB, Cowman FA. 1996. Characterization of promoters and stable transfection by homologous and nonhomologous recombination in *Plasmodium falciparum*. Proc Natl Acad Sci U S A 93:7289–7294.

52. Epp C, Raskolnikov D, Deitsch WK. 2008. A regulatable transgene expression system for cultured *Plasmodium falciparum* parasites. Malar J 7.

53. Nkrumah JL, Muhle AR, Moura AP, Ghosh P, Hatfull FG, Jacobs RW, Fidock AD. 2006. Efficient site-specific integration in *Plasmodium falciparum* chromosomes mediated by mycobacteriophage Bxb1 integrase. Nat Methods 3:615–621.

54. Spalding DM, Allary M, Gallagher RJ, Prigge TS. 2010. Validation of a modified method for Bxb1 mycobacteriophage integrase-mediated recombination in *Plasmodium falciparum* by localization of the H-protein of the glycine cleavage complex to the mitochondrion. Mol Biochem Parasitol 172:156–160.

55. Mata-Cantero L, Lafuente MJ, Sanz L, Rodriguez MS. 2014. Magnetic isolation of *Plasmodium falciparum* schizonts iRBCs to generate a high parasitaemia and synchronized in vitro culture. Malar J 13:112.

56. Olszewski KL, Llinás M. 2013. Extraction of hydrophilic metabolites from *Plasmodium falciparum*-infected erythrocytes for metabolomic analysis. Methods Mol Biol 923:259–66.

Chapter 3

The Essentiality and Role of the SUF Iron-Sulfur Cluster Biosynthetic Pathway in the Apicoplast of *P. falciparum* Parasites

Attributions:

- The growth curves for each deletion line were generated by Hans Liu
  The IspH genetic deletion was generated by Dr. Krithika Rajaram

ABSTRACT

The apicoplast is essential for *Plasmodium falciparum*. However, it has been shown that blood-stage parasites can survive without this organelle as long as the isoprenoid precursor isopentenyl pyrophosphate (IPP) is supplemented. While this suggests that IPP is the only indispensable product of the organelle during this stage, other pathways within the apicoplast play accessory functions to its production, or are involved in the maintenance and replication of the organelle and thus are also required for blood-stage parasite survival. Previous work showed that the SUF iron-sulfur cluster biosynthetic pathway within the organelle is required for blood-stage parasite survival in addition to being essential for the maintenance of the apicoplast. However, the roles that the individual iron-sulfur cluster dependent proteins play in apicoplast maintenance has remained unknown. To help answer this question we utilized our PfMev parasite line, which provides a metabolic bypass that allows for the deletion of essential apicoplast-specific proteins. Genetic deletions in this line also allowed us to determine the importance of these genes in apicoplast maintenance by analyzing the resulting organelle phenotype. Through a series of genetic deletions, we have been able to determine that a number of iron-sulfur cluster dependent proteins are required for the survival of blood-stage parasites, while others are dispensable. However, individually none of the predicted apicoplast-resident iron-sulfur cluster dependent proteins are required for the maintenance of the organelle. We went on to demonstrate that additionally, none of the nuclear encoded genes involved in iron-sulfur cluster generation are required for organelle maintenance either, with the exception of the cysteine desulfurase SufS. These results contradict previous findings showing that SufC is required for organelle maintenance. We found that the requirement for SufS in apicoplast maintenance is not driven by its function in iron-sulfur cluster generation, but instead is likely driven by its role in the

generation of sulfur for use by MnmA, a tRNA modifying enzyme predicted to be present within the apicoplast.

INTRODUCTION

With increasing resistance to current front-line antimalarials there is a crucial need to find new therapeutic interventions with novel mechanisms of action (1, 2). In efforts to find new potential drug targets, the apicoplast organelle within the parasite has often been considered because it is necessary for parasite survival and contains unique biochemical pathways dissimilar from the human host (3). While the production of the isoprenoid precursors isopentenyl pyrophosphate (IPP) and dimethylallyl pyrophosphate (DMAPP) are thought to be the only essential products of the apicoplast in the blood-stage of *Plasmodium falciparum* parasites (4), the organelle remains an attractive source of drug targets due to other resident pathways playing essential accessory functions (5). One such essential pathway in the apicoplast is the SUF iron-sulfur cluster biosynthetic pathway, responsible for the generation of iron-sulfur cluster cofactors within the organelle (6). Previous work has shown that the SUF pathway is likely essential for blood-stage parasite survival, since the genes involved in this pathway are refractory to deletion (7). Additional work has shown that the pathway appears to be essential for the maintenance of the apicoplast organelle, based on results generated through the expression of a SufC dominant negative mutant (6).

Iron-sulfur clusters are cofactors composed of inorganic sulfur and iron, and are ubiquitous in nature, being found in organisms within every domain of life (8, 9). Iron-sulfur cluster cofactors are extremely versatile and can serve a variety of functions including single electron transfer, enzyme catalysis, and initiation of free-radical chemistry, among others (9).

Iron-sulfur clusters are typically generated within eukaryotes by the iron-sulfur cluster formation (ISC) pathway, residing within the mitochondrion (10, 11). The ISC pathway generates iron-sulfur clusters for proteins within the mitochondrion in addition to exporting the sulfur component to the cytosolic iron-sulfur protein assembly (CIA) pathway, forming iron-sulfur clusters for transfer to proteins within the cytosol and other subcellular locations, such as the nucleus (12, 13). Prokaryotic organisms can also contain the ISC iron-sulfur cluster assembly pathway, as well as the sulfur utilization factor (SUF) pathway (14). However, some eukaryotic cells, such as those that contain a chloroplast or plastid, typically possess their own self-contained SUF iron-sulfur cluster assembly pathway within the organelle, inherited from a cyanobacterial endosymbiont ancestor (15, 16).

Plasmodium parasites are believed to possess the ISC, CIA, and SUF pathways (17, 18). The activity and localization of these pathways is believed to replicate what has been found in other systems, with the ISC pathway being localized to the mitochondrion (6, 19), generating iron-sulfur clusters for usage within the organelle, in addition to transferring sulfur to the cytosolic iron-sulfur protein assembly (CIA) machinery for the generation and transfer of iron-sulfur clusters for usage in other areas within the cell (17). The SUF system is believed to reside within the apicoplast and generates iron-sulfur clusters exclusively for proteins within that organelle (6, 20, 21).

Fe-S cluster biosynthesis is organized in three main steps: sulfur acquisition, cluster assembly, and cluster transfer. For the SUF pathway sulfur is acquired through the cysteine desulfurase SufS, which mobilizes sulfur from *L*-cysteine resulting in a bound persulfide (22). SufE interacts with SufS increasing the cysteine desulfurase activity (23) and also acquires sulfur from SufS and transfers it to SufB of the SufBCD iron-sulfur cluster assembly complex (24). The SufBCD complex serves as a scaffold for iron-sulfur cluster

formation (25) with the ATPase activity of SufC being essential for the accumulation of iron (26). SufA and NifU (SufU) have been shown to receive iron-sulfur clusters from the SufBCD complex (27) and transfer them to downstream target proteins (28, 29).

In *Plasmodium*, all components of the SUF system are nuclear encoded and trafficked to the organelle with the exception of SufB, which is encoded by the ~35kb apicoplast organellar genome (30). The activity of multiple components of the SUF pathway from *Plasmodium* have been confirmed. The cysteine desulfurase activity of SufS and its interaction with SufE have been confirmed and localized (6, 21). SufB and SufC have been shown to interact (31) and the ATPase activity of SufC has been shown to be present and essential (6, 31). Additionally, SufA has been demonstrated to interact with SufB of the SufBCD complex and accept iron-sulfur clusters (32), with NifU (SufU) also believed to accept and transfer iron-sulfur clusters (33).

As mentioned previously, the apicoplast can be disrupted in blood-stage *P. falciparum* parasites as long as they are supplemented with 200μM of IPP (4). Our lab has previously taken advantage of this apicoplast chemical bypass system, using it to investigate the role and importance of iron-sulfur cluster biogenesis through the generation of a SufC (K140A) dominant negative mutant (6). The expression of SufC (K140A), containing a point mutation designed to ablate the essential ATPase activity of SufC (26), was reliant on IPP supplementation for survival and resulted in the disruption and loss of the apicoplast organelle. This demonstrated that SufC is not only an essential protein, but is also required for the maintenance of the organelle (6). By extension, these results also suggest that the SUF pathway and the formation and utilization of iron-sulfur clusters is also essential for apicoplast maintenance as well.

While the generation of a SufC (K140A) dominant negative mutant suggested that iron-sulfur cluster biosynthesis is required for the maintenance of the apicoplast, the ultimate mechanism by which it is responsible for this process has not been elucidated. However, the only proposed function of the SUF pathway is the generation of iron-sulfur cluster cofactors for usage by five predicted apicoplast localized target proteins: lipoic acid synthase (LipA) involved in the lipoylation of pyruvate dehydrogenase (PDH) (34, 35), MiaB predicted to function as a tRNA modifying enzyme (36–40), IspG and IspH involved in the last two steps of the MEP isoprenoid precursor production pathway (37, 41), and ferredoxin (Fd) which is part of the ferredoxin/ferredoxin NADP+ reductase (FNR) redox system within the apicoplast (42–44) (**Figure 3-1**). Thus, we hypothesized that inhibition of iron-sulfur cluster formation likely results in the disruption of the apicoplast due to the loss of function of one of the downstream enzymes that has been deprived of its essential iron-sulfur cluster cofactor.

In order to better determine the ultimate mechanism by which iron-sulfur clusters are required for apicoplast maintenance, our goal was to delete each of the five proposed iron-sulfur cluster dependent proteins. As outlined in chapter 2 of this thesis, we developed an alternative apicoplast bypass in the form of the PfMev parasite line, and demonstrated that we can use this line to generate deletions of essential apicoplast-specific genes and analyze the resulting apicoplast phenotype. Thus, we used this line for the generation of all targeted genetic deletions.

We were successful in generating deletions of all of the proposed iron-sulfur cluster dependent proteins, but found that individually, none were required for the maintenance of the apicoplast. We searched for additional potential apicoplast localized iron-sulfur cluster containing proteins that may be essential for organelle maintenance using bioinformatic

approaches, and were ultimately unsuccessful. Thus, we went on to delete each component of the SUF pathway, with the exception of SufB encoded within the apicoplast organelle genome, to better determine which SUF proteins are required for apicoplast maintenance. We found that both iron-sulfur-cluster transfer, mediated by SufA and NifU, and iron-sulfur cluster formation, mediated by the SufBCD complex are not required for the maintenance of the organelle. These results contradict what has been previously found with the SufC dominant negative mutant, but more conclusively demonstrate that iron-sulfur clusters are not required for apicoplast maintenance.

Surprisingly, we did find that the SufS cysteine desulfurase of the SUF pathway is required for apicoplast maintenance, suggesting that a pathway reliant on sulfur, other than the SUF pathway is required for organelle maintenance. Upon further analysis, we found that the cysteine desulfurase activity of SufS is likely required for apicoplast maintenance due to its role in generating sulfur for tRNA modifications mediated by the putative tRNA modifying enzyme 5-methylaminomethyl-2-thiouridylate methyltransferase, also referred to as MnmA.

Overall, the work outlined here provides multiple insights into the apicoplast resident SUF iron-sulfur cluster biosynthetic pathway and the proteins dependent on these cofactors, and their roles in parasite survival and organelle maintenance. We have demonstrated that iron-sulfur cluster usage and generation are required for parasite survival, but not for organelle maintenance. We additionally discovered that the SufS cysteine desulfurase enzyme of this pathway is required for organelle maintenance, but not due to its role in iron-sulfur cluster biogenesis, but instead by its likely role in sulfur generation for its usage by the tRNA modifying enzyme MnmA.

RESULTS

Iron Sulfur Cluster Dependent Proteins are not Required for Apicoplast Maintenance

Having the proof of concept that the PfMev line is a viable platform to generate deletions of essential apicoplast-specific genes, we wanted to use this system to follow up on previous results demonstrating that the generation of a SufC (K140A) dominant negative mutant results in disruption of the apicoplast (6). We hypothesized that the ultimate mechanism by which iron-sulfur clusters are required for apicoplast maintenance is due to the loss of function of one of the iron-sulfur cluster dependent proteins. Thus, we generated deletions of each of the proposed iron-sulfur cluster dependent proteins within the organelle including LipA, MiaB, IspG, IspH, and Fd. For each targeted gene, a series of tests were performed to confirm the genetic deletion, ascertain whether the gene is required for blood-stage parasite survival, and to determine if the gene is essential for the maintenance of the apicoplast, following what had been done previously for DXPR as outlined in chapter 2 of this thesis.

Of the predicted iron-sulfur cluster containing proteins, we first targeted the gene encoding lipoate synthase (LipA) (PF3D7_1344600) for disruption. LipA is responsible for the lipoylation of the PDH E2 subunit (34, 45), enabling it to generate acetyl-CoA for usage by the FASII pathway (46). While the FASII pathway is dispensable for blood-stage parasites (46, 47), LipA has remained refractory to deletion (48). Thus, in order to determine if LipA is essential for blood-stage parasite survival and potentially apicoplast maintenance we deleted the gene in the PfMev line using Cas9-mediated editing (49), under continuous supplementation with 50μM mevalonate. We were successful in knocking out LipA and confirmed the deletion using PCR by screening for integration at both the 5' and 3' ends of

the recombinant locus (Δ5' and Δ3'), in addition to screening for the potential presence of any wild type parasites as well, at the 5' and 3' loci. We also conducted these same reactions using the PfMev parental line as a control (**Figure 3-2a**). We went on to determine whether this gene deletion resulted in disruption of the apicoplast by attempting to PCR amplify SufB from the apicoplast genome, in addition to lactate dehydrogenase (LDH) from the nuclear genome and cytochrome C oxidase (Cox1) from the mitochondrial genome as PCR controls, as previously described (50). We were successful in amplifying SufB, demonstrating that the apicoplast genome was still present (**Figure 3-2b**). We went on to confirm the phenotype of the apicoplast using live epifluorescent microscopy and found that the apicoplast remained intact in the LipA deletion line (**Figure 3-2c**). We additionally found that LipA is not required for blood-stage parasite survival by demonstrating that ΔLipA parasites continue to grow in the absence of mevalonate supplementation (**Figure 3-2d**).

We next targeted the gene encoding MiaB (PF3D7_0622200) for deletion. MiaB is predicted to be an iron-sulfur cluster dependent tRNA modifying enzyme within the apicoplast (36, 37), and is believed to potentially assist in the read-through of a premature stop codon in the RpoC2 gene within the apicoplast genome (30, 37). However, we were successful in deleting MiaB in the PfMev parasites under continuous supplementation with 50μM mevalonate and were able to show that this gene is not required for organelle maintenance or replication. Additionally, we were able to demonstrate that this gene is also dispensable in blood-stage parasites, as it is not reliant on mevalonate for growth (**Figure 3-3**).

We next moved on to deleting IspG (PF3D7_1022800) and IspH (PF3D7_0104400) of the MEP pathway. IspG and IspH are involved in the last two steps of the MEP isoprenoid precursor production pathway (37, 41). Since these enzymes are involved in the

production of IPP and DMAPP within the parasite, we reasoned that they were likely to be essential, but we wanted to determine if they are also required for apicoplast maintenance. To answer this question, we targeted both for deletion in the PfMev line under continuous supplementation with 50μM mevalonate and were able to confirm that both are essential for blood-stage parasite survival, as evidenced by their reliance on exogenous mevalonate for parasite growth and survival. We then analyzed their potential role in apicoplast maintenance by attempting to amplify SufB from the apicoplast genome, and examining the morphology of the apicoplast via live epifluorescence microscopy. We found that the organelle genome was still present and that the apicoplast remained intact in both the ΔIspG (**Figure 3-4**) and ΔIspH (**Figure 3-5**) parasites, indicating that these genes are not required for apicoplast maintenance.

We finally targeted ferredoxin (Fd) (PF3D7_1318100) and ferredoxin reductase (FNR) (PF3D7_0623200) for deletion in the PfMev line. As discussed previously, the generation of a SufC (K140A) dominant negative mutant resulted in disruption of the apicoplast (6). In that publication the authors speculated that the ultimate mechanism by which the dominant negative mutant resulted in disruption of the apicoplast was likely due to the loss of function of the Fd/FNR redox system (6). The Fd/FNR redox system is the only known redox system within the apicoplast, which is believed to deliver reducing power to IspG, LipA, and MiaB in addition to other proteins within the SUF pathway (37, 42, 51, 52). Thus, we went on to test this hypothesis by attempting to delete both Fd and FNR in the PfMev line under continuous supplementation with 50μM mevalonate. We successfully deleted both genes and found that both Fd and FNR are required for blood-stage parasite survival. However, neither the ΔFd (**Figure 3-6**) or ΔFNR (**Figure 3-7**) parasite lines

resulted in disruption of the apicoplast, demonstrating that these genes are not required for organelle maintenance.

Through the findings described above, we were successful in determining which predicted apicoplast-specific iron-sulfur cluster dependent proteins are required for blood-stage parasite survival. However, these results demonstrate that the individual deletion of any of the proposed iron-sulfur cluster dependent proteins did not result in disruption of the apicoplast.

Searching for Additional Apicoplast Iron-Sulfur Cluster Dependent Proteins

Deletion of any of the individual predicted iron-sulfur cluster dependent proteins did not replicate the phenotype seen with the SufC (K140A) dominant negative mutant (6). This led us to believe that there may be additional apicoplast resident iron-sulfur cluster dependent proteins that are playing essential roles in apicoplast maintenance that have not yet been annotated or discovered. In order to search for additional apicoplast trafficked iron-sulfur cluster containing proteins we downloaded the amino acid sequences of every known and putative protein of the *P. falciparum* 3D7 genome through PlasmoDB (53). We then ran the amino acid sequences through the program MetalPredator, which is a program designed to predict iron-sulfur cluster binding proteins (54). Through this program we were able to generate a list of all of the predicted iron-sulfur cluster binding proteins (**Table 3-1**). We then ran this list of proteins through PlasmoAP, a program designed to predict the likelihood of a given protein being trafficked to the apicoplast (55). Finally, we checked if the genes are predicted to be essential through prior work done using forward genetic screens in *P. berghei* (56) and *P. falciparum* (57). However, after this analysis we found no candidate genes that looked promising in terms of having a high likelihood of being trafficked to the

apicoplast and were likely to be essential proteins. Thus, we were unable to identify any other potential apicoplast localized iron-sulfur-cluster dependent proteins that represented viable targets to pursue further through the generation of additional genetic knockouts or other methods.

Iron-Sulfur Cluster Transfer is not Required for Apicoplast Maintenance

The previous genetic deletions were all done individually, leading to the possibility that the loss of the apicoplast may be due to a combinatorial effect from multiple iron-sulfur cluster dependent genes lacking their required cofactors. There also still remained the possibility that there may be additional apicoplast localized iron-sulfur cluster dependent proteins that are essential for organelle maintenance that our previous bioinformatic analysis did not identify. Thus, in an effort to address these questions we attempted to delete the genes involved in iron-sulfur cluster transfer in order to prevent all apicoplast proteins from acquiring iron-sulfur-cluster cofactors.

Two genes are proposed to be involved in iron-sulfur cluster transfer within the apicoplast, SufA (PF3D7_0522700) and NifU (SufU) (PF3D7_0921400). In *E. coli* both SufA and NfuA (a homolog of NifU) have been shown to receive iron-sulfur clusters from the SufBCD iron-sulfur cluster assembly complex (27) and transfer those clusters to downstream target enzymes (28, 29). Some of this activity has been confirmed in *Plasmodium,* showing interactions between SufA and SufB of the SufBCD complex (32). Both SufA and NifU have been previously localized to the apicoplast, and have been shown individually to be dispensable at every stage of the parasite lifecycle in *P. berghei* (7, 33). However, this work has not been replicated in *P. falciparum*. Thus, we targeted both of these genes for deletion in the PfMev line, and were successful in the individual deletion of both genes. We found that

both SufA and NifU are dispensable for *P. falciparum* blood-stage parasite survival, and that parasite growth was unaffected by the removal of mevalonate. Additionally, we were able to show that neither SufA (**Figure 3-8**) or NifU (**Figure 3-9**) are required for apicoplast maintenance or replication by assaying for the presence of the apicoplast genome and determining the morphology of the organelle. This reproduces previous results in *P. berghei* also demonstrating that individually SufA (7) and NifU (33) are not essential.

It has been hypothesized that SufA and NifU are functionally redundant and are both able to recognize all potential substrate proteins (7, 33). In other organisms it has been shown that detrimental effects are only observed when more than one of the cluster transfer genes are targeted for deletion (58). Thus, in order to determine if iron-sulfur cluster transfer is essential for apicoplast maintenance we generated a double knockout of SufA and NifU. The deletion of both of these genes should continue to allow for the formation of iron-sulfur clusters through the actions of SufS/SufE and the SufBCD complex, but inhibit the transfer of those clusters to any downstream proteins that receive these cofactors. We were successful in generating ΔSufA/ΔNifU PfMev parasite lines, and found that together these genes are essential for blood-stage parasite survival. However, these genetic deletions did not result in the disruption of the apicoplast (**Figure 3-10**).

Taken together, these data suggest that SufA and NifU are functionally redundant as indicated by the lack of phenotype observed upon the individual deletion of either gene (58). The essentiality of SufA and NifU together suggests that iron-sulfur cluster transfer is required for the survival of blood-stage parasites. However, the observation that ΔSufA/ΔNifU PfMev parasite lines retain the apicoplast suggests that iron-sulfur cluster transfer or usage is not required for apicoplast maintenance. Additionally, these results suggest that there are no additional iron-sulfur cluster dependent proteins in the apicoplast

that are essential for organelle maintenance, since the ΔSufA/ΔNifU double deletion should presumably prevent the transfer of iron-sulfur clusters to all apicoplast proteins.

Iron Sulfur Cluster Formation is not Required for Apicoplast Maintenance

Since the transfer or usage of iron-sulfur clusters is not essential for apicoplast maintenance, we wanted to determine at which point inhibition of the SUF pathway would result in disruption of the organelle. It was previously demonstrated that the expression of a SufC (K140A) dominant negative mutant resulted in apicoplast disruption. The introduction of the K140A point mutation abolishes the ATPase activity of SufC, which is essential for iron acquisition and cluster formation *in vivo* (26, 59). However, the work outlined up to this point has only involved deletion of the iron-sulfur cluster dependent proteins and iron-sulfur cluster transfer proteins. Thus, it remains a possibility that iron-sulfur cluster formation, but not transfer or usage is required for organelle maintenance. This may be the case due to previous work showing that iron-sulfur cluster formation may be essential for iron homeostasis (60–63). Thus, we next sought to determine whether interfering with the iron-sulfur cluster assembly complex may result in apicoplast disruption.

The $SufBC_2D$ complex is predicted to form from a SufBC dimer and a SufDC dimer (64), with SufC transiently dimerizing upon hydrolyzing ATP (25). It has previously been demonstrated that SufD is required for iron incorporation into the complex *in vivo* (26, 65), and thus should play an essential role in iron-sulfur cluster formation. Thus, we attempted to delete SufD (PF3D7_1103400) of the SufBCD iron-sulfur cluster assembly complex. Using the PfMev line we were successful in deleting SufD, and found it to be essential for blood-stage parasite survival as evidenced by its reliance on mevalonate for growth. However, deletion of SufD did not result in the disruption of the apicoplast (**Figure 3-11**).

This finding demonstrating that SufD is not required for organelle maintenance, but is essential for parasite survival suggests that the process of iron-sulfur cluster formation itself is not required for the maintenance of the apicoplast. The requirement of SufD for iron-sulfur cluster formation is supported by prior work in other systems (26). However, SufB and SufD are paralogs, sharing 17% sequence identity in *E. coli* (66), and 21% identity in *P. falciparum*. It is predicted that SufD arose from a gene duplication event of SufB, with ancestral iron-sulfur cluster assembly complexes consisting of only SufB and SufC (67). Indeed there are many organisms that contain genes for SufC and SufB, but lack SufD (67). It has even been shown that organisms that contain SufD are capable of forming $SufB_2C_2$ complexes (16, 68). Thus, in order to confirm the essentiality of iron-sulfur cluster formation, we targeted the SufC ATPase for deletion.

Using the PfMev line we were successful in generating a SufC (PF3D7_1413500) deletion line. We were able to determine that SufC is essential for blood-stage parasite survival, but is not required for apicoplast maintenance or replication (**Figure 3-12**). The deletion of SufC resulted in a similar phenotype as that seen for the deletion of SufD, helping to further support the finding that iron-sulfur cluster formation is not required for organelle maintenance. Additionally, we went on to more conclusively establish that iron-sulfur cluster formation is not required for organelle maintenance by generating a dual deletion of both SufC and SufD in the PfMev line. While SufE has previously been shown to only transfer sulfur from SufS to SufB in the presence of SufC (24), and both SufC and SufD have been demonstrated to perform critical functions in iron acquisition and iron-sulfur cluster assembly (26), we wanted to eliminate as many components of the SufBCD cluster assembly complex to eliminate any doubt that iron-sulfur cluster formation is essential for apicoplast maintenance. These are the only components of the system that we

are able to knockout, since SufB is encoded by the apicoplast organelle genome (30), and current genetic tools make organelle genome modification unfeasible. However, we were successful in generating a ΔSufC/ΔSufD dual deletion in the PfMev parasite line, and found that even when both components were deleted they were required for blood-stage survival, but were not essential for apicoplast maintenance (**Figure 3-13**). Thus, these results more conclusively demonstrate that iron-sulfur cluster formation is not required for apicoplast maintenance.

SufE is Required for Parasite Survival, but is not Essential for Apicoplast Maintenance

Having established that iron-sulfur cluster formation is not required for apicoplast maintenance, we continued to move up in the SUF pathway to determine if sulfur acquisition and transfer is essential for apicoplast maintenance. Thus, we chose to delete SufE (PF3D7_0206100), which has previously been characterized as a sulfur transfer protein, and has been shown to accept sulfur from SufS and transfer it to SufB of the SufBCD complex (24, 69). Additionally, SufE has been shown to increase the cysteine desulfurase activity of SufS up to 8 fold (23), and in other systems up to 50 fold (22). SufE has been shown to be essential for iron-sulfur cluster synthesis in *E. coli* (23, 24). In *Plasmodium*, SufE is predicted to be essential due to the inability to generate SufE deletion lines (7). Using the PfMev line we were successful in generating a genetic knock out of SufE, and found the gene to be essential for parasite survival, but found that it is not required for apicoplast maintenance (**Figure 3-14**).

SufS is Required for Organelle Maintenance

As mentioned previously, SufS (PF3D7_0716600) is an apicoplast resident cysteine desulfurase (6, 21), that acquires sulfide through the conversion of *L*-cysteine to *L*-alanine (69). SufS has been shown to then transfer this sulfide to SufE, which in turn transfers it to SufB of the SufBCD complex for iron-sulfur cluster formation (24). As outlined in the work above, we were able to demonstrate that SufE is required for parasite survival, but is not essential for organelle maintenance. While SufE has previously been shown to play a role in sulfur transfer between SufS and SufB (24), in addition to increasing the cysteine desulfurase activity of SufS (23), it does not appear to be absolutely required for cysteine desulfurase activity. SufS in the absence of SufE still displays a basal cysteine desulfurase activity (23), and it may be possible that its activity can be enhanced by other interacting partners besides SufE. Some organisms lack SufE altogether, demonstrating that its activity may not be essential for the cysteine desulfurase activity of SufS (70). Additionally, in other systems cysteine desulfurase enzymes have been shown to be required for other pathways in addition to iron-sulfur cluster formation including the biosynthesis of thiamine, biotin, lipoic acid, molybdopterin, and tRNA modifications (71), and the transfer of sulfur between SufS and the target proteins likely does not require SufE (72–74). We were successful in deleting SufS in the PfMev line and found the gene to be essential for blood-stage parasite survival, in addition to being essential for apicoplast maintenance (**Figure 3-15**). These results suggest that the cysteine desulfurase activity of SufS is essential for apicoplast maintenance, but its role in that process is likely not due to its function in generating sulfur for usage by the SUF iron-sulfur cluster formation pathway.

MnmA is Essential and Required for Organelle Maintenance

The previous results demonstrate that SufS is required for apicoplast maintenance. However, none of the genes involved in iron-sulfur cluster generation, transfer, or usage are required for this process. This suggests that the reliance on sulfur for organelle maintenance is not driven by its requirement for iron-sulfur cluster generation, but instead by a separate pathway. As mentioned above, cysteine desulfurase enzymes can also be involved in the biosynthesis of thiamine, biotin, lipoic acid, molybdopterin, and sulfur containing tRNA modifications (71). Having analyzed which of these pathways are present within the parasite, likely to be localized to the apicoplast, and potentially essential for the survival of the parasite, the only pathway that potentially fit this description was tRNA thiolation, mediated by a putative MnmA (37). While this gene has not been investigated or characterized in *Plasmodium*, MnmA has previously been predicted to be localized to the apicoplast (37), with its activity being reliant on a cysteine desulfurase (75).

After searching the genome of *P. falciparum,* we found a gene that potentially possesses MnmA activity, that is currently annotated as a tRNA methyltransferase (PF3D7_1019800). Using the apicoplast targeting prediction algorithm PlasmoAP, the gene product is likely trafficked to the apicoplast (76). Additionally, further analysis of the protein sequence shows that there is a domain present that shows homology to the bacterial MnmA, with eukaryotic homologs typically termed TrmU or Mtu1, which act as a tRNA-specific 2-thiouridylase involved in the 2-thiolation of the wobble base uridine at position 34 (U34) of tRNA(Lys), tRNA(Glu) and tRNA(Gln), generating the s^2U34 tRNA modification (77). This modification has been shown to improve reading frame maintenance, with its absence responsible for a growth defect in bacteria, attributed to potential translational frameshifting (78–81). In order to determine if the s^2U34 tRNA modification, potentially catalyzed by the putative *P. falciparum* MnmA (PF3D7_1019800) is required for organelle maintenance, we

deleted this gene in the PfMev parasite line and found this gene to be essential for blood-stage survival in addition to being required for apicoplast maintenance (**Figure 3-16**). Overall, these results suggest that the ultimate reason why SufS is required for apicoplast maintenance is likely due to its role in sulfur generation for utilization by the putative MnmA gene for tRNA modification.

CONCLUSIONS AND DISCUSSION

Previous work using the IPP chemical bypass system (4), showed that the apicoplast organelle becomes disrupted when the SufC (K140A) dominant negative mutant is expressed (6). This work suggested that iron-sulfur cluster biosynthesis is required for organelle maintenance, but a more refined etiology was not provided. The ultimate mechanism by which the SufC (K140A) dominant negative mutant resulted in organelle loss was suggested to be due to the loss of function of one or more of the five proposed iron-sulfur cluster containing proteins within the organelle, with ferredoxin being hypothesized as the most likely candidate (6). To capitalize on these insights, we individually deleted each of the five proposed iron-sulfur cluster dependent proteins in the apicoplast, including LipA, MiaB, IspG, IspH, and Fd using the PfMev parasite line described in chapter 2 of this thesis. We determined the role of each protein in parasite survival and in the maintenance of the apicoplast, as summarized in **Table 3-2**.

We first targeted lipoic acid synthase (LipA) for deletion. As described previously, LipA is predicted to be an apicoplast-resident iron-sulfur cluster dependent protein (35, 46, 82), involved the lipoylation of the apicoplast-resident pyruvate dehydrogenase (PDH) complex (34, 35). LipA is involved in the second step of lipoate synthesis, preceded by the

octanoyltransferase LipB, which transfers an octanoyl group from ACP onto the E2 subunit of apicoplast resident pyruvate dehydrogenase (PDH) (34, 45, 46). LipA is responsible for the insertion of two sulfur atoms into the octanoyl moiety of PDH, converting it to the active lipoylated form of the enzyme (34, 35, 83). Lipoate functions as an essential cofactor of PDH, which converts pyruvate into acetyl-CoA, which in turn is utilized by the type II fatty acid biosynthetic pathway (FASII) within the apicoplast (46). Previous attempts to delete LipA in *P. falciparum* have been unsuccessful (48). However, genes relevant to the activity and function of LipA, such as LipB (84), the E1α subunit of PDH (85), and multiple components of the FASII pathway (46, 47) have been amenable to deletion in blood-stage *P. falciparum* parasites, suggesting that LipA should be able to be deleted as well. As detailed above, we were successful in deleting LipA and found it to be not essential for the growth of blood-stage parasites. The deletion was generated in the PfMev bypass line under supplementation with 50μM mevalonate. However, upon the removal of mevalonate, the ΔLipA parasites continued to grow at a rate similar to those with supplementation with 50μM mevalonate, demonstrating the dispensability of the gene in blood-stage parasites.

We next targeted MiaB for deletion. In *P. falciparum* MiaB (PF3D7_0622200) is predicted to be another apicoplast-resident iron-sulfur cluster containing enzyme (36–38). MiaB is predicted to function as a tRNA modifying enzyme, acting downstream of another tRNA modifying enzyme MiaA (PF3D7_1207600) (37). MiaA is a tRNA isopentenyltransferase, transferring the isopentenyl group from DMAPP to the N^6-nitrogen of adenine at base 37 of the target tRNA, to form the modification (i^6A37) (39, 40). MiaB is then predicted to function as a tRNA methylthiotransferase (38), catalyzing the methylthiolation of the i^6A37 base, further modifying it to generate the 2-methylthio-*N*^{6}-isopentenyl-adenosine (ms^2i^6A) tRNA modification (36, 86). In other systems, the ms^2i^6A

tRNA modification generated by MiaA and MiaB is involved in increasing translational fidelity, reducing frameshifting, assisting in stop codon suppression, and reading frame maintenance (81, 87–89). These modifications are also present in tRNAs within chloroplast organelles, and are required for tRNA ribosome binding (90, 91). The apicoplast organelle genome contains an internal stop codon in the RpoC2 gene (30), and the MiaA/MiaB modification was previously predicted to be essential for the translation of this gene (37). MiaA is involved in tRNA isopentenylation reliant on DMAPP (92), produced within the organelle. However, previous work suggested that isoprenoid biosynthesis is not essential for organelle maintenance (50). Our work certainly confirms this conclusion since the deletions of MEP pathway enzymes DXS, DXPR, IspG, or IspH did not result in loss of the apicoplast. Formation of i^6A37 tRNA would only be possible in these deletion lines if supplemented isoprenoid precursors were able to enter the apicoplast from the cytosol. MiaA and MiaB have been proven to be non-essential in other systems such as *E. coli* (93) and we found MiaB to not be essential in our system as well. Based on our results, we found that the deletion of MiaB had no discernible detrimental effect on the growth of blood-stage parasites.

We moved on to delete IspG and IspH, two proteins predicted to contain iron-sulfur-clusters and localize to the apicoplast (37, 42, 94, 95). IspG and IspH are responsible for the last two steps of isoprenoid precursor production (37, 41), with IspG predicted to catalyze the conversion of methylerythritol cyclic diphosphate (MEcPP) to (*E*)-4-hydroxy-3-methylbut-2-enyl diphosphate (HMBPP) (96), followed by IspH which converts HMBPP into IPP and DMAPP (42, 97). Previous work reported in the chapter 2 of this thesis demonstrated that DXPR, which catalyzes the second step in the MEP pathway, is essential for blood-stage parasite survival, but is not required for organelle maintenance. We expected

the same phenotype to be shared by ΔIspG and ΔIspH parasites, however, there was the possibility that another phenomenon, such as the buildup of a toxic substrate, could lead to apicoplast disruption in these lines. Ultimately, this proved not to be the case, and the MEP pathway enzymes IspG, IspH, and DXPR all are essential for parasite survival, but are not required for apicoplast maintenance.

Ferredoxin is another apicoplast-resident iron-sulfur cluster dependent protein (42) involved in the apicoplast Fd/FNR redox system (43), the only known redox system present in the apicoplast (44, 52, 98). FNR harvests two electrons (through hydride transfer) from NADPH and uses these electrons to reduce two Fd proteins (one electron each), which in turn deliver reducing power throughout the organelle (52). Fd has been demonstrated to function as an electron donor to IspH (42), and is also believed to deliver reducing power to multiple other enzymes and pathways within the organelle, such as IspG, LipA, MiaB, and other proteins within the SUF iron-sulfur cluster generation pathway (37, 42, 51, 52). It was hypothesized that loss of the Fd iron-sulfur cluster would lead to redox dysfunction, DNA damage, and loss of the organelle (6). In *E. coli*, loss of the Fd/FNR system led to increased sensitivity to oxidative stress (50, 99). However, while we found that Fd and FNR are both essential for parasite survival, we found that neither are required for the maintenance of the organelle. Since redox homeostasis should be critical for organelle maintenance, these results suggest that there could be some other mechanisms for maintaining redox balance and oxidative defense.

Our results showed that all of the known apicoplast iron-sulfur cluster proteins can be individually deleted without loss of the organelle. It remained possible that other undiscovered iron-sulfur proteins existed, or that the combined loss of multiple iron-sulfur proteins could lead to apicoplast loss. In order to explore these hypotheses, we targeted the

only two proposed iron-sulfur cluster transfer proteins, SufA and NifU, both individually and together. These proteins should be required for transferring the clusters formed by the SufBCD complex to all target proteins (7, 33, 100). Thus, loss of the transfer proteins should behave like a functional deletion of all iron-sulfur proteins, including any that have yet to be discovered. We found that individually SufA and NifU are dispensable, however, the simultaneous deletion of both SufA and NifU demonstrated that together they are required for parasite survival. These data support previous findings suggesting that they are functionally redundant, as parasites lacking either can complete the entire parasite lifecycle in *P. berghei* (7, 33). Our results indicate that SufA and NifU are likely the only iron-sulfur cluster transfer proteins within the organelle, since the deletion of both results in parasite death. Dual deletion, however, did not result in the disruption of the apicoplast. Thus, functional loss of all apicoplast iron-sulfur cluster proteins does not trigger disruption of the organelle.

There do not appear to be any other iron storage proteins located in the apicoplast. The iron-sulfur cluster assembly machinery may have an important role in sequestering free iron and sulfide, which would be toxic otherwise. This hypothesis is supported by previous researching demonstrating the importance of iron-sulfur cluster generation in iron homeostasis and metabolism (60–63). Thus, we chose to delete SufD and SufC of the SufBCD iron-sulfur cluster assembly complex (26). As mentioned above SufD is a paralog of SufB, with SufB being encoded by the apicoplast organellar genome (37, 67, 101), with its activity being essential for iron acquisition and cluster formation (26). We were successful in individually deleting SufD and SufC, and while they were shown to be essential for parasite survival, neither was required for organelle maintenance. Consistent with this result, we generated a dual deletion of SufC and SufD, and still observed an intact apicoplast,

demonstrating that the SufBCD complex is not essential for organelle maintenance, and thus likely not required for iron homeostasis and metabolism in the organelle.

Our results make it clear that iron-sulfur cluster generation, transfer or usage is not required for organelle maintenance. The discrepancy in the results between the SufC dominant negative mutant and SufC genetic deletion are not immediately clear. For one, the mechanisms of gene disruption were different, with the previous method relying on a SufC (K140A) dominant negative mutant. This method relied on the exogenous expression of a second copy of the gene containing the point mutation, with its expression controlled by either the ribosomal L2 (RL2) or calmodulin promoters (50). Overexpression of the protein could have led to general toxicity as has been observed by others (6), however, expression of the native SufC using the same promoters (RL2 and calmodulin) did not lead to toxicity and apicoplast loss (50). In our current work, protein overexpression is not an issue because we targeted proteins for deletion. Additionally, the method of bypass was different in the previous work and what is outlined here, with the previous dominant negative mutant expression relying on the exogenous supplementation with 200 μM IPP. The effect of this concentration of IPP on parasite fitness over the time-course needed for this experiment (>30 days) has not been studied, however, the isomer of IPP, DMAPP has been shown to toxic to parasites (4). Our method relies on supplementation with only 50μM mevalonate, and while this has not been experimentally confirmed, this may be better tolerated by the parasite. As far as how the previous phenotype manifested, it is unclear, but may be a combinatorial effect of increased protein trafficking to the organelle as well as the metabolic bypass method, but it is clear that the resulting phenotype was not due to SufC being required for organelle maintenance.

We completed our investigation of the SUF pathway by targeting the sulfur acquisition step catalyzed by SufS and SufE. We attempted to knockout SufE, which is an accessory partner to SufS, and functions as a sulfur transfer protein. Once sulfur is liberated from *L*-cysteine by SufS, the persulfide sulfur is transferred from SufS to SufE (69). SufE can then in turn transfer it to SufB of the SufBCD complex, with analysis showing that there is no transfer of sulfur directly from SufS to SufB (24), and thus SufE is required for this process. Additionally, bacterial SufE has been shown to enhance the cysteine desulfurase activity of SufS, increasing its activity up to 50-fold (22). Similar experiments have been conducted analyzing the *P. falciparum* proteins and found that SufS cysteine desulfurase activity was enhanced up to 17-fold by the addition of SufE (21). We were successful in deleting SufE and SufS in *P. falciparum*, and showed that both proteins are required for parasite survival, consistent with their roles in iron-sulfur cluster synthesis. However, SufS proved to be essential for apicoplast maintenance while SufE was not. While SufE has been shown to enhance the cysteine desulfurase activity of SufS, it does not appear to be absolutely required for its activity (21). SufS may be capable of liberating and transferring sulfur to other pathways within the organelle that are essential for its maintenance, independent of SufE. In addition to iron-sulfur cluster assembly there are other pathways that rely on sulfur harvested from *L*-cysteine by cysteine desulfurases, such as the biosynthesis of thiamine, biotin, lipoic acid, molybdopterin, in addition to the sulfur modifications of tRNAs (71). We analyzed each of these potential pathways to determining if they are likely to be present in *P. falciparum,* and if their activity is likely to be required for apicoplast maintenance.

The current model of thiamine biosynthesis relies on the joining of 5-(2-hydroxyethyl)-4-methylthiazole (THZ) with 4-amino-2-methyl-5-hydroxymethylpyrimidine

pyrophosphate (HMP-PP) by the enzyme ThiE (102), with an additional pathway for thiamine scavenging (102, 103). The biosynthesis of THZ is the step in thiamine biosynthesis reliant on cysteine desulfurase activity, and parasites have been shown to survive in thiamine depleted media as long as HMP is supplemented, suggesting that the parasites can synthesize THZ, but not HMP (102). However, multiple enzymes involved in THZ synthesis including ThiG/H/L have not been identified in *Plasmodium* species (102, 104), and should be required for its biosynthesis (105, 106). Additionally, there is a pathway present for the scavenging of THZ, as evidenced by the presence of the ThiM (102, 107). The biosynthesis of THZ does require a cysteine desulfurase, and while it is currently unclear what proteins are involved in this pathway or if this pathway is present in the parasite at all, a potential role for SufS cannot be ruled out. However, thiamine biosynthesis is unlikely to play a role in apicoplast maintenance. Within the parasite, thiamine is predicted to be used by transketolase, 3-methyl-2-oxobutanoate dehydrogenase (BCKDK), and 2-oxoglutarate dehydrogenase (OxoDH) outside of the apicoplast, and by 1-deoxy-D-xylose phosphate synthase (DXS) and the E1 subunit of the pyruvate dehydrogenase (PDH) complex within the apicoplast (107, 108). The dependent enzymes outside of the apicoplast are unlikely to play a role in organelle maintenance, and of the dependent enzymes within the apicoplast, both have been deleted and have been shown to not be required for organelle maintenance. The PDH E1α subunit has previously been deleted and was demonstrated to not be essential for blood-stage survival (85). Additionally, as outlined in chapter 4 of this manuscript, we deleted DXS and found the gene to be essential for parasite survival but not for organelle maintenance. Thus, overall it appears unlikely that SufS has a key role in thiamine biosynthesis, and even if it does, the cofactor would not be required for organelle maintenance.

Other pathways potentially reliant on a cysteine desulfurase include lipoic acid and biotin biosynthesis. For lipoic acid biosynthesis, LipA is predicted to be an iron-sulfur cluster dependent protein that catalyzes the conversion of PDH E2 bound octanoate into lipoate through the addition of two sulfur atoms (34, 46). Within the parasite, the only enzymes predicted to be reliant on lipoic acid include the branched-chain alpha-ketoacid dehydrogenase (BCDH), alpha-ketoglutarate dehydrogenase (KDH), and the glycine cleavage system within the mitochondria (109), and the PDH E2 subunit within the apicoplast (46). However, due to LipA being an iron-sulfur cluster dependent protein, in addition to the above demonstration that deletion of the gene has no discernible effect on apicoplast morphology, LipA is clearly not responsible for organelle maintenance. For biotin biosynthesis the final step typically involves the conversion of dethiobiotin into biotin by biotin synthase (BioB), an iron-sulfur cluster dependent protein (110, 111). However, acetyl-CoA carboxylase (ACC) is the only protein predicted to be biotinylated within the parasite (104), and it has been demonstrated to not be essential for the blood-stage survival of the parasite (112). Furthermore, the parasite is predicted to scavenge biotin (113), and lacks the ability to synthesize it on their own (104). Thus, for these reasons lipoate and biotin biosynthesis are unlikely to be responsible for apicoplast maintenance.

Additionally, another pathway reliant on cysteine desulfurase is the biosynthesis of molybdopterin (71). However, the enzymes involved in the production of this cofactor are not likely to be present in *P. falciparum* based on bioinformatic analysis of the parasite genome (114).

When analyzing which pathways may be present in the apicoplast and playing a role in the maintenance of the organelle, the pathway that appeared to be the most likely was tRNA thiolation. These modifications can include the 4-thiouridine (s4U) modification at

position 8 on the tRNA, or the 2-thiouridine (s2U) modification at position 34 of the tRNA (71). The s4U modification typically relies on IscS and ThiL of the thiamine biosynthetic pathway (115–117). However, *Plasmodium* does not have a ThiL, and instead contains the homologous thiamine phosphate kinase (TPK) (37, 107), which is believed to act solely within the cytosol of the parasite (118). The s2U modification relies on MnmA (119), which has previously been predicted to be localized to the apicoplast organelle (37).

MnmA is an 5-methylaminomethyl-2-thiouridylate methyltransferase enzyme involved in the 2-thiouridine modification (s^2) of position 2 of the pyrimidine ring at the wobble base position (U34) of $tRNA^{Glu}_{UUC}$, $tRNA^{Gln}_{UUG}$, and $tRNA^{Lys}_{UUU}$ (75), helping to generate the mnm^5s^2U34 tRNA modification (77). While requiring sulfur, this modification has been shown to occur independently of iron-sulfur clusters (120). This modification typically occurs in parallel to modifications mediated by the MnmE/MnmG complex, which catalyzes the addition of an aminomethyl or carboxymethylaminomethyl group to the C5 position at the U34 wobble base of $tRNA^{Glu}_{UUC}$, $tRNA^{Gln}_{UUG}$, $tRNA^{Lys}_{UUU}$, $tRNA^{Leu}_{UAA}$, $tRNA^{Arg}_{UCU}$, and $tRNA^{Gly}_{UCC}$ (121, 122). In *E. coli,* the $tRNA^{Glu}_{UUC}$ and $tRNA^{Lys}_{UUU}$ can then be further converted into a 5-methylaminomethyl (mnm^5) group by MnmC (121). However, while MnmE and MnmG are evolutionarily conserved, MnmC is not, with some organisms lacking this gene (123). This appears to be the case in *P. falciparum*, with genes sharing a high sequence homology to the *E. coli* MnmA (PF3D7_1019800), MnmE (PF3D7_0817100), and MnmG (PF3D7_1244000) present in the parasite genome. Additionally, each of these genes are predicted to likely be trafficked to the apicoplast (76), and predicted to be essential as determined by the forward genetic screen conducted by Dr. John Adams (57). With the MnmA and MnmG also predicted to be essential in *P. berghei,* as predicted by a separate forward genetic screen (56). Through the work detailed above we were able to show that

MnmA is likely to be present in the apicoplast and essential for its maintenance, as evidenced through its deletion in the PfMev line. Additionally, it appears that other proteins involved in this pathway are present and essential in the *P. falciparum* apicoplast organelle as well.

In the MnmA pathway in *E. coli*, sulfur is typically liberated by IscS and the transferred through the Tus sulfur relay system (TusABCDE) to MnmA for modification of the tRNA (74). While MnmA is conserved, TusBCD and E are often not found in numerous organisms (124) and it has been shown that this modification can occur independent of the Tus system (72). Additionally, the liberation of sulfur for usage by MnmA has been shown to be generated by other cysteine desulfurases besides IscS, such as yrvO in *B. subtilis* (72), or by NifS within the mitochondria (77), and SufS is predicted to fulfill this role in *T. parva* (125). These modified tRNAs are also believed to be present within chloroplasts (126).

MnmA shows extreme evolutionary conservation, being present even in the most reduced bacterial genomes (127), and is even hypothesized to also be responsible for the retention of SufS and IscS, due to the lack of conservation of the other pathways that would be reliant on these enzymes (128). The (x)nm^{5}S^{2}U34 modification is also conserved in the mitochondrial and chloroplast organelles (126), with the eukaryotic homolog of MnmA, Mtu, having been shown to be essential for mitochondrial translation and organelle biogenesis (129–131). While MnmA has been shown to not be essential in *E. coli* or *S. enterica*, MnmA deletion mutants do display a slower growth phenotype (75, 126) and MnmA/MnmE double mutants in *E. coli* and *S. enterica* demonstrated that these genes together are critical for growth (122, 126). The reduction in growth is believed to be caused by an increase in missense errors (126).

While the specific role the putative MnmA is playing in the apicoplast of *P. falciparum* is unclear, the S^{2}U34 modification predicted to be catalyzed by this enzyme has been shown

to be important in other systems for tRNA ribosome binding (132), the recognition of wobble codons (133, 134), reading frame maintenance (78), and reducing +1 +2 frameshifts (81, 135). Additionally, tRNA modifications in general are ubiquitous and critical for translation across all domains of life (136). Due to *P. falciparum* presumably encoding all of the tRNAs needed for translation within the apicoplast genome itself (30), there is likely no import of tRNAs into the organelle. Thus, all modifications of the apicoplast tRNAs must also likely occur within the organelle as well. Previous work showed that ribosome binding and wobble codon recognition was prevented with hypomodified $tRNA^{Lys}_{UUU}$, but was restored upon S^2U34 modification (132, 133). This suggests that there may be a minimal set of tRNA modifications required for translation, with the S^2U34 modification potentially being one of them. This hypothesis is supported by the retention of MnmA in extremely reduced bacterial genomes (127, 137–139).

Overall, this work has helped to better elucidate the biochemistry and roles of the various components of the SUF pathway and the downstream proteins reliant on it. We have been able to demonstrate which are essential for parasite survival and which are required for the maintenance and replication of the organelle.

METHODS

P. falciparum culture and maintenance

Unless otherwise noted, blood-stage *P. falciparum* parasites were cultured in human erythrocytes at 1% hematocrit in a 10mL total volume of CMA (complete medium with Albumax) medium containing RPMI 1640 media with L-glutamine (USBiological Life Sciences), supplemented with 25mM HEPES, 0.2% sodium bicarbonate, 12.5μg/mL

hypoxanthine, 5g/L Albumax II (Life Technologies) and 25µg/mL gentamicin. Cultures were maintained in gassed flasks (94% N_2, 3% O_2, 3% CO_2) and incubated in sealed 25cm^2 flasks at 37°C.

Generation of *P. falciparum* transfection constructs for gene deletion

Homology arms of ~300-600bp for each gene were amplified using the homology arm (HA) 1 and 2 forward and reverse primers corresponding to each gene (**Table 3-3**) from blood-stage *P. falciparum* NF54-attb gDNA. HA1 and HA2 primers were designed to contain ~15bp overhangs for insertion into the cut the pL8, pRS or pRSng plasmids using In-Fusion (Clontech) ligation independent cloning methods. The pRS and pRSng are modified versions of the pL8 plasmid. The pRS plasmid contains a synthetic LacZ cassette flanked by two BsaI sites to allow for blue/white colony screening within the site used for guide RNA insertion. The pRSng plasmid has the guide RNA expression cassette removed entirely, reliant on gRNA expression from the paired pCasG plasmid, which also contains the gene encoding the Cas9 enzyme.

For generation of the deletion constructs, the pL8 and pRS(ng) plasmids were digested with NotI for insertion of HA1, and with NgoMIV for HA2. Digests with either endonuclease were also treated with recombinant shrimp alkaline phosphatase (rSAP) and then ethanol precipitated before insertion of the homology arms. The pL8, pRS, and pCasG plasmids contain a guide RNA (gRNA) expression cassette. Guide RNA sequences were synthesized as oligos (**Table 3-5**), annealed, and inserted into the pL8, pRS, or pCasG plasmids via In-Fusion cloning after being digested with BsaI and also treated with rSAP, and then ethanol precipitated.

The SufA/NifU double knock-out construct was generated by cutting the existing pRSng SufA plasmid with BamHI and HindIII in the presence of rSAP and ethanol precipitating it. The blasticidin deaminase drug resistance cassette was then amplified from a separate plasmid containing the sequence, using the primers listed in **Table 3-8** (pRsBSD F and pRsBSD R). The amplicon was then ethanol precipitated and inserted into the cut plasmid using In-Fusion cloning.

P. falciparum transfections for Gene Deletion

Transfections were conducted as previously described (140, 141). Briefly, 400µL of red blood cells were washed with 5mL of CytoMix and resuspended in 340µL of CytoMix. The red blood cells were then electroporated with 75µg each of the pUF1-Cas9 and pL8-gene specific knock out plasmids (49) or the pCasG and pRS(ng) gene specific plasmids. The electroporated RBCs were then mixed with ~2.5mL of 10mL PfMev parasites synchronized as schizonts at 1% hematocrit and ~10% parasitemia and given 10mL CMA with 50µM mevalonate. After 48 hours, transfectants were selected with 1.5µM DSM1, 2.5nM WR99210, and 50µM mevalonate for seven days. After seven days, the parasites were switched to media containing only 50µM mevalonate. Infected red blood cells (iRBC) were first observed between 17 and 30 days after beginning drug selection. Once parasites were observed the medium was switched to 2.5nM WR99210 and 50µM mevalonate.

For generation of the double SufA/NifU double knockout ΔSufA parasites were transfected following the above mentioned standard protocol with the NifU gene-specific pRSng and pCasG plasmids, with the pRSng plasmid having been modified to contain the BSD drug resistance cassette. Parasites were then selected for 7 days with 2.5ng/mL blasticidin, 1.5µM DSM1, and 50µM mevalonate in addition to 2.5nM WR99210. After

seven days, the media was switched to 50μM mevalonate and 2.5nM WR99210 until parasites were seen ~20-25 days post selection, after which they were maintained on media containing 2.5ng/mL blasticidin, 2.5nM WR99210, and 50μM mevalonate.

Confirmation of knockout genotype

In order to screen for integration and successful gene knockout, in addition to the presence of any contaminating residual wild type parasites, a set of six primers were used: 5'F, 3'R, pL8 HA1 R, pL8 HA2F, 5' WT R and 3' WT F (**Table 3-6**). These primers were designed to screen for integration and gene disruption at the 5' and 3' ends (Δ5' and Δ3') in addition to 5' and 3' regions of the WT gene (5' and 3'). The same reactions were also performed on the parental PfMev line concurrently as a control. Samples for PCR were collected when the parasitemia reached been 5-10%, as determined by Giemsa stain. Approximately 100μL of a resuspended parasite culture was placed in a heat block at 90°C for 2 minutes and stored at -20°C. For the PCR reaction, 1μL of the parasite sample was added to reactions with a 50μL total volume. Reactions were conducted using a Veriti 96 well thermal cycler (Applied Biosystems) and Phusion High-Fidelity DNA polymerase (Thermo Fisher Scientific). PCR products were separated on a 1.5% agarose gel stained with ethidium bromide for visualization.

The PCR reaction volumes were as follows:

Water 34.5μL
5x Phusion HF buffer 10μL
Forward primer (10 μM)1.5μL
Reverse primer (10 μM) 1.5μL
dNTPs (10mM) 1μL
Phusion polymerase 0.5μL
parasite lysate 1μL

Total volume 50μL

The PCR program was as follows:

95°C 3.5 minutes
95°C 30 seconds
62°C 1 minute
62°C 4 minutes
4° C ∞

(steps 2 and 3 were repeated 35 times)

Confirmation of apicoplast loss

The loss of the apicoplast was confirmed via PCR with primers specific for a gene within the nuclear (Lactate Dehydrogenase), apicoplast (SufB), and mitochondrial (Cox1) genomes (**Table 3-7**). Failure to amplify a gene from the apicoplast genome, while amplifying genes from the nuclear and mitochondrial genomes would indicate loss of the organelle [31]. To collect samples for PCR, approximately 100μL of a resuspended parasite culture at ~5-10% parasitemia was placed in a 90°C heat block for 2 minutes, and then frozen at -20°C. For the PCR reaction, 1μL of the parasite sample was added to reactions with a 50μL total volume. Reactions were conducted using a Veriti 96 well thermal cycler (Applied Biosystems) and Phusion High-Fidelity DNA polymerase (Thermo Fisher Scientific). PCR products were separated by size on a 1.5% agarose gel stained with ethidium bromide. The parental PfMev line was always used as a positive control for apicoplast detection.

The PCR reaction volumes were as follows:

Water 34.5μL
5x Phusion HF buffer 10μL

Forward primer (10 μM)1.5μL
Reverse primer (10 μM) 1.5μL
dNTPs (10mM) 1μL
Phusion polymerase 0.5μL
parasite lysate 1μL
Total volume 50μL

The PCR program was as follows:

95°C 3.5 minutes
95°C 30 seconds
63°C 30 seconds
72°C 1 minute
72°C 4 minutes
4° C ∞

(steps 2-4 were repeated 35 times)

Live cell epifluorescent microscopy

For sample preparation, 100μL of parasite culture with a hematocrit of 1% and a parasitemia between 8-10% was obtained. Parasites were stained with 30nM MitoTracker CMX-Ros (Invitrogen) and 1μg/mL 4, 6-diamidino-2-phenylindole (DAPI), and incubated for 30 minutes at 37°C. Cells were then pelleted via mini-centrifuge (Fischer Scientific) for 10 seconds, and the media was aspirated and the cells were resuspended in 100μL of CMA media and incubated for 5 minutes at 37°C. This was done three times to wash the cells, with the cells being resuspended in 20μL of CMA and then pipetted onto slides and sealed with wax (2 parts paraffin, 1 part Vaseline) for observation on a Zeiss AxioImager M2 microscope. A series of images spanning 5μm were acquired with 0.2μm spacing and images were deconvolved with VOLOCITY software (PerkinElmer) to report a single combined z - stack image.

Testing mevalonate dependence in PfMev deletion mutants via growth curve

For each of the PfMev deletion lines, the parasitemia was determined via Gimesa stain, with the appropriate amount of the parental culture removed to seed quadruplicate samples with or without mevalonate. This volume was resuspended in a total of 10mL CMA and centrifuged at 1,600rcf at room temperature (~25°C) for 5 minutes, washed a second time with an additional 10mL CMA, and then resuspended in the appropriate volume of CMA, and then split equally into two tubes. To one of the tubes, the appropriate volume of a 10mM stock of mevalonate was added to bring to final concentration to 50μM mevalonate. Parasites were seeded in a 96-well plate at 0.5% starting parasitemia, 2% hematocrit, and at a total volume of 250μL per well in quadruplicate. Additionally, 150μL of the appropriate media was replaced in each well on days 1, 2, and 3. Parasite samples were collected every 24 hours for four days, and the parasitemia was counted via SYBR green staining and flow-cytometry as outlined below.

Flow cytometry for parasite growth curve determination

Growth curves were generated by staining parasites with SYBR Green and counting parasitemia via flow cytometry. In order to setup the growth curve, the parasitemia of the starting culture was determined via Giemsa stain. Based on the determined parasitemia the culture was used to seed a 96-well flat bottom cell culture plate (Corning) at a 0.5% starting parasitemia and 2% hematocrit, at a total volume of 250μL in quadruplicate. In order to minimize evaporation and edge effects, the surrounding wells were filled with 250μL of 1mM EDTA. Plates were incubated in chambers gassed with 94% N_2, 3% O_2, 3% CO_2 for 1 minute and 15 seconds, and incubated at 37°C.

Parasite samples were collected immediately after seeding and analyzed via flow cytometry to verify the starting parasitemia and then collected every 24 hours thereafter.

Samples collected on days 1-3 were diluted 1:10 in phosphate-buffered saline (PBS) and stored in a 96-well plate (Corning) at 4°C. We have previously verified that storage under these conditions and subsequent staining with SYBR Green reflects accurate parasitemia values.

On day 4 parasites were stained with SYBR Green by transferring 1μL of parasite culture, or 10μL of the 1:10 dilutions (the day 1-3 samples), to a 96-well plate containing 100μL of 1x SYBR Green (Invitrogen) in PBS. The samples were then incubated for 30 minutes on a platform Titramax 101 shaker (Heidolph) at 950rpm while protected from light. Post-incubation, 150μL of PBS was added to each well to dilute unbound SYBR Green dye. A control consisting of uninfected RBCs was also prepared in parallel and treated in the same manner as listed above.

Samples were analyzed with an Attune Nxt Flow Cytometer (Thermo Fisher Scientific). With a 50μL acquisition volume, 250μL total sample volume, and a running speed of 25μL/minute with 10,000 total events were collected within the R2 gate.

For flow cytometer gating, the R1 gate used forward-scatter area by side-scatter area to identify total RBCs from the sample. The R2 gate used forward-scatter height to identify single cells, and the R3 gate was used to measure parasitemia using fluorescence from the SYBR Green staining of parasite DNA (ratio of SYBR Green positive cells to total cells).

Parasite cloning through limiting dilution

Single cloning of each parasite line was carried out via limiting dilution. For each parasite line, the type of media used for the dilution and media change is the same as that within the flask from which the sample is derived. The parasitemia for each culture was determined using Giemsa staining, and used to calculate the number of infected RBCs

(iRBCs) per μL of culture. Based on the this iRBC concentration, a sample consisting of 1,000 iRBCs/μL in media was prepared. This sample was then diluted 1:10 thrice sequentially, yielding a parasite sample with a final concentration of 1 iRBC/μL. Then, a 2% hematocrit media was deposited into row A of a 96-well flat bottom cell culture plate (Corning, cat. #3595) at 200μL per well, followed by the diluted parasite sample at 100μL per well. Finally, a 1:3 serial dilution was carried out from row to row starting form row A and all the way down to row H. The prepared plate was placed into a Modular Incubator Chamber (Billups-Rothenberg Inc.), and gassed with 92% N_2, 3% O_2, 5% CO_2 for 1 min and 15 seconds prior to incubation at 37°C.

After seeding on day 0, the media was changed on days 5, 7, 9, 12, and 14. On days 5 and 12, a 0.5% hematocrit media was used; on days 7, 9, and 14, pure media (without any blood) was used. On day 16, selected iRBC-positive wells that are the most dilute (i.e., closest to row H) were picked and transferred into a 24-well flat bottom cell culture plate (Corning, cat. #S3524) at 2% hematocrit and 1mL total volume per well. The 24-well plate was then maintained and routinely monitored. Upon reaching a high enough parasitemia (~8%), the content within the well was transferred into a 75cm^2 sealed cell culture flask and further maintained. For each cloned parasite line, the genotype and the (nuclear, apicoplast, and mitochondrial) genome status were confirmed by genotyping PCR and SufB PCR, respectively.

FIGURES

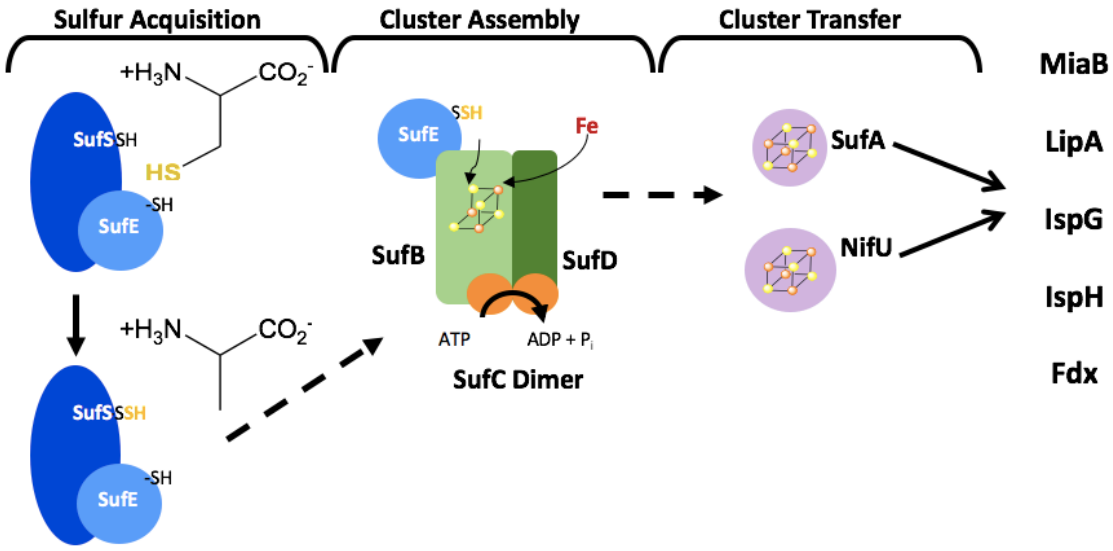

Figure 3-1 Iron-sulfur cluster assembly and transfer in the apicoplast

Iron-sulfur cluster assembly takes place in three steps: sulfur acquisition, cluster assembly and cluster transfer. Sulfur acquisition is mediated by the cysteine desulfurase SufS along with SufE. Sulfur is transferred by SufE to the SufBCD cluster assembly complex. Fe-S clusters are handed off to SufA or NifU, which transfer the Fe-S clusters to the terminal acceptors within the apicoplast: MiaB, LipA, IspG, IspH, and Fd.

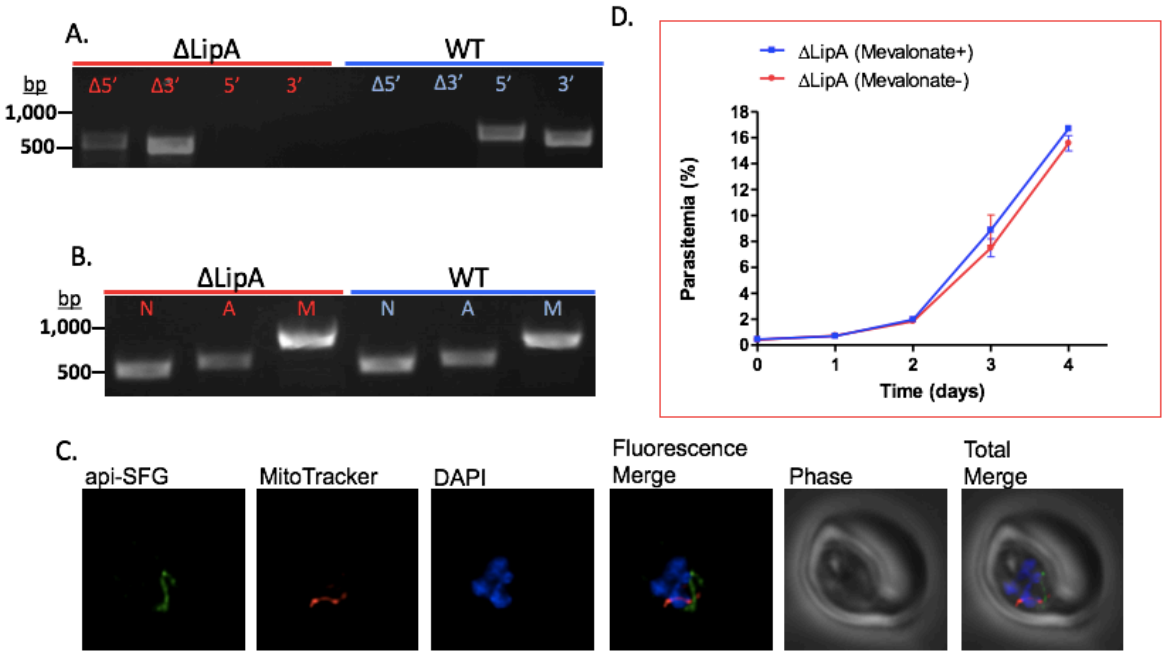

Figure 3-2 Characterization of the PfMev ΔLipA parasite line

A.) Genotyping PCR confirming deletion of the LipA locus, as compared to WT parasites

B.) PCR detection of the lactate dehydrogenase, SufB, and Cox1 genes from the nuclear (N), apicoplast (A), and mitochondrial (M) genomes, respectively. We successfully amplified SufB from the *Pf*Mev ΔLipA parasite line, indicating presence of the apicoplast organelle genome.

C.) Live fluorescence microscopy of the PfMev ΔLipA parasite line. This parasite line expresses api-SFG (green), and is also stained with mitoTracker (red) and DAPI (blue).

D.) Growth curve of PfMev ΔLipA parasites cultured with or without 50μM mevalonate.

Microscopy images are 10μM long by 10μM wide.

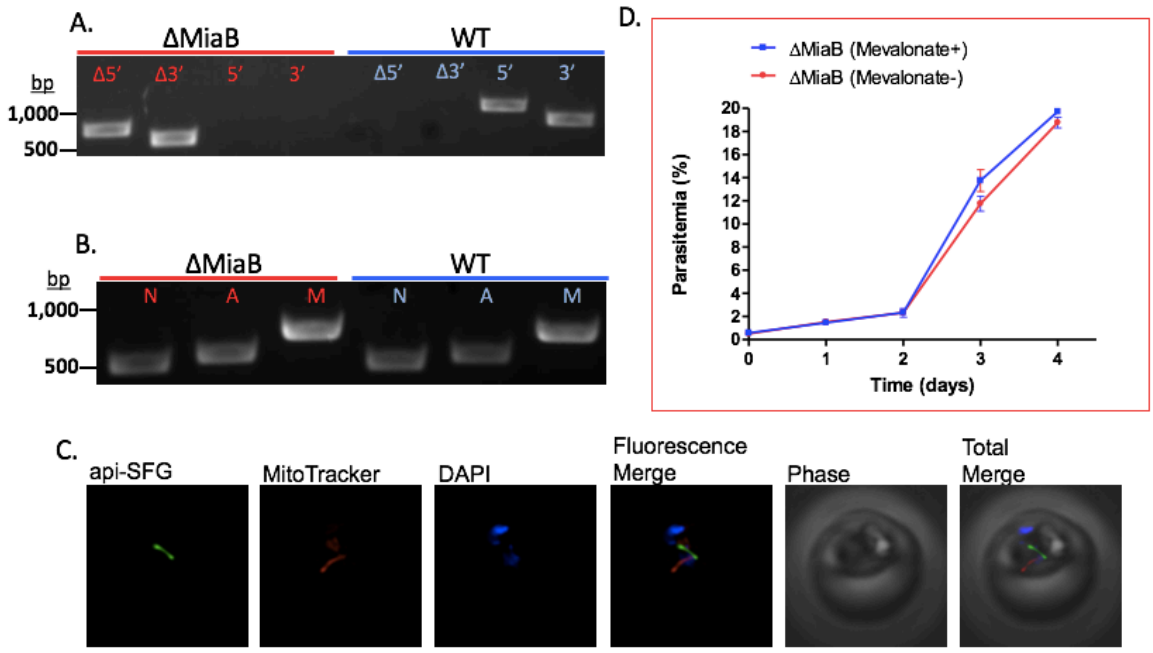

Figure 3-3 Characterization of the PfMev ΔMiaB parasite line

A.) Genotyping PCR confirming deletion of the MiaB locus, as compared to WT parasites

B.) PCR detection of the lactate dehydrogenase, SufB, and Cox1 genes from the nuclear (N), apicoplast (A), and mitochondrial (M) genomes, respectively. We successfully amplified SufB from the *Pf*Mev ΔMiaB parasite line, indicating presence of the apicoplast organelle genome.

C.) Live fluorescence microscopy of the PfMev ΔMiaB parasite line. This parasite line is expressing api-SFG (green), and is also stained with mitoTracker (red) and DAPI (blue).

D.) Growth curve of PfMev ΔMiaB parasites cultured with or without 50μM mevalonate.

Microscopy images are 10μM long by 10μM wide.

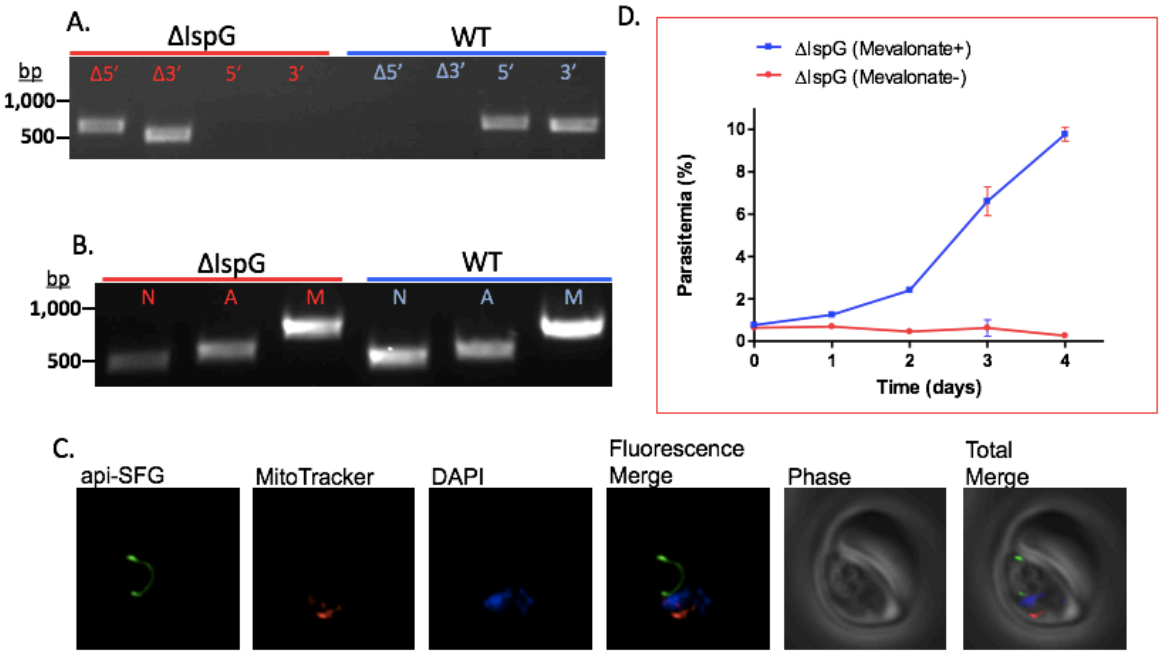

Figure 3-4 Characterization of the PfMev ΔIspG parasite line

A.) Genotyping PCR confirming deletion of the IspG locus, as compared to WT parasites

B.) PCR detection of the lactate dehydrogenase, SufB, and Cox1 genes from the nuclear (N), apicoplast (A), and mitochondrial (M) genomes, respectively. We successfully amplified SufB from the *Pf*Mev ΔIspG parasite line, indicating presence of the apicoplast organelle genome.

C.) Live fluorescence microscopy of the PfMev ΔIspG parasite line. This parasite line expresses api-SFG (green), and is also stained with mitoTracker (red) and DAPI (blue).

D.) Growth curve of PfMev ΔIspG parasites cultured with or without 50μM mevalonate.

Microscopy images are 10μM long by 10μM wide.

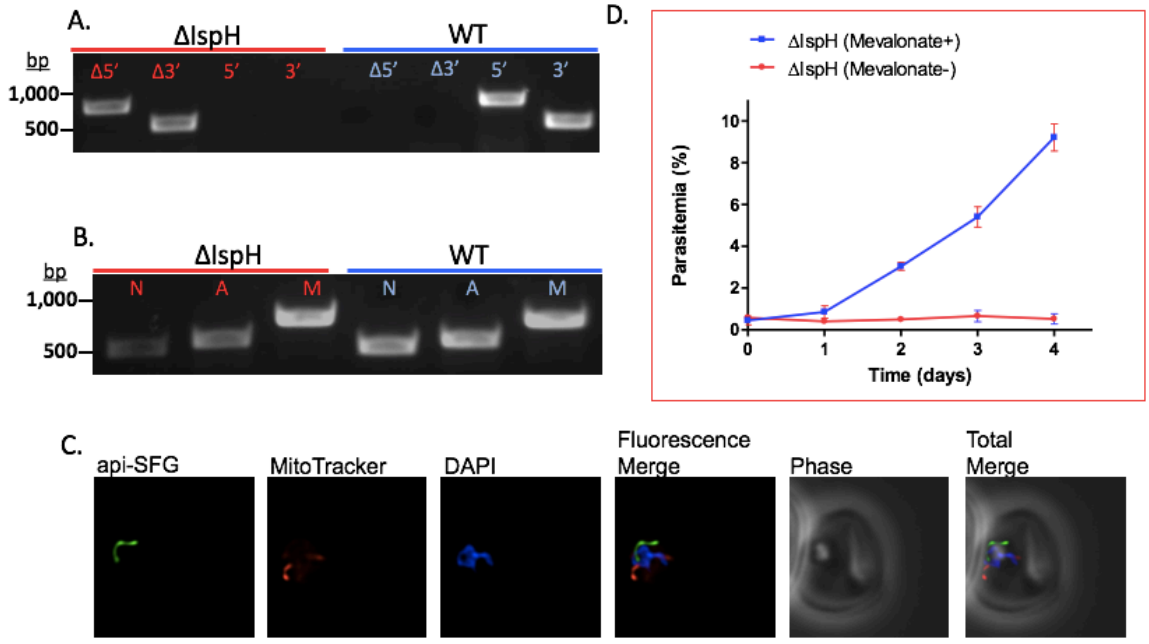

Figure 3-5 Characterization of the PfMev ΔIspH parasite line

A.) Genotyping PCR confirming deletion of the IspH locus, as compared to WT parasites

B.) PCR detection of the lactate dehydrogenase, SufB, and Cox1 genes from the nuclear (N), apicoplast (A), and mitochondrial (M) genomes, respectively. We successfully amplified SufB from the *Pf*Mev ΔIspH parasite line, indicating presence of the apicoplast organelle genome.

C.) Live fluorescence microscopy of the PfMev ΔIspH parasite line. This parasite line expresses api-SFG (green), and is also stained with mitoTracker (red) and DAPI (blue).

D.) Growth curve of PfMev ΔIspH parasites cultured with or without 50μM mevalonate.

Microscopy images are 10μM long by 10μM wide.

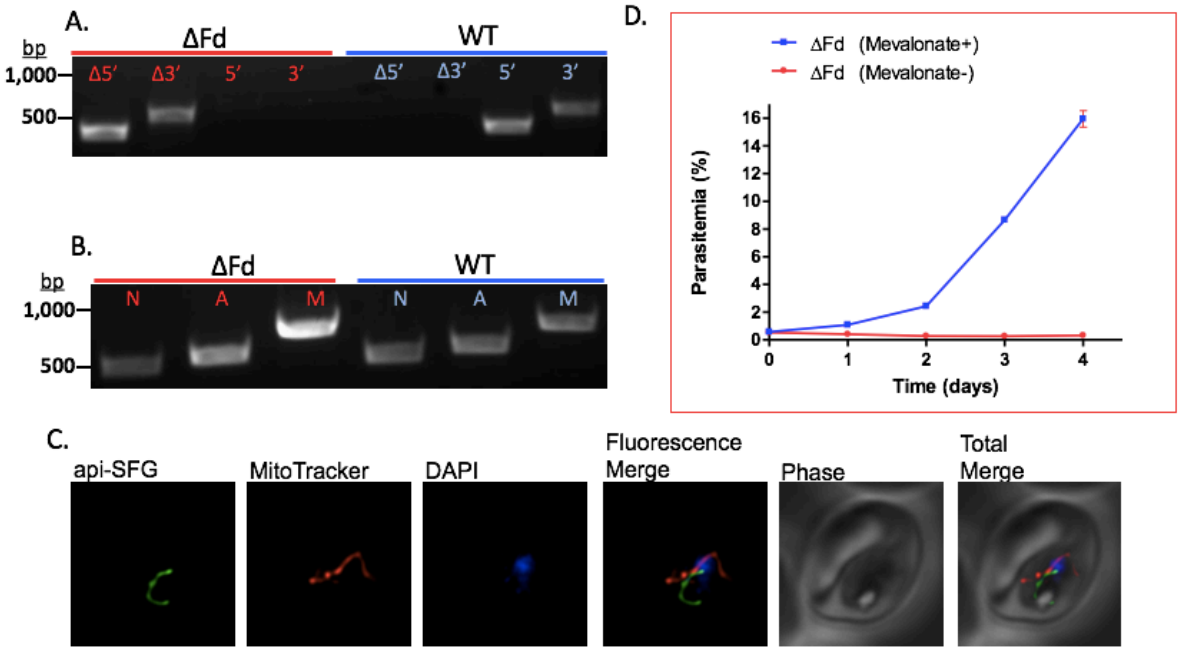

Figure 3-6 Characterization of the PfMev ΔFd parasite line

A.) Genotyping PCR confirming deletion of the Fd locus, as compared to WT parasites

B.) PCR detection of the lactate dehydrogenase, SufB, and Cox1 genes from the nuclear (N), apicoplast (A), and mitochondrial (M) genomes, respectively. We successfully amplified SufB from the *Pf*Mev ΔFd parasite line, indicating presence of the apicoplast organelle genome.

C.) Live fluorescence microscopy of the PfMev ΔFd parasite line. This parasite line expresses api-SFG (green), and is also stained with mitoTracker (red) and DAPI (blue).

D.) Growth curve of PfMev ΔFd parasites cultured with or without 50μM mevalonate.

Microscopy images are 10μM long by 10μM wide.

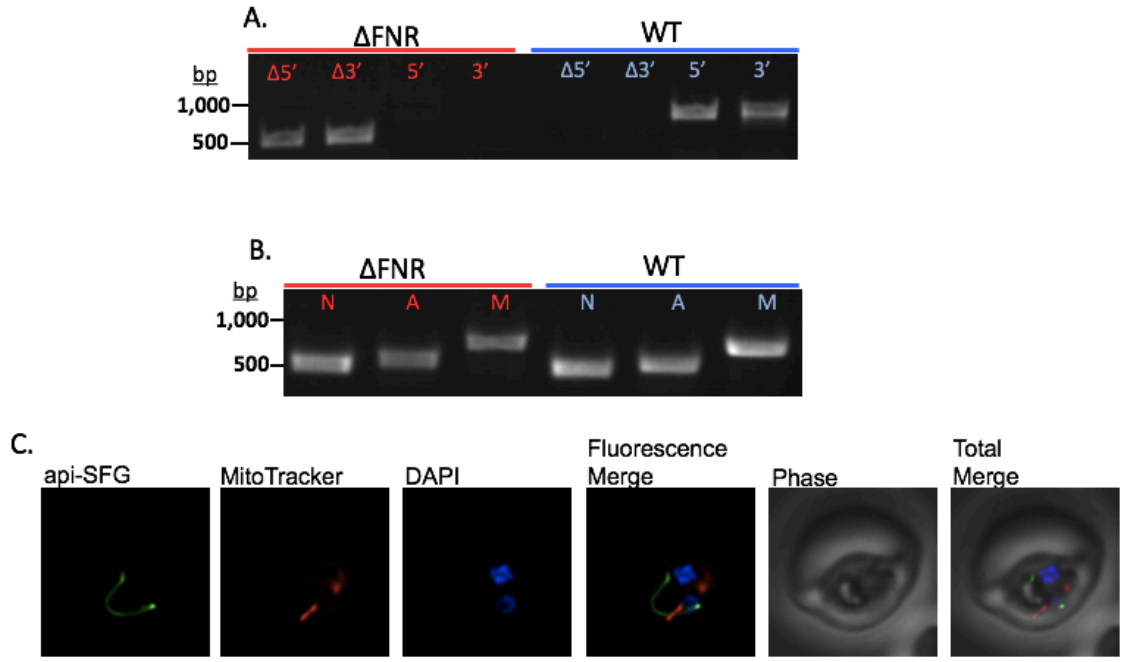

Figure 3-7 Characterization of the PfMev ΔFNR parasite line

A.) Genotyping PCR confirming deletion of the FNR locus, as compared to WT parasites

B.) PCR detection of the lactate dehydrogenase, SufB, and Cox1 genes from the nuclear (N), apicoplast (A), and mitochondrial (M) genomes, respectively. We successfully amplified SufB from the *Pf*Mev ΔFNR parasite line, indicating presence of the apicoplast organelle genome.

C.) Live fluorescence microscopy of the PfMev ΔFNR parasite line. This parasite line expresses api-SFG (green), and is also stained with mitoTracker (red) and DAPI (blue). Microscopy images are 10μM long by 10μM wide.

Table 3-1 List of potential iron-sulfur cluster binding proteins in *P. falciparum* 3D7

Gene ID	Gene Name	Signal peptide	Transit peptide	Plasmogem Phenotype (56)	PiggyBac Phenotype (142)
PF3D7_0910800	Cytosolic Fe-S cluster assembly factor NBP35	++	++	Essential	Slow
PF3D7_1344600	Lipoyl synthase	++	++	Dispensable	Essential
PF3D7_0921400	NifU-like scaffold protein	++	++	Dispensable	Essential
PF3D7_1103400	SufD Fe-S cluster assembly protein SufD	++	++	Essential	Essential
PF3D7_0716600	SufS cysteine desulfurase	++	++	Slow	Slow/ Dispensable
PF3D7_0522700	SufA iron-sulfur assembly protein	++	++	Dispensable	Essential
PF3D7_1318100	ferredoxin	++	++	Essential	Slow/ Dispensable
PF3D7_0622200	Radical SAM protein	+	++	Dispensable	Dispensable
PF3D7_1022800	IspG 4-hydroxy-3-methylbut-2-en-1-yl diphosphate synthase	+	++	Essential	Essential
PF3D7_0910900	DNA primase large subunit	-	++	Essential	Essential
PF3D7_1342100	Aconitate hydratase	-	++	Essential	Slow/ Dispensable
PF3D7_1214600	Adrenodoxin-type ferredoxin	-	++	Essential	Slow/ Essential
PF3D7_1454500	ISU iron-sulfur cluster assembly protein	-	++	Essential	Essential
PF3D7_0207200	IscA1 iron-sulfur assembly protein	-	++	Essential	Essential
PF3D7_0727200	NFS cysteine desulfurase	-	++	Essential	Slow/ Essential
PF3D7_0720400	Apoptosis-inducing factor	-	++	NA	Dispensable
PF3D7_0614800	Endonuclease III homologue	-	++	NA	Dispensable

PF3D7_1220500	ribosome biogenesis protein TSR3	-	++	NA	Essential
PF3D7_1361600	Fe-S assembly protein IscX	-	++	NA	Essential
PF3D7_1439400	Cytochrome b-c1 complex subunit Rieske	-	++	NA	Dispensable
PF3D7_0927300	Fumarate hydratase	-	++	NA	Essential
PF3D7_1212800	Iron-sulfur subunit of succinate dehydrogenase	-	++	Dispensable	Dispensable
PF3D7_0709200	Glutaredoxin-like protein	-	++	Dispensable	Dispensable
PF3D7_0416700	CDGSH iron-sulfur domain-containing protein	-	++	Dispensable	Dispensable
PF3D7_0930900	NifU-like protein	-	++	Dispensable	Dispensable
PF3D7_1306300	SAM dependent methyltransferase	-	++	Dispensable	Dispensable
PF3D7_API04700	SufB Fe-S cluster assembly protein SufB	-	++	NA	NA
PF3D7_1472700	DNA-directed RNA polymerase, alpha subunit	+	+	NA	Essential
PF3D7_1406900	Radical SAM protein	-	+	Essential	Essential
PF3D7_0322500	IscA2 iron-sulfur assembly protein	-	+	NA	Dispensable
PF3D7_0824600	Fe-S cluster assembly protein DRE2	-	-	Essential	Essential
PF3D7_1017000	DNA polymerase delta catalytic subunit	-	-	Essential	Essential
PF3D7_0934100	TFIIH basal transcription factor complex helicase XPD subunit	-	-	Essential	Essential
PF3D7_1128500	Fe-S cluster assembly protein	-	-	Essential	Essential
PF3D7_1227800	Elongator complex protein 3	-	-	Essential	Dispensable/Slow
PF3D7_1022900	CDGSH iron-sulfur domain-containing protein	-	-	Essential	Dispensable

PF3D7_0524900	tRNA-YW synthesizing protein	-	-	Essential	Dispensable
PF3D7_1458700	Exonuclease V, mitochondrial	-	-	Slow	Essential
PF3D7_1238800	Acyl-CoA synthetase	-	-	Slow	Essential
PF3D7_1435300	NAD(P)H-dependent glutamate synthase	-	-	Slow	Dispensable
PF3D7_0606900	Glutaredoxin-like protein	-	-	Slow	Essential
PF3D7_1408400	FANCJ-like helicase	-	-	Slow	Essential
PF3D7_1143300	DNA-directed RNA polymerases I and III subunit RPAC1	-	-	NA	Essential
PF3D7_0515800	BolA-like protein	-	-	NA	Essential
PF3D7_1415200	DNA-directed RNA polymerases I and III subunit RPAC2	-	-	NA	Essential
PF3D7_1413800	Diphthamide biosynthesis protein 1	-	-	NA	Slow/ Dispensable
PF3D7_0923000	DNA-directed RNA polymerase II subunit RPB3	-	-	NA	Essential
PF3D7_0614200	Cytosolic Fe-S cluster assembly factor NAR1	-	-	NA	Essential
PF3D7_1324500	DEAD box helicase	-	-	NA	Essential
PF3D7_0302700	CDGSH iron-sulfur domain-containing protein	-	-	NA	Essential
PF3D7_1129500	A/G-specific adenine glycosylase	-	-	Dispensable	Dispensable
PF3D7_0306300	Glutaredoxin 1	-	-	Dispensable	Essential
PF3D7_0104400	IspH 4-hydroxy-3-methylbut-2-enyl diphosphate reductase	-	-	NA	Dispensable
PF3D7_1368200	ABC transporter E family member 1	-	0	Essential	Essential

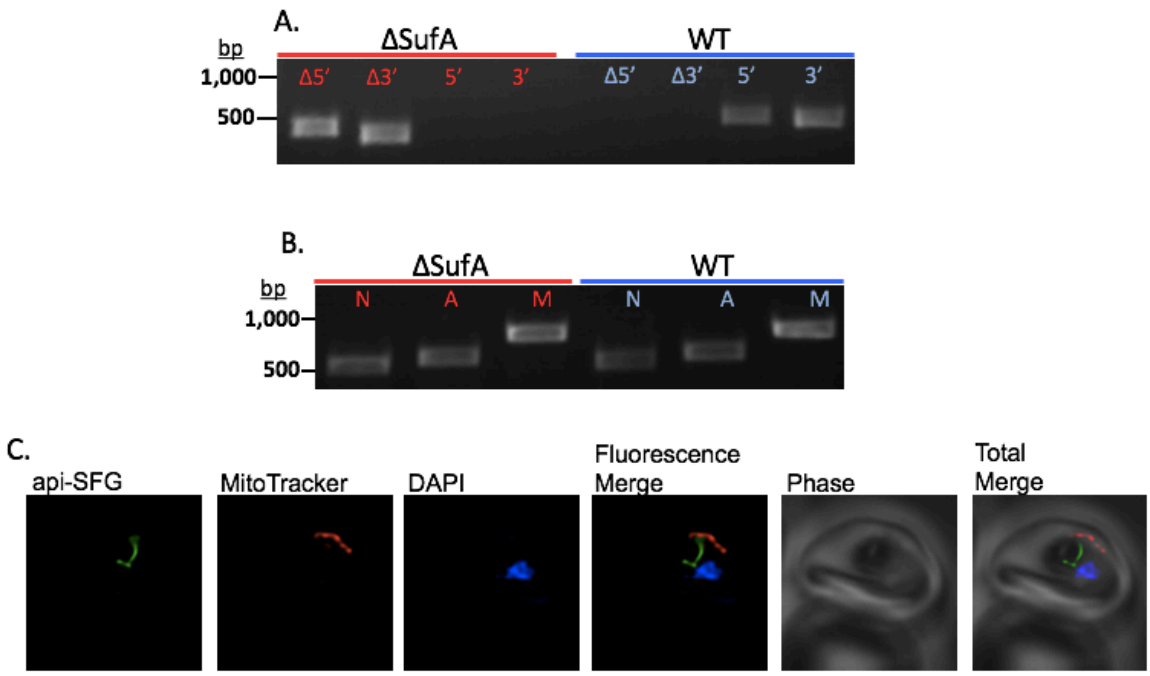

Figure 3-8 Characterization of the PfMev ΔSufA parasite line

A.) Genotyping PCR confirming deletion of the SufA locus, as compared with WT parasites B.) PCR detection of the lactate dehydrogenase, SufB, and Cox1 genes from the nuclear (N), apicoplast (A), and mitochondrial (M) genomes, respectively. We successfully amplified SufB from the *Pf*Mev ΔSufA parasite line, indicating presence of the apicoplast organelle genome. C.) Live fluorescence microscopy of the PfMev ΔSufA parasite line. This parasite line expresses api-SFG (green), and is also stained with mitoTracker (red) and DAPI (blue). D.) Growth curve of PfMev ΔSufA parasites cultured with or without 50μM mevalonate. Microscopy images are 10μM long by 10μM wide.

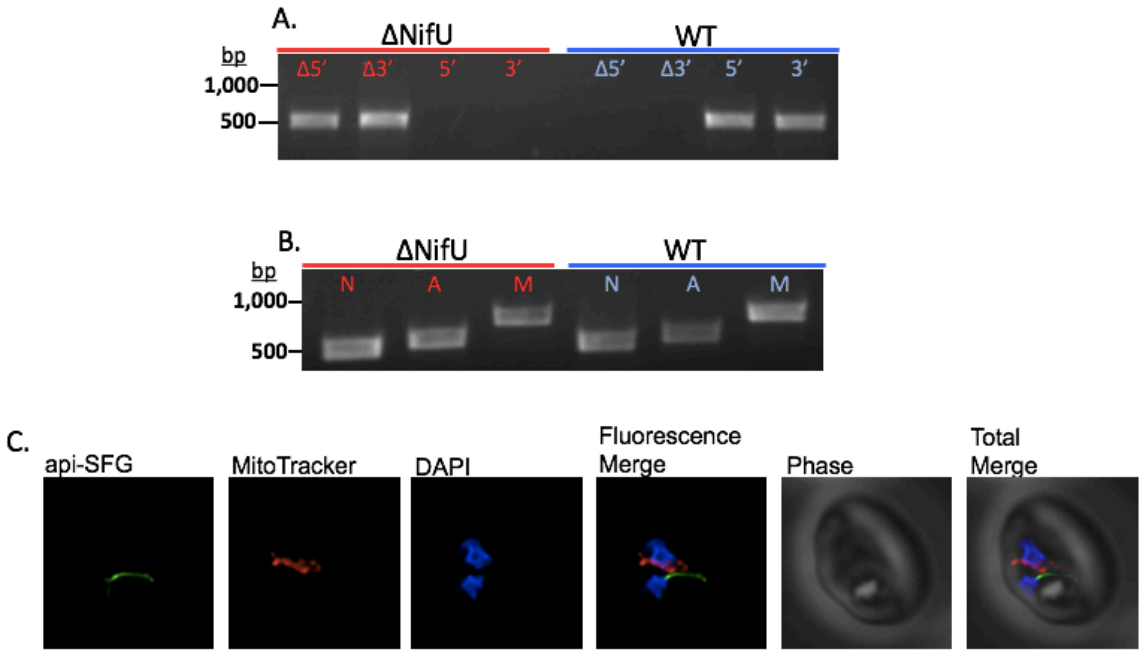

Figure 3-9 Characterization of the PfMev ΔNifU parasite line

A.) Genotyping PCR confirming deletion of the NifU locus, as compared with WT parasites B.) PCR detection of the lactate dehydrogenase, SufB, and Cox1 genes from the nuclear (N), apicoplast (A), and mitochondrial (M) genomes, respectively. We successfully amplified SufB from the *Pf*Mev ΔNifU parasite line, indicating presence of the apicoplast organelle genome. C.) Live fluorescence microscopy of the PfMev ΔNifU parasite line. This parasite line expresses api-SFG (green), and is also stained with mitoTracker (red) and DAPI (blue). D.) Growth curve of PfMev ΔNifU parasites cultured with or without 50μM mevalonate. Microscopy images are 10μM long by 10μM wide.

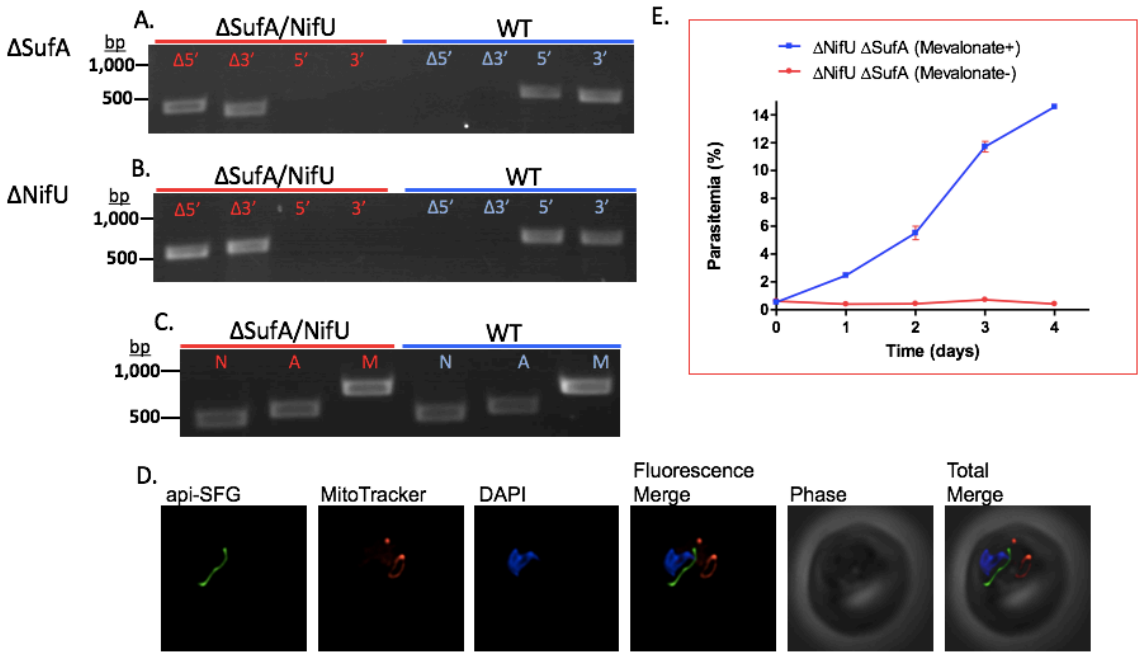

Figure 3-10 Characterization of the PfMev ΔSufA/NifU parasite line

A.) Genotyping PCR confirming deletion of the SufA locus in the PfMev ΔSufA/ΔNifU line, as compared with WT parasites

B.) Genotyping PCR confirming deletion of the NifU locus in the PfMev ΔSufA/ΔNifU line, as compared with WT parasites

C.) PCR detection of the lactate dehydrogenase, SufB, and Cox1 genes from the nuclear (N), apicoplast (A), and mitochondrial (M) genomes, respectively. We successfully amplified SufB from the *Pf*Mev ΔSufA/ΔNifU parasite line, indicating presence of the apicoplast organelle genome.

D.) Live fluorescence microscopy of the PfMev ΔSufA/ΔNifU parasite line. This parasite line expresses api-SFG (green), and is also stained with mitoTracker (red) and DAPI (blue).

E.) Growth curve of PfMev ΔSufA/ΔNifU parasites supplemented with either 50μM or 0μM mevalonate.

Microscopy images are 10μM long by 10μM wide.

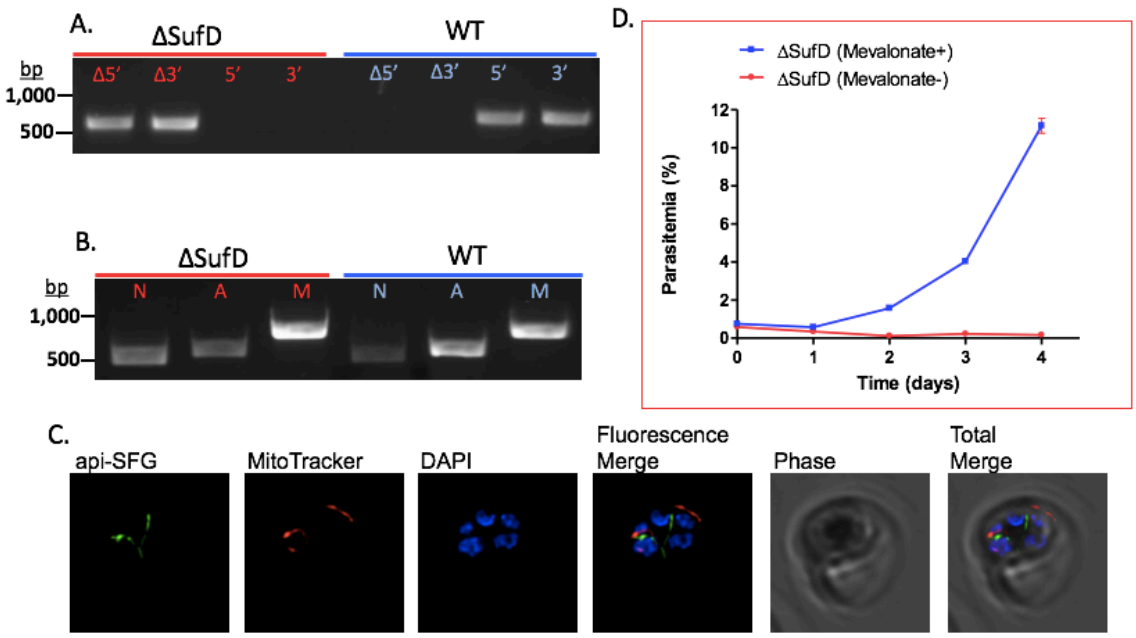

Figure 3-11 Characterization of the PfMev ΔSufD parasite line

A.) Genotyping PCR confirming deletion of the SufD locus, as compared with WT parasites B.) PCR detection of the lactate dehydrogenase, SufB, and Cox1 genes from the nuclear (N), apicoplast (A), and mitochondrial (M) genomes, respectively. We successfully amplified SufB from the *Pf*Mev ΔSufD parasite line, indicating presence of the apicoplast organelle genome. C.) Live fluorescence microscopy of the PfMev ΔSufD parasite line. This parasite line expresses api-SFG (green), and is also stained with mitoTracker (red) and DAPI (blue). D.) Growth curve of PfMev ΔSufD parasites cultured with or without 50μM mevalonate. Microscopy images are 10μM long by 10μM wide.

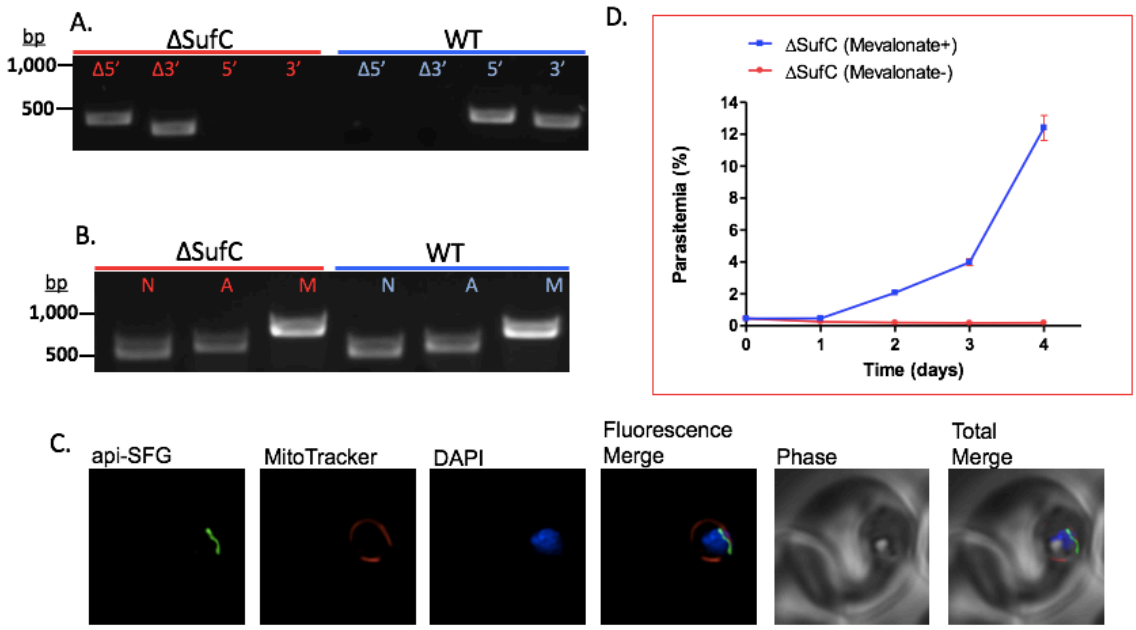

Figure 3-12 Characterization of the PfMev ΔSufC parasite line

A.) Genotyping PCR confirming deletion of the SufC locus, as compared with WT parasites B.) PCR detection of the lactate dehydrogenase, SufB, and Cox1 genes from the nuclear (N), apicoplast (A), and mitochondrial (M) genomes, respectively. We successfully amplified SufB from the *Pf*Mev ΔSufC parasite line, indicating presence of the apicoplast organelle genome. C.) Live fluorescence microscopy of the PfMev ΔSufC parasite line. This parasite line expresses api-SFG (green), and is also stained with mitoTracker (red) and DAPI (blue). D.) Growth curve of PfMev ΔSufC parasites cultured with or without 50μM mevalonate. Microscopy images are 10μM long by 10μM wide.

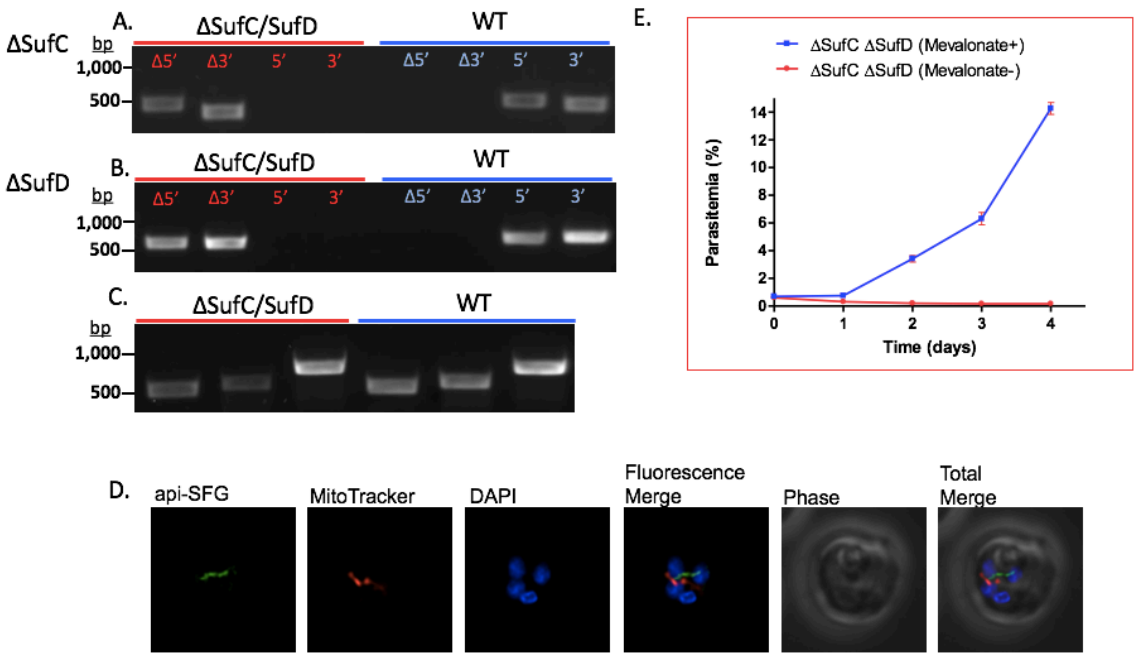

Figure 3-13 Characterization of the PfMev ΔSufC/SufD parasite line

A.) Genotyping PCR confirming deletion of the SufC locus in the ΔSufC/SufD line, as compared with WT parasites

B.) Genotyping PCR confirming deletion of the SufD locus in the ΔSufC/SufD line, as compared with WT parasites

C.) PCR detection of the lactate dehydrogenase, SufB, and Cox1 genes from the nuclear (N), apicoplast (A), and mitochondrial (M) genomes, respectively. We successfully amplified SufB from the *Pf*Mev ΔSufC/ΔSufD parasite line, indicating presence of the apicoplast organelle genome.

D.) Live fluorescence microscopy of the PfMev ΔSufC/SufD parasite line. This parasite line expresses api-SFG (green), and is also stained with mitoTracker (red) and DAPI (blue).

E.) Growth curve of PfMev ΔSufC/SufD parasites supplemented with either 50μM or 0μM mevalonate

Microscopy images are 10μM long by 10μM wide.

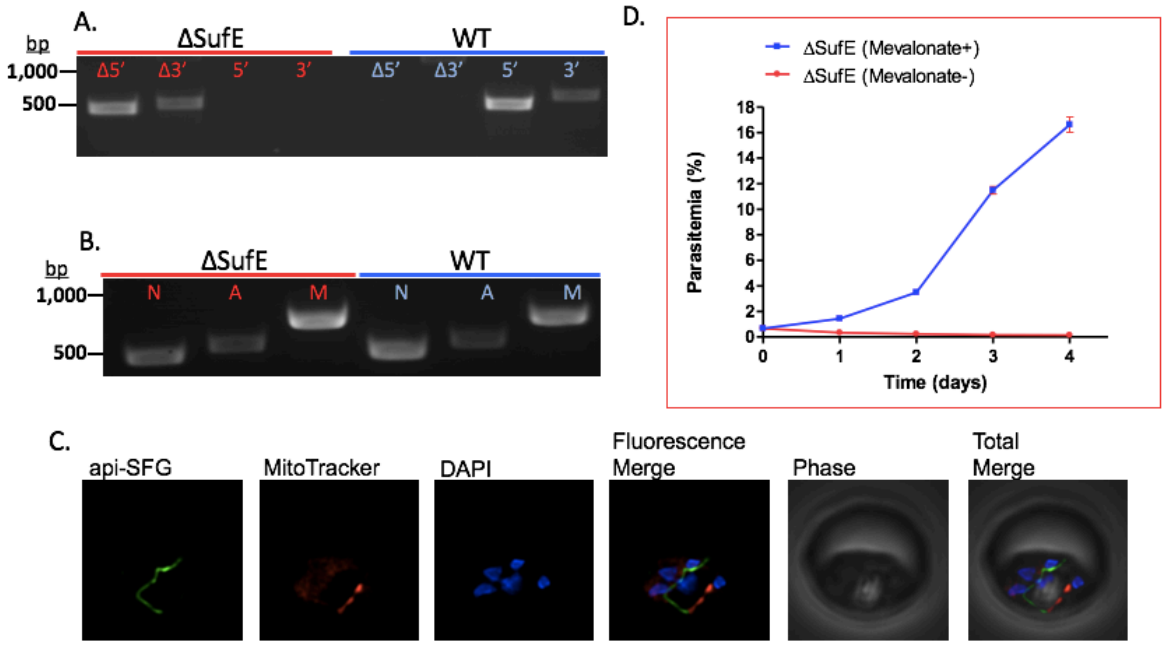

Figure 3-14 Characterization of the PfMev ΔSufE parasite line

A.) Genotyping PCR confirming deletion of the SufE locus, as compared with WT parasites B.) PCR detection of the lactate dehydrogenase, SufB, and Cox1 genes from the nuclear (N), apicoplast (A), and mitochondrial (M) genomes, respectively. We successfully amplified SufB from the *Pf*Mev ΔSufE parasite line, indicating presence of the apicoplast organelle genome. C.) Live fluorescence microscopy of the PfMev ΔSufE parasite line. This parasite line expresses api-SFG (green), and is also stained with mitoTracker (red) and DAPI (blue). D.) Growth curve of PfMev ΔSufE parasites cultured with or without 50μM mevalonate. Microscopy images are 10μM long by 10μM wide.

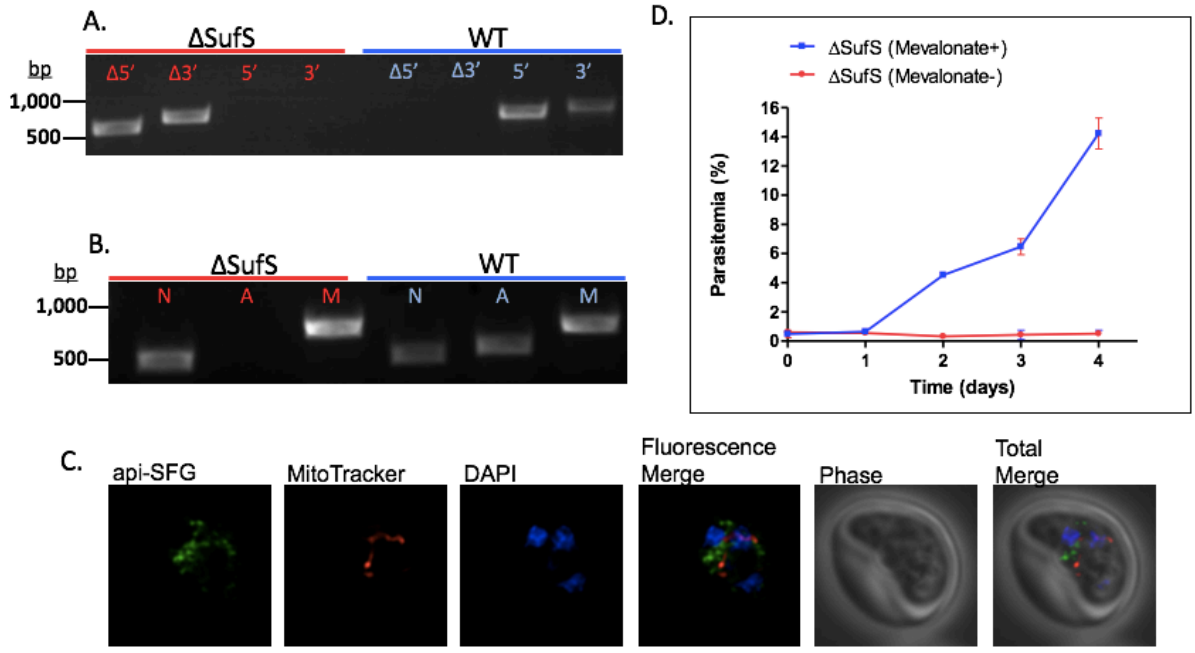

Figure 3-15 Characterization of the PfMev ΔSufS parasite line

A.) Genotyping PCR confirming deletion of the SufS locus, as compared with WT parasites

B.) PCR detection of the lactate dehydrogenase, SufB, and Cox1 genes from the nuclear (N), apicoplast (A), and mitochondrial (M) genomes, respectively. We were unsuccessful in amplifying SufB from the *Pf*Mev ΔSufS parasite line, indicating loss of the apicoplast organelle genome.

C.) Live fluorescence microscopy of the PfMev ΔSufS parasite line. This parasite line expresses api-SFG (green), and is also stained with mitoTracker (red) and DAPI (blue).

D.) Growth curve of PfMev ΔSufS parasites cultured with or without 50μM mevalonate. Microscopy images are 10μM long by 10μM wide.

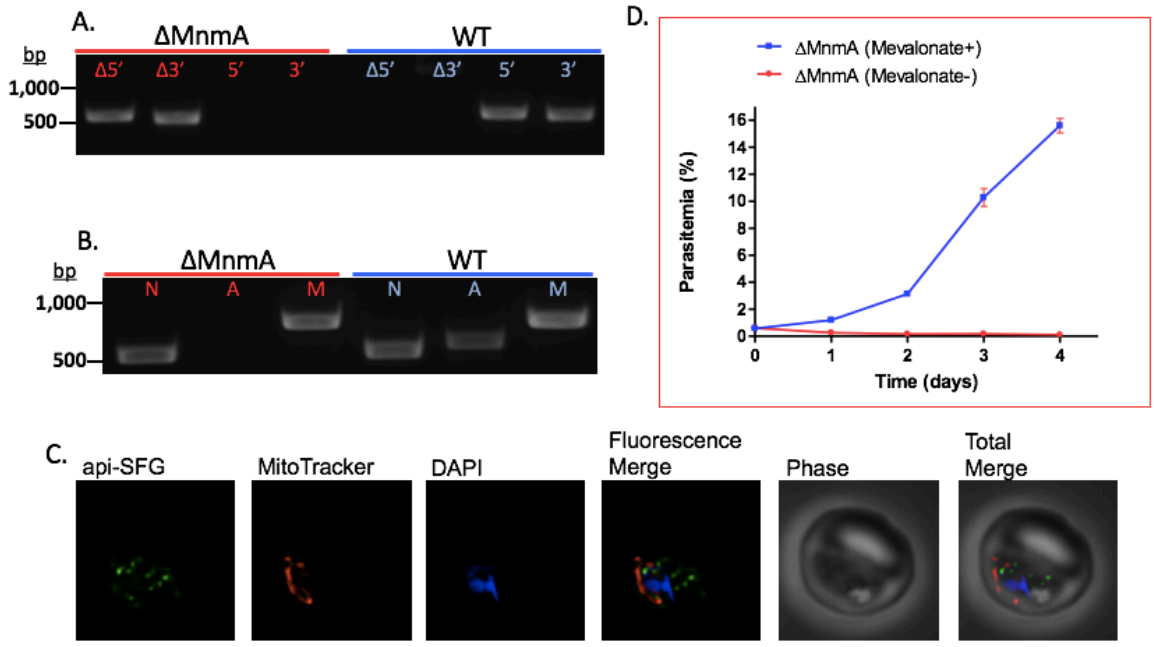

Figure 3-16 Characterization of the PfMev ΔMnmA parasite line

A.) Genotyping PCR confirming deletion of the MnmA locus, as compared with WT parasites

B.) PCR detection of the lactate dehydrogenase, SufB, and Cox1 genes from the nuclear (N), apicoplast (A), and mitochondrial (M) genomes, respectively. We were unsuccessful in amplifying SufB from the *Pf*Mev ΔSufS parasite line, indicating loss of the apicoplast organelle genome.

C.) Live fluorescence microscopy of the PfMev ΔMnmA parasite line. This parasite line expresses api-SFG (green), and is also stained with mitoTracker (red) and DAPI (blue).

D.) Growth curve of PfMev ΔMnmA parasites cultured with or without 50μM mevalonate.

Microscopy images are 10μM long by 10μM wide.

Table 3-2 Resulting apicoplast-specific gene deletion phenotypes

Gene ID	Gene Name	Phenotype
PF3D7_1344600	LipA	Nonessential
PF3D7_0622200	MiaB	Nonessential
PF3D7_1022800	IspG	Essential
PF3D7_0104400	IspH	Essential
PF3D7_1318100	Ferredoxin (Fd)	Essential
PF3D7_0623200	Ferredoxin reductase (FNR)	Essential
PF3D7_0522700	SufA	Nonessential
PF3D7_0921400	NifU	Nonessential
See above	SufA + NifU	Essential
PF3D7_1103400	SufD	Essential
PF3D7_1413500	SufC	Essential
PF3D7_0206100	SufE	Essential
PF3D7_0716600	SufS	Essential and Maintenance
PF3D7_1019800	MnmA	Essential and Maintenance

Table 3-3 Primer sequences used to amplify homology arms for genetic knock outs

Primer Name	Primer Sequence
SufS HA1 F	GCCACGAGCGGCGCTTAATAAATATTTTCTATTATGTCAT
SufS HA1 R	AAGCGCAGCGGCATTATATTATTTCTTCATTTTATTACC
SufS HA2 F	CGACAGACGCCGGTAGTAATATAATAACTAATGTTTCTAA
SufS HA2 R	GGCCACCAGCCGGTGTGTTATAAAAATATATGGATATCC
MiaB HA1 F	GCCACGAGCGGCCTTAGCAGGAGGAGGAACGTATTAC
MiaB HA1 R	AAGCGCAGCGGCCTAAATGGGTCCATGTTATTATCTGTAG
MiaB HA2 F	CGACAGACGCCGGTTTTTCTGATATAGAAAATGAATATTG
MiaB HA2R	GGCCACCAGCCGGTACGCACCCACATACAATAATTTTTAT
Fd HA1 F	GCCACGAGCGGCCACCAAAAAGGCTATTGCATCAATAAAC
Fd HA1 R	AAGCGCAGCGGCCTCAAAAATAATTTACTCTTTTGGCTTC
Fd HA2 F	CGACAGACGCCGGTAGTTGTTCTACATGCGCAGCAAAAT
Fd HA2 R	GGCCACCAGCCGGAGGAAATTTTATCATTCCCCATTTCAA
FNR HA1 F	GCCACGAGCGGCCTGAAAATTCGTTTCGTCTTTATCTTGT
FNR HA1 R	AAGCGCAGCGGCCTTCCAAATATTTAAAGAGACCAT
FNR HA2 F	CGACAGACGCCGGTGCACATGGATATTTTAATTTACCA
FNR HA2 R	GGCCACCAGCCGGTCATGACTTTTCAAAATATCCATAAC
LipA HA1 F	GTGCCACGAGCGGCCCCCATCCCTTTTTTACTTGTATATC
LipA HA1 R	TTAAGCGCAGCGGCCCAGCTACATGAAACCAGTCTG
LipA HA2 F	TTCGACAGACGCCGGGCTAGTCATTTTGCTAAAACAGTAG
LipA HA2 R	ATGGCCACCAGCCGGCGAACTAAAGGGCCGCTG
IspH HA1 F	GTGCCACGAGCGGCCATGTCAGTTACCACATTTTGTTC
IspH HA1 R	TTAAGCGCAGCGGCCCTTATCTGTTCTTGTTTTCCGAAG
IspH HA2 F	TCGACAGACGCCGGGATTGTGCACTTATCGTACAAAAACT
IspH HA2 R	ATGGCCACCAGCCGGTGCAAGAGATTCTTGGGAAGC

IspG HA1 F	GTGCCACGAGCGGCCTCCCAACACGAGAAGTAGTTATTG
IspG HA1 R	TTAAGCGCAGCGGCCCTACCATACCTAATGGTGTATCTCC
IspG HA2 F	TTCGACAGACGCCGGGCAGGAAGTTGTTTGATGGAT
IspG HA2 R	TGGCCACCAGCCGGCAATTTATCACAAGCTTCTTCCTCAG
SufA HA1 F	GCCACGAGCGGCCACCAAAAAGGCTATTGCATCAATAAAC
SufA HA1 R	AAGCGCAGCGGCCTCAAAAATAATTTACTCTTTTGGCTTC
SufA HA2 F	CGACAGACGCCGGTAGTTGTTCTACATGCGCAGCAAAAT
SufA HA2 R	GGCCACCAGCCGGAGGAAATTTTATCATTCCCCATTTCAA
NifU HA1 F	GCCACGAGCGGCCGAACGGTTCAGGTAAAATTTAGAAAAA
NifU HA1 R	AAGCGCAGCGGCCCTAAGGTTTTTCACATACACAAAAAAA
NifU HA2 F	CGACAGACGCCGGGTTCCCTACATTAACTGTTAATTTTGA
NifU HA2 R	GGCCACCAGCCGGTCCTTTTATTTATTTGTTTGTTTGTTT
SufC HA1 F	GCCACGAGCGGCCTATGCATCCTTTTGAAACCCTTCAACT
SufC HA1 R	AAGCGCAGCGGCCTTGTTATTTTCCATATGCACGACATTC
SufC HA2 F	CGACAGACGCCGGAGGAGAAAAAAAAAGAAATGAAATATT
SufC HA2 R	GGCCACCAGCCGGCTATTCCTTAAGAAATTGAGAGTACCCC
SufD HA1 F	GCCACGAGCGGCCTTTGATTATGTTGAGAGTAAACATTGG
SufD HA1 R	AAGCGCAGCGGCCAAATGGGTAGCATTATTAATCTTTAGA
SufD HA2 F	CGACAGACGCCGGATGGATTCTCAAGAATTTGTTTAGAAG
SufD HA2 R	GGCCACCAGCCGGGTGATTTGCACATTCTATATCACTTGG
SufE HA1 F	GCCACGAGCGGCCTTGTTTTCGGGCATACCATTTAATATGC
SufE HA1 R	AAGCGCAGCGGCCTGGAGATTACTGAAAAATAAATTGGAGTCA
SufE HA2 F	CGACAGACGCCGGCAGGGGTGTCAATCGGTAGTATATATTTAC
SufE HA2 R	GGCCACCAGCCGGTGTCCATATTCTTCAATATATTGGTGCAGA
MnmA HA1 F	GCCACGAGCGGCCATCATTTTGTAAATCTATTAAGGTCACACA
MnmA HA1 R	AAGCGCAGCGGCCTATAGCCATAAATAAAATTTCATCACACC

MnmA HA2 F	CGACAGACGCCGGAGGGGAAATTACCTGCATGTATAAAAAAG
MnmA HA2 R	GGCCACCAGCCGGCAAGAAATTGATTACTTATTGTTGCTGAAC

Table 3-4 Oligonucleotides designed for In-Fusion insertion of gRNA sequences

Name	Oligonucleotide Sequence
SufS gRNA F	TAAGTATATAATATTAAATTTAAACCATTGTTATAGTTTTAGAGCTAGAA
SufS gRNA R	TTCTAGCTCTAAAACTATAACAATGGTTTAAATTTAATATTATATACTTA
MiaB gRNA F	TAAGTATATAATATTTGCTTATCAACATCTTCCTCGTTTTAGAGCTAGAA
MiaB gRNA R	TTCTAGCTCTAAAACGAGGAAGATGTTGATAAGCAAATATTATATACTTA
Fd gRNA F	TAAGTATATAATATTTTACCATATAGTTGTAGGGGGTTTTAGAGCTAGAA
Fd gRNA R	TTCTAGCTCTAAAACCCCCTACAACTATATGGTAAAATATTATATACTTA
FNR gRNA F	TAAGTATATAATATTTATTTGGAAGGCCATACTTGGTTTTAGAGCTAGAA
FNR gRNA R	TTCTAGCTCTAAAACCAAGTATGGCCTTCCAAATAAATATTATATACTTA
LipA gRNA F	TAAGTATATAATATTAGAGATGATTTACCAGATGGGTTTTAGAGCTAGAA
LipA gRNA R	TTCTAGCTCTAAAACCCATCTGGTAAATCATCTCTAATATTATATACTTA
IspH gRNA F	TAAGTATATAATATTTACACAAACCACACTAAGTAGTTTTAGAGCTAGAA
IspH gRNA R	TTCTAGCTCTAAAACTACTTAGTGTGGTTTGTGTAAATATTATATACTTA
IspG gRNA F	TAAGTATATAATATTACCATTAGGTATGGTAGAATGTTTTAGAGCTAGAA
IspG gRNA R	TTCTAGCTCTAAAACATTCTACCATACCTAATGGTAATATTATATACTTA
SufA gRNA F	TAAGTATATAATATTAGTAATGATTTAATTAGTGGGTTTTAGAGCTAGAA
SufA gRNA R	TTCTAGCTCTAAAACCCACTAATTAAATCATTACTAATATTATATACTTA
NifU gRNA F	TAAGTATATAATATTTGTCATATTGTAAGATGCTAGTTTTAGAGCTAGAA
NifU gRNA R	TTCTAGCTCTAAAACTAGCATCTTACAATATGACAAATATTATATACTTA
SufC gRNA F	TAAGTATATAATATTGTTAATTATGGATTTAGTGGGTTTTAGAGCTAGAA
SufC gRNA R	TTCTAGCTCTAAAACCCACTAAATCCATAATTAACAATATTATATACTTA
SufD gRNA F	TAAGTATATAATATTAGTAATAGTGGACTAGTTAAGTTTTAGAGCTAGAA
SufD gRNA R	TTCTAGCTCTAAAACTTAACTAGTCCACTATTACTAATATTATATACTTA
SufE gRNA F	TAAGTATATAATATTATATAATCTACACATAACAGGTTTTAGAGCTAGAA
SufE gRNA R	TTCTAGCTCTAAAACCTGTTATGTGTAGATTATATAATATTATATACTTA

MnmA gRNA F	TAAGTATATAATATTACAATATAAAATGGATAGAGGTTTTAGAGCTAGAA
MnmA gRNA R	TTCTAGCTCTAAAACCTCTATCCATTTTATATTGTAATATTATATACTTA

Table 3-5 Primer sequences used for confirmation of gene deletions

Primer Name	Primer Sequence
pl8insHA1R	TACAAAATGCTTAAGCGCAGCGGCC
pl8insHA2F	CATATTTATTAAATCTAGAATTCGACAGACGCCG
SufS 5'F	CAGAAAATGAGTGAGTTTTATAAAAAGGAAAACTC
SufS 3'R	CAATTTGCTGTGCCAAATATTTGATTTC
SufS 5'WT R	CCATATAACAATGGTTTAAATTTATATTTTGATG
SufS 3' WT F	CCAGATATATTAATAACATCTGGTCATAAATTTTG
MiaB 5'F	GATATTAAATGGGAAAGCAAAACTTATAAGTTTTTTATTC
MiaB 3'R	GTGATACATTTTCAAATATCTCCATATCTTTTTCTG
MiaB 5' WT R	GATGTTGATAAGCATTCCAAGTCATATTCTC
MiaB 3' WT F	GGATGTGCTCATAATAGTTCAGATTCTG
Fd 5'F	CTGGTATATTATAGTTTATATTTAATAAGAAAAGGGC
Fd 3'R	GGTAGCGAAGTTAATACATACACATATATATATGTG
Fd 5' WT R	CGAATGTAATGAAGATGAATATATATTAGATGCTAG
Fd 3' WT F	GGTAGCGAAGTTAATACATACACATATATATATGTG
FNR 5' F	GAGAAGTTTTCTTTATATCATCCTATTTTTTTTGTCATAT
FNR 3' R	AACTAGTACACCTCAACGTGCACCCTT
FNR 5' WT R	CCTGAACAATAACCATAATTTGTAATATTGGGAG
FNR 3' WT F	GTGGTATTATACCTTACTATAATGAACTTGATAATAATCC
LipA 5' F	CCTACATAAACTGTAATGTTTCAATATGACC
LipA 3' R	GGTTAACTAAATTTTTTATAAAATATTCACCTGC
LipA 5' WT R	GTGCTTCTTCACATACGGTATGTAAG
LipA 3' WT F	CTTTCAATACAGCTAAAGCTATATGTGAATG
IspH 5' F	CCAGTAAGCAAAATATATCCATTCTGTATAC
IspH 3' R	TGTGATTTCATTTTTCTCTTTCTTTTATCA

IspH 5' WT R	GGGTACATATATATTTTTCGATTCCCATC
IspH 3' WT F	CCATTAAATAAAAAGTTATTCTATGTTACACAAACC
IspG 5' F	CTAAATGAAGAAGGGAATTCTTCAAAAAAG
IspG 3' R	CATATTCAATTTATGGATCTTTCCATTTG
IspG 5' WT R	CAATACATAAATCAGAAAACTCAAAAGCC
IspG 3' WT F	GTATTAATAACCAGAAGAATTAATGAACTTTTACAATC
SufA 5'F	CTTTTTTCTCCTTTTAATATTAAAAAGAAAAAAG
SufA 3'R	CCTAAAGATATATATTTATGTGTTATCTTATATATTTTTG
SufA 5' WTR	GCTCTTATTGTTATATAAAAATGTTTTTGGAG
SufA 3' WTF	GATATAGAACGAAATTGAAGAAGATGATTATATAC
NifU 5'F	ATACGAAATGAAATTAGTTTTTTAATAATATATTTATACC
NifU 3'R	CGTTAATGTGGAGAAAATTCAAAGACCTAC
NifU 5' WTR	CGAAATTATTTTGTATAAATAACACCTTTGC
NifU 3' WTF	CACACAACGTTAAAAATGAAATAACAGAAAG
SufE 5'F	CATTTCATTCATTTTGGTAGTTAAAAAGAAAAGG
SufE 3'R	TCATTTTATTAAAAACATATTTCATTTAATTTGTAAGA
SufE 5'WT R	CATGAGCATATTATATATAAAACAAAGAAATGTGC
SufE 3' WT F	CCTGATAAACATAAAATTAGACAAAATCAAGTTTTGG
SufC 5'F	GGGATTTGTCATACATATAAATATGTATAAAAAGGTCC
SufC 3'R	TAAGTACAAAATAATATCATATGTACATTATAAAATCCAC
SufC 5'WT R	CTTCTTCTAAATTTTTTAATAAAGATAATCTATCCATATC
SufC 3' WT F	GAGATAAGTGTAAGTGAATTTAATTTAATGATGATAGAAG
SufD 5'F	GTGTATATAATTTTTTGAAAAAAATGATTTAGCTAACACA
SufD 3'R	CAGATATTCCTCTTGTCATTAATGAGAAGATTGG
SufD 5'WT R	GTGTTTTCTCTTCATTTTGATGTCTATAGTTTTTTATAC
SufD 3' WT F	CCAATAACAAATCCTAGATTAGTTGTATATGTAAAAGG

MnmA 5'F	CTACTTTGATGTTTTTTTATTTTTGCACATTTTATG
MnmA 3'R	GGTATTTTTTATTTGCTCATGTTTAAATCATTTATCTG
MnmA 5'WT R	CTTTATACTATTGTTTCTTTGTTCGTCTTCATCAATTTG
MnmA 3' WT F	CTTACTAAAAATTATGACCAAGATTTATTTACACATATACG

Table 3-6 Primer sequences used to detect genes from the nuclear and organellar genomes

Primer Name	Primer Sequence
LDH F	GGAGATGTAGTTTTGTTCGATATTG
LDH R	CTTGTAAAGGGATACCACCTACAG
SufB F	CATGTAGCTATAGTAGAAATAATAGTAAAAGATTATGG
SufB R	GACTCTGAAATACTTAAACCACGTTGC
Cox1 F	CTTCATCTTTAAGAATAATTGCACAAGAAAATGTAAATC
Cox1 R	GTACATATGATGTACCCATACTAAGCTTCC

Table 3-7 Primer sequences used to generate the pRSng SufA (BSD) plasmid

Primer Name	Primer Sequence
pRsBSD F	ACCTAATAGAAATATATCAGGATCCATGGCAAAACCTTTG
pRsBSD R	TCTATTATTAAATAAGCTTATTCCCAAACATAACCAGATG

REFERENCES

1. Trape JF. The public health impact of chloroquine resistance in Africa. Am J Trop Med Hyg 64:12–7.

2. Dondorp MA, Nosten F, Yi P, Das D, Phyo PA, Tarning J, Lwin MK, Ariey F, Hanpithakpong W, Lee JS, Ringwald P, Silamut K, Imwong M, Chotivanich K, Lim P, Herdman T, An S Sen, Yeung S, Singhasivanon P, Day JNP, Lindegardh N, Socheat D, White JN. 2009. Artemisinin resistance in *Plasmodium falciparum* malaria. N Engl J Med 361:455–467.

3. Lim L, McFadden GI. 2010. The evolution, metabolism and functions of the apicoplast. Philos Trans R Soc Lond B Biol Sci 365:749–63.

4. Yeh E, DeRisi LJ. 2011. Chemical rescue of malaria parasites lacking an apicoplast defines organelle function in blood-stage *Plasmodium falciparum*. PLoS Biol 9.

5. Mukherjee A, Sadhukhan CG. 2016. Anti-malarial Drug Design by Targeting Apicoplasts: New Perspectives. J pharmacopuncture 19:7–15.

6. Gisselberg EJ, Dellibovi-Ragheb AT, Matthews AK, Bosch G, Prigge TS. 2013. The suf iron-sulfur cluster synthesis pathway is required for apicoplast maintenance in malaria parasites. PLoS Pathog 9.

7. Haussig MJ, Matuschewski K, Kooij ATW. 2014. Identification of vital and dispensable sulfur utilization factors in the *Plasmodium* apicoplast. PLoS One 9.

8. Fontecave M. 2006. Iron-sulfur clusters: ever-expanding roles. Nat Chem Biol 2:171–174.

9. Johnson CD, Dean RD, Smith DA, Johnson KM. 2003. Structure, function, and formation of biological iron-sulfur clusters. Annu Rev Biochem 74:247–281.

10. Lill R. 2009. Function and biogenesis of iron-sulphur proteins. Nature 460:831–838.

11. Lill R, Mühlenhoff U. 2004. Iron-sulfur protein biogenesis in eukaryotes: components and mechanisms. Annu Rev Cell Dev Biol 22:457–486.

12. Stehling O, Lill R. 2013. The role of mitochondria in cellular iron-sulfur protein biogenesis: mechanisms, connected processes, and diseases. Cold Spring Harb Perspect Biol 5.

13. Sharma KA, Pallesen JL, Spang JR, Walden EW. 2010. Cytosolic iron-sulfur cluster assembly (CIA) system: factors, mechanism, and relevance to cellular iron regulation. J Biol Chem 285:26745–26751.

14. Fontecave M, Ollagnier-de-Choudens S. 2008. Iron–sulfur cluster biosynthesis in bacteria: Mechanisms of cluster assembly and transfer. Arch Biochem Biophys

474:226–237.

15. Balk J, Pilon M. 2011. Ancient and essential: the assembly of iron–sulfur clusters in plants. Trends Plant Sci 16:218–226.

16. Takahashi Y, Tokumoto U. 2002. A third bacterial system for the assembly of iron-sulfur clusters with homologs in archaea and plastids. J Biol Chem 277:28380–28383.

17. Dellibovi-Ragheb AT, Gisselberg EJ, Prigge TS. 2013. Parasites FeS up: iron-sulfur cluster biogenesis in eukaryotic pathogens. PLoS Pathog 9.

18. Seeber F. 2002. Biogenesis of iron-sulphur clusters in amitochondriate and apicomplexan protists. Int J Parasitol 32:1207–1217.

19. Sato S, Rangachari K, Wilson MRJ. 2003. Targeting GFP to the malarial mitochondrion. Mol Biochem Parasitol 130:155–158.

20. Ellis EK, Clough B, Saldanha WJ, Wilson JR. 2001. Nifs and Sufs in malaria. Mol Microbiol 41:973–981.

21. Charan M, Singh N, Kumar B, Srivastava K, Siddiqi IM, Habib S. 2014. Sulfur mobilization for Fe-S cluster assembly by the essential SUF pathway in the *Plasmodium falciparum* apicoplast and its inhibition. Antimicrob Agents Chemother 58:3389–3398.

22. Loiseau L, Ollagnier-de-Choudens S, Nachin L, Fontecave M, Barras F. 2003. Biogenesis of Fe-S cluster by the bacterial Suf system: SufS and SufE form a new type of cysteine desulfurase. J Biol Chem 278:38352–38359.

23. Outten WF, Wood JM, Munoz MF, Storz G. 2003. The SufE protein and the SufBCD complex enhance SufS cysteine desulfurase activity as part of a sulfur transfer pathway for Fe-S cluster assembly in *Escherichia coli*. J Biol Chem 278:45713–45719.

24. Layer G, Gaddam AS, Ayala-Castro NC, Ollagnier-de Choudens S, Lascoux D, Fontecave M, Outten WF. 2007. SufE transfers sulfur from SufS to SufB for iron-sulfur cluster assembly. J Biol Chem 282:13342–13350.

25. Hirabayashi K, Yuda E, Tanaka N, Katayama S, Iwasaki K, Matsumoto T, Kurisu G, Outten WF, Fukuyama K, Takahashi Y, Wada K. 2015. Functional Dynamics Revealed by the Structure of the SufBCD Complex, a Novel ATP-binding Cassette (ABC) Protein That Serves as a Scaffold for Iron-Sulfur Cluster Biogenesis. J Biol Chem 290:29717–29731.

26. Saini A, Mapolelo TD, Chahal KH, Johnson KM, Outten WF. 2010. SufD and SufC ATPase activity are required for iron acquisition during in vivo Fe-S cluster formation on SufB. Biochemistry 49:9402–9412.

27. Chahal KH, Dai Y, Saini A, Ayala-Castro C, Outten WF. 2009. The SufBCD Fe-S scaffold complex interacts with SufA for Fe-S cluster transfer. Biochemistry

48:10644–10653.

28. Gupta V, Sendra M, Naik GS, Chahal KH, Huynh HB, Outten WF, Fontecave M, de Choudens S. 2009. Native *Escherichia coli* SufA, coexpressed with SufBCDSE, purifies as a [2Fe-2S] protein and acts as an Fe-S transporter to Fe-S target enzymes. J Am Chem Soc 131:6149–6153.

29. Py B, Gerez C, Angelini S, Planel R, Vinella D, Loiseau L, Talla E, Brochier-Armanet C, Garcia Serres R, Latour J-M, Ollagnier-de Choudens S, Fontecave M, Barras F. 2012. Molecular organization, biochemical function, cellular role and evolution of NfuA, an atypical Fe-S carrier. Mol Microbiol 86:155–171.

30. Wilson RJ, Denny PW, Preiser PR, Rangachari K, Roberts K, Roy A, Whyte A, Strath M, Moore DJ, Moore PW, Williamson DH. 1996. Complete gene map of the plastid-like DNA of the malaria parasite *Plasmodium falciparum*. J Mol Biol 261:155–72.

31. Kumar B, Chaubey S, Shah P, Tanveer A, Charan M, Siddiqi IM, Habib S. 2011. Interaction between sulphur mobilisation proteins SufB and SufC: evidence for an iron-sulphur cluster biogenesis pathway in the apicoplast of *Plasmodium falciparum*. Int J Parasitol 41:991–999.

32. Pala RZ, Saxena V, Saggu SG, Yadav KS, Pareek PR, Kochar KS, Kochar KD, Garg S. 2016. Structural and functional characterization of an iron-sulfur cluster assembly scaffold protein-SufA from *Plasmodium* vivax. Gene 585:159–165.

33. Haussig MJ, Matuschewski K, Kooij ATW. 2013. Experimental Genetics of *Plasmodium* berghei NFU in the Apicoplast Iron-Sulfur Cluster Biogenesis Pathway. PLoS One 8.

34. Wrenger C, Müller S. 2004. The human malaria parasite *Plasmodium falciparum* has distinct organelle-specific lipoylation pathways. Mol Microbiol 53:103–113.

35. Thomsen-Zieger N, Schachtner J, Seeber F. 2003. Apicomplexan parasites contain a single lipoic acid synthase located in the plastid. FEBS Lett 547:80–6.

36. Pierrel F, Björk RG, Fontecave M, Atta M. 2002. Enzymatic modification of tRNAs: MiaB is an iron-sulfur protein. J Biol Chem 277:13367–13370.

37. Ralph SA, van Dooren GG, Waller RF, Crawford MJ, Fraunholz MJ, Foth BJ, Tonkin CJ, Roos DS, McFadden GI. 2004. Tropical infectious diseases: metabolic maps and functions of the *Plasmodium falciparum* apicoplast. Nat Rev Microbiol 2:203–16.

38. Hernández HL, Pierrel F, Elleingand E, García-Serres R, Huynh BH, Johnson MK, Fontecave M, Atta M. 2007. MiaB, a Bifunctional Radical- *S*- Adenosylmethionine Enzyme Involved in the Thiolation and Methylation of tRNA, Contains Two Essential [4Fe-4S] Clusters †. Biochemistry 46:5140–5147.

39. Moore JA, Poulter CD. 1997. *Escherichia coli* Dimethylallyl Diphosphate:tRNA Dimethylallyltransferase: A Binding Mechanism for Recombinant Enzyme †. Biochemistry 36:604–614.

40. Leung CH, Chen Y, Winkler EM. 1997. Regulation of substrate recognition by the MiaA tRNA prenyltransferase modification enzyme of *Escherichia coli* K-12. J Biol Chem 272:13073–13083.

41. Saggu SG, Garg S, Pala RZ, Yadav KS, Kochar KS, Kochar KD, Saxena V. 2017. Characterization of 4-hydroxy-3-methylbut-2-en-1-yl diphosphate synthase (IspG) from *Plasmodium vivax* and it's potential as an antimalarial drug target. Int J Biol Macromol 96:466–473.

42. Röhrich CR, Englert N, Troschke K, Reichenberg A, Hintz M, Seeber F, Balconi E, Aliverti A, Zanetti G, Köhler U, Pfeiffer M, Beck E, Jomaa H, Wiesner J. 2005. Reconstitution of an apicoplast-localised electron transfer pathway involved in the isoprenoid biosynthesis of *Plasmodium falciparum*. FEBS Lett 579:6433–6438.

43. Balconi E, Pennati A, Crobu D, Pandini V, Cerutti R, Zanetti G, Aliverti A. 2009. The ferredoxin-NADP+ reductase/ferredoxin electron transfer system of *Plasmodium falciparum*. FEBS J 276:3825–3836.

44. Vollmer M, Thomsen N, Wiek S, Seeber F. 2001. Apicomplexan parasites possess distinct nuclear-encoded, but apicoplast-localized, plant-type ferredoxin-NADP+ reductase and ferredoxin. J Biol Chem 276:5483–5490.

45. Jordan WS, Cronan EJ. 2003. The Escherichia coli lipB gene encodes lipoyl (octanoyl)-acyl carrier protein: protein transferase. J Bacteriol 185:1582–1589.

46. Foth JB, Stimmler ML, Handman E, Crabb SB, Hodder NA, McFadden IG. 2005. The malaria parasite *Plasmodium falciparum* has only one pyruvate dehydrogenase complex, which is located in the apicoplast. Mol Microbiol 55:39–53.

47. van Schaijk LBC, Kumar STR, Vos WM, Richman A, van Gemert G-J, Li T, Eappen GA, Williamson CK, Morahan JB, Fishbaugher M, Kennedy M, Camargo N, Khan MS, Janse JC, Sim LK, Hoffman LS, Kappe ISH, Sauerwein WR, Fidock AD, Vaughan MA. 2014. Type II fatty acid biosynthesis is essential for *Plasmodium falciparum* sporozoite development in the midgut of Anopheles mosquitoes. Eukaryot Cell 13:550–559.

48. Günther S, Storm J, Müller S. 2009. *Plasmodium falciparum*: organelle-specific acquisition of lipoic acid. Int J Biochem Cell Biol 41:748–752.

49. Ghorbal M, Gorman M, Macpherson CR, Martins RM, Scherf A, Lopez-Rubio J-J. 2014. Genome editing in the human malaria parasite *Plasmodium falciparum* using the CRISPR-Cas9 system. Nat Biotechnol 32:819–21.

50. Gisselberg JE, Dellibovi-Ragheb TA, Matthews KA, Bosch G, Prigge ST. 2013. The

suf iron-sulfur cluster synthesis pathway is required for apicoplast maintenance in malaria parasites. PLoS Pathog 9:e1003655.

51. Seeber F, Soldati-Favre D. 2010. Metabolic Pathways in the Apicoplast of Apicomplexa. Int Rev Cell Mol Biol 281:161–228.

52. Seeber F, Aliverti A, Zanetti G. 2005. The plant-type ferredoxin-NADP+ reductase/ferredoxin redox system as a possible drug target against apicomplexan human parasites. Curr Pharm Des 11:3159–72.

53. Bahl A, Brunk B, Crabtree J, Fraunholz JM, Gajria B, Grant RG, Ginsburg H, Gupta D, Kissinger CJ, Labo P, Li L, Mailman DM, Milgram JA, Pearson SD, Roos SD, Schug J, Stoeckert JC, Whetzel P. 2003. PlasmoDB: the *Plasmodium* genome resource. A database integrating experimental and computational data. Nucleic Acids Res 31:212–215.

54. Valasatava Y, Rosato A, Banci L, Andreini C. 2016. MetalPredator: a web server to predict iron-sulfur cluster binding proteomes. Bioinformatics 32:2850–2852.

55. Foth JB, Ralph AS, Tonkin JC, Struck SN, Fraunholz M, Roos SD, Cowman FA, McFadden IG. 2003. Dissecting apicoplast targeting in the malaria parasite *Plasmodium falciparum*. Science 299:705–708.

56. Schwach F, Bushell E, Gomes AR, Anar B, Girling G, Herd C, Rayner JC, Billker O. 2015. PlasmoGEM, a database supporting a community resource for large-scale experimental genetics in malaria parasites. Nucleic Acids Res 43:D1176-82.

57. Zhang M, Wang C, Otto TD, Oberstaller J, Liao X, Adapa SR, Udenze K, Bronner IF, Casandra D, Mayho M, Brown J, Li S, Swanson J, Rayner JC, Jiang RHY, Adams JH. 2018. Uncovering the essential genes of the human malaria parasite *Plasmodium falciparum* by saturation mutagenesis. Science 360:eaap7847.

58. Lu J, Yang J, Tan G, Ding H. 2008. Complementary roles of SufA and IscA in the biogenesis of iron-sulfur clusters in *Escherichia coli*. Biochem J 409:535–543.

59. Nachin L, Loiseau L, Expert D, Barras F. 2003. SufC: an unorthodox cytoplasmic ABC/ATPase required for [Fe-S] biogenesis under oxidative stress. EMBO J 22:427–437.

60. Schilke B, Voisine C, Beinert H, Craig E. 1999. Evidence for a conserved system for iron metabolism in the mitochondria of *Saccharomyces cerevisiae*. Proc Natl Acad Sci U S A 96:10206–11.

61. Uhrigshardt H, Singh A, Kovtunovych G, Ghosh M, Rouault TA. 2010. Characterization of the human HSC20, an unusual DnaJ type III protein, involved in iron–sulfur cluster biogenesis. Hum Mol Genet 19:3816–3834.

62. Chillappagari S, Seubert A, Trip H, Kuipers OP, Marahiel MA, Miethke M. 2010.

Copper stress affects iron homeostasis by destabilizing iron-sulfur cluster formation in *Bacillus subtilis*. J Bacteriol 192:2512–24.

63. Ye H, Rouault TA. 2010. Human iron-sulfur cluster assembly, cellular iron homeostasis, and disease. Biochemistry 49:4945–56.

64. Wollers S, Layer G, Garcia-Serres R, Signor L, Clemancey M, Latour J-M, Fontecave M, Ollagnier de Choudens S. 2010. Iron-sulfur (Fe-S) cluster assembly: the SufBCD complex is a new type of Fe-S scaffold with a flavin redox cofactor. J Biol Chem 285:23331–41.

65. Nachin L, El Hassouni M, Loiseau L, Expert D, Barras F. 2001. SoxR-dependent response to oxidative stress and virulence of Erwinia chrysanthemi: the key role of SufC, an orphan ABC ATPase. Mol Microbiol 39:960–72.

66. Pérard J, Ollagnier de Choudens S. 2018. Iron–sulfur clusters biogenesis by the SUF machinery: close to the molecular mechanism understanding. JBIC J Biol Inorg Chem 23:581–596.

67. Boyd ES, Thomas KM, Dai Y, Boyd JM, Outten FW. 2014. Interplay between Oxygen and Fe–S Cluster Biogenesis: Insights from the Suf Pathway. Biochemistry 53:5834–5847.

68. Wada K, Sumi N, Nagai R, Iwasaki K, Sato T, Suzuki K, Hasegawa Y, Kitaoka S, Minami Y, Outten FW, Takahashi Y, Fukuyama K. 2009. Molecular Dynamism of Fe–S Cluster Biosynthesis Implicated by the Structure of the SufC2–SufD2 Complex. J Mol Biol 387:245–258.

69. Ollagnier-de-Choudens S, Lascoux D, Loiseau L, Barras F, Forest E, Fontecave M. 2003. Mechanistic studies of the SufS-SufE cysteine desulfurase: evidence for sulfur transfer from SufS to SufE. FEBS Lett 555:263–267.

70. Huet G, Daffe M, Saves I. 2005. Identification of the *Mycobacterium tuberculosis* SUF Machinery as the Exclusive Mycobacterial System of [Fe-S] Cluster Assembly: Evidence for Its Implication in the Pathogen's Survival. J Bacteriol 187:6137–6146.

71. H. M, N. E. 2002. Bacterial cysteine desulfurases: their function and mechanisms. Appl Microbiol Biotechnol 60:12–23.

72. Black KA, Dos Santos PC. 2015. Abbreviated Pathway for Biosynthesis of 2-Thiouridine in *Bacillus subtilis*. J Bacteriol 197:1952–62.

73. Palenchar PM, Buck CJ, Cheng H, Larson TJ, Mueller EG. 2000. Evidence that ThiI, an enzyme shared between thiamin and 4-thiouridine biosynthesis, may be a sulfurtransferase that proceeds through a persulfide intermediate. J Biol Chem 275:8283–6.

74. Ikeuchi Y, Shigi N, Kato J, Nishimura A, Suzuki T. 2006. Mechanistic Insights into

Sulfur Relay by Multiple Sulfur Mediators Involved in Thiouridine Biosynthesis at tRNA Wobble Positions. Mol Cell 21:97–108.

75. and RK, Lauhon* CT. 2003. MnmA and IscS Are Required for *in Vitro* 2-Thiouridine Biosynthesis in *Escherichia coli*†.

76. Cilingir G, Broschat SL, Lau AOT. 2012. ApicoAP: The First Computational Model for Identifying Apicoplast-Targeted Proteins in Multiple Species of Apicomplexa. PLoS One 7:e36598.

77. Umeda N, Suzuki T, Yukawa M, Ohya Y, Shindo H, Watanabe K, Suzuki T. 2005. Mitochondria-specific RNA-modifying enzymes responsible for the biosynthesis of the wobble base in mitochondrial tRNAs. Implications for the molecular pathogenesis of human mitochondrial diseases. J Biol Chem 280:1613–24.

78. Nilsson K, Lundgren HK, Hagervall TG, Björk GR. 2002. The cysteine desulfurase IscS is required for synthesis of all five thiolated nucleosides present in tRNA from *Salmonella enterica* serovar typhimurium. J Bacteriol 184:6830–5.

79. Agris PF. 1991. Wobble position modified nucleosides evolved to select transfer RNA codon recognition: a modified-wobble hypothesis. Biochimie 73:1345–9.

80. Ogle JM, Brodersen DE, Clemons WM, Tarry MJ, Carter AP, Ramakrishnan V. 2001. Recognition of Cognate Transfer RNA by the 30S Ribosomal Subunit. Science (80-) 292:897–902.

81. Urbonavicius J, Qian Q, Durand JM, Hagervall TG, Björk GR. 2001. Improvement of reading frame maintenance is a common function for several tRNA modifications. EMBO J 20:4863–4873.

82. Cicchillo MR, Lee K-H, Baleanu-Gogonea C, Nesbitt MN, Krebs C, Booker JS. 2004. *Escherichia coli* lipoyl synthase binds two distinct [4Fe-4S] clusters per polypeptide. Biochemistry 43:11770–11781.

83. Miller RJ, Busby WR, Jordan WS, Cheek J, Henshaw FT, Ashley WG, Broderick BJ, Cronan EJ, Marletta AM. 2000. Escherichia coli LipA is a lipoyl synthase: in vitro biosynthesis of lipoylated pyruvate dehydrogenase complex from octanoyl-acyl carrier protein. Biochemistry 39:15166–15178.

84. Günther S, Wallace L, Patzewitz E-M, McMillan JP, Storm J, Wrenger C, Bissett R, Smith KT, Müller S. 2007. Apicoplast lipoic acid protein ligase B is not essential for *Plasmodium falciparum*. PLoS Pathog 3.

85. Cobbold SA, Vaughan AM, Lewis IA, Painter HJ, Camargo N, Perlman DH, Fishbaugher M, Healer J, Cowman AF, Kappe SHI, Llinás M. 2013. Kinetic flux profiling elucidates two independent acetyl-CoA biosynthetic pathways in *Plasmodium falciparum*. J Biol Chem 288:36338–50.

86. Esberg B, Leung HC, Tsui HC, Björk GR, Winkler ME. 1999. Identification of the miaB gene, involved in methylthiolation of isopentenylated A37 derivatives in the tRNA of *Salmonella typhimurium* and *Escherichia coli*. J Bacteriol 181:7256–65.

87. Thompson MK, Gottesman S. 2014. The MiaA tRNA modification enzyme is necessary for robust RpoS expression in *Escherichia coli*. J Bacteriol 196:754–761.

88. Connolly DM, Winkler ME, Connolly DM, Winkler ME, Bacteriol J. 1991. Structure of *Escherichia coli* K-12 miaA and Characterization of the Mutator Phenotype Caused by miaA Insertion Mutations Previously, we reported several unusual relationships between the 2-methylthio-N6-(A2-isopentenyl)adeno-sine-37 (ms2i6A-37) tRNA modification and spontaneous mutagenesis in Escherichia coli.

89. Petrullo LA, Gallagher PJ, Elseviers D. 1983. The role of 2-methylthio-N6-isopentenyladenosine in readthrough and suppression of nonsense codons in *Escherichia coli*. Mol Gen Genet 190:289–94.

90. Hall RH. 1970. N6-(delta 2-isopentenyl)adenosine: chemical reactions, biosynthesis, metabolism, and significance to the structure and function of tRNA. Prog Nucleic Acid Res Mol Biol 10:57–86.

91. Persson BC, Esberg B, Olafsson O, Björk GR. 1994. Synthesis and function of isopentenyl adenosine derivatives in tRNA. Biochimie 76:1152–60.

92. Lamichhane TN, Blewett NH, Maraia RJ. 2011. Plasticity and diversity of tRNA anticodon determinants of substrate recognition by eukaryotic A37 isopentenyltransferases. RNA 17:1846–1857.

93. Baba T, Ara T, Hasegawa M, Takai Y, Okumura Y, Baba M, Datsenko KA, Tomita M, Wanner BL, Mori H. 2006. Construction of *Escherichia coli* K-12 in-frame, single-gene knockout mutants: the Keio collection. Mol Syst Biol 2:2006.0008.

94. Zepeck F, Gräwert T, Kaiser J, Schramek N, Eisenreich W, Bacher A, Rohdich F. 2005. Biosynthesis of isoprenoids. purification and properties of IspG protein from *Escherichia coli*. J Org Chem 70:9168–9174.

95. Lee M, Gräwert T, Quitterer F, Rohdich F, Eppinger J, Eisenreich W, Bacher A, Groll M. 2010. Biosynthesis of isoprenoids: crystal structure of the [4Fe-4S] cluster protein IspG. J Mol Biol 404:600–610.

96. Xiao Y, Zahariou G, Sanakis Y, Liu P. 2009. IspG enzyme activity in the deoxyxylulose phosphate pathway: roles of the iron-sulfur cluster. Biochemistry 48:10483–10485.

97. Altincicek B, Duin EC, Reichenberg A, Hedderich R, Kollas A-K, Hintz M, Wagner S, Wiesner J, Beck E, Jomaa H. 2002. LytB protein catalyzes the terminal step of the 2- *C* -methyl- D -erythritol-4-phosphate pathway of isoprenoid biosynthesis. FEBS Lett 532:437–440.

98. Mulo P. 2011. Chloroplast-targeted ferredoxin-NADP+ oxidoreductase (FNR): Structure, function and location. Biochim Biophys Acta - Bioenerg 1807:927–934.

99. Krapp RA, Rodriguez ER, Poli OH, Paladini HD, Palatnik FJ, Carrillo N. 2002. The flavoenzyme ferredoxin (flavodoxin)-NADP(H) reductase modulates NADP(H) homeostasis during the soxRS response of *Escherichia coli*. J Bacteriol 184:1474–1480.

100. Sendra M, Ollagnier de Choudens S, Lascoux D, Sanakis Y, Fontecave M. 2007. The SUF iron-sulfur cluster biosynthetic machinery: Sulfur transfer from the SUFS-SUFE complex to SUFA. FEBS Lett 581:1362–1368.

101. Arisue N, Hashimoto T, Mitsui H, Palacpac QNM, Kaneko A, Kawai S, Hasegawa M, Tanabe K, Horii T. 2012. The *Plasmodium* apicoplast genome: conserved structure and close relationship of *P. ovale* to rodent malaria parasites. Mol Biol Evol 29:2095–2099.

102. Wrenger C, Eschbach M-L, Müller IB, Laun NP, Begley TP, Walter RD. 2006. Vitamin B1 de novo synthesis in the human malaria parasite *Plasmodium falciparum* depends on external provision of 4-amino-5-hydroxymethyl-2-methylpyrimidine. Biol Chem 387:41–51.

103. Chan XWA, Wrenger C, Stahl K, Bergmann B, Winterberg M, Müller IB, Saliba KJ. 2013. Chemical and genetic validation of thiamine utilization as an antimalarial drug target. Nat Commun 4:2060.

104. Müller S, Kappes B. 2007. Vitamin and cofactor biosynthesis pathways in *Plasmodium* and other apicomplexan parasites. Trends Parasitol 23:112–21.

105. Webb E, Claas K, Downs DM. 1997. Characterization of thiI, a new gene involved in thiazole biosynthesis in *Salmonella typhimurium*. J Bacteriol 179:4399–402.

106. Gralnick J, Webb E, Beck B, Downs D. 2000. Lesions in gshA (Encoding gamma-L-glutamyl-L-cysteine synthetase) prevent aerobic synthesis of thiamine in *Salmonella enterica* serovar typhimurium LT2. J Bacteriol 182:5180–7.

107. Bozdech Z, Ginsburg H. 2005. Data mining of the transcriptome of *Plasmodium falciparum*: the pentose phosphate pathway and ancillary processes. Malar J 4:17.

108. Müller IB, Hyde JE, Wrenger C. 2010. Vitamin B metabolism in *Plasmodium falciparum* as a source of drug targets. Trends Parasitol 26:35–43.

109. Allary M, Lu JZ, Zhu L, Prigge ST. 2007. Scavenging of the cofactor lipoate is essential for the survival of the malaria parasite *Plasmodium falciparum*. Mol Microbiol 63:1331–1344.

110. Ugulava NB, Gibney BR, Jarrett JT. 2001. Biotin synthase contains two distinct iron-sulfur cluster binding sites: chemical and spectroelectrochemical analysis of iron-sulfur cluster interconversions. Biochemistry 40:8343–51.

111. Ugulava NB, Gibney BR, Jarrett JT. 2000. Iron-sulfur cluster interconversions in

biotin synthase: dissociation and reassociation of iron during conversion of [2Fe-2S] to [4Fe-4S] clusters. Biochemistry 39:5206–14.

112. Goodman DC, Mollard V, Louie T, Holloway AG, Watson GK, McFadden IG. 2014. Apicoplast acetyl Co-A carboxylase of the human malaria parasite is not targeted by cyclohexanedione herbicides. Int J Parasitol 44:285–289.

113. Dellibovi-Ragheb TA, Jhun H, Goodman CD, Walters MS, Ragheb DRT, Matthews KA, Rajaram K, Mishra S, McFadden GI, Sinnis P, Prigge ST. 2018. Host biotin is required for liver stage development in malaria parasites. Proc Natl Acad Sci U S A 115:E2604–E2613.

114. Carlton JM, Angiuoli S V., Suh BB, Kooij TW, Pertea M, Silva JC, Ermolaeva MD, Allen JE, Selengut JD, Koo HL, Peterson JD, Pop M, Kosack DS, Shumway MF, Bidwell SL, Shallom SJ, van Aken SE, Riedmuller SB, Feldblyum T V., Cho JK, Quackenbush J, Sedegah M, Shoaibi A, Cummings LM, Florens L, Yates JR, Raine JD, Sinden RE, Harris MA, Cunningham DA, Preiser PR, Bergman LW, Vaidya AB, van Lin LH, Janse CJ, Waters AP, Smith HO, White OR, Salzberg SL, Venter JC, Fraser CM, Hoffman SL, Gardner MJ, Carucci DJ. 2002. Genome sequence and comparative analysis of the model rodent malaria parasite *Plasmodium yoelii yoelii*. Nature 419:512–519.

115. Mueller EG, Buck CJ, Palenchar PM, Barnhart LE, Paulson JL. 1998. Identification of a gene involved in the generation of 4-thiouridine in tRNA. Nucleic Acids Res 26:2606–10.

116. Kambampati R, Lauhon CT. 1999. IscS is a sulfurtransferase for the in vitro biosynthesis of 4-thiouridine in *Escherichia coli* tRNA. Biochemistry 38:16561–8.

117. Kambampati R, Lauhon CT. 2000. Evidence for the transfer of sulfane sulfur from IscS to ThiI during the in vitro biosynthesis of 4-thiouridine in *Escherichia coli* tRNA. J Biol Chem 275:10727–30.

118. Eschbach M-L, Müller IB, Gilberger T-W, Walter RD, Wrenger C. 2006. The human malaria parasite *Plasmodium falciparum* expresses an atypical N-terminally extended pyrophosphokinase with specificity for thiamine. Biol Chem 387:1583–91.

119. Sullivan MA, Cannon JF, Webb FH, Bock RM. 1985. Antisuppressor mutation in *Escherichia coli* defective in biosynthesis of 5-methylaminomethyl-2-thiouridine. J Bacteriol 161:368–76.

120. Čavužić M, Liu Y. 2017. Biosynthesis of Sulfur-Containing tRNA Modifications: A Comparison of Bacterial, Archaeal, and Eukaryotic Pathways. Biomolecules 7.

121. Moukadiri I, Garzón M-J, Björk GR, Armengod M-E. 2014. The output of the tRNA modification pathways controlled by the *Escherichia coli* MnmEG and MnmC enzymes depends on the growth conditions and the tRNA species. Nucleic Acids Res 42:2602–2623.

122. Armengod ME, Meseguer S, Villarroya M, Prado S, Moukadiri I, Ruiz-Partida R, Garzón MJ, Navarro-González C, Martínez-Zamora A. 2014. Modification of the wobble uridine in bacterial and mitochondrial tRNAs reading NNA/NNG triplets of 2-codon boxes. RNA Biol 11:1495–1507.

123. Moukadiri I, Villarroya M, Benítez-Páez A, Armengod M-E. 2018. *Bacillus subtilis* exhibits MnmC-like tRNA modification activities. RNA Biol 15:1167–1173.

124. KOTERA M, BAYASHI T, HATTORI M, TOKIMATSU T, GOTO S, MIHARA H, KANEHISA M. 2010. COMPREHENSIVE GENOMIC ANALYSIS OF SULFUR-RELAY PATHWAY GENES, p. 104–115. *In* Genome Informatics 2010. IMPERIAL COLLEGE PRESS.

125. Gardner MJ, Bishop R, Shah T, de Villiers EP, Carlton JM, Hall N, Ren Q, Paulsen IT, Pain A, Berriman M, Wilson RJM, Sato S, Ralph SA, Mann DJ, Xiong Z, Shallom SJ, Weidman J, Jiang L, Lynn J, Weaver B, Shoaibi A, Domingo AR, Wasawo D, Crabtree J, Wortman JR, Haas B, Angiuoli S V, Creasy TH, Lu C, Suh B, Silva JC, Utterback TR, Feldblyum T V, Pertea M, Allen J, Nierman WC, Taracha ELN, Salzberg SL, White OR, Fitzhugh HA, Morzaria S, Venter JC, Fraser CM, Nene V. 2005. Genome Sequence of *Theileria parva*, a Bovine Pathogen That Transforms Lymphocytes. Science (80-) 309:134–137.

126. Nilsson K, Jäger G, Björk GR. 2017. An unmodified wobble uridine in tRNAs specific for Glutamine, Lysine, and Glutamic acid from *Salmonella enterica* Serovar Typhimurium results in nonviability—Due to increased missense errors? PLoS One 12:e0175092.

127. Bjork GR, Ericson JU, Gustafsson CED, Hagervall TG, Jonsson YH, Wikstrom PM. 1987. Transfer RNA Modification. Annu Rev Biochem 56:263–285.

128. McCutcheon JP, Moran NA. 2011. Extreme genome reduction in symbiotic bacteria.

129. Zhang Q, Zhang L, Chen D, He X, Yao S, Zhang Z, Chen Y, Guan M-X. 2018. Deletion of Mtu1 (Trmu) in zebrafish revealed the essential role of tRNA modification in mitochondrial biogenesis and hearing function. Nucleic Acids Res 46:10930–10945.

130. Wang X, Yan Q, Guan M-X. 2010. Combination of the loss of cmnm5U34 with the lack of s2U34 modifications of tRNALys, tRNAGlu, and tRNAGln altered mitochondrial biogenesis and respiration. J Mol Biol 395:1038–48.

131. Wu Y, Wei F-Y, Kawarada L, Suzuki T, Araki K, Komohara Y, Fujimura A, Kaitsuka T, Takeya M, Oike Y, Suzuki T, Tomizawa K. 2016. Mtu1-Mediated Thiouridine Formation of Mitochondrial tRNAs Is Required for Mitochondrial Translation and Is Involved in Reversible Infantile Liver Injury. PLOS Genet 12:e1006355.

132. ASHRAF SS, SOCHACKA E, CAIN R, GUENTHER R, MALKIEWICZ A, AGRIS PF. 1999. Single atom modification (O → S) of tRNA confers ribosome

binding. RNA 5:S1355838299981529.

133. Yarian C, Marszalek M, Sochacka E, Malkiewicz A, Guenther R, Miskiewicz A, Agris PF. 2000. Modified nucleoside dependent Watson-Crick and wobble codon binding by tRNALysUUU species. Biochemistry 39:13390–5.

134. Vendeix FAP, Murphy F V., Cantara WA, Leszczyńska G, Gustilo EM, Sproat B, Malkiewicz A, Agris PF. 2012. Human tRNALys3UUU Is Pre-Structured by Natural Modifications for Cognate and Wobble Codon Binding through Keto–Enol Tautomerism. J Mol Biol 416:467–485.

135. Brégeon D, Colot V, Radman M, Taddei F. 2001. Translational misreading: a tRNA modification counteracts a +2 ribosomal frameshift. Genes Dev 15:2295–306.

136. Diwan GD, Agashe D. 2018. Wobbling Forth and Drifting Back: The Evolutionary History and Impact of Bacterial tRNA Modifications. Mol Biol Evol 35:2046–2059.

137. Grosjean H, Breton M, Sirand-Pugnet P, Tardy F, Thiaucourt F, Citti C, Barré A, Yoshizawa S, Fourmy D, de Crécy-Lagard V, Blanchard A. 2014. Predicting the Minimal Translation Apparatus: Lessons from the Reductive Evolution of Mollicutes. PLoS Genet 10:e1004363.

138. McCutcheon JP, Moran NA. 2012. Extreme genome reduction in symbiotic bacteria. Nat Rev Microbiol 10:13–26.

139. Gil R, Peretó J. 2015. Small genomes and the difficulty to define minimal translation and metabolic machineries. Front Ecol Evol 3:123.

140. Nkrumah JL, Muhle AR, Moura AP, Ghosh P, Hatfull FG, Jacobs RW, Fidock AD. 2006. Efficient site-specific integration in *Plasmodium falciparum* chromosomes mediated by mycobacteriophage Bxb1 integrase. Nat Methods 3:615–621.

141. Spalding DM, Allary M, Gallagher RJ, Prigge TS. 2010. Validation of a modified method for Bxb1 mycobacteriophage integrase-mediated recombination in *Plasmodium falciparum* by localization of the H-protein of the glycine cleavage complex to the mitochondrion. Mol Biochem Parasitol 172:156–160.

142. Zhang M, Wang C, Otto TD, Oberstaller J, Liao X, Adapa SR, Udenze K, Bronner IF, Casandra D, Mayho M, Brown J, Li S, Swanson J, Rayner JC, Jiang RHY, Adams JH. 2018. Uncovering the essential genes of the human malaria parasite *Plasmodium falciparum* by saturation mutagenesis. Science 360:eaap7847.

Chapter 4

The Role of Carbon Metabolism in the Apicoplast of *P. falciparum* Parasites

Attributions:
- The PfMev PDH E2 deletion mutant was generated by Dr. Krithika Rajaram, and the PfMev DXS deletion mutant was generated by Bobby Kwan
- All growth curves were generated by Hans Liu
- PyrKII *E. coli* purification and enzyme activity assays were conducted by Cyrianne Keutcha
- Microarray analysis of the PyrKII-CLD line was conducted by the Johns Hopkins Genomic Analysis and Sequencing Core Facility

ABSTRACT

In this chapter, we determined which genes involved in carbon backbone metabolism within the apicoplast are essential for the maintenance of the organelle. In order to determine this, we made knockouts of the genes involved in this pathway in our PfMev bypass line under mevalonate supplementation and then determined the resulting organellar phenotypes. We demonstrated that deletion of the inner triosephosphate transporter (iTPT), responsible for the import of three-carbon phosphates, was essential for the maintenance of the organelle. We were also able to show that pyruvate kinase II (PyrKII), the sole predicted source of pyruvate and ATP within the apicoplast, was essential for the maintenance of the organelle as well. The pyruvate generated by PyrKII is subsequently fed into the MEP isoprenoid precursor pathway as well as the FASII fatty acid biosynthetic pathway. Deletion of enzymes within these pathways did not result in organelle disruption, suggesting that the utilization of pyruvate is not required for the maintenance of the organelle. This suggests that the essentiality of PyrKII for apicoplast maintenance is instead driven by its ability to generate ATP. Given this, we went on to further characterize this enzyme by determining the substrate specificity of recombinant purified PyrKII against various NDPs and dNDPs to determine which nucleotide triphosphates might be supplied by PyrKII. Through this work we were able to determine that PyrKII does not have a high level of substrate specificity, indicating that it may be capable of generating all NTPs and dNTPs within the organelle. We also generated a parasite line that allows for the conditional mislocalization of PyrKII, and used this line to examine how loss of PyrKII affects transcription within the apicoplast and disruption of the organelle. We were able to show that upon mislocalization of PyrKII there was a rapid decrease in transcript level within the apicoplast that far preceded apicoplast disruption, helping to further support the hypothesis that PyrKII is

essential for organelle maintenance due to its role in nucleotide triphosphate generation within the apicoplast.

INTRODUCTION

The apicoplast is a plastid organelle present in most Apicomplexa species (1). The apicoplast is an organelle surrounded by four membranes, a result of its evolutionary origin resulting from a secondary endosymbiotic process. In the first endosymbiotic event, the chloroplast of an algal cell was formed from an engulfed cyanobacterium (2). The algal cell was then phagocytosed, and lost all of its cellular contents except for its chloroplast organelle (3),(4). Over the course of endosymbiosis the apicoplast has become extremely reduced in terms of the biochemical processes present within the organelle in addition to the genetic material that it possesses (5). However, the *P. falciparum* apicoplast has kept some of its own genetic material in the form of a reduced 35kb organellar genome that encodes a full set of tRNAs, rRNAs, and just a few proteins (6). The remainder, and majority, of apicoplast-specific proteins are now encoded within the nucleus of the parasite and trafficked to the organelle, likely resulting from multiple gene transfer events that have occurred over the course of endosymbiosis (7–9). Due to the unique eubacterial origin of the organelle, the apicoplast retains some bacterial-like pathways that are highly dissimilar from that of the human host, making it an attractive source of potential drug targets (10).

In *Plasmodium falciparum* malaria parasites, the apicoplast is home to the FASII fatty acid and MEP (methylerythritol phosphate) isoprenoid precursor biosynthetic pathways, in addition to containing its own iron-sulfur cluster machinery, and sharing the heme biosynthetic pathway with the mitochondrion (10). While the apicoplast is required at every

stage of the parasite lifecycle (11–14), it appears that the only essential product of the organelle during the asexual blood-stage of the parasite is the isoprenoid precursor isopentenyl pyrophosphate (IPP) (15). However, enzymes within the MEP pathway are not the only potential apicoplast blood-stage drug targets. There are over 400 proteins predicted to be trafficked to the apicoplast, representing ~7% of the parasite genome (16–20), many of which are likely involved in accessory pathways that are required to support isoprenoid production by producing substrates or cofactors, and others that are essential for the maintenance and replication of the organelle that houses these pathways.

In order to fuel the metabolic pathways in the apicoplast, sources of reducing power, carbon skeletons, and energy in the form of nucleotide triphosphates are required. Other plastid organelles, such as chloroplasts, can generate these products through photosynthesis and export them (21, 22). However, when not exposed to light, chloroplasts must import the resources needed for the anabolic processes that occur within the organelle (23, 24). Since the apicoplast is non-photosynthetic, it has been referred to as a plastid 'in the dark' and is reliant on the cell to provide these resources (25).

The way in which the apicoplast acquires energy and reducing power remains unknown. While chloroplasts can acquire carbon backbones, energy, and reducing power through the import of glucose-6-phosphate and its breakdown by glycolytic (26) or pentose phosphate pathways (27), it does not appear that this occurs in *P. falciparum*, since the apicoplast does not seem to contain the proteins required to import or breakdown hexose or pentose sugars (16). Additionally, chloroplasts can also import ATP in exchange for ADP with ATP/ADP antiporters (24, 28), but these transporters have not been found to be associated with the apicoplast of *Plasmodium* (16). Instead, the apicoplast appears to meet its

carbon backbone, energy, and reducing power needs solely through the import and metabolism of 3-carbon phosphates generated by parasite glycolysis (16, 29).

Three-carbon phosphates are imported by two different transporters, the inner triose phosphate transporter (iTPT), which is embedded in the inner apicoplast membrane, with its trafficking directed by a N-terminal signal and transit peptide, as well as the outer triose phosphate transporter (oTPT), embedded in the outer apicoplast membrane, which lacks a targeting sequence (30, 31). These transporters have been biochemically characterized *ex vivo* and have been shown to be capable of importing triose phosphate compounds including phosphoenolpyruvate (PEP), dihydroxyacetone phosphate (DHAP), and 3-phosphoglyceric acid (3PGA), which it exchanges for inorganic phosphate (**Figure 4-1**) (29). Previous work investigated the essentiality of these transporters in *P. berghei*, and found oTPT to be essential, while iTPT was dispensable in blood-stage parasites, but was required in mosquito and liver stage parasites (32). Based on these results, it was hypothesized that there may be some functional redundancy between iTPT and oTPT (32). However, the essentiality or potential redundancy of these transporters has not been determined in *P. falciparum* parasites.

The import of three carbon phosphates is critical for metabolism within the apicoplast. Imported DHAP, mediated by iTPT/oTPT (29), is believed to interact with triose phosphate isomerase (TPI) as a substrate to generate GA3P (16), which is then fed into the MEP isoprenoid pathway for the production of essential isoprenoid precursors (33). Additionally, DHAP is also believed to be converted by glycerol phosphate dehydrogenase (GpdA) to form glycerol-3-phosphate (G3P) for phospholipid biosynthesis within the apicoplast (16, 34). DHAP may also be involved in the generation of reducing power within the organelle. One hypothesized source of reducing power is a triose phosphate isomerase (TPI) / glyceraldehyde 3-phosphate dehydrogenase (GAPDH) cycle, in which imported

DHAP is converted by TPI to form GA3P, which in turn is converted into 1,3-diphosphoglycerate (1,3-DPGA) by GAPDH, reducing NAD+ to NADPH in the process (35, 36). The 1,3-DPGA can then presumably be exchanged for DHAP by the triose phosphate transporters, creating an electron shuttle (35). A putative TPI has been found and is predicted to localize to the apicoplast, but only a single GAPDH has been found (37) and does not appear to localize to the apicoplast (38). This is in contrast to the related parasite species *Toxoplasma gondii* which has an apicoplast GAPDH and cytosolic GAPDH (36), and presumably has a functional apicoplast TPI/GAPDH cycle. However, it has yet to be determined if this cycle is present and active in *P. falciparum*. In general, the source of reducing power in the apicoplast remains unclear.

Another three-carbon phosphate imported into the apicoplast is phosphoenolpyruvate (PEP) (29). PEP is believed to be used along with ADP as substrates by the enzyme pyruvate kinase II (PyrKII), which transphosphorylates PEP to ADP to generate the products pyruvate and ATP (8, 39, 40). As the name implies, there are two pyruvate kinase enzymes within *Plasmodium*, one within the cytosol, Pyruvate kinase I (PyrKI) (41), and another within the apicoplast called pyruvate kinase II (PyrKII) (42). In eukaryotes, pyruvate kinase plays a key role in glycolysis, catalyzing the final step of this pathway, and is also one of the key control points of glycolysis (43). In Apicomplexan parasites such as *T. gondii* and *P. falciparum,* two isoforms of pyruvate kinase have been found, that are referred to as Type-I and Type-II isozymes, or PyrKI and PyrKII (39, 42). PyrKI is found within the cytoplasm and plays a typical glycolytic role, while PyrKII has been found to localize to both the mitochondria and apicoplast in *T. gondii* and solely to the apicoplast in *P. falciparum* (39, 42). Within the apicoplast of *P. falciparum* PyrKII provides the only predicted source of both ATP and pyruvate (29). The pyruvate produced is believed to enter into the FASII and MEP

pathways (33), and becomes incorporated into fatty acid and isoprenoid products (44). The ATP generated presumably powers all energy requiring reactions within the organelle and provides adenine bases for RNA synthesis. It is not clear how the apicoplast acquires the other NTPs for RNA synthesis and other reactions since apicoplast transporters for NMPs or NDPs have not been described and there is no other predicted source of NTPs within the organelle (16). The activity of the *T. gondii* PyrKII has been characterized *in vitro* and shows a near-exclusive substrate preference for GDP instead of using ADP (39). Researchers have so far been unable to produce recombinant *P. falciparum* PyrKII in *E. coli*, and its substrate specificity remains unknown (42).

The import of PEP and DHAP by the triose phosphate transporters and their conversion by the PyrKII and TPI provides the substrates required for the FASII and MEP anabolic pathways, and presumably supplies energy and reducing power for apicoplast metabolism. Although carbon metabolism appears to be an essential process, the importance of these proteins in parasite survival or the maintenance of the apicoplast in *P. falciparum* has not been elucidated. Thus, we utilized the PfMev apicoplast bypass parasite line described in chapter 2 of this thesis to determine the required roles of the apicoplast carbon metabolism proteins. As demonstrated in chapters 2 and 3 of this thesis, the PfMev parasite line allows for the deletion of essential apicoplast resident genes, while under mevalonate supplementation. The PfMev parasite line also contain a fluorescently labeled apicoplast, which enables us to determine the impact a given gene deletion has on the organellar phenotype (15). We have previously shown that deletion of essential apicoplast-resident genes, such as DXPR has no discernible effect on the morphology of the organelle. However, other genetic disruptions, such as SufS and MnmA, can result in breakdown of the organelle, suggesting that the gene product plays an essential role in the maintenance of the

organelle (45). In the work outlined this chapter, we utilized the PfMev line to interrogate carbon metabolism within the apicoplast through a series of genetic deletions, and have been able to determine which genes are required for blood-stage parasite survival, in addition to determining which are essential for the maintenance of the apicoplast organelle.

Our results show that PyrKII, an enzyme believed to be the sole source of pyruvate and ATP in the organelle (16), is essential for apicoplast maintenance. Deletion of iTPT, the transporter responsible for the PEP substrate (29) used by PyrKII replicated the phenotype, helping to confirm the original finding. To assess the importance of the pyruvate generated from PyrKII for apicoplast metabolism, we deleted the two enzymes predicted to use the pyruvate generated by PyrKII. We deleted the PDH (pyruvate dehydrogenase) E2 subunit, responsible for the generation of acetyl-CoA from pyruvate (46), and found that it was dispensable. This replicates what has been shown previously through deletions of other enzymes in the FASII pathway (47). We also deleted DXS (DOXP synthase), which is responsible for the condensation of pyruvate and G3P to form DOXP in the MEP pathway. We found that while DXS is essential for parasite growth, it is not needed for maintenance of the apicoplast organelle. These data indicate that pyruvate generated by PyrKII is not required for the maintenance of the organelle. Instead the requirement of PyrKII for apicoplast maintenance is likely driven by its role in generating ATP (or NTP) products.

Given these results we went on to further characterize the PyrKII enzyme by determining the substrate specificity of recombinant purified PyrKII against various NDPs and dNDPs. While PyrKII was most active against ADP and GDP, it was also found to be active against all NDPs and dNDPs that were tested, and did not show a high level of substrate specificity. Thus, this led us to hypothesize that the deletion of PyrKII resulted in the loss of NTPs and dNTPs, which in turn inhibited the processes reliant on these

substrates, such as energy consuming reactions (ATP), protein translation (GTP), mRNA production (NTPs), and DNA replication (dNTPs). Based on the hypothesis that mRNA levels may decline as a result of PyrKII deletion we generated a parasite line that would allow us to controllably knockdown PyrKII and measure the rate of loss of mRNA levels via microarray as a proxy for measuring the change in NTP production. Using this approach, we found that apicoplast mRNA levels decreased rapidly (over the course of hours) while the organelle itself remained intact for much longer (~4 days), helping to support the conclusion that PyrKII is involved in NTP/dNTP production within the apicoplast.

RESULTS

The goal of this work is to interrogate the role and necessity of genes involved in carbon metabolism within the apicoplast. In order to accomplish this, we began by attempting to delete these genes in our PfMev line under mevalonate supplementation, which should allow for the deletion of essential apicoplast-specific genes. A given genetic deletion should give us two pieces of information. First, it should allow us to determine if the gene is essential by testing whether the deletion line is reliant on mevalonate for growth and survival. Second, it should allow us to determine if the gene is required for the maintenance or replication of the apicoplast organelle. Previous genetic disruptions of essential genes localized in the apicoplast have shown no discernable phenotype, such as the deletion of DXPR, while others such as SufS or MnmA have proven to be essential for the maintenance or replication of the organelle (48).

Deletion of Triose Phosphate Isomerase

Triose phosphates imported into the apicoplast are predicted to be substrates for PyrKII and TPI. As mentioned above, imported DHAP is predicted to be used as a substrate by TPI to generate GA3P, which is fed into the MEP isoprenoid pathway for the generation of isoprenoid precursors (33). In order to determine the importance of TPI within the apicoplast, in addition to the parasite overall, we attempted to delete this gene in the PfMev parasite line under constant supplementation with 50μM mevalonate using Cas9-mediated genome editing (49, 50). Through this approach we were successful in deleting the TPI gene. Once parasites were obtained the presence of recombinant parasites containing the genetic deletion were confirmed using PCR by screening for integration at the 5' and 3' ends of the locus (Δ5' and Δ3'), in addition to screening for the original locus (5' and 3') to determine if there was any contamination by residual wild type parasites. These same reactions were also used to screen the PfMev parental line as a control for the PCR reactions (**Figure 4-2a**). We went on to characterize the ΔTPI line by determining whether the gene disruption resulted in the loss of the organelle by screening for the presence or absence of the apicoplast organelle genome using PCR techniques that have been previously described (45). We attempted to amplify SufB from the apicoplast genome, as well as lactate dehydrogenase (LDH) from the nuclear genome and cytochrome C oxidase (Cox1) from the mitochondrial genome as PCR controls, as previously described (48). We were able to amplify SufB, indicating that the apicoplast organellar genome is intact (**Figure 4-2b**). Using epifluorescent microscopy, we observed an intact apicoplast organelle in ΔTPI parasites (**Figure 4-2c**), confirming that deletion of TPI does not affect organelle morphology. Additionally, when we removed the mevalonate supplement from the growth medium, there was no significant change in parasite growth, demonstrating that TPI is not essential for asexual parasite survival (**Figure 4-2d**).

TPI was previously believed to play a potentially essential role in converting DHAP to GA3P for usage by the MEP isoprenoid pathway (16). However, the ability to delete TPI may be explained by the relative lack of substrate specificity by the triosephosphate transporters (oTPT and iTPT), which have been shown to be capable of importing PEP, DHAP, and 3PGA (29) and may be capable of importing other 3-carbon phosphate compounds as well, as seen in homologous transporters found in chloroplast membranes (51). Thus, TPI may be dispensable in blood-stage parasites due to the ability of these transporters to directly import GA3P for the MEP pathway. Additionally, TPI was thought to potentially play an important role in the generation of reducing power (NADPH) in the organelle along with a hypothetical GAPDH (16). The successful deletion of TPI and the failure to identify a candidate apicoplast GAPDH makes it more likely that this cycle is not present in malaria parasites (16).

Deletion of Pyruvate Kinase II

We next targeted the apicoplast PyrKII for deletion since it is predicted to be the sole source of pyruvate in the organelle, and should be required for the FASII and MEP pathways (16). We were successful in deleting PyrKII in PfMev parasites under mevalonate supplementation and confirmed the deletion by PCR (**Figure 4-3a**). When assaying for the presence of the apicoplast, we were able to amplify genes from the nuclear and mitochondrial genomes, but were unable to amplify SufB, consistent with loss of the apicoplast genome due to disruption of the organelle (**Figure 4-3b**). Using live epifluorescent microscopy, we observed multiple vesicles throughout the cell instead of the discrete intact structure that is typically seen in wild type parasites (15, 48), further demonstrating that the apicoplast was disrupted in ΔPyrKII parasites (**Figure 4-3c**).

Additionally, when we removed the mevalonate supplement from the growth medium, there was a rapid reduction in parasite growth, demonstrating that PyrKII is an essential protein (**Figure 4-3d**). These data suggest that PyrKII is an essential gene required for blood-stage parasite survival, and is also essential for the maintenance of the apicoplast organelle. However, based on these results the mechanism by which PyrKII was essential for apicoplast maintenance remained unclear, and could be due to its enzymatic activity or some other essential binding or structural role.

Attempted Deletion of the Inner and Outer Triose Phosphate Transporters

We next attempted to delete the inner and outer triose phosphate transporters (iTPT/oTPT) since these proteins are responsible for importing the PyrKII substrate PEP into the apicoplast (29). If the enzymatic activity of PyrKII is indeed essential for organelle maintenance, then these transporters, either individually or together, should also be required. Previous deletions in *P. berghei* showed iTPT to be dispensable in blood-stage parasites, while oTPT was essential (32). Using the PfMev line we were successful in deleting iTPT under mevalonate supplementation (**Figure 4-4a**). When assessing the apicoplast phenotype we observed results similar that of the ΔPyrKII parasite line including loss of the apicoplast organelle genome (**Figure 4-4b**) and accumulation of multiple vesicles instead of an intact apicoplast organelle (**Figure 4-4c**). The apicoplast disruption phenotype shared by ΔPyrKII and ΔiTPT parasite lines is consistent with the hypothesis that iTPT is needed to import PEP to support PyrKII activity which is essential for apicoplast maintenance. Additionally, upon removal of mevalonate there was a rapid inhibition of parasite growth, indicating that this gene is essential for blood-stage parasite survival (**Figure 4-4d**), contradicting what was

previous found in *P. berghei* in which the deletion did not cause significant growth defects (32).

Using the same techniques, we also attempted to delete oTPT, but were unsuccessful after multiple attempts (**Table 4-1**). These results are somewhat similar to those seen in *P. berghei,* in which the attempted deletion was apparently successful, but did not survive beyond a few replicative cycles, suggesting that the gene is essential for blood-stage survival (32). However, in our case, we should have been able to delete oTPT in the presence of the mevalonate bypass as long as oTPT has a role that is limited to apicoplast function. It could be that the molecular techniques we used were not designed in a way that facilitated successful deletion of the gene. Although, another possibility is that oTPT has an essential role for the parasite beyond its function associated with the apicoplast. While oTPT has been localized to the apicoplast (31) it still remains a possibility that a small portion of the protein may be located elsewhere in the cell. Regardless of where it is located, our results suggest that oTPT plays an essential role in parasite survival in parasites that cannot be bypassed with mevalonate.

The Role of Pyruvate in the Apicoplast

Our results so far implicate PyrKII enzymatic activity in apicoplast maintenance and suggest that one of the PyrKII products, pyruvate or ATP, is responsible for this phenomenon. We first investigated the role of pyruvate by targeting enzymes for deletion within the only two pathways predicted to use pyruvate as a substrate, the FASII and MEP pathways. All of the carbon in fatty acids synthesized by the FASII pathway comes from acetyl-CoA which is produced by PDH (pyruvate dehydrogenase) (46), with the production of acetyl-CoA reliant on pyruvate produced by PyrKII (52, 53). Previous deletions of several

FASII pathway enzymes showed that this pathway is dispensable in blood-stage parasites (12, 54). Subunits of the PDH complex were also shown to be dispensable in *P. yoelli* (E1α and E3) (55) and *P. falciparum* (E1α) (56). Although these results are quite convincing, the PDH E2 subunit, which forms the catalytic core of the PDH complex, has not been successfully deleted in any parasite species. We targeted the PDH E2 subunit for deletion, and confirmed deletion via PCR as previously described (**Figure 4-5a**). We also characterized the PDH E2 deletion line using the previously described apicoplast genome PCR and epifluorescent microscopy techniques, and found that the parasites retained the apicoplast genome and contained a discrete intact organellar structure (**Figure 4-5b and c**). We also found that the deletion line grows normally when the mevalonate supplement is removed from the growth medium, showing that PDH E2 is dispensable in blood-stage parasites (**Figure 4-5d**). Taken together, these results show that the PDH E2 is dispensable in blood-stage parasites, consistent with what has been seen previously in deletions of other genes involved in the FASII pathway (12, 54–56). If pyruvate is essential for apicoplast maintenance, PDH and the FASII pathway are not the reason why.

The MEP isoprenoid pathway is the only other pathway within the apicoplast believed to be reliant on pyruvate. The first enzyme in this pathway, DOXP synthase (DXS), mediates the first step of the MEP pathway, converting pyruvate along with GA3P into 1-deoxy-*D*-xylulose 5-phosphate (DOXP) (44, 57). However, beyond its role in isoprenoid production, DXS may be playing a yet to be discovered role in the maintenance of the organelle. In order to determine the role and essentiality of this enzyme, we deleted it in the PfMev parasite line under mevalonate supplementation. We confirmed the deletion via PCR, as previously described (**Figure 4-6a**). Upon assessing the apicoplast phenotype we were able to detect the organellar genome by PCR (**Figure 4-6b**) and we observed an intact

apicoplast organelle via epifluorescent microscopy **(Figure 4-6c**). We also found that ΔDXS parasites are mevalonate-dependent, demonstrating that DXS is an essential enzyme (**Figure 4-6d**). These results show that DXS is essential for parasite survival, but is not required for the maintenance of the apicoplast. This phenotype is consistent with the effects of the MEP pathway inhibitor fosmidomycin which kills parasites but can be bypassed with IPP without disrupting the apicoplast organelle (48). Taken together, our results targeting PDH E2 and DXS show that the enzymes predicted to use pyruvate can be deleted without loss of the apicoplast. This suggests that the enzymatic activity of PyrKII that is essential for organelle maintenance is likely to be the generation of ATP, or other nucleotide triphosphates, rather than the generation of pyruvate.

Enzymatic Characterization of Purified Recombinant *P. falciparum* PyrKII

Due to the deletion of enzymes within the pathways known to be reliant on pyruvate not replicating the apicoplast loss phenotype seen with the deletion of PyrKII, this suggests that the essential product of PyrKII that is required for organelle maintenance is the generation of ATP, or potentially the generation of many or all NTPs and dNTPs within the organelle. Thus, in order to investigate the generation of nucleotide triphosphates by PyrKII, we produced pure recombinant protein for enzymatic assays. It was previously reported that the *P. falciparum* PyrKII enzyme cannot be produced in *E. coli* (42), so we generated a codon harmonized version of the gene to overcome problems with protein translation, and appended an N-terminal maltose binding protein (MBP) to increase the solubility and folding of recombinant PyrKII. The MBP-PyrKII fusion protein was purified by amylose affinity chromatography and cleaved with tobacco etch virus (TEV) protease to remove the MBP domain. Cut PyrKII was purified by metal chelate chromatography and yielded about

10mg of pure PyrKII per liter of *E. coli* culture. We measured enzymatic activity using a lactate dehydrogenase (LDH) coupled spectrophotometric assay that tracks the consumption of NADH by LDH as it converts pyruvate generated by PyrKII to lactate (58). Using a saturating level of ADP (3mM), we determined that the K_M for PEP was 0.61±0.09mM and we subsequently used a saturating level of PEP (5mM) to assess the kinetic parameters of nucleotide diphosphate substrates. Our results indicate that PyrKII is fairly nonspecific and converts all of the NDPs and dNDPs that we tested into the corresponding triphosphates (**Table 4-2**). In comparison, the kcat/Km values for the *T. gondii* PyrKII were 337-fold higher for GDP than for ADP (39). However, for the *P. falciparum* PyrKII, the preference for GDP over ADP was less than l-fold, and the greatest difference in activity between GDP and dCDP only differed by 38-fold. These results indicate that PyrKII does not have a high substrate specificity and may have an important role in nucleotide metabolism. Currently, there is no other known source of dNTPs or NTPs within the apicoplast of malaria parasites, neither the enzymes responsible for their generation, nor the transporters capable of importing them (16).

Inducible Knock Down of PyrKII using the TetR DOZI System

Genetic deletion of PyrKII in the PfMev line offers information on the terminal effect of the loss of the gene, which results in disruption of the organelle. In order to study the chain of events, and thus potential mechanism leading to loss of the organelle, we needed to generate a controllable system to remove PyrKII from the apicoplast. To accomplish this, we tagged the endogenous PyrKII gene with a C-terminal aptamer array that is part of the TetR-DOZI tetracycline-on system that has previously been developed for *P. falciparum* (59). We used genome editing methods to insert a linearized version of the

plasmid pMG74 immediately after the PyrKII gene, adding the aptamer array and other elements (such as the expression cassette to produce the TetR-DOZI fusion protein and the blasticidin S-deaminase drug selection marker) to the 3' end of the PyrKII gene. Parasites were selected with blasticidin and maintained in the permissive state with 0.5μM aTc (anhydrotetracycline). Once generated, we then assayed the line to determine what effect the knockdown of PyrKII would have on parasite growth (**Figure 4-7**). These results show that upon removal of aTc, there is a rapid reduction in parasite growth, occurring during the second parasite intraerythrocytic growth cycle, confirming that PyrKII is an essential protein. However, importantly the PyrKII-TetR-DOZI line also gives us a controllable system in which to better investigate the importance of PyrKII in parasite survival and organelle maintenance and replication.

Conditional Localization of PyrKII

We also developed a separate conditional PyrKII line in which we replaced the apicoplast trafficking region of the endogenous PyrKII with an artificial conditional localization domain (CLD) (60). This system allows for the mislocalization of PyrKII, which will, upon the addition of the ligand Shield1, be secreted into the parasitophorous vacuole instead of being trafficked to the apicoplast (60). We also tested the CLD-PyrKII line by adding Shield1 and measuring the growth of the parasite line. The addition of Shield1 resulted in a rapid reduction of parasite growth (**Figure 4-8**). The reduction in growth was more rapid than that found with the PyrKII-TetR-DOZI line (**Figure 4-7**), and thus we used this line in subsequent experiments investigating the effect that PyrKII loss has on apicoplast maintenance.

Tracking Loss of the Apicoplast Post-mislocalization of PyrKII

Based on the previous genetic knockout of PyrKII we know that deletion of the gene in the PfMev line results in loss of the organelle. However, this only gives us an endpoint result and does not give us information on the rate of potential NTP/dNTP loss or the kinetics of organelle disruption. We hypothesized that if PyrKII was indeed involved in NTP/dNTP production, then mislocalization would result in a rapid reduction of NTPs and that this could be detected by measuring the levels of mRNA transcripts generated from the organelle genome. We also hypothesized that if PyrKII were involved in NTP/dNTP production then the reduction in apicoplast mRNA levels post-mislocalization would occur much more rapidly than the loss of the organelle, as opposed to apicoplast mRNA levels being reduced because of organelle loss. Thus, we first wanted to determine the kinetics of apicoplast loss following mislocalization of PyrKII. In order to accomplish this, we synchronized the CLD-PyrKII line and added Shield1 to ring stage parasites and determined the apicoplast morphology at ~24 hour intervals for 5 days. We observed the pattern of api-SFG fluorescence and found that disruption of the organelle occurred primarily after 4-5 days, or during the transition between the second and third lifecycle of the parasite (**Figure 4-9**). The percentage of parasites containing an intact organelle was ~90-100% at the 0, 16, 40, and 64-hour time points, and then dropped precipitously in the transition between the second and third 48-hour growth cycle. Approximately 25% of parasites contain an intact apicoplast at the 88-hour (day 4) time point, and less than 5% of parasites containing an intact apicoplast at the 110-hour (day 5) time point (**Figure 4-10**).

Measuring Apicoplast mRNA Levels Post-mislocalization of PyrKII

Loss of the apicoplast primarily occurred 4-5 days after mislocalization of PyrKII. We hypothesized that apicoplast transcript levels would be reduced much faster, if PyrKII is playing a critical role in NTP production, which would be required for the generation of new mRNA transcripts within the organelle. Thus, in order to determine the kinetics of apicoplast transcript loss we replicated the same procedure used to determine the phenotype of the organelle mentioned above. CLD-PyrKII parasites were synchronized and Shield1 was added to ring stage parasites. Parasites were collected every 8 hours for 48 hours and analyzed via microarray. We found that mislocalization of PyrKII triggers a rapid reduction in apicoplast transcript levels, beginning to occur within the first ~8-16 hours (**Figure 4-11**). The reduction in apicoplast transcript levels happens much more rapidly than the disruption of the organelle, which occurs between the second and third parasite growth cycle after mislocalization of PyrKII. Thus, disruption of apicoplast gene transcription is a very early consequence of interfering with PyrKII activity. This finding is consistent with the hypothesis that PyrKII is involved the production of NTPs, which are required for mRNA production within the organelle.

CONCLUSIONS AND DISCUSSION

Through the work outlined in this thesis chapter we explored the roles of apicoplast proteins predicted to be involved in the import and metabolism of three carbon sugars in the apicoplast organelle. The apicoplast is thought to meet its carbon backbone, energy, and reducing power needs through the import of 3-carbon phosphates using the inner and outer triose phosphate transporters (iTPT and oTPT) (16, 29). We were successful in deleting iTPT, and found it to be essential for parasite survival, in addition to maintenance of the

apicoplast. These findings contradict previous results, which found this gene to be dispensable in blood-stage *P. berghei* parasites (32). What is driving this discrepancy is unclear, but may be due to differences in the metabolic requirements or modes of substrate import into the apicoplast between blood-stage *P. berghei* and *P. falciparum* parasites. However, our results are consistent with forward genetic screens conducted by Oliver Billker in *P. berghei* suggesting that this gene is essential (61), and by John Adams in *P. falciparum* showing that disruption causes a large reduction in fitness (62). While iTPT can transport PEP and DHAP (63), the reason that it is required for organelle maintenance is most likely to be the utilization of PEP by PyrKII for the generation of NTPs. Imported DHAP may be used by the phospholipid biosynthetic pathway or the MEP pathway, however, deletions of genes involved in these pathways do not result in disruption of the apicoplast (34).

Additionally, we attempted to delete the outer triose phosphate transporter (oTPT), but failed after multiple attempts. The reason for this failure is unclear. It may be due to inefficiencies associated with the design of the guide RNA or repair construct. Alternatively, it may be due to the inability of the oTPT deletion to be bypassed by mevalonate supplementation in the PfMev line because it is playing an essential role in the parasite beyond the function of the apicoplast. These results are consistent with what has been previously shown, in which the gene could not be deleted in *P. berghei* (32), and also appears to be essential as determined by a forward genetic screen in *P. falciparum* (62). However, even if the gene is essential, we should have been able to delete it in the presence of our mevalonate bypass as long as it's essential function is exclusively associated with the apicoplast.

PyrKII is a central player in apicoplast carbon metabolism and is involved in generating the only predicted source of both pyruvate and ATP within the organelle (29).

Through our work here we were able to show that PyrKII is an essential gene that is required for blood-stage parasite survival and the maintenance of the apicoplast organelle. We went on to investigate the mechanism by which PyrKII is essential for apicoplast maintenance by deleting genes in the two pathways predicted to be reliant on pyruvate within the apicoplast, including DXS from the MEP pathway and the PDH E2 subunit from the FASII pathway. While the deletion of DXS demonstrated that this gene is essential for parasite survival, it was shown to not be required for the maintenance of the organelle, reproducing what we found when deleting the DXPR, IspG, and IspH enzymes, which are also components of this pathway. We additionally deleted the E2 subunit of PDH, which is involved in the conversion of pyruvate into acetyl-CoA and the generation of NADH within the apicoplast (64). While PDH provides the only predicted source of NADH, and potentially all reducing power within the organelle (16, 46), we were able to demonstrate that this gene is dispensable in blood-stage parasites. This replicates what has been seen previously with the deletion of another PDH subunit in *P. falciparum* (52). Overall, the result that the deletion of enzymes within the two pathways predicted to be reliant on pyruvate within the apicoplast did not replicate the organelle-loss phenotype seen with the deletion of PyrKII suggested that the generation or usage of pyruvate within the apicoplast is not required for organelle maintenance.

We found that the activity of PyrKII that is essential for organelle maintenance is instead likely due to its role in the generation of nucleoside triphosphates. While PyrKII generates the only predicted source of energy in the apicoplast, it may also be involved in the generation of all NTPs and dNTPs within the organelle, since there is no other predicted source for these compounds within the apicoplast (16). This activity would not be totally unprecedented as other pyruvate kinase enzymes have been shown to be relatively non-

specific in their use of purine or pyrimidine nucleoside substrates (65–69). In other systems, pyruvate kinase enzymes have been shown to play an important role in nucleoside triphosphate generation, and are potentially able to function as a nucleoside diphosphate kinase (66). Through our work outlined in this chapter, we were able to demonstrate that PyrKII has a relatively low substrate specificity, with only a slightly higher activity against purine nucleotide substrates. These data indicate that PyrKII may be capable of generating any or all NTPs and dNTPs within the apicoplast. Additionally, using transcript abundance within the apicoplast as a proxy for measuring NTP levels within the organelle, we were able to demonstrate that mislocalization of PyrKII results in the rapid loss of transcripts within the apicoplast. The drop in transcript levels began within ~8 hours, which far preceded disruption of the apicoplast, which was not observed until ~88-110 hours after mislocalization. The rapid loss of apicoplast transcript levels upon removal of PyrKII from the organelle suggests that PyrKII may be playing an important role in NTP generation within the apicoplast. Loss of the NTP generating activity of PyrKII is the likely cause of subsequent apicoplast disruption.

Within the apicoplast the ferredoxin/ferredoxin reductase system is the only known redox system within the organelle, and is believed to deliver reducing power to LipA, NifU, MiaB, IspG and IspH (16, 70–72). The generation and utilization of reducing power within the apicoplast has been predicted to be essential for parasite survival (10). We were able to confirm this by demonstrating that the deletion of either component of the ferredoxin/ferredoxin reductase system results in parasite death, as outlined in chapter 3 of this thesis. However, the source of reducing power within the apicoplast has remained unclear. One hypothesized source has been a triose phosphate isomerase (TPI), working along with a hypothetical glyceraldehyde 3-phosphate dehydrogenase (GAPDH) in a cycle.

TPI would convert DHAP into GA3P, which would be used by GAPDH to generate 1,3-diphosphoglycerate (1,3-DPGA) with the concomitant production of NADPH (35, 36). However, we were able to demonstrate that TPI is dispensable in blood-stage parasites, and the single GAPDH in malaria parasites has been localized to the cytosol (38). This is the only predicted source of NADPH within the apicoplast, and due to the apparent absence of GAPDH from the organelle, the apicoplast is predicted to rely entirely on NADH for reducing power (16). The only predicted source of NADH, and thus potentially all reducing power within the organelle is the PDH complex, converting pyruvate into acetyl-CoA, and forming NADH from in the process (73). However, we have been able to demonstrate that PDH is dispensable for blood-stage parasite survival, replicating what had been seen previously with deletions of other PDH subunits in *P. falciparum* (52). Thus, the source of reducing power within the apicoplast remains a mystery, and cannot be attributed exclusively to TPI or PDH.

TPI is also believed to provide the MEP pathway with carbon backbones through the conversion of DHAP to GA3P (16). While the MEP pathway is essential, we have demonstrated that TPI is dispensable. The dispensability of TPI can potentially be attributed to the lack of specificity of the upstream iTPT/oTPT transporters. Homologous transporters in plant plastids are relatively nonspecific and can import various triose phosphate compounds (51). The *P. falciparum* iTPT and oTPT triose phosphate transporters were also demonstrated to be relative nonspecific when tested *in vitro*, capable of importing 3PGA, a compound not predicted to be used within the organelle (29). Thus, it is possible that the iTPT/oTPT transporters can import GA3P directly, bypassing the need for the conversion of DHAP to GA3P by TPI.

Through the work outlined here we have been able to draw numerous conclusions about the metabolic requirements of the apicoplast organelle during the asexual stage of the parasite. We were able to demonstrate that PyrKII is essential for apicoplast maintenance and replication. The requirement of PyrKII for this process is apparently not due to its role in the generation of pyruvate, as evidenced by pathways reliant on pyruvate not being essential for this process, but instead can likely be attributed to the role of PyrKII in NTP production. Additionally, PyrKII may potentially be responsible for the generation of all NTPs and dNTPs within the apicoplast due to the relative lack of specificity of the enzyme, and the rapid loss of apicoplast transcript levels upon removal of the enzyme, occurring within the same intraerythrocytic growth cycle that the mislocalization was induced. This is also bolstered by the lack of any other identified sources of NTPs/dNTPs within the apicoplast. Additionally, we were able to demonstrate that TPI is dispensable for blood-stage survival, suggesting an alternate source of GA3P, such as the direct import of the metabolite. The dispensability of TPI also suggests that it is unlikely to play a role in the generation of reducing power; this is supported by previous findings demonstrating that the required partner enzyme, GAPDH, is not localized to the apicoplast. The dispensability of PDH, the only other potential source of reducing power opens up further questions, as to what the source of reducing power is within organelle, which remains an open question. Furthermore, we were unable to delete oTPT, after numerous attempts, potentially suggestive of an essential function beyond its current known role in importing three-carbon phosphate compounds into the apicoplast.

METHODS

P. falciparum culture and maintenance

Unless otherwise noted, blood-stage *P. falciparum* parasites were cultured in human erythrocytes at 1% hematocrit in a 10mL total volume of CMA (complete medium with AlbuMAX) medium containing RPMI 1640 media with L-glutamine (USBiological Life Sciences), supplemented with 25mM HEPES, 0.2% sodium bicarbonate, 12.5μg/ml hypoxanthine, 5g/L Albumax II (Life Technologies) and 25μg/mL gentamicin. Cultures were maintained in gassed flasks (94% N_2, 3% O_2, 3% CO_2) and incubated in sealed 25cm^2 flasks at 37°C.

Generation of Cas9 gene deletion constructs

Cas9 mediated gene deletion constructs were generated generally following methods previously described (49). Briefly, homology arms of ~300-600bp for each gene were amplified using the homology arm (HA) 1 and 2 forward and reverse primers corresponding to each gene (**Table 4-3**) from blood-stage *P. falciparum* NF54-attb gDNA. HA1 and HA2 primers were designed to contain ~15bp overhangs for insertion into the cut the pL8 or pRSng plasmids using In-Fusion (Clontech) cloning methods. The pL8 and pRSng plasmids contain the hDHFR drug resistance cassette for selection, which is flanked by endonuclease sites for insertion of the homology arms. The pL8 or pRSng plasmids were digested with NotI for insertion of HA1, and with NgoMIV for HA2. Digests with either endonuclease were also treated with recombinant shrimp alkaline phosphatase (rSAP) and then ethanol precipitated. The pL8 and pCasG plasmids also contain a guide RNA (gRNA) expression cassette. For insertion of the gRNA sequence, the plasmids were digested with BsaI and also treated with rSAP and then ethanol precipitated. Guide RNA sequences were synthesized as

oligos (**Table 4-4**), annealed, and inserted into the pL8 or pCasG plasmids via In-Fusion cloning.

P. falciparum transfections for gene deletion

Transfections were conducted as previously described (74, 75). Briefly, 400µL of red blood cells were washed with 5mL of CytoMix and resuspended in 400µL of CytoMix. The red blood cells were then electroporated with 75µg each of the pUF1-Cas9 and pL8 gene specific knock out plasmids or the pCasG and pRSng gene specific knock out plasmids (49). The electroporated RBCs were then mixed with ~2.5mL PfMev parasites synchronized as schizonts at 1% hematocrit and ~10% parasitemia and given 10mL CMA with 50µM mevalonate. After 48 hours, transfectants were selected with 0.75µM DSM1, 2.5nM WR99210, and 50µM mevalonate for seven days. After seven days, the parasites were switched to media containing only 50µM mevalonate. Infected red blood cells (iRBC) were first observed between 17 and 30 days after beginning drug selection. Once parasites were observed, the medium was switched to 2.5nM WR99210 and 50µM mevalonate.

Confirmation of knockout genotype

In order to screen for integration and successful gene knockout, in addition to the presence of any contaminating residual wild type parasites, a set of six primers were used: 5'F, 3'R, pL8 HA1 R, pL8 HA2F, 5' WT R and 3' WT F (**Table 4-5**). These primers were designed to screen for integration and gene disruption at the 5' and 3' ends (Δ5' and Δ3') in addition to 5' and 3' regions of the WT gene (5' and 3'). The same reactions were also performed on the parental PfMev line concurrently as a control. Samples for PCR were collected when the parasitemia reached been 5-10%, as determined by Giemsa stain.

Approximately 100µL of a resuspended parasite culture was placed in a heat block at 90°C for 2 minutes and stored at -20°C. For the PCR reaction, 1µL of the parasite sample was added to reactions with a 50µL total volume. Reactions were conducted using a Veriti 96 well thermal cycler (Applied Biosystems) and Phusion High-Fidelity DNA polymerase (Thermo Fisher Scientific). PCR products were separated on a 1.5% agarose gel stained with ethidium bromide for visualization.

The PCR reaction volumes were as follows:

parasite lysate 1µl
5x Phusion HF buffer 10µl
Forward primer (10 µM)1.5µl
Reverse primer (10 µM) 1.5µl
dNTPs (10mM) 1µl
Phusion polymerase 0.5µl
Water 34.5µl
Total volume 50µl

The PCR program was as follows:

95°C 3.5 minutes
95°C 30 seconds
62°C 1 minute
62°C 4 minutes
4°C stable

(steps 2 and 3 were repeated 35 times)

Confirmation of apicoplast loss

The loss of the apicoplast was confirmed via PCR with primers specific for a gene within the nuclear (Lactate Dehydrogenase), apicoplast (SufB), and mitochondrial (Cox1) genomes (**Table 4-6**). Failure to amplify a gene from the apicoplast genome, while amplifying genes from the nuclear and mitochondrial genomes would indicate loss of the organelle (45). To collect samples for PCR, approximately 100µL of a resuspended parasite

culture at ~5-10% parasitemia was placed in a 90°C heat block for 2 minutes, and then frozen at -20°C. For the PCR reaction, 1µL of the parasite sample was added to reactions with a 50µL total volume. Reactions were conducted using a Veriti 96 well thermal cycler (Applied Biosystems) and Phusion High-Fidelity DNA polymerase (Thermo Fisher Scientific). PCR products were separated by size on a 1.5% agarose gel stained with ethidium bromide. The parental PfMev line was always used as a positive control for apicoplast detection.

The PCR reaction volumes were as follows:

parasite lysate 1µl
5x Phusion HF buffer 10µl
Forward primer (10 µM)1.5µl
Reverse primer (10 µM) 1.5µl
dNTPs (10mM) 1µl
Phusion polymerase 0.5µl
Water 34.5µl
Total volume 50µl

The PCR program was as follows:

95°C 3.5 minutes
95°C 30 seconds
63°C 30 seconds
72°C 1 minute
72°C 4 minutes
4°C stable

(steps 2-4 were repeated 35 times)

Live cell epifluorescent microscopy

For sample preparation, 100µL of parasite culture with a hematocrit of 1% and a parasitemia between 8-10% was obtained. Parasites were stained with 30nM mitoTracker CMX-Ros (Invitrogen) and 1µg/mL 4', 6-diamidino-2-phenylindole (DAPI), and incubated

for 30 minutes at 37°C. Cells were then pelleted via mini-centrifuge (Fischer Scientific) for 10 seconds, and the media was aspirated and the cells were resuspended in 100μL of CMA media and incubated for 5 minutes at 37°C. This was done three times to wash the cells, with the cells being resuspended in 20μL of CMA and then pipetted onto slides and sealed with wax (2 parts paraffin, 1 part Vaseline) for observation on a Zeiss AxioImager M2 microscope. A series of images spanning 5μm were acquired with 0.2μm spacing and images were deconvolved with VOLOCITY software (PerkinElmer) to report a single combined z - stack image.

Testing mevalonate dependence in PfMev deletion mutants via growth curve

For each of the PfMev deletion lines, the parasitemia was determined via Gimesa stain, with the appropriate amount of the parental culture removed to seed quadruplicate samples with or without mevalonate. This volume was resuspended in a total of 10 mL CMA and centrifuged at 1,600rcf at room temperature (~25°C) for 5 minutes, washed a second time with an additional 10 mL CMA, and then resuspended in the appropriate volume of CMA, and then split equally into two tubes. To one of the tubes, the appropriate volume of a 10mM stock of mevalonate was added to bring to final concentration to 50 μM mevalonate. Parasites were seeded in a 96-well plate at 0.5% starting parasitemia, 2% hematocrit, and at a total volume of 250μL per well in quadruplicate. Additionally, 150μL of the appropriate media was replaced in each well on days 1, 2, and 3. Parasite samples were collected every 24 hours for four days, and the parasitemia was counted via SYBR green staining and flow-cytometry as outlined below.

Flow cytometry for parasite growth curve determination

Growth curves were generated by staining parasites with SYBR Green and counting parasitemia via flow cytometry. In order to setup the growth curve, the parasitemia of the starting culture was determined via Giemsa stain. Based on the determined parasitemia the culture was used to seed a 96-well flat bottom cell culture plate (Corning) at a 0.5% starting parasitemia and 2% hematocrit, at a total volume of 250µL in quadruplicate. In order to minimize evaporation and edge effects, the surrounding wells were filled with 250µL of 1mM EDTA. Plates were incubated in chambers gassed with 94% N_2, 3% O_2, 3% CO_2 for 1 minute and 15 seconds, and incubated at 37°C.

Parasite samples were collected immediately after seeding and analyzed via flow cytometry to verify the starting parasitemia and then collected every 24 hours thereafter. Samples collected on days 1-3 were diluted 1:10 in phosphate-buffered saline (PBS) and stored in a 96-well plate (Corning) at 4°C. We have previously verified that storage under these conditions and subsequent staining with SYBR Green reflects accurate parasitemia values.

On day 4 parasites were stained with SYBR Green by transferring 1µL of parasite culture, or 10µL of the 1:10 dilutions (the day 1-3 samples), to a 96-well plate containing 100µL of 1x SYBR Green (Invitrogen) in PBS. The samples were then incubated for 30 minutes on a platform Titramax 101 shaker (Heidolph) at 950rpm while protected from light. Post-incubation, 150µL of PBS was added to each well to dilute unbound SYBR Green dye. A control consisting of uninfected RBCs was also prepared in parallel and treated in the same manner as listed above.

Samples were analyzed with an Attune Nxt Flow Cytometer (Thermo Fisher Scientific). With a 50µL acquisition volume, 250µL total sample volume, and a running speed of 25µL/minute with 10,000 total events were collected within the R2 gate.

For flow cytometer gating, the R1 gate used forward-scatter area by side-scatter area to identify total RBCs from the sample. The R2 gate used forward-scatter height to identify single cells, and the R3 gate was used to measure parasitemia using fluorescence from the SYBR Green staining of parasite DNA (ratio of SYBR Green positive cells to total cells).

Generation of the PyrKII *E. coli* Expression Vector

The *P. falciparum* PyrKII was codon harmonized for expression in *E. coli* cells. The PyrKII gene was synthesized consisting of amino acids 42-745 of the protein. This region corresponds to what we predict to be the mature full-length protein, post-processing of the signal/transit peptide. The PyrKII gene was then amplified from the plasmid containing the codon harmonized sequence using the primers listed in **Table 4-7**. The amplicon was then inserted into the EcoRI and HindIII sites in the pMAL-cHT expression vector (76) using ligation independent cloning (In-Fusion, Clontech). The pMAL-cHT expression vector generates a fusion protein tagging the PyrKII protein with an N-terminal MBP (maltose binding protein) followed by a TEV (Tobacco Etch Virus) protease site and a six-histidine tag. Cleavage with TEV protease liberates histidine-tagged PyrKII (76).

Expression and Purification of Recombinant PyrKII from *E.coli*

The pMAL-cHT PyrKII expression plasmid was transformed into BL21 Star (DE3) *E. coli* cells (ThermoFisher) also harboring the pRIL plasmid from BL21-CodonPlus-RIL cells (Agilent), that we refer to as *RIL cells. The fusion protein was expressed in *RIL cells grown in LB medium, and shaken at 220 rpm at 37°C until an OD600 of 0.6 was reached. At this point, expression was induced with 0.4mM isopropyl β-thiogalactoside (IPTG) and the cells were then incubated for an additional 4 hours at 27°C degrees.

Cells were isolated via centrifugation and then lysed with 20mM Tris-HCl at pH 7.5, 100mM KCl, 1mg/mL lysozyme (Sigma), 2.5mg/mL DNAse I (Sigma), and 100mM PMSF. Cells were then sonicated at 40% amplitude for 30 seconds two times, and then pelleted via centrifugation. The MBP-PyrKII protein was then purified from the resulting lysate using a 5mL MBPTrap HP column (GE Healthcare). The protein was eluted with 100mM maltose. The resulting protein was then cleaved with TEV protease and further purified using a 5mL HisTrap column (GE Healthcare). The protein was then eluted with an imidazole gradient, and peak fractions were collected, pooled, and concentrated for storage in 20mM Tris-HCl (pH 7.5), 100mM KCl, 10% glycerol at -80 °C. The PyrKII protein concentration was determined by a Bradford assay using bovine serum albumin as a standard. The purity of recombinant pyruvate kinase was analyzed by electrophoresis on a 4-12% acrylamide gel, and detected by Coomassie Brilliant Blue staining.

PyrKII Enzyme Assays

The activity of the PyrKII protein was determined by a continuous assay coupled to lactate dehydrogenase (LDH), as previously described (39). Pyruvate generated by PyrKII is converted into lactate by LDH with concomitant oxidation of NADH, which can be monitored via spectrophotometer at 340nm. The standard reaction mixture for assaying PyrKII activity contained 1µL of the PyrKII enzyme, 5mM PEP (neutralized to pH 7), 10mM $MgCl_2$, 0.2mM NADH, 2 units of rabbit muscle lactate dehydrogenase (Sigma), 26.5mM Tris-HCl at pH 7.5, and 50mM KCl. Appropriate dilution of PyrKII enzyme was made to ensure that the reaction remained in the linear range over the complete time course. All reactions were initiated by adding a given NDP or dNDP. The concentrations assayed for ADP and GDP ranged from 0mM to 3.0mM, specifically at 0mM, 50µM, 125µM,

250μM, 500μM, 1.02mM, 1.01mM, and 3mM. CDP, UDP, TDP, dATP, dGDP, dCTP, and dTDP were assayed at concentrations between 0mM to 6mM, specifically at 0mM, 128μM, 254μM, 510μM, 1.08mM, 2.07mM, 4.05mM, and 6.03mM. All reactions were carried out in final volume of 100μL in triplicate in a 96-well plate, and monitored for 20 minutes. The initial enzyme velocity was calculated from a tangent that was fitted to the reaction curve. Kinetic parameters were calculated using Prism (GraphPad).

Generation of the TetR-DOZI PyrKII Parasite Line

The PyrKII TetR-DOZI line was generated as previously described (59). Briefly, the pMG74 plasmid was used, generously sent to us by the laboratory of Dr. Jacquin Niles. The pMG74 plasmid encodes the TetR-DOZI system, which allows for the inducible knockdown of a gene through the removal of aTc. This method relies on the insertion of the entire linearized pMG74 plasmid immediately following the gene to be knocked down. This work by generating two homology arms corresponding to the 3' end of the gene, and another corresponding to the 3' UTR, which are separated by endonuclease cut-site, such as EcoRV. The gene of interest is then cut with a gene-specific gRNA, using the linearized gene-specific pMG74 plasmid as a repair template. This results in the insertion of the entire pMG74 plasmid, which generates a C-terminal HA and flag tag that will become appended to the 3' end of the gene, followed by an aptamer array. This aptamer array is part of the TetR-DOZI system which is encoded elsewhere within the inserted plasmid.

The gene-specific pMG74 line was generated by using the primers in **Table 4-8**. Briefly, the PyrKIItet HA1 F and PyrKIItet HA1 R primers were used to amplify the region of the gene corresponding to homology arm 1 (HA1), and the PyrKIItet HA2 F and PyrKIItet HA2 R primers were used to amplify the region of the gene corresponding to

homology arm 2 (HA2). The amplicons were then ethanol precipitated and a small amount from each was used as a template for another PCR reaction, this time using PyrKIItet HA2 F and PyrKIItet HA1 R primers to join the two fragments together, containing the intervening EcoRV site. The resulting amplicon was then ethanol precipitated. The pMG74 plasmid was then cut with AscI and AatII restriction enzymes in the presence of rSAP, and ethanol precipitated. The HA1/HA2 fragment was then inserted into this plasmid using In-Fusion (Clontech) cloning methods. The resulting pMG74 plasmid was validated and then linearized with EcoRV for transfection into PfMev parasites.

Insertion of the pMG74 plasmid also relies on cutting of the genetic region using a gene-specific gRNA encoded by the pCasG plasmid. The pCasG plasmid was digested as previously described, with BsaI and also treated with rSAP. Guide RNAs were synthesized as oligos and (**Table 4-4**), annealed, and inserted in the pCasG plasmid via In-Fusion cloning.

The linearized PyrKII pMG74 plasmid along with the genetic-specific pCasG plasmid were co-transfected into the PfMev line, using the same transfection protocol as described previously. The parasites were then selected for 7 days with 2.5ng/mL blasticidin, 1.5μM DSM1, and 0.5μM aTc. After 7 days, the drug pressure was removed and the parasites were cultured with CMA media, and continuously cultured in the presence of 0.5μM aTc. Resulting parasites were single-cloned following the single-cloning methods listed later this section.

Magnetic purification and synchronization of parasite cultures

Parasite lines were synchronized via magnetic purification, isolating late-stage parasites mostly in the schizont stage (77). This was accomplished by passing 10mL of a

mixed stage culture at ~5-10% parasitemia and 1% hematocrit through a MACS LS column (Miltenyi BioTec) placed in a custom-made magnet with a field strength of about ~8,000g The column was washed with 1mL CMA, and the parasites were eluted with 1mL of the appropriate media (in the absence of a magnet) into a flask containing 9mL pre-warmed media and 200µL of 50% hematocrit blood to generate a synchronized culture at 1% hematocrit.

TetR-DOZI PyrKII Growth Curve

Growth curves for the TetR-DOZI PyrKII line were conducted using cultures that had been synchronized using magnetic purification, as mentioned above, 6 hours prior to seeding. Once the parasite lines were synchronized, the parasitemia was counted via Giemsa stain in order to determine how much culture was needed to seed wells at the desired parasitemia. Once this was calculated, the required volume was removed from the parental flask and transferred to a 15mL conical tube, and CMA media pre-warmed to 37°C was added until a final volume of 10mL was reached. The culture was then centrifuged at 1,600xg at room temperature (~25°C) for 5 minutes. The media was aspirated, and the pellet was resuspended in 10mL of CMA. The washing was done an additional time to ensure removal of any residual aTc from the parental culture. The culture was then resuspended in the appropriate volume required for seeding. This volume was then split in half, with one half receiving 0.5µM aTc, while the other did not. Parasites from both conditions were then seeded in a 96-well flat bottom cell culture plate (Corning) at a starting parasitemia of 0.5% at 2% hematocrit, at a total volume of 250µL in quadruplicate. For each well, 150µL of the appropriate media was replaced daily. Parasite samples were collected every 24 hours and counted via SYBR green staining and flow cytometry as outlined above.

On day 4 of the growth curve, $1/10^{th}$ of the culture was used to seed another 96-well plate with identical growth and culture conditions as the original plate to show the growth kinetics of the lines after a 1:10 cut. This helped to remove any dead parasite that may have been detected and counted as a parasite via flow cytometry (which would artificially raise the parasitemia count). These 1:10 cut cultures were then treated in the same manner as previously mentioned, with samples being collected every 24 hours and 150μL of the appropriate media replaced daily until day 8.

Generation of the PyrKII Conditional Localization Line

The conditional localization domain was added to the endogenous PyrKII enzyme using CRISPR-Cas9 genome editing techniques, and relied on markerless selection. To engineer this line two constructs were created, a pCasG plasmid, and a repair template plasmid. The pCasG plasmid expresses the Cas9 enzymes and a gene-specific gRNA. The pCasG plasmid was digested as previously described, with BsaI and also treated with rSAP. Guide RNAs were synthesized as oligos and (**Table 4-4**), annealed, and inserted in the pCasG plasmid via In-Fusion cloning.

The repair construct was generated by first synthesizing a piece of DNA that corresponded to the first 250 nucleotides of 5'UTR of the PyrKII gene, ending immediately before the start codon. This was immediately followed by the conditional localization domain, that had been previously generated and validated (60), followed by a BsaI type IIs restriction site for the insertion of the PyrKII genetic sequence corresponding to what we predict to be the start of the PyrKII protein after processing of the signal and transit peptide, and thus begins at the 42^{nd} amino acid. The 5' UTR and genetic region of PyrKII included in this repair construct function as homology arms for the homology directed repair and thus

insertion of an N-terminal CLD into the endogenous PyrKII gene sequence. For insertion of the PyrKII genetic sequence, the above-mentioned plasmid was digested with BsaI in the presence of rSAP and then ethanol precipitated. The PyrKII genetic region was then amplified using the primers in **Table 4-9** (PyrKII HA2 F, and PyrKII HA2 F), and inserted into the cut plasmid via In-Fusion cloning. This sequence was then validated and inserted into the pRSng plasmid, by first cutting the plasmid with NotI, and then ethanol precipitating it. The entire genetic region containing the 5' UTR, CLD and PyrKII genetic sequence was then amplified with the primers listed in **Table 4-9** (PyrKII pRSHA1F, and PyrKII pRSHA2R), and then inserted into the previously cut pRSng plasmid.

The pRSng-PyrKII-CLD plasmid along with the genetic-specific pCasG plasmid were co-transfected into the PfMev line, using the same transfection protocol as described previously. The parasites were then selected for 14 days with 1.5μM DSM1 and 2.5nM WR99210. After 14 days, the drug pressure was removed and the parasites were cultured with CMA media. The insertion of the CLD was validated using the primers listed in **Table 4-10**. This method looked for insertion of the CLD as well as the potential presence of any contaminating wild-type parasites. Insertion at the 5' end was done by pairing the PyrKcld.5.F and CLD.R primers. Insertion at the 5' end was done by pairing the PyrKcld.3.R and CLD.F primers. The presence of any residual wild-type parasites was screened at the 5' end of the PyrKII gene by pairing the PyrKcld.5.F and PyrkcldWT.5.R, and screened at the 3' end of the gene by pairing the Pyrkcld.wt.3.F and PyrKcld.3.R primers. These reactions were also replicated for the parental PfMev line as a control. These PCR reactions were conducted on the lines, but there was still some contaminating wild-type parasites. Thus, the parasites were single-cloned following the below mentioned methods, and screened again via PCR. After single cloning, we were successful in obtaining a clonal

line of parasites that contained the conditional localization domain on the N-terminal end of the PyrKII gene.

Parasite cloning through limiting dilution

Single cloning of the PyrKII TetR-DOZI and CLD lines were carried out via limiting dilution. For each parasite line, the type of media used for the dilution and media change is the same as that within the flask from which the sample is derived. The parasitemia for each culture was determined using Giemsa staining, and used to calculate the number of infected RBCs (iRBCs) per μL of culture. Based on the iRBC concentration, a sample consisting of 1,000 iRBCs/μL in media was prepared. This sample was then diluted 1:10 three times sequentially, yielding a parasite sample with a final concentration of 1 iRBC/μL. Then, a 2% hematocrit media was pipetted into row A of a 96-well flat bottom cell culture plate (Corning) at 200μL per well, followed by the diluted parasite sample at 100uL per well. Finally, a 1:3 serial dilution was carried out from row to row starting from row A and all the way down to row H. The prepared plate was placed into a Modular Incubator Chamber (Billups-Rothenberg Inc.), and gassed with 92% N_2, 3% O_2, 5% CO_2 for 1 min and 15 seconds prior to incubation at 37°C.

After seeding on day 0, the media was changed on days 5, 7, 9, 12, and 14. On days 5 and 12, a 0.5% hematocrit media was used; on days 7, 9, and 14, pure media (without any blood) was used. On day 16, selected iRBC-positive wells that are the most dilute (i.e., closest to row H) were picked and transferred into a 24-well flat bottom cell culture plate (Corning) at 2% hematocrit and 1mL total volume per well. The 24-well plate was then maintained and routinely monitored. Upon reaching a high enough parasitemia (~8%), the content within the well was transferred into a 75cm^2 sealed cell culture flask and further

maintained. For each cloned parasite line, the genotype confirmed via PCR using the above-mentioned primer sets.

CLD-PyrKII Growth Curve

The growth curve for the CLD-PyrKII line was conducted identically as described for the TetR-DOZI line (*vide ante*), with the exception that the parental line was not washed, as there was no need to remove any ligand. Additionally, once parasite cultures were split, one culture received 500nM Shield1, while the other did not.

CLD-PyrKII Sample Collection for Microarray

A mixed stage CLD-PyrKII line at ~5-10% parasitemia was synchronized via magnetic purification as detailed above. Six hours post synchronization, the parasitemia of the culture was counted in order to determine the volume required for seeding. The determined volume was taken from the parental flask and used to seed a 50mL culture flask at 1% parasitemia and 2% hematocrit with 500nM Shield1, with this point considered as time 0.

To collect the sample at each time point, 5mL of the culture was taken and transferred to a 15mL conical tube, which was then centrifuged at 1,600g at room temperature (~25°C) for 5 minutes. The media was then aspirated and ~100µL of the pelleted cells were transferred to a 1.5mL cryo tube and snap frozen by submerging the tube in a slurry of dry ice and 70% ethanol and stored at -80°C until the samples were processed for microarray analysis. Samples were collected for microarray analysis every 8 hours for 56 hours, at times 0, 8, 16, 24, 32, 40, 48, 56 hours post Shield1 addition. To ensure that

parasite growth was not hindered by the lack of nutrients, the media was replaced with the appropriate volume of pre-warmed media containing 500nM Shield1 at 16, and 40 hours.

Samples were sent to the Johns Hopkins Genomic Analysis and Sequencing Core Facility for microarray analysis using Agilent microarray chip AMADID 037237. This same experiment was conducted three separate times, and the data shown are based on averages of the data collected.

Tracking apicoplast loss via live epi-fluorescent microscopy

While the above experiment was being conducted the morphology of the apicoplast was also tracked by taking 100μL samples from the culture for analysis via live epifluorescent microscopy at times 0, 16, 40, 64, 88, and 110 hours. For each of these time points the parasites were prepared for analysis via microscopy following the same protocol listed as above, including staining with DAPI and mitoTracker CMX-Ros (Invitrogen). For each time point, images were collected using the same method as listed above, for a minimum of 15 parasite cells. The images were processed and deconvolved using the same methods as listed above. Apicoplast morphology was assessed by visual inspection to determine whether the apicoplast was intact or disrupted multiple discrete vesicles. Parasitized cells in which the status of the apicoplast was unclear, such as with late stage schizont parasites were discarded to avoid misclassification. Average data are presented from three independent biological replicates.

FIGURES

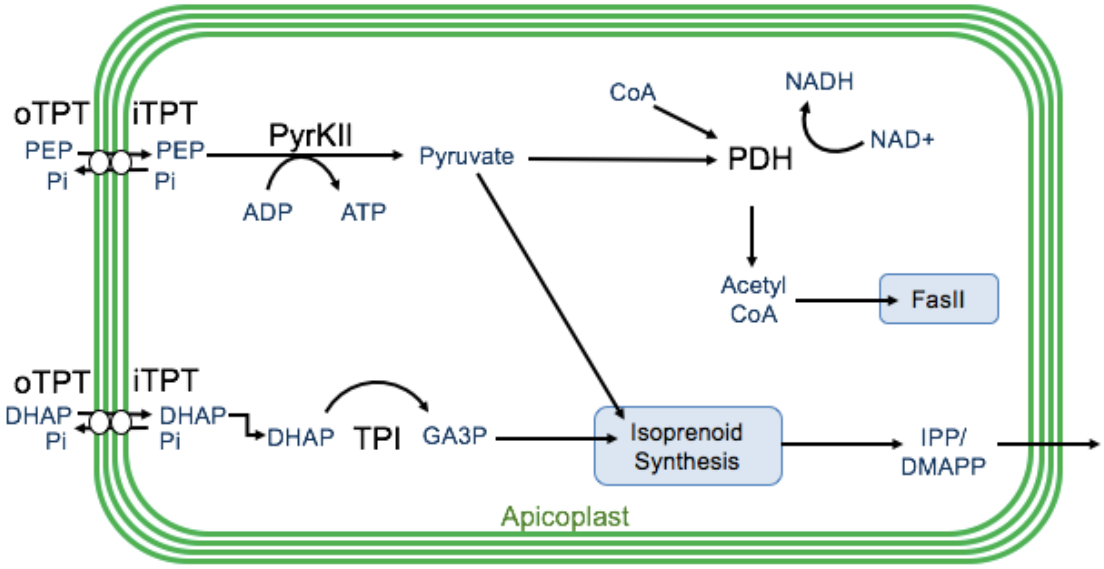

Figure 4-1 Carbon metabolism in the apicoplast

Carbon backbones are imported into the apicoplast organelle in the form of 3-carbon phosphates by the apicoplast membrane outer triose phosphate transporter (oTPT) and inner triose phosphate transporter (iTPT). Pyruvate kinase II (PyrKII) converts substrates phosphoenolpyruvate (PEP) and adenosine diphosphate (ADP) into products pyruvate and adenosine triphosphate (ATP). Pyruvate is used by the FASII fatty acid biosynthesis pathway as well as the MEP isoprenoid precursor pathway.

Triose phosphate isomerase (TPI) converts dihydroxyacetone phosphate (DHAP) into glyceraldehyde-3-phosphate (GA3P), which is also required for the isoprenoid precursor pathway.

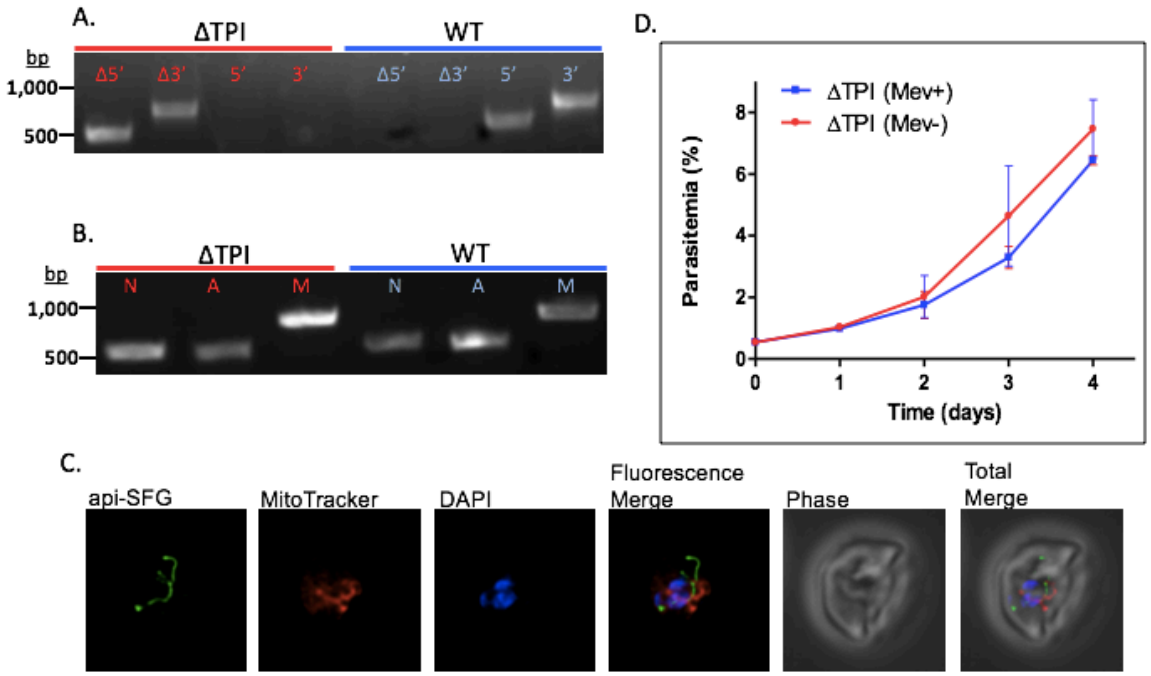

Figure 4-2 Characterization of the PfMev ΔTPI parasite line

A.) Genotyping PCR confirming the deletion of TPI, with amplification demonstrating integration at the Δ5' and Δ3' loci, and lack of wild type parasites due to failure to amplify at the wild type 5' and 3' loci, as compared to the parental control.

B.) PCR detection of the lactate dehydrogenase, SufB, and Cox1 genes from the nuclear (N), apicoplast (A), and mitochondrial (M) genomes, respectively. We successfully amplified SufB from the PfMev ΔTPI parasite line, indicating retention of the apicoplast organelle genome.

C.) Live fluorescence microscopy of the PfMev ΔTPI parasite line. This parasite line expresses api-SFG (green), and is also stained with MitoTracker (red) and DAPI (blue).

D.) Growth curve of PfMev ΔTPI parasites cultured with or without 50μM mevalonate.

Microscopy images are 10μM long by 10μM wide.

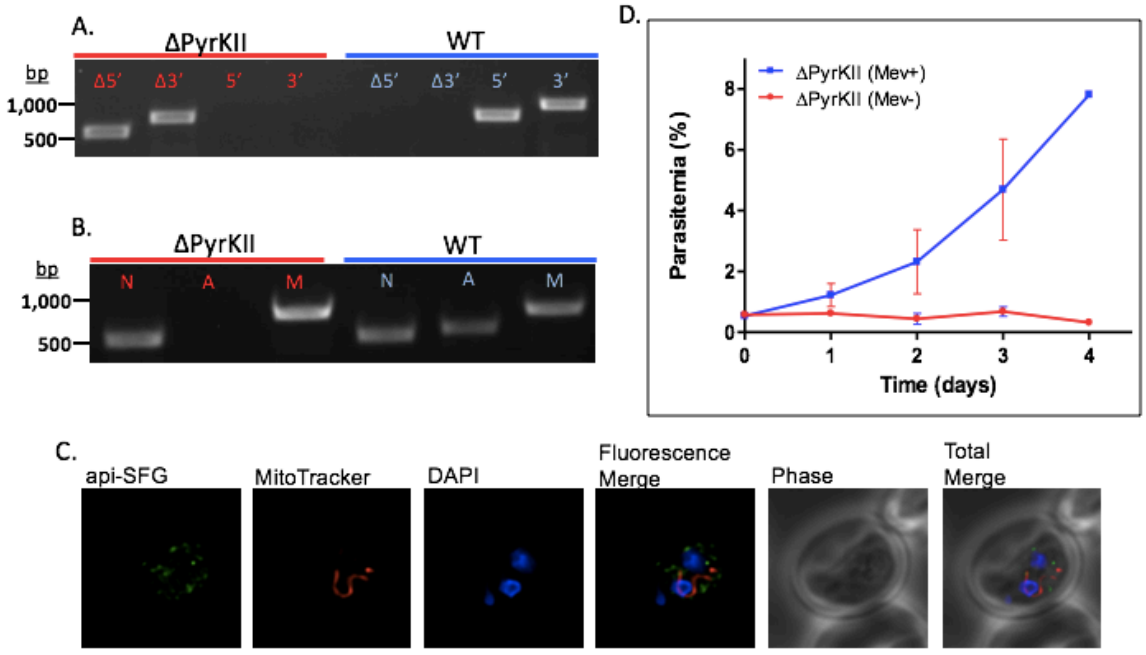

Figure 4-3 Characterization of the PfMev ΔPyrKII parasite line

A.) Genotyping PCR confirming the deletion of PyrKII, with amplification demonstrating integration at the Δ5' and Δ3' loci, and lack of wild type parasites due to failure to amplify at the wild type 5' and 3' loci, as compared to the parental control.

B.) PCR detection of the lactate dehydrogenase, SufB, and Cox1 genes from the nuclear (N), apicoplast (A), and mitochondrial (M) genomes, respectively. We failed to amplify SufB from the PfMev ΔPyrKII parasite line, indicating loss of the apicoplast organelle genome.

C.) Live fluorescence microscopy of the PfMev ΔPyrKII parasite line. This parasite line expresses api-SFG (green), and is also stained with MitoTracker (red) and DAPI (blue).

D.) Growth curve of PfMev ΔPyrKII parasites cultured with or without 50μM mevalonate.

Microscopy images are 10μM long by 10μM wide.

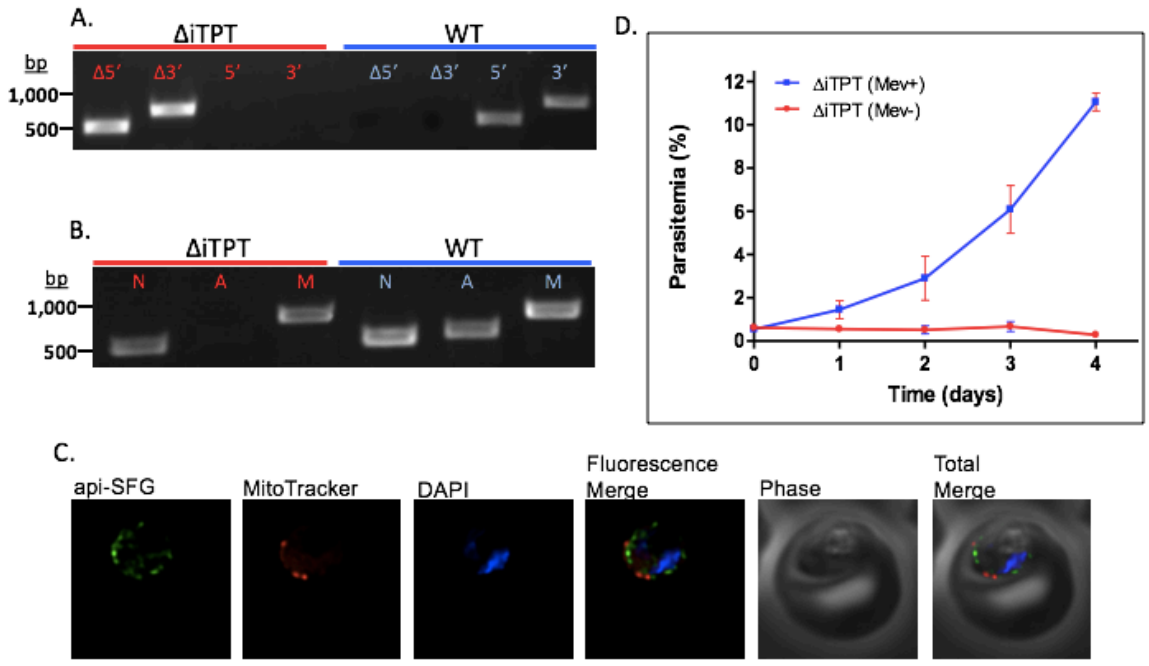

Figure 4-4 Characterization of the PfMev ΔiTPT parasite line

A.) Genotyping PCR confirming the deletion of iTPT, with amplification demonstrating integration at the Δ5' and Δ3' loci, and lack of wild type parasites due to failure to amplify at the wild type 5' and 3' loci, as compared to the parental control.

B.) PCR detection of the lactate dehydrogenase, SufB, and Cox1 genes from the nuclear (N), apicoplast (A), and mitochondrial (M) genomes, respectively. We failed to amplify SufB from the PfMev ΔiTPT parasite line, indicating loss of the apicoplast organelle genome.

C.) Live fluorescence microscopy of the PfMev ΔiTPT parasite line. This parasite line expresses api-SFG (green), and is also stained with MitoTracker (red) and DAPI (blue).

D.) Growth curve of PfMev ΔiTPT parasites cultured with or without 50μM mevalonate.

Microscopy images are 10μM long by 10μM wide.

Plasmids	Time of selection	Successful?
Puf1-Cas9/pL8-oTPT-HA1/2+g (14s16)	31 days	No
Puf1-Cas9/pL8-oTPT-HA1/2+g (20s16)	40 days	No
Puf1-Cas9/pL8-oTPT-HA1/2+g (27s16)	40 days	No
Puf1-Cas9/pL8-oTPT-HA1/2+g (3o16)	40 days	No
Puf1-Cas9/pL8-oTPT-HA1/2+g (31o16)	40 days	No
Puf1-Cas9/pL8-oTPT-HA1/2+g (8n16)	40 days	No
Puf1-Cas9/pL8-oTPT-HA1/2+g (28n16)	40 days	No

Table 4-1 oTPT deletion transfection attempts

We attempted to knockout the outer triose phosphate transporter (oTPT) gene. In none of the seven independent transfections were we successful in deleting the oTPT gene.

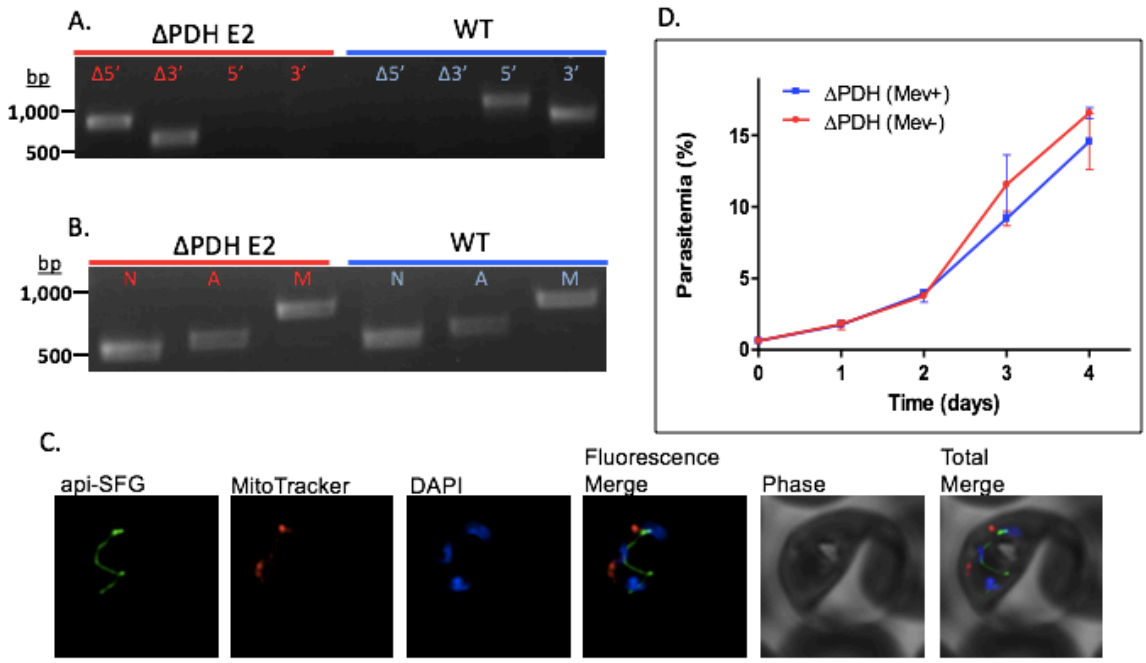

Figure 4-5 Characterization of the PfMev ΔPDH E2 parasite line

A.) Genotyping PCR confirming the deletion of PDH E2, with amplification demonstrating integration at the Δ5' and Δ3' loci, and lack of wild type parasites due to failure to amplify at the wild type 5' and 3' loci, as compared to the parental control.

B.) PCR detection of the lactate dehydrogenase, SufB, and Cox1 genes from the nuclear (N), apicoplast (A), and mitochondrial (M) genomes, respectively. We successfully amplified SufB from the PfMev ΔPDH E2 parasite line, indicating retention of the apicoplast organelle genome.

C.) Live fluorescence microscopy of the PfMev ΔPDH E2 parasite line. This parasite line expresses api-SFG (green), and is also stained with MitoTracker (red) and DAPI (blue).

D.) Growth curve of PfMev ΔPDH E2 parasites cultured with or without 50μM mevalonate.

Microscopy images are 10μM long by 10μM wide.

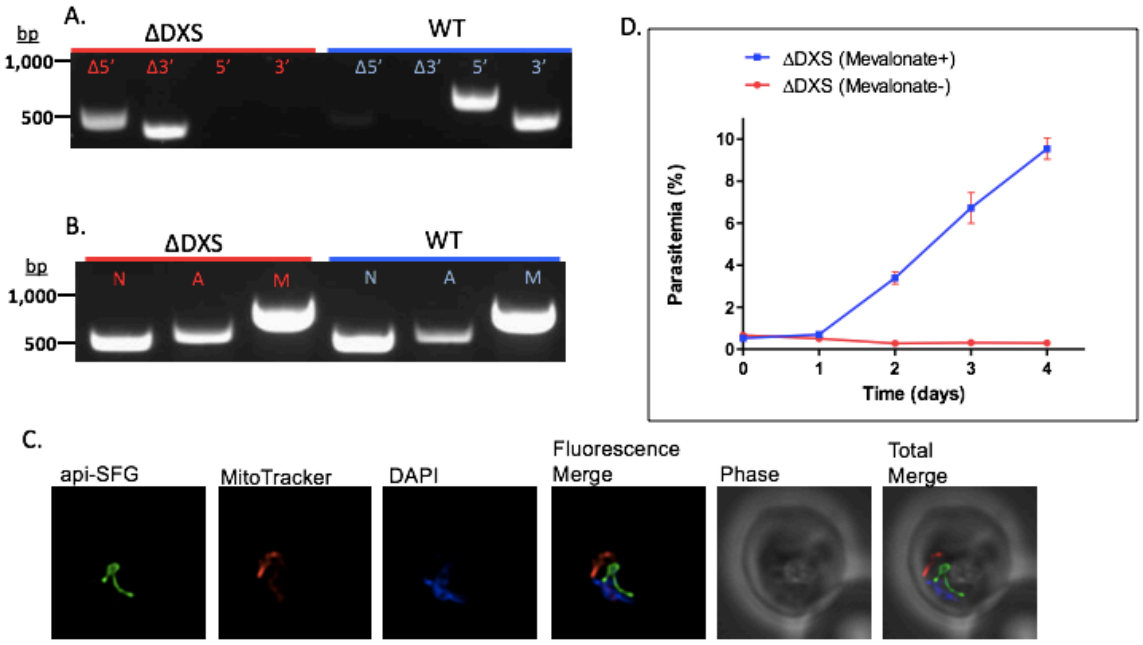

Figure 4-6 Characterization of the PfMev ΔDXS parasite line

A.) Genotyping PCR confirming the deletion of DXS, with amplification demonstrating integration at the Δ5' and Δ3' loci, and lack of wild type parasites due to failure to amplify at the wild type 5' and 3' loci, as compared to the parental control.

B.) PCR detection of the lactate dehydrogenase, SufB, and Cox1 genes from the nuclear (N), apicoplast (A), and mitochondrial (M) genomes, respectively. We successfully amplified SufB from the PfMev ΔDXS parasite line, indicating retention of the apicoplast organelle genome.

C.) Live fluorescence microscopy of the PfMev ΔDXS parasite line. This parasite line expresses api-SFG (green), and is also stained with MitoTracker (red) and DAPI (blue).

D.) Growth curve of PfMev ΔDXS parasites cultured with or without 50μM mevalonate.

Microscopy images are 10μM long by 10μM wide.

Substrate	K_{cat} (min^{-1})	K_M (mM)	K_{cat}/K_M (mM^{-1} min^{-1})	Organism
ADP	**790** +/-190	**0.25** +/-0.10	3,170	*P. falciparum*
GDP	**400** +/-45	**0.10** +/-0.05	5,670	
CDP	**440** +/-70	**1.00** +/-0.10	430	
UDP	**250** +/-40	**0.80** +/-0.20	310	
dADP	**400** +/-30	**0.40** +/-0.05	1058	
dGDP	**90** +/-5	**0.30** +/-0.50	321	
dCDP	**80** +/-5	**0.50** +/-0.10	150	
ADP	**2850** +/-80	**8.0** +/-0.40	360	*T. gondii*
GDP	**6600**+/-240	**0.05** +/-0.006	121,320	

Table 4-2 Enzyme kinetics of pure recombinant PyrKII as compared to *T. gondii* PyrKII

Activity of PyrKII was measured using various NPDs and dNDPs as substrates. Values are reported for the kinetic parameters K_{cat}, K_M, and K_{cat}/K_M (catalytic efficiency).

Kinetic parameters for *T. gondii* PyrKII from Saito and coworkers are shown for comparison (39).

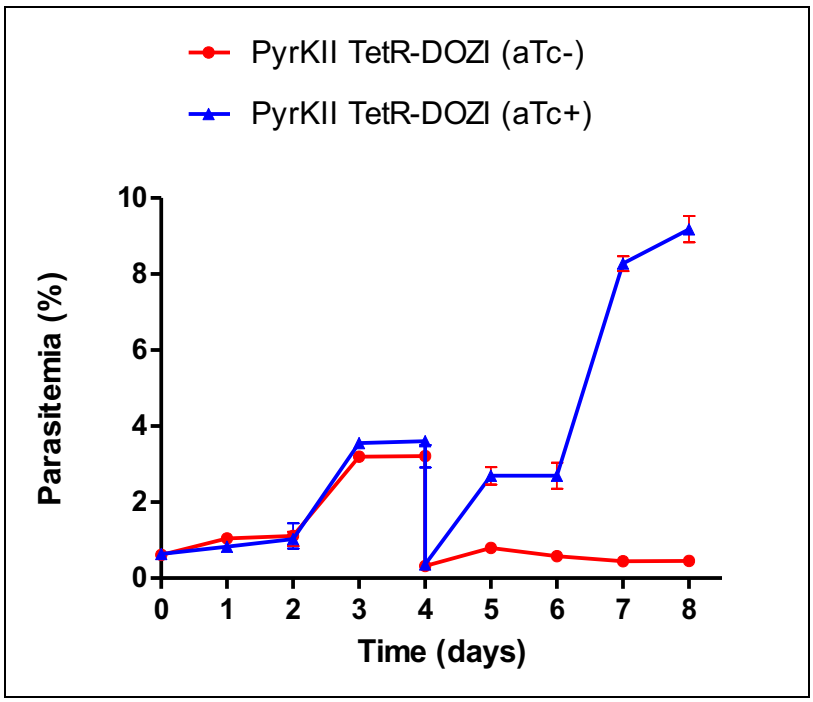

Figure 4-7 Growth of the PfMev PyrKII TetR-DOZI line under permissive and non-permissive knockdown conditions

Synchronized PfMev PyrKII TetR-DOZI parasites were seeded at 0.5% parasitemia and cultured without the mevalonate supplement in the permissive (with aTc) or non-permissive (no aTc) conditions for 8 days. Parasites were collected daily and parasitemia was determined via flow cytometry. Upon the removal of aTc, parasites exhibit a decrease in growth, which was more pronounced after the cultures are cut 1:10 on day 4. Error bars represent the standard error of the mean from two experiments, each conducted in quadruplicate.

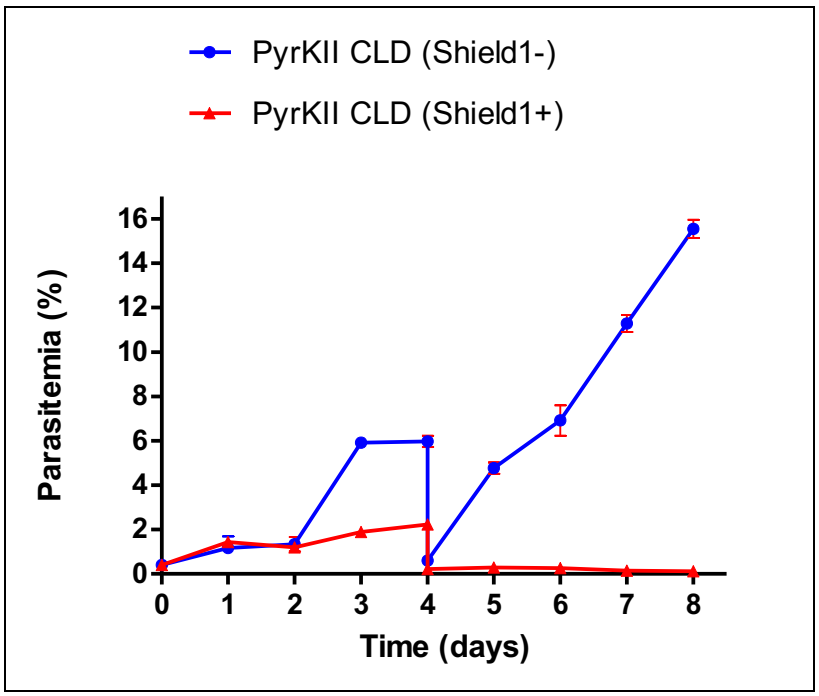

Figure 4-8 Growth of the PfMev PyrKII-CLD line under permissive and non-permissive conditional localization conditions

Synchronized PfMev PyrKII-CLD parasites were seeded at 0.5% parasitemia and cultured without the mevalonate supplement in the permissive (no Shield1) or non-permissive (500nM Shield1) conditions for 8 days. Parasites were collected daily and parasitemia was determined via flow cytometry. Upon the addition of Shield1, parasites exhibit a rapid decrease in growth, which can be seen clearly by day 3, but is more pronounced after the cultures are cut 1:10 on day 4. Error bars represent the standard error of the mean from two experiments, each conducted in quadruplicate.

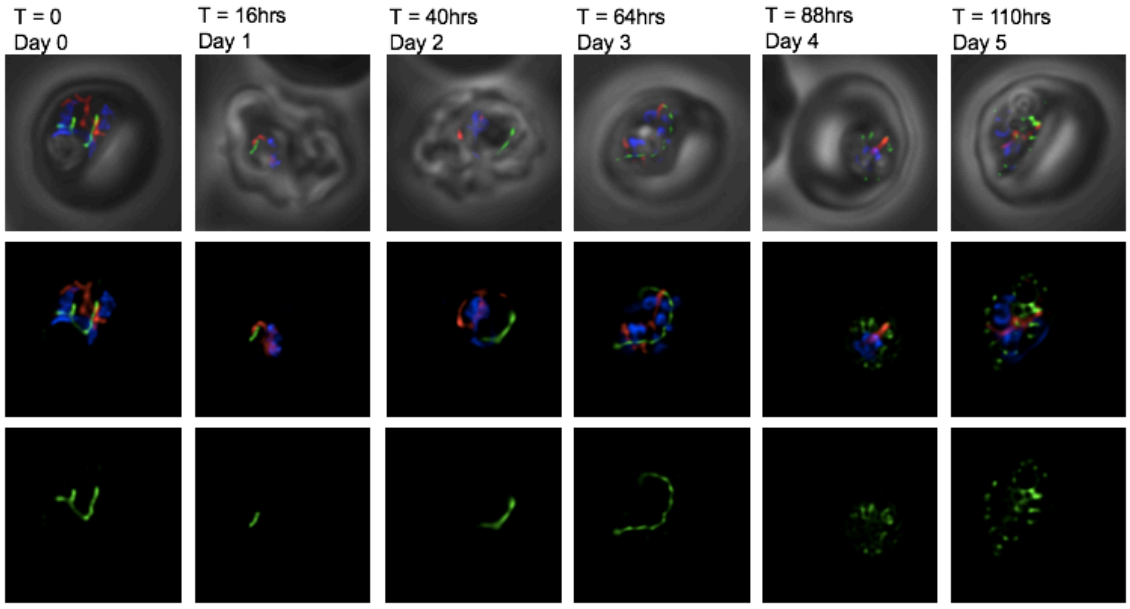

Figure 4-9 Tracking apicoplast disruption in PyrKII-CLD parasites via live epifluorescent microscopy

Live fluorescence microscopy of the PfMev PyrKII-CLD parasite line after Shield1 treatment. This parasite line expresses api-SFG (green), and is also stained with MitoTracker (red) and DAPI (blue). The above images are representative images of the state of the apicoplast organelle at the corresponding time points. Each day, a minimum 15 microscopy images were taken to determine apicoplast morphology (intact or disrupted), with average values from three independent experiments displayed in the previous graph. Microscopy images are 10μM long by 10μM wide.

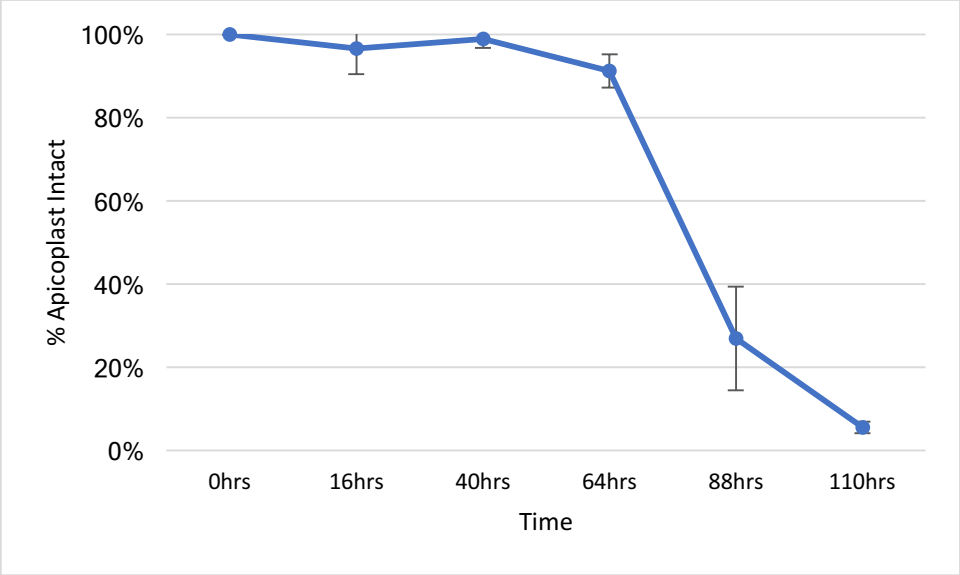

Figure 4-10 Quantifying apicoplast disruption in PyrKII-CLD parasites via live epifluorescent microscopy

Graph of the percentage of disrupted apicoplast organelles in synchronized PyrKII-CLD parasite lines after Shield1 treatment. Each day a minimum 15 microscopy images were taken to determine apicoplast morphology (intact or disrupted) based on api-SFG fluorescence. The percentage of parasites containing an intact apicoplast dropped precipitously between the second and third growth cycle of the parasite, corresponding to the 64 and 88-hour time points. Error bars represent the standard deviation from three independent experiments.

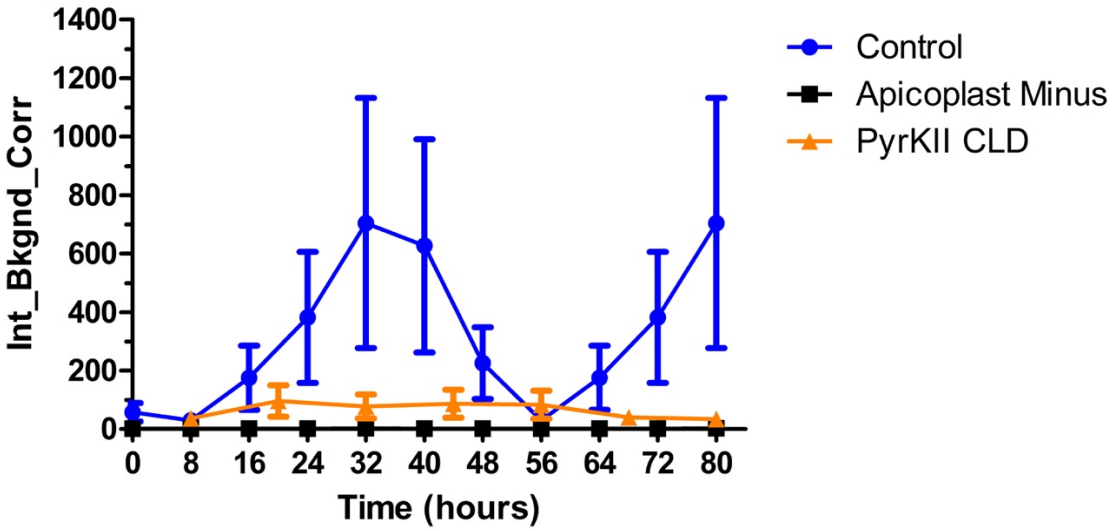

Figure 4-11 Measuring apicoplast transcript levels in Shield1-treated PyrKII-CLD parasites

Synchronized ring-stage PyrKII-CLD parasites were treated with of Shield1, with samples collected every 8 hours for 48 hours to be used for microarray analysis. The intensity background corrected average mRNA levels of genes encoded by the apicoplast organelle genome were compared to an untreated control line as well as a IPP-dependent apicoplast minus parasite line that had previously been treated with azithromycin for 10 days.

Table 4-3 Primer sequences used to amplify homology arms for genetic knock outs

Primer Name	Primer Sequence
PyrKII HA1 F	GCCACGAGCGGCCTATGATAAATTTTATAAGCAAGGAAG
PyrKII HA1 R	AAGCGCAGCGGCCTGTTTTGGTTACCTAATGAATTC
PyrKII HA2 F	CGACAGACGCCGGTTTCTGTATTCCTAATATGATTATGCC
PyrKII HA2 R	GGCCACCAGCCGGTAAATTGGATAAATTCGTTTCGATTC
iTPT HA1 F	GCCACGAGCGGCCCATATAAATATTATGCCTTGCCCAACC
iTPT HA1 R	AAGCGCAGCGGCCTTCCTATTAATTTGTGAAGGACGTTTG
iTPT HA2 F	CGACAGACGCCGGGTGCTGGTGCTATTAGTTTTGTTCATA
iTPT HA2 R	GGCCACCAGCCGGCTGTGCTTGCAACAGCATGTGTAATAT
oTPT HA1 F	GCCACGAGCGGCCGTAGTTATTTTATTACGTGAGACCTCA
oTPT HA1 R	AAGCGCAGCGGCCGGATTTTTTTCATTCCACTTATCCAAT
oTPT HA2 F	CGACAGACGCCGGGTGCAACCTTATCAAATTTTGGTTCAT
oTPT HA2R	GGCCACCAGCCGGAATGTCATCGTTAAAATGCCACAATTC
TPI HA1 F	GCCACGAGCGGCCCCATTATGGTGATATTTGTTCATCTTG
TPI HA1 R	AAGCGCAGCGGCCGTTCATCATGGGTTAATATATTTTCCA
TPI HA2 F	CGACAGACGCCGGTGCTATAGGTACAGGACAACCTGTATC
TPI HA2 R	GGCCACCAGCCGGCACAGGGAAAATATGCTAATGATCTAC
PDH E2 HA1 F	GCCACGAGCGGCCCGTGGAAGCATTTGATGAAGGTATAAC
PDH E2 HA1 R	AAGCGCAGCGGCCTCCACTTCTATGGTGCTTTTATCATCC
PDH E2 HA2 F	CGACAGACGCCGGATTACCAGATTCTCTATTAACTCCTGT
PDH E2 HA2 R	GGCCACCAGCCGGCAATACTTCCAATATTTGTGCCGATTG
DXS HA1 F	GCCACGAGCGGCCGAATAGGTTGTCAAGGAAAAATTCGTTATG
DXS HA1 R	AAGCGCAGCGGCCATTAGCTAGTTTGTCCTGTTCATGTGAC
DXS HA2 F	CGACAGACGCCGGTGGTTTAACAGGTGGAATGGC
DXS HA2 R	GGCCACCAGCCGGAGCTCTTCTGTATTATTACCATTCACAACACC

Table 4-4 Oligonucleotides designed for In-Fusion insertion of gRNA sequences

Primer Name	Primer Sequence
PyrKII gRNA F	TAAGTATATAATATTAATTTAATTGTACCCTGTTTGTTTTAGAGCTAGAA
PyrKII gRNA R	TTCTAGCTCTAAAACAAACAGGGTACAATTAAATTAATATTATATACTTA
iTPT gRNA F	TAAGTATATAATATTTCTATTATCTGTTATTGCTAGTTTTAGAGCTAGAA
iTPT gRNA R	TTCTAGCTCTAAAACTAGCAATAACAGATAATAGAAATATTATATACTTA
oTPT gRNA F	TAAGTATATAATATTATTTTACTTGGATAGCTTTTGTTTTAGAGCTAGAA
oTPT gRNA R	TTCTAGCTCTAAAACAAAAGCTATCCAAGTAAAATAATATTATATACTTA
TPI gRNA F	TAAGTATATAATATTTAATCATAGCCTTTGAGCCAGTTTTAGAGCTAGAA
TPI gRNA R	TTCTAGCTCTAAAACTGGCTCAAAGGCTATGATTAAATATTATATACTTA
PDH E2 gRNA F	TAAGTATATAATATTGTTAATATAGGAAATGCATTGTTTTAGAGCTAGAA
PDH E2 gRNA R	TTCTAGCTCTAAAACAATGCATTTCCTATATTAACAATATTATATACTTA
DXS gRNA F	TAAGTATATAATATTATTGCTATTATAGGAGATGGGTTTTAGAGCTAGAA
DXS gRNA R	TTCTAGCTCTAAAACCCATCTCCTATAATAGCAATAATATTATATACTTA
PyrKIITetR gRNA F	TAAGTATATAATATTCCATGTCTAACAAATTAGCAGTTTTAGAGCTAGAA
PyrKIITetR gRNA R	TTCTAGCTCTAAAACTGCTAATTTGTTAGACATGGAATATTATATACTTA
PyrKIICLD gRNA F	TAAGTATATAATATTTCCATTGCCAGAACCTACAAGTTTTAGAGCTAGAA
PyrKIICLD gRNA R	TTCTAGCTCTAAAACTTGTAGGTTCTGGCAATGGAAATATTATATACTTA

Table 4-5 Primer sequences used for confirmation of gene deletions

Primer Name	Primer Sequence
pl8insHA1R	TACAAAATGCTTAAGCGCAGCGGCC
pl8insHA2F	CATATTTATTAAATCTAGAATTCGACAGACGCCG
PyrKII 5' F	GTTAATTGCATAAAAAAGAATAACAAACATATTGC
PyrKII 3'R	CCATCATTTGTGTTGCTACAATTACTGG
PyrKII 5' WT R	CCTTTTTTACTATATAATTTTCCACCTGTTAAAACTTGTA
PyrKII 3' WT F	GGGTACAATTAAATTATCCAGAATTAATAAAGAATGC
iTPT 5'F	GCTTATATTGTAAACAATGATTGTTATTGC
iTPT 3'R	CAAGAGAATATACAAATGTTCCACCAAC
iTPT 5'WT R	GGAATAGAAAAAACGGGTATATTAAATGC
iTPT 3' WT F	CCTTAATCAAAGGATTCCAAAAATACG
oTPT 5'F	TCCTTACACATATTACAAAGTATTTAAAAGGA
oTPT 3'R	GACTAAAACGATTTCTTAAATGTCAAAAGG
oTPT 5' WT R	ACCAAAATGAACAAATATATGACATACAC
oTPT 3' WT F	CCTTATTAATTATTGTAGGTGGTGTTGTTTG
TPI 5'F	GTGTATAATATTATGGGATTTAATATATATATGTGTG
TPI 3'R	GGAAGTCACGAAATAAAATTAAAAAAAAAAAAAGAATC
TPI 5' WT R	GCTTCCTCTTTTGATAAATAGCATTTCC
TPI 3' WT F	CCATATTTTATTTTCCCCAGCTTATC
PDH E2 5'F	GCCAGCTCTATCTAGTACCATGACG
PDH E2 3'R	CGCTGCTGCATGGGATCCATAG
PDH E2 5' WT R	GTCTAAATCTACGAACTGTCCTTCCTTGAC
PDH E2 3' WT F	CCGTTCCAGTGTTCCGTGTTACTC
DXS 5'F	GAACTTTGTACCAGTTGTTCTATACATTCTCC
DXS 3'R	CGATTTTTTTGTACGTACATGAAGAACAGTAGC
DXS 5' WT R	GTGCAATTTTTTTTTTTATAGGCCTTATGCAG
DXS 3' WT F	CCTTCAGATGTGGTAGGAAGAGAAAATACG

Table 4-6 Primer sequences used to detect genes from the nuclear and organellar genomes

Primer Name	Primer Sequence
LDH F	GGAGATGTAGTTTTGTTCGATATTG
LDH R	CTTGTAAAGGGATACCACCTACAG
SufB F	CATGTAGCTATAGTAGAAATAATAGTAAAAGATTATGG
SufB R	GACTCTGAAATACTTAAACCACGTTGC
Cox1 F	CTTCATCTTTAAGAATAATTGCACAAGAAAATGTAAATC
Cox1 R	GTACATATGATGTACCCATACTAAGCTTCC

Table 4-7 Primer sequences used to amplify harmonized PyrKII for In-Fusion insertion into the pMAL-cHT expression plasmid

Primer Name	Primer Sequence
PfPyrKIIpMAL F	ATCACCATCAC**GAATTC**ATGGGCAGTGGAAACGGCTCAGG
PfPyrKIIpMAL R	CGGCCAGTGCC**AAGCTT**AGTTGGTGAGGCACGGCTGACAC

Endonuclease sites are marked in bold.

Table 4-8 Primer sequences used for generation of the PyrKII-TetR-DOZI line

Primer Name	Primer Sequence
PyrKIITetR HA1F	GATATCGTCCACCTGGATATCGAGCAAGATATTCAAAATAATATATCCTATTTTG
PyrKIITetR HA1R	CATAAGGATAGACGTCATTTGTTAGACATGGTTGACATAAATAAAGTAA
PyrKIITetR HA2F	CCCTTTCCGGGCGCGCCTTCATCTTACACATATTTATGTGCC
PyrKIITetR HA2R	GATATCCAGGTGGACGATATCCTTTCATAACAACATAGGATTATTAATTATGAGG

Table 4-9 Primer sequences used for generation of the PyrKII-CLD line

Primer Name	Primer Sequence
PyrKII HA2F	TTGCTAAAGTTAGAAGGTTCTGGCAATGGATCGGGGGATT
PyrKII HA2R	TTACGCCGCGGCCGCCATCTATACCATTTAAGTATAATTT
PyrKII pRSHA1F	GCGGCCGTGCCACGAGCGGCCGACGCGTAAAGTAAATGAT
PyrKII pRSHA2R	AAATGCTTAAGCGCAGCGGCCGCCATCTATACCATTTAAG

Table 4-10 Insertion validation primers for the PfPyrKII-CLD line

Primer Name	Primer Sequence
PyrKcld.5.F	CGTATATTGAAATGGGCCCTACATAGAAATATTTATAGG
PyrkcldWT.5.R	GTTATTCTTTTTTATGCAATTAACATAACATTTTATTACT
Pyrkcld.wt.3.F	CCTATGATAAATTTTATAAGCAAGGAAGTAATACCATTG
PyrKcld.3.R	CATTTTCATTTATTTGATTTTTTTCAAATTCTCCTATTC
CLD.F	CAAGTAGGGATAGAAATAAACCATTTAAATTTATGCTAG
CLD.R	CTTGTTTTCCTAGCATAAATTTAAATGGTTTATTTCTATC

REFERENCES

1. Sato S. 2011. The apicomplexan plastid and its evolution. Cell Mol Life Sci 68:1285–96.

2. McFadden GI. 2014. Origin and evolution of plastids and photosynthesis in eukaryotes. Cold Spring Harb Perspect Biol 6:a016105.

3. Janouskovec J, Horák A, Oborník M, Lukes J, Keeling JP. 2010. A common red algal origin of the apicomplexan, dinoflagellate, and heterokont plastids. Proc Natl Acad Sci U S A 107:10949–10954.

4. Lemgruber L, Kudryashev M, Dekiwadia C, Riglar DT, Baum J, Stahlberg H, Ralph SA, Frischknecht F. 2013. Cryo-electron tomography reveals four-membrane architecture of the *Plasmodium* apicoplast. Malar J 12:25.

5. McFadden GI. 2000. Mergers and acquisitions: malaria and the great chloroplast heist. Genome Biol 1:reviews1026.1.

6. Wilson RJ, Denny PW, Preiser PR, Rangachari K, Roberts K, Roy A, Whyte A, Strath M, Moore DJ, Moore PW, Williamson DH. 1996. Complete gene map of the plastid-like DNA of the malaria parasite *Plasmodium falciparum*. J Mol Biol 261:155–72.

7. McFadden GI. 2000. Mergers and acquisitions: malaria and the great chloroplast heist. Genome Biol 1:reviews1026.1.

8. Lim L, McFadden GI. 2010. The evolution, metabolism and functions of the apicoplast. Philos Trans R Soc Lond B Biol Sci 365:749–63.

9. Martin W. 2003. Gene transfer from organelles to the nucleus: Frequent and in big chunks. Proc Natl Acad Sci 100:8612–8614.

10. Lim L, McFadden IG. 2010. The evolution, metabolism and functions of the apicoplast. Philos Trans R Soc Lond B Biol Sci 365:749–763.

11. Wiley DJ, Merino FE, Krai MP, McLean JK, Tripathi KA, Vega-Rodríguez J, Jacobs-Lorena M, Klemba M, Cassera BM. 2015. Isoprenoid precursor biosynthesis is the essential metabolic role of the apicoplast during gametocytogenesis in *Plasmodium falciparum*. Eukaryot Cell 14:128–139.

12. Vaughan MA, O'Neill TM, Tarun SA, Camargo N, Phuong MT, Aly IAS, Cowman FA, Kappe ISH. 2009. Type II fatty acid synthesis is essential only for malaria parasite late liver stage development. Cell Microbiol 11:506–520.

13. Nagaraj VA, Sundaram B, Varadarajan NM, Subramani PA, Kalappa DM, Ghosh SK, Padmanaban G. 2013. Malaria Parasite-Synthesized Heme Is Essential in the Mosquito and Liver Stages and Complements Host Heme in the Blood-stages of Infection. PLoS Pathog 9:e1003522.

14. Charan M, Choudhary HH, Singh N, Sadik M, Siddiqi IM, Mishra S, Habib S. 2017. [Fe-S] cluster assembly in the apicoplast and its indispensability in mosquito stages of the malaria parasite. FEBS J 284:2629–2648.

15. Yeh E, DeRisi JL. 2011. Chemical rescue of malaria parasites lacking an apicoplast defines organelle function in blood-stage *Plasmodium falciparum*. PLoS Biol 9.

16. Ralph SA, van Dooren GG, Waller RF, Crawford MJ, Fraunholz MJ, Foth BJ, Tonkin CJ, Roos DS, McFadden GI. 2004. Tropical infectious diseases: metabolic maps and functions of the *Plasmodium falciparum* apicoplast. Nat Rev Microbiol 2:203–16.

17. Foth JB, Ralph AS, Tonkin JC, Struck SN, Fraunholz M, Roos SD, Cowman FA, McFadden IG. 2003. Dissecting apicoplast targeting in the malaria parasite *Plasmodium falciparum*. Science 299:705–708.

18. Zuegge J, Ralph S, Schmuker M, McFadden GI, Schneider G. 2001. Deciphering apicoplast targeting signals – feature extraction from nuclear-encoded precursors of *Plasmodium falciparum* apicoplast proteins. Gene 280:19–26.

19. Cilingir G, Lau AOT, Broschat SL. 2013. ApicoAMP: The first computational model for identifying apicoplast-targeted transmembrane proteins in Apicomplexa. J Microbiol Methods 95:313–319.

20. Cilingir G, Broschat SL, Lau AOT. 2012. ApicoAP: The First Computational Model for Identifying Apicoplast-Targeted Proteins in Multiple Species of Apicomplexa. PLoS One 7:e36598.

21. Schleucher J, Vanderveer PJ, Sharkey TD. 1998. Export of carbon from chloroplasts at night. Plant Physiol 118:1439–45.

22. Alberts B, Johnson A, Lewis J, Raff M, Roberts K, Walter P. 2002. Chloroplasts and Photosynthesis.

23. Emes MJ, Neuhaus HE. 1997. Metabolism and transport in non-photosynthetic plastids. J Exp Bot 48:1995–2005.

24. Flugge U-I, Hausler RE, Ludewig F, Gierth M. 2011. The role of transporters in supplying energy to plant plastids. J Exp Bot 62:2381–2392.

25. Ralph AS, van Dooren GG, Waller FR, Crawford JM, Fraunholz JM, Foth JB, Tonkin JC, Roos SD, McFadden IG. 2001. Metabolic maps and functions of the *Plasmodium falciparum* apicoplast. Nat Rev Microbiol 2.

26. Plaxton WC. 1996. THE ORGANIZATION AND REGULATION OF PLANT GLYCOLYSIS. Annu Rev Plant Physiol Plant Mol Biol 47:185–214.

27. Schnarrenberger C, Flechner A, Martin W. 1995. Enzymatic Evidence for a Complete Oxidative Pentose Phosphate Pathway in Chloroplasts and an Incomplete Pathway in

the Cytosol of Spinach Leaves. Plant Physiol 108:609–614.

28. Neuhaus HE, Thom E, Möhlmann T, Steup M, Kampfenkel K. 1997. Characterization of a novel eukaryotic ATP/ADP translocator located in the plastid envelope of *Arabidopsis thaliana* L. Plant J 11:73–82.

29. Lim L, Linka M, Mullin KA, Weber APM, McFadden GI. 2010. The carbon and energy sources of the non-photosynthetic plastid in the malaria parasite. FEBS Lett 584:549–554.

30. Mullin KA, Lim L, Ralph SA, Spurck TP, Handman E, McFadden GI. 2006. Membrane transporters in the relict plastid of malaria parasites. Proc Natl Acad Sci U S A.

31. Lim L, Sayers CP, Goodman CD, McFadden GI. 2016. Targeting of a Transporter to the Outer Apicoplast Membrane in the Human Malaria Parasite *Plasmodium falciparum*. PLoS One 11:e0159603.

32. Banerjee T, Jaijyan KD, Surolia N, Singh PA, Surolia A. 2012. Apicoplast triose phosphate transporter (TPT) gene knockout is lethal for *Plasmodium*. Mol Biochem Parasitol 186:44–50.

33. Lim L, McFadden GI. 2010. The evolution, metabolism and functions of the apicoplast. Philos Trans R Soc Lond B Biol Sci 365:749–63.

34. Lindner SE, Sartain MJ, Hayes K, Harupa A, Moritz RL, Kappe SHI, Vaughan AM. 2014. Enzymes involved in plastid-targeted phosphatidic acid synthesis are essential for *Plasmodium yoelii* liver-stage development. Mol Microbiol 91:679–693.

35. Waller FR, Keeling JP, Donald GR, Striepen B, Handman E, Lang-Unnasch N, Cowman FA, Besra SG, Roos SD, McFadden IG. 1998. Nuclear-encoded proteins target to the plastid in *Toxoplasma gondii* and *Plasmodium falciparum*. Proc Natl Acad Sci U S A 95:12352–12357.

36. Fleige T, Fischer K, Ferguson DJP, Gross U, Bohne W. 2007. Carbohydrate metabolism in the *Toxoplasma gondii* apicoplast: localization of three glycolytic isoenzymes, the single pyruvate dehydrogenase complex, and a plastid phosphate translocator. Eukaryot Cell 6:984–96.

37. Gardner MJ, Hall N, Fung E, White O, Berriman M, Hyman RW, Carlton JM, Pain A, Nelson KE, Bowman S, Paulsen IT, James K, Eisen JA, Rutherford K, Salzberg SL, Craig A, Kyes S, Chan M-S, Nene V, Shallom SJ, Suh B, Peterson J, Angiuoli S, Pertea M, Allen J, Selengut J, Haft D, Mather MW, Vaidya AB, Martin DMA, Fairlamb AH, Fraunholz MJ, Roos DS, Ralph SA, McFadden GI, Cummings LM, Subramanian GM, Mungall C, Venter JC, Carucci DJ, Hoffman SL, Newbold C, Davis RW, Fraser CM, Barrell B. 2002. Genome sequence of the human malaria parasite *Plasmodium falciparum*. Nature 419:498–511.

38. Daubenberger CA, Tisdale EJ, Curcic M, Diaz D, Silvie O, Mazier D, Eling W, Bohrmann B, Matile H, Pluschke G. 2003. The N'-Terminal Domain of Glyceraldehyde-3-Phosphate Dehydrogenase of the Apicomplexan *Plasmodium falciparum* Mediates GTPase Rab2-Dependent Recruitment to Membranes. Biol Chem 384:1227–37.

39. Saito T, Nishi M, Lim IM, Wu B, Maeda T, Hashimoto H, Takeuchi T, Roos SD, Asai T. 2008. A novel GDP-dependent pyruvate kinase isozyme from *Toxoplasma gondii* localizes to both the apicoplast and the mitochondrion. J Biol Chem 283:14041–14052.

40. Israelsen JW, Vander Heiden GM. 2015. Pyruvate kinase: function, regulation and role in cancer. Semin Cell Dev Biol 43:43–51.

41. Chan M, Tan DSH, Sim TS. 2007. *Plasmodium falciparum* pyruvate kinase as a novel target for antimalarial drug-screening. Travel Med Infect Dis 5:125–131.

42. Maeda T, Saito T, Harb SO, Roos SD, Takeo S, Suzuki H, Tsuboi T, Takeuchi T, Asai T. 2009. Pyruvate kinase type-II isozyme in *Plasmodium falciparum* localizes to the apicoplast. Parasitol Int 58:101–105.

43. Gray RL, Tompkins CS, Taylor BE. 2014. Regulation of pyruvate metabolism and human disease. Cell Mol life Sci C 71:2577–2604.

44. Guggisberg MA, Amthor ER, Odom RA. 2014. Isoprenoid biosynthesis in *Plasmodium falciparum*. Eukaryot Cell 13:1348–1359.

45. Gisselberg JE, Dellibovi-Ragheb T a., Matthews K a., Bosch G, Prigge ST. 2013. The Suf Iron-Sulfur Cluster Synthesis Pathway Is Required for Apicoplast Maintenance in Malaria Parasites. PLoS Pathog 9.

46. Foth JB, Stimmler ML, Handman E, Crabb SB, Hodder NA, McFadden IG. 2004. The malaria parasite *Plasmodium falciparum* has only one pyruvate dehydrogenase complex, which is located in the apicoplast: The single, plastidic PDH of *Plasmodium falciparum*. Mol Microbiol 55.

47. Vaughan AM, O'Neill MT, Tarun AS, Camargo N, Phuong TM, Aly ASI, Cowman AF, Kappe SHI. 2009. Type II fatty acid synthesis is essential only for malaria parasite late liver stage development. Cell Microbiol 11:506–20.

48. Gisselberg JE, Dellibovi-Ragheb TA, Matthews KA, Bosch G, Prigge ST. 2013. The suf iron-sulfur cluster synthesis pathway is required for apicoplast maintenance in malaria parasites. PLoS Pathog 9:e1003655.

49. Ghorbal M, Gorman M, Macpherson CR, Martins RM, Scherf A, Lopez-Rubio J-J. 2014. Genome editing in the human malaria parasite *Plasmodium falciparum* using the CRISPR-Cas9 system. Nat Biotechnol 32:819–21.

50. Wagner JC, Platt RJ, Goldfless SJ, Zhang F, Niles JC. 2014. Efficient CRISPR-Cas9–mediated genome editing in *Plasmodium falciparum*. Nat Methods 11:915–8.

51. Fischer K, Kammerer B, Gutensohn M, Arbinger B, Weber A, Häusler RE, Flügge UI. 1997. A new class of plastidic phosphate translocators: a putative link between primary and secondary metabolism by the phosphoenolpyruvate/phosphate antiporter. Plant Cell 9:453–62.

52. Cobbold SA, Vaughan AM, Lewis IA, Painter HJ, Camargo N, Perlman DH, Fishbaugher M, Healer J, Cowman AF, Kappe SHI, Llinás M. 2013. Kinetic flux profiling elucidates two independent acetyl-CoA biosynthetic pathways in *Plasmodium falciparum*. J Biol Chem 288:36338–50.

53. Foth BJ, Stimmler LM, Handman E, Crabb BS, Hodder AN, McFadden GI. 2004. The malaria parasite *Plasmodium falciparum* has only one pyruvate dehydrogenase complex, which is located in the apicoplast. Mol Microbiol 55:39–53.

54. Yu M, Kumar STR, Nkrumah JL, Coppi A, Retzlaff S, Li DC, Kelly JB, Moura AP, Lakshmanan V, Freundlich SJ, Valderramos J-C, Vilcheze C, Siedner M, Tsai H-CJ, Falkard B, Sidhu SAB, Purcell AL, Gratraud P, Kremer L, Waters PA, Schiehser G, Jacobus PD, Janse JC, Ager A, Jacobs RW, Sacchettini CJ, Heussler V, Sinnis P, Fidock AD. 2008. The fatty acid biosynthesis enzyme FabI plays a key role in the development of liver-stage malarial parasites. Cell Host Microbe 4:567–578.

55. Pei Y, Tarun AS, Vaughan AM, Herman RW, Soliman JMB, Erickson-Wayman A, Kappe SHI. 2010. *Plasmodium* pyruvate dehydrogenase activity is only essential for the parasite's progression from liver infection to blood infection. Mol Microbiol 75:957–971.

56. Cobbold SA, Vaughan AM, Lewis IA, Painter HJ, Camargo N, Perlman DH, Fishbaugher M, Healer J, Cowman AF, Kappe SHI, Llinás M. 2013. Kinetic flux profiling elucidates two independent acetyl-CoA biosynthetic pathways in *Plasmodium falciparum*. J Biol Chem 288:36338–50.

57. Frank A, Groll M. 2017. The Methylerythritol Phosphate Pathway to Isoprenoids. Chem Rev 117:5675–5703.

58. Kahn A, Marie J. 1982. Pyruvate kinases from human erythrocytes and liver. Methods Enzymol 90 Pt E:131–40.

59. Goldfless SJ, Wagner JC, Niles JC. 2014. Versatile control of *Plasmodium falciparum* gene expression with an inducible protein-RNA interaction. Nat Commun 5:5329.

60. Roberts A. 2017. Development and validation of a conditional localization domain to control trafficking of secretory proteins in *Plasmodium falciparum*.

61. Schwach F, Bushell E, Gomes AR, Anar B, Girling G, Herd C, Rayner JC, Billker O. 2015. PlasmoGEM, a database supporting a community resource for large-scale

experimental genetics in malaria parasites. Nucleic Acids Res 43:D1176-82.

62. Zhang M, Wang C, Otto TD, Oberstaller J, Liao X, Adapa SR, Udenze K, Bronner IF, Casandra D, Mayho M, Brown J, Li S, Swanson J, Rayner JC, Jiang RHY, Adams JH. 2018. Uncovering the essential genes of the human malaria parasite *Plasmodium falciparum* by saturation mutagenesis. Science 360:eaap7847.

63. Mullin KA, Lim L, Ralph SA, Spurck TP, Handman E, McFadden GI. 2006. Membrane transporters in the relict plastid of malaria parasites. Proc Natl Acad Sci 103:9572–9577.

64. Foth JB, Stimmler ML, Handman E, Crabb SB, Hodder NA, McFadden IG. 2005. The malaria parasite *Plasmodium falciparum* has only one pyruvate dehydrogenase complex, which is located in the apicoplast. Mol Microbiol 55:39–53.

65. Boehme C, Bieber F, Linnemann J, Breitling R, Lorkowski S, Reissmann S. 2013. Chemical and enzymatic characterization of recombinant rabbit muscle pyruvate kinase. Biol Chem 394:695–701.

66. Saeki T, Hori M, Umezawa H. 1974. Pyruvate kinase of *Escherichia coli*. Its role in supplying nucleoside triphosphates in cells under anaerobic conditions. J Biochem 76:631–7.

67. Knowles VL, Smith CS, Smith CR, Plaxton WC. 2001. Structural and Regulatory Properties of Pyruvate Kinase from the Cyanobacterium *Synechococcus* PCC 6301 . J Biol Chem 276:20966–20972.

68. Abbe K, Yamada T. 1982. Purification and properties of pyruvate kinase from *Streptococcus mutans*. J Bacteriol 149:299–305.

69. Plowman KM, Krall AR. 1965. A kinetic study of nucleotide interactions with pyruvate kinase. Biochemistry 4:2809–14.

70. Röhrich CR, Englert N, Troschke K, Reichenberg A, Hintz M, Seeber F, Balconi E, Aliverti A, Zanetti G, Köhler U, Pfeiffer M, Beck E, Jomaa H, Wiesner J. 2005. Reconstitution of an apicoplast-localised electron transfer pathway involved in the isoprenoid biosynthesis of *Plasmodium falciparum*. FEBS Lett 579:6433–6438.

71. Balconi E, Pennati A, Crobu D, Pandini V, Cerutti R, Zanetti G, Aliverti A. 2009. The ferredoxin-NADP+ reductase/ferredoxin electron transfer system of *Plasmodium falciparum*. FEBS J 276:3825–3836.

72. Vollmer M, Thomsen N, Wiek S, Seeber F. 2001. Apicomplexan parasites possess distinct nuclear-encoded, but apicoplast-localized, plant-type ferredoxin-NADP+ reductase and ferredoxin. J Biol Chem 276:5483–5490.

73. Laine LM, Biddau M, Byron O, Müller S. 2015. Biochemical and structural characterization of the apicoplast dihydrolipoamide dehydrogenase of *Plasmodium*

falciparum. Biosci Rep 35.

74. Nkrumah JL, Muhle AR, Moura AP, Ghosh P, Hatfull FG, Jacobs RW, Fidock AD. 2006. Efficient site-specific integration in *Plasmodium falciparum* chromosomes mediated by mycobacteriophage Bxb1 integrase. Nat Methods 3:615–621.

75. Spalding DM, Allary M, Gallagher RJ, Prigge TS. 2010. Validation of a modified method for Bxb1 mycobacteriophage integrase-mediated recombination in *Plasmodium falciparum* by localization of the H-protein of the glycine cleavage complex to the mitochondrion. Mol Biochem Parasitol 172:156–160.

76. Muench SP, Rafferty JB, McLeod R, Rice DW, Prigge ST. 2003. Expression, purification and crystallization of the *Plasmodium falciparum* enoyl reductase. Acta Crystallogr D Biol Crystallogr 59:1246–8.

77. Mata-Cantero L, Lafuente MJ, Sanz L, Rodriguez MS. 2014. Magnetic isolation of *Plasmodium falciparum* schizonts iRBCs to generate a high parasitaemia and synchronized in vitro culture. Malar J 13:112.

Chapter 5

CoA Biosynthesis in *P. falciparum* Parasites

Attributions:
- The parental plasmid for the generation of the PfMev CLD-EcDPCK-mCherry-apt line was generated by Dr. Sean Prigge and Dr. Krithika Rajaram
- The growth curves for Figures 5-11 and 5-13 were generated by Hans Liu

ABSTRACT

The survival of blood-stage *P. falciparum* parasites has long been known to rely on the vitamin pantothenate, which is metabolized by a series of enzymes to generate Coenzyme A (CoA). All of the enzymes involved in this pathway are predicted to reside in the cytosol except for the last enzyme in the pathway, dephospho-CoA kinase (DPCK), which is predicted to localize to the apicoplast organelle. This enzyme should be essential for the production of CoA and the survival of blood-stage parasites, which makes its putative localization in the apicoplast interesting. Previous work demonstrated that the apicoplast can be disrupted in blood-stage parasites, if isopentenyl pyrophosphate (IPP) is supplemented in the growth medium. This has been interpreted as IPP production being the only essential function of the apicoplast during this stage. In the work described here, we confirmed that DPCK is indeed localized to the apicoplast organelle. We were unable to delete the gene encoding DPCK, even in the presence of an apicoplast bypass system, unless we first expressed the *E. coli* DPCK (*Ec*DPCK) to complement the loss of the parasite enzyme. Ultimately, we were able to demonstrate that DPCK activity is required for parasite survival, and that DPCK remains functional and essential in 'apicoplast negative' parasites that contain a disrupted apicoplast organelle. Taken together, these results show that the apicoplast is an essential source of CoA in blood-stage malaria parasites. CoA also appears to be required in the apicoplast for the 4'-phosphopantetheine modification of the acyl-carrier protein (ACP). Both ACP and ACP Synthase (ACP-S), the enzyme that catalyzes the modification of ACP, are essential for parasite survival and organelle maintenance. Thus, ACP modified with the 4'-phosphopantetheine group from CoA has an essential non-canonical function in the apicoplast outside of its known role in the FasII fatty acid biosynthetic pathway.

INTRODUCTION

P. falciparum parasites rely on exogenous pantothenate (vitamin B5) (1, 2), which they use for the *de novo* synthesis of Coenzyme A (CoA) (3). Within the parasite, CoA functions as an essential cofactor used for a variety of biosynthetic pathways (4), including the generation of acetyl-CoA, fatty acid biosynthesis and modification, and cellular oxidation and metabolism (5). The CoA biosynthetic pathway has been considered an attractive source of drug targets, with studies showing that pantothenate analogs inhibit this pathway and are effective in inhibiting the growth of the asexual red blood cell (RBC) stage of the parasite (6–8).

In *Plasmodium,* pantothenate is imported into the infected red blood cell (iRBC) via the new permeability pathway (NPP) transporter (9), diffuses across the parasitophorous vacuole (10), and then crosses the parasite plasma membrane through the pantothenate transporter (PAT) (11–13). Once inside the parasite, pantothenate is converted into CoA through a series of five enzyme-mediated steps. The first four enzymes, including pantothenate kinase 1 or 2 (PanK1/2), phosphopantothenoylcysteine synthase (PPCS), phosphopantothenoylcysteine decarboxylase (PPCDC), and phosphopantetheine adenylyltransferase (PPAT) are believed to be localized to the cytosol of the parasite (4). However, the last step of this pathway, involving the conversion of dephospho-CoA to CoA by the dephospho-CoA kinase (DPCK) enzyme is predicted to occur within the apicoplast of the parasite (**Figure 5-1**) (14).

All of these enzymes have been targeted for deletion in *Plasmodium yoelli,* and it was found that PAT, Pank1, PanK2, PPCS and PPCDC were dispensable for blood-stage

survival, while the last two enzymes in this pathway, PPAT and DPCK, appear to be essential (12, 15, 16). However, in *P. falciparum* PAT was refractory to deletion (11). The dispensability or essentiality of these genes was explained by a potential alternate CoA biosynthetic route in which pantetheine is imported and phosphorylated by PanK1 or PanK2 to form 4' phosphopantetheine, which is used directly by PPAT to form dephospho-CoA, bypassing PPCS and PPCDC (15). While parasites are able to tolerate the deletion of multiple enzymes within the pathway, it still represents a viable drug target that is deserving of further investigation.

The last enzyme in this pathway, DPCK, is predicted to localize to the apicoplast due to the presence of a N-terminal bipartite apicoplast trafficking peptide (14). The CoA generated within the apicoplast is then presumably exported out of the organelle for utilization throughout the rest of the cell, by a transporter that is yet to be identified. Within the apicoplast, CoA is predicted to be used to modify the acyl-carrier protein (ACP) with a 4-phosphopantethine cofactor (17). This modification is catalyzed by ACP synthase (ACP-S), and is required to form the mature and biologically active form of ACP (4, 17). ACP plays a central role in the FasII pathway within the apicoplast (14, 18), however this pathway has been demonstrated to be nonessential in blood-stage parasites (19, 20).

It has previously been demonstrated that the apicoplast organelle can be disrupted in blood-stage *P. falciparum* parasites if supplemented with sufficient quantities of isoprenoid precursor isopentenyl pyrophosphate (IPP) (21). Parasites with a disrupted apicoplast lose the 35kb apicoplast genome and no longer contain an intact organelle, instead accumulating vesicles throughout the cell (21, 22). One interpretation of this result is that IPP is the only essential product generated by the apicoplast during the blood-stage of the parasite. However, DPCK is predicted to be an essential gene (15), and is thought to be localized to

the apicoplast (14). Thus, disruption of the apicoplast should require supplementation with CoA as well as IPP if DPCK is an essential apicoplast enzyme whose product, CoA, is needed by the rest of the cell.

The vast majority of apicoplast-specific proteins are encoded within the nucleus (23), and then trafficked to the apicoplast through the recognition of an N-terminal hydrophobic signal peptide followed by a positively charged transit peptide (24). This bipartite peptide is necessary and sufficient to target proteins, such as the green-fluorescent protein (GFP) to the apicoplast (25). The signal peptide mediates co-translational import into the endoplasmic reticulum and is cleaved, exposing the transit peptide which mediates vesicular trafficking to the organelle (26–28). When the apicoplast is disrupted, there is an accumulation of vesicles throughout the cell (21, 22) that have been shown to contain nuclear-encoded apicoplast proteins (26). Thus, it remains a possibility that the vesicles that accumulate in parasites containing a disrupted apicoplast contain apicoplast-specific proteins that are biochemically active and fulfilling their functional role in the cell.

Through the work described here, we attempted to generate a genetic knockout of DPCK, and were unsuccessful, even when using an apicoplast metabolic bypass , suggesting that DPCK is playing an essential role in the parasite beyond its potential function within the apicoplast. However, we were successful in deleting the endogenous *P. falciparum* DPCK, when complementing the parasite with the *E. coli* DPCK (*Ec*DPCK), helping to both confirm its functionality as a DPCK enzyme, and providing additional evidence that it is likely to be essential. We provided further evidence that DPCK activity is essential for parasite survival by knocking down the complemented *Ec*DPCK in the ΔDPCK line, which resulted in the inhibition of parasite growth. We also showed that DPCK is present and active in the vesicles of parasites containing a disrupted apicoplast. Furthermore, we

demonstrated that CoA is likely needed within the apicoplast for the 4-phosphopanthethine modification of ACP by ACP-S. We found that both ACP and ACP-S are essential for parasite survival and organelle maintenance, suggesting that these proteins have an essential and non-canonical role outside of their known function in the FASII fatty acid synthesis pathway.

RESULTS

DPCK Localization to the Apicoplast Organelle

In *P. falciparum,* DPCK is predicted to localize to the apicoplast (14), however this has yet to be experimentally confirmed. In order to determine the localization of DPCK we took advantage of certain features of the PfMev parasite line that we generated previously. Namely, PfMev parasites are engineered to express a more stable green fluorescent protein, super-folder green (SFG), which is directed to the apicoplast by the trafficking peptide of the *P. falciparum* acyl-carrier protein, fluorescently labeling the organelle (api-SFG). Systems such as these have been used previously to visualize the apicoplast (21, 22, 29). Thus, we generated a construct to express the *P. falciparum* DPCK containing a C-terminal mCherry tag, under the control of the calmodulin promoter. The entire construct was then integrated into the genome of PfMev parasites that had been further modified to contain an additional attb site within the p230p locus of the genome using attP/attB recombination (30, 31). We then analyzed the resulting line using live epifluorescent microscopy. Upon analysis, we observed co-localization of the api-SFG and mCherry signals, indicating that DPCK is indeed localized to the apicoplast (**Figure 5-2**).

DPCK is Not Amenable to Genetic Deletion Even in the Presence of Exogenous Mevalonate and CoA

Using the PfMev line, we attempted to delete DPCK using Cas9-mediated genome editing methods (32) under continuous supplementation with 50μM mevalonate, which should allow DPCK to be deleted even if it is essential for apicoplast function. However, we failed to delete DPCK in six independent attempts, suggesting that DPCK is essential for parasite survival and likely fulfills a metabolic requirement outside of the apicoplast. We also tried direct supplementation with CoA, since CoA has been shown to rescue the growth of parasites that have been treated with inhibitors that are thought to target CoA biosynthesis (33, 34). We were also not successful in deleting DPCK in two additional attempts using both 50μM mevalonate and 5mM CoA as culture medium supplements (**Table 5-2**). This result seems to suggest that DPCK is either essential for some function that does not involve CoA, or that the parasites are unable to scavenge CoA. However, it is not clear from previous supplementation experiments whether parasites can scavenge intact CoA (33, 34). In these experiments, CoA may have broken down into components like pantetheine or 4' phosphopantetheine and then taken up by the parasites. If 4' phosphopantetheine can be scavenged, it can be used directly by PPAT and DPCK, bypassing the other CoA synthesis pathway enzymes and their inhibitors. Since DPCK is the last enzyme in the pathway, only acquisition of intact CoA would rescue deletion of the enzyme.

DPCK Can be Knocked Out if Complemented With the *E. coli* DPCK in the Apicoplast

Since our previous knockout attempts were inconclusive, we wanted to determine if we could delete DPCK if the parasite was complemented with an alternate copy of DPCK in

the apicoplast. Thus, we generated an expression construct in which we appended the signal and transit peptide of *P. falciparum* ACP to the N-terminus of the *E. coli* DPCK (*Ec*DPCK), along with a C-terminal mCherry tag to confirm trafficking of the protein to the apicoplast (**Figure 5-3a**). The expression of this gene was controlled by the calmodulin promoter, and the construct was integrated into the genome using attP/attB integration in the PfMev p230p attb line. The resulting parasite line (PfMev Api-*Ec*DPCK-mCherry) was then analyzed by live fluorescent microscopy. We found that the mCherry signal was co-localized with the api-SFG signal, demonstrating that the *E. coli* DPCK was being expressed and trafficked to the apicoplast (**Figure 5-3b**). Upon confirming this, we again targeted the endogenous DPCK for deletion, with the same construct previously used unsuccessfully in attempts to delete this gene in non-complemented PfMev parasites. However, this time in the complemented PfMev Api-*Ec*DPCK-mCherry line, we were successful in deleting DPCK. We confirmed the deletion of this gene using PCR (**Figure 5-3c**). We then analyzed this line again using live epifluorescent microscopy and confirmed that the api-SFG and mCherry signals continued to be co-localized in the apicoplast (**Figure 5-3d**). These results indicate that *Ec*DPCK can complement the loss of the parasite DPCK. Since the *E. coli* DPCK (encoded by the *coaE* gene) has already been biochemically characterized (35), complementation further indicates that the parasite DPCK has dephospho-CoA kinase enzymatic activity.

The *E. coli* DPCK is Present and Active in the Vesicles of Parasites Containing a Disrupted Apicoplast Organelle

Once we generated the DPCK knockout line expressing the apicoplast localized *E. coli* DPCK (PfMev Api-*Ec*DPCK-mCherry ΔDPCK), we wanted to determine whether the

*Ec*DPCK enzyme could be active in the vesicles resulting from disruption of the apicoplast organelle. Thus, we treated the PfMev Api-*Ec*DPCK-mCherry ΔDPCK line with 100nM azithromycin in the presence of 50μM mevalonate for 7 days. After azithromycin treatment, we were no longer able to detect the presence of the apicoplast genome by PCR, indicating that the organelle had been disrupted (**Figure 5-4a**). We then analyzed this line by live epifluorescent microscopy and observed the presence of multiple vesicular bodies in the parasites, consistent with loss of the single apicoplast organelle (**Figure 5-4b**). Both the api-SFG and mCherry signals remained co-localized (**Figure 5-4b**), indicating that the *E. coli* DPCK was present and active in the vesicles of the parasite.

DPCK Can be Knocked Out if Complemented with the *E. coli* DPCK in the Cytosol

It is not clear why the last step of CoA synthesis occurs in the apicoplast . Within the apicoplast, CoA is an important cofactor needed for the FASII fatty acid biosynthetic pathway (36), however, this pathway is dispensable in blood-stage parasites (19, 20). We have previously failed to delete DPCK under mevalonate supplementation, suggesting that CoA is essential for processes outside of the apicoplast organelle. However, we could delete DPCK in a parasite line expressing *E. coli* DPCK in the apicoplast organelle. This raised the question of whether CoA has to be produced in the apicoplast, potentially being required for within the organelle for maintenance or replication, or whether it could be produced in the cytosol. In order to determine this, we generated a second complementation parasite line in which we expressed the *E. coli* DPCK protein with a C-terminal mCherry tag, but did not append a N-terminal trafficking peptide to the construct (**Figure 5-5a**).

We were successful in integrating the *Ec*DPCK-mCherry cytosolic expression construct into the genome of the PfMev p230p attb parasite line using attB/attP integration,

and observed a pattern of mCherry fluorescence consistent with cytosolic protein expression (**Figure 5-5b**). Using this parasite line, we were successful in deleting the endogenous DPCK gene under supplementation with 50μM mevalonate (**Figure 5-5c**). We then analyzed the resulting apicoplast phenotype to determine whether deletion of DPCK had any effect on the maintenance or replication of the organelle. PCR analysis indicated that the apicoplast genome is present in the knockout line (**Figure 5-5d**), and we observed intact apicoplast morphology via epifluorescent microscopy (**Figure 5-5e**). Additionally, we removed mevalonate from the culture medium and found that these parasites continued to grow and replicate, demonstrating that CoA production within the apicoplast is not required for organelle maintenance or parasite survival. Taken together, these results indicate that either CoA is not needed in the apicoplast, or that the organelle has the ability to import CoA from the cytosol.

Knockdown of *E. coli* DPCK in ΔDPCK Parasites Results in a Modest Growth Defect

Our results so far strongly suggest that DPCK is an essential gene, but they are not entirely conclusive since they are based on the failure to delete DPCK unless *Ec*DPCK is expressed. In order to demonstrate that DPCK activity is essential, we took advantage of the TetR-DOZI knockdown system, which inhibits the translation of the target protein in the absence of the tetracycline analog aTc (anhydrotetracycline) (37). We also used a new conditional localization domain (CLD) approach that does not affect protein trafficking to the apicoplast until a CLD binding ligand (Shield1) is added to the parasite culture, causing the targeted protein to be secreted to the parasitophorous vacuole (38). Using both of these systems, we generated an additional expression construct containing the *E. coli* DPCK, with

an N-terminal CLD and a C-terminal mCherry tag for visualization, followed by an aptamer array providing binding sites for the tetR-DOZI fusion protein to bind and silence mRNA transcripts. The expression was controlled by a calmodulin promoter, with the construct also containing the TetR-DOZI system, required for the function of the knockdown (**Figure 5-6a**) (37). We were successful in integrating this construct into the genome of the PfMev p230p attb parasite line using attP/attB integration, with the resulting line being named PfMev CLD-*Ec*DPCK-mCherry-apt (aptamer). We confirmed expression of the protein using live epifluorescent microscopy (**Figure 5-6b**), and found it to be localized to the apicoplast as expected. We then went on to delete the endogenous DPCK gene in this line, confirming the successful deletion of the gene by PCR (**Figure 5-6c**), and generating what we called the PfMev-CLD-*Ec*DPCK-mCherry-apt ΔDPCK line.

After validating that the *E. coli* DPCK-mCherry protein was being appropriately expressed (**Figure 5-7a**), we confirmed the functionality of the individual knockdown systems through the removal of aTc (**Figure 5-7b**), the addition of Shield1 (**Figure 5-7c**), or the simultaneous removal of aTc and the addition of Shield1 (**Figure 5-7d**). Analysis of mCherry signal after 48 hours of treatment under these conditions indicated that the TetR-DOZI knockdown and the CLD systems were both functional. The removal of aTc resulted in a highly diminished mCherry signal, consistent with knockdown of the protein. The addition of Shield1 resulted in mislocalization of the protein away from the apicoplast, confirming the functionality of the CLD. In the non-permissive state with both systems applied (aTc removed and Shield1 added), we were not able to detect mCherry signal. We conducted a growth assay under this non-permissive condition and tracked growth over 6 days. We observed a modest effect on parasite growth, with the parasitemia differing by ~50% on day 6 (**Figure 5-8**). However, it should be noted that this experiment was

conducted in singlicate, as an initial proof of concept to test whether DPCK may be essential. The reduced growth of the PfMev *Ec*DPCK-mCherry-apt ΔDPCK line upon the removal of aTc and addition of Shield1 suggested that DPCK is playing an important role in parasite growth.

Knockdown of *E. coli* DPCK in ΔDPCK Parasites is Exacerbated Under Limiting Concentrations of Pantothenate

The mild growth inhibition of PfMev *Ec*DPCK-mCherry-apt ΔDPCK parasites grown in the non-permissive state may be partially explained by strong overexpression of *Ec*DPCK by the calmodulin promoter. Thus, even if the knockdown and CLD approaches were effective in reducing *Ec*DPCK levels in the apicoplast, there still may be enough enzyme activity to sustain parasite growth, albeit at a reduced level. We reasoned that we could further reduce DPCK activity and parasite growth by limiting that amount of pantothenate in the growth medium. Thus, we determined the minimal concentration of pantothenate that is required to sustain parasite growth to near wild type levels. RPMI-1640 parasite growth medium contains is approximate 1μM pantothenate; we titrated the concentration of pantothenate and found that as little as 100nM was sufficient to restore parasite growth to near wild-type levels. Parasites failed to replicate at concentrations of less than 10nM pantothenate (**Figure 5-9**). This gave us a starting point to test additional pantothenate concentrations within the range required for parasite growth. Thus, we next measured growth of the PfMev *Ec*DPCK-mCherry-apt ΔDPCK parasite line under permissive and non-permissive conditions, with pantothenate supplemented at concentrations of 100nM, 50nM, 25nM, and 10nM, supplemented with 0nM as a negative control and used CMA as a positive control (**Figure 5-10**). Based on these data, we found

that parasites supplemented with as little as 50nM pantothenate grew at near wild type levels under permissive conditions, and essentially failed to replicated under non-permissive conditions. It should be noted that both of these pantothenate titration experiments were done in singlicate as initial ranging experiments. Thus, we ran one additional experiment measuring the growth of the PfMev *Ec*DPCK-mCherry-apt ΔDPCK parasite line under the permissive and non-permissive conditions in the presence of 50nM pantothenate with an appropriate number of technical and biological replicates. Under limiting pantothenate concentrations we saw a severe defect in parasite replication in the non-permissive condition. These results demonstrate that DPCK activity is essential for parasite growth (**Figure 5-11**).

DPCK is Present and Active in Disrupted Apicoplast Vesicles and is Essential for Parasite Survival

It is not clear whether apicoplast-localized DPCK could continue to function if the organelle becomes disrupted. This would require the enzyme to be expressed and functional in the vesicles that result from apicoplast disruption, and these vesicles would have to provide the appropriate biochemical environment. To explore this question, we treated the PfMev CLD-*Ec*DPCK-mCherry-apt ΔDPCK line with 100nM azithromycin in the presence of 50μM mevalonate for seven days. Azithromycin treatment resulted in the formation of multiple punctate vesicles containing fluorescent signals corresponding to both api-SFG and mCherry, indicating that *Ec*DPCK is produced and trafficked to the vesicles in apicoplast disrupted parasites (**Figure 5-12a**). We were no longer able to detect the presence of the apicoplast genome by PCR in these parasites, confirming that the organelle had been disrupted (**Figure 5-12b**). We then wanted to demonstrate that the vesicle localized activity

of the *Ec*DPCK is essential for parasite survival, and thus induced the dual knockdown and CLD systems in the presence of 50μM mevalonate and the reduced level of 50nM pantothenate. Based on these results, we found that parasites grew poorly in the non-permissive condition, indicating that *Ec*DPCK is essential for parasite survival in apicoplast disrupted parasites (**Figure 5-13**). These results reinforced the finding that DPCK activity within the apicoplast is essential for parasite growth, and demonstrated that the vesicles resulting from apicoplast disruption can contain essential processes despite the absence of an intact organelle.

ACP is Essential for Blood-Stage Parasite Survival and Apicoplast Maintenance

We showed thus far that CoA synthesis is essential, but we next wanted to know whether CoA is specifically required in the apicoplast. Pyruvate dehydrogenase (PDH) uses CoA to generate acetyl-CoA within the apicoplast, however this activity has previously been demonstrated to be dispensable in blood-stage parasites (39). Within the apicoplast, ACP synthase (ACP-S) uses CoA and catalyzes the posttranslational modification of ACP with a 4'-phosphopantetheine cofactor (4, 17, 40). ACP is known to function in the FASII fatty acid biosynthetic pathway (36), and although this pathway is dispensable in blood-stage parasites (19, 20), ACP itself has not been targeted for deletion.

In order to test the potential essentiality of ACP within the with the apicoplast, we attempted to delete this gene in the PfMev parasite line using Cas9-mediated editing (32), under continuous supplementation with 50μM mevalonate. We were successful in knocking out ACP, and confirmed the deletion using PCR (**Figure 5-14a**). Surprisingly, PCR analysis indicated that the organellar genome was no longer present in the ACP deletion line (**Figure 5-14b**), and we observed multiple vesicles instead of an intact apicoplast in epifluorescent

microscopy images, confirming the loss of the organelle (**Figure 5-14c**). Consistent with these findings, the ΔACP parasite line relies on mevalonate for survival, and these parasites fail to grow in its absence. These results demonstrate the ACP is not only essential for the blood-stage survival of the parasite, but is additionally required for the maintenance and replication of the organelle. Due to the dispensability of other components of the FASII pathway ACP must be essential for a previously unpredicted and essential non-canonical function.

ACP Synthase is Essential for Blood-Stage Parasite Survival and Apicoplast Maintenance

Our previous results show that ACP is essential, but this does not necessarily mean that CoA or the 4'-phosphopantethine modification of ACP is required. To investigate the importance of this posttranslational modification, we attempted to delete ACP-S in the PfMev parasite line under continuous supplementation with 50μM mevalonate. We were successful in deleting this gene, confirming the knockout using PCR (**Figure 5-15a**). We observed a phenotype similar that of the ΔACP parasite line including loss of the apicoplast organelle genome (**Figure 5-15b**), accumulation of multiple vesicles (**Figure 5-15b**), and dependence on mevalonate supplementation for survival. These results indicate that ACP-S and its substrate CoA are likely required in the apicoplast for the 4'-phosphopantethine modification of ACP, and that this posttranslational modification is essential for organelle maintenance and parasite survival.

FabD is Not Required for Blood-Stage Parasite Survival

While the multiple deletions of genes within the FASII pathway demonstrated that this pathway is dispensable for blood-stage parasite survival (19, 20) the first enzyme in the pathway, FabD, has not been targeted for deletion (18). FabD catalyzes the transfer of the malonyl group from malonyl-CoA to ACP, to form malonyl-ACP (36). It is possible that FabD generates malonyl-ACP or another acyl-ACP species that has an important role in apicoplast maintenance. To investigate these possibilities, we targeted FabD for deletion and confirmed the deletion via PCR (**Figure 5-16a**). Unlike the ΔACP and ΔACP-S parasite lines, we could detect the apicoplast organellar genome in the ΔFabD line (**Figure 5-16b**), and found that the apicoplast remained intact in this line (**Figure 5-16c**). Additionally, we found that ΔFabD parasites grow without mevalonate supplementation, demonstrating that FabD is not required for blood-stage parasite survival. Thus, the essential role of holo-ACP in the apicoplast does not rely on acylation by FabD, and is instead seemingly due to a previously unpredicted non-canonical activity.

CONCLUSIONS AND DISCUSSION

Through the work outlined here we have been able to confirm that the generation of CoA is essential for parasite survival. We have also been able to demonstrate that the last enzyme in the CoA synthesis pathway, DPCK, is located in the apicoplast, and confirmed its function as a DPCK through complementation with the *E. coli* enzyme. We were also able to demonstrate that DPCK likely remains present and active in the vesicles of a parasite containing a disrupted organelle. Furthermore, we have been able to show that CoA is likely needed within the apicoplast for its utilization by ACP-S to modify ACP with a 4-phosphopantethine cofactor. Additionally, ACP and ACP-S are essential for parasite survival

and the maintenance of the organelle, likely related to some unpredicted non-canonical activity unrelated to their previously described role in the FASII pathway. As mentioned previously, *P. falciparum* parasites are reliant on the supplementation of exogenous pantothenate, which they use to generate CoA (3). The enzymes involved in this process include PanK1/2, PPCS, PPCDC, and PPAT within the cytosol, with the final step mediated by DPCK within the apicoplast (4, 14). Most of these enzymes have been targeted for deletion in *P. yoelli,* and all except for the last two (PPAT and DPCK) are dispensable for blood-stage parasite survival (12, 15, 16). This pathway has not been investigated to the same degree in other species of *Plasmodium*, such as *P. berghei* or *P. falciparum*, but previous forward genetic screens attempting to determine gene essentiality have been instructive (41, 42). The results from these screens are not totally concordant with what has been found previously, but mostly confirm that the initial steps in the CoA biosynthetic pathway are likely to be dispensable, and that DPCK is likely to be essential (**Table 5-2**). As stated previously, the dispensability of the upstream enzymes involved in this pathway is likely related to the ability of parasites to use pantetheine or 4'-phosphopantetheine directly; PPAT and DPCK would then be required to form dephospho-CoA and CoA, respectively (15).

Table 5-1 Predicted essentiality of genes via forward genetic screens

Gene Name	ID #	PiggyBac	PlasmoGem
PAT	PF3D7_0206200	Dispensable	Not studied
PanK1	PF3D7_1420600	Essential	Dispensable
PanK2	PF3D7_1437400	Dispensable	Dispensable
PPCS	PF3D7_1102400	Dispensable	Dispensable
PPCS2	PF3D7_0412300	Dispensable	Absent in *P. berghei*
PPCDC	PF3D7_0816100	Essential	Dispensable
PPAT	PF3D7_0704700	Dispensable	Not studied
DPCK	PF3D7_1443700	Essential	Essential
ACP	PF3D7_0208500	Essential	Essential

ACP-S	PF3D7_0420200	Essential	Not studied
FabD	PF3D7_1312000	Essential	Dispensable

While the *P. falciparum* DPCK has been predicted to be one of the few enzymes within the pantothenate pathway that is absolutely required for parasite survival, it has not been well studied. DPCK is predicted to reside within the apicoplast, performing the essential function of CoA generation for the parasite. However, *P. falciparum* DPCK had previously not been localized or functionally characterized, and its essentiality had not been demonstrated. Through the work outlined here, we were able to localize DPCK to the apicoplast organelle. This was accomplished by expressing a second copy of the DPCK with a C-terminal mCherry tag, which co-localized with the apicoplast marker api-SFG when analyzed via live epifluorescent microscopy, indicating apicoplast localization. We were also able to demonstrate that DPCK is likely functioning as a DPCK, by complementing the parasite with *E. coli* DPCK. This complementation not only helped to functionally validate DPCK, but also helped confirm its essentiality, since deletion of the endogenous DPCK was only successful when completed with the expression of *Ec*DPCK. The essentiality of DPCK was more conclusively shown through the knockdown of the complemented *Ec*DPCK in a ΔDPCK line. In this knockdown line *Ec*DPCK was under the control of a CLD to alter its trafficking to the parasitophorous vacuole (PV) instead of the apicoplast, in addition to containing a C-terminal aptamer array that allowed for knockdown of the protein upon the removal of aTc. This knockdown and mislocalization resulted in a reduction of parasite growth, which was dramatically exacerbated by limiting the concentration of pantothenate in the culture medium, confirming the essentiality of the gene. Additionally, DPCK could not be knocked out even when supplied with 5mM of exogenous CoA, indicating that the parasites may be unable to scavenged intact CoA.

It had been previously hypothesized that DPCK is apicoplast localized and essential for parasite survival (14, 15), and our work shows that both of these predictions are true. However, previous work also demonstrated that the apicoplast can be disrupted if parasites are supplemented with sufficient concentrations of IPP (21). The resulting disrupted apicoplast phenotype has been characterized, with the normally discrete intact structure of the organelle no longer seen, but instead there appears to be an accumulation of vesicles throughout the cell (21, 22). This can be visualized by tagging a green fluorescent protein with an N-terminal apicoplast-specific signal and transit peptide, to direct its trafficking to the organelle (24, 25). Additionally, the ~35kb apicoplast genome becomes lost in this process as well, which can be confirmed via PCR (22). Once parasites have reached this disrupted apicoplast state, they are entirely reliant on IPP supplementation for survival, and can continue to survive and replicate in perpetuity as long as IPP is provided (21). These results have been described as proof that IPP is the only essential product generated by the apicoplast during the blood-stage of the parasite. However, when the apicoplast is disrupted, nuclear-encoded apicoplast-specific proteins are still presumably being made. Based our own transcriptomic analysis of apicoplast negative parasites, it appears that there is no significant difference in the transcription of nuclear-encoded apicoplast-specific proteins that would be trafficked to the organelle. Additionally, previous work suggests that apicoplast trafficked proteins are still being translated, packaged, and sent out into the cell, but accumulate due to the destination organelle no longer being present (26). It is assumed that the all proteins and pathways once active in the intact organelle are no longer functional once the organelle has become disrupted. However, this conclusion is hard to reconcile with the need for CoA generated in the apicoplast. CoA is needed outside of the organelle and it does not make sense that IPP supplementation could bypass the need for CoA elsewhere in the cell. Our

results show that DPCK plays an essential role within the organelle that cannot by bypassed with apicoplast metabolic bypass systems. This was demonstrated through the localization of DPCK to the apicoplast, along with the multiple failed attempts to delete DPCK, even in the presence of exogenous mevalonate. Furthermore, we demonstrated that the vesicles of a parasite containing a disrupted organelle continue to be biochemically active. This was shown through the continued survival and co-localization of DPCK-mCherry with the api-SFG apicoplast marker in parasites containing a disrupted organelle, indicating that it remained biochemically active within these vesicles. We were also able to demonstrate that the DPCK activity within these vesicles is essential, since parasites grow poorly when DPCK is knocked down and mislocalized, even in the presence of mevalonate, fueling the apicoplast metabolic bypass. While the exact mechanism is unclear, the likely scenario is that DPCK is present and active within the vesicles, and there are functional transporters embedded within the membrane of the vesicles that are allowing for the import of substrates and the export of the product CoA for usage throughout the cell. One could further speculate that the environmental conditions (pH, redox potential, ion concentration) are also maintained in the vesicles at levels compatible with enzymatic activity.

We investigated whether CoA is essential for apicoplast function in addition to requirements outside of the organelle. We found that ACP and ACP-S, and likely CoA, are essential for apicoplast maintenance, but it is not clear why they are required in the organelle. ACP-S is involved in catalyzing the addition of a 4'-phosphopantetheine prosthetic group to ACP, converting the apo form of the protein to the functional mature form of the protein (holo-ACP) (4, 17). ACP was shown to function in the FASII fatty acid biosynthetic pathway (14, 18), with FabD first catalyzing the transfer of a malonyl group from malonyl-CoA to ACP, forming malonyl-ACP. Every subsequent step of fatty acid synthesis involves further

modification of acyl-ACP. FabH condenses malonyl-ACP and acetyl-CoA to form acetoacetyl-ACP (36). These steps are followed by the elongation stage of FASII in which fatty acids are extended by the enzymes FabF, FabG, FabZ and FabI (43). However, after a series of knockouts in *Plasmodium* it was concluded that the pathway is not required in blood-stage parasites (44, 45). With knockouts of ACC (46), FabF (20), FabI (44), and the PDH E1α subunit (39) in *P. falciparum* showing no clear deleterious effects in blood-stage parasites. Thus, the essential role of ACP and ACP-S is likely not related to their role in the FASII pathway.

It is likely that ACP and ACP-S have some secondary function yet to be elucidated that is required both for parasite survival in addition to apicoplast maintenance. It is possible that both proteins have secondary functions, while ACP has a similar secondary structure to the other acyl carrier proteins and acyl carrier protein-like domains (47) it has been shown to have additional enzymatic activity *in vitro*, being able to function as a malonyl-transferase (48) in addition to showing the ability to self-acylate (49). In regards to ACP-S, it appears to be bifunctional, containing a metal-dependent hydrolase domain (50). Additionally, the 4-phosphopanthethine modification has been shown to increase the stability of ACP, which may be important for any cryptic role that ACP may be playing (47). In other organisms, ACP has been shown to be important for additional roles beyond fatty acid biosynthesis. In *Saccharomyces cerevisiae*, ACP, and specifically the 4'-phosphopantetheine prosthetic group, was shown to play an important role in iron-sulfur cluster biosynthesis in mitochondria (51). The *S. cerevisiae* ACP has been shown to interact and form a complex with ISD11, the cysteine desulfurase NFS1, and ISCU (51, 52). However, this may not be the case in the *P. falciparum* apicoplast. The *P. falciparum* ACP and *S. cerevisiae* ACP are evolutionarily distinct, and found in entirely different organelles which contain different iron-sulfur cluster synthesis pathways

(22). The *P. falciparum* homologs of the proteins found within the mitochondria of *S. cerevisiae* are found in the mitochondrion of *P. falciparum* including ISD11 (53), ISCU (PF3D7_1454500) (54) and NFS1 (55). In the closely related species *T. gondii*, ACP has also been shown to be essential for parasite survival and organelle maintenance (56), but that has been assumed to be due to its role in fatty acid biosynthesis, which is not required in *P. falciparum*. However, it is possible that ACP is playing an essential role in *T. gondii* parasites and other apicomplexan species that is unrelated to fatty acid biosynthesis as well.

Expression of cytosolic *Ec*DPCK complemented the deletion of apicoplast DPCK. This deletion did not result in the loss of the apicoplast. This is surprising since the deletions of ACP and ACP-S result in the loss of the organelle, and it seems that CoA would be needed within the apicoplast for the 4'-phosphopantethine modification of ACP. Thus, it is possible that the CoA generated within the cytosol by *Ec*DPCK may be able to be imported back into the apicoplast. Presumably, there is one or more transporters that bring dephospho-CoA into the apicoplast and export CoA during the normal operation of the apicoplast. These transporters may either be sufficiently nonspecific, or have the ability to work in reverse to bring CoA into the organelle, allowing production of CoA in the cytosol to fulfill requirements in the apicoplast.

Overall, the work here demonstrated that DPCK is an essential apicoplast-localized protein that is required for parasite survival and whose activity cannot be bypassed with IPP. We also found that the vesicles of parasites with disrupted apicoplast organelles continue to be biochemically active, at least in the case of DPCK. Additionally, it is likely that CoA is required within the apicoplast as the 4'-phosphopantethine modification of ACP by ACP-S is essential for organelle maintenance and parasite survival, and that this essentiality is not driven by the predicted role of these proteins in the FASII biosynthetic pathway.

METHODS

P. falciparum culture and maintenance

Unless otherwise noted, blood-stage *P. falciparum* parasites were cultured in human erythrocytes at 1% hematocrit in a 10mL total volume of CMA (complete medium with AlbuMAX) medium containing RPMI 1640 media with L-glutamine (USBiological Life Sciences), supplemented with 25mM HEPES, 0.2% sodium bicarbonate, 12.5µg/mL hypoxanthine, 5g/L Albumax II (Life Technologies) and 25µg/mL gentamicin. Cultures were maintained in gassed flasks (94% N_2, 3% O_2, 3% CO_2) and incubated in sealed 25cm^2 flasks at 37°C.

Generation of the P. *falciparum* DPCK localization line

In order to determine the subcellular localization of the *P. falciparum* DPCK protein we generated a plasmid for the expression of DPCK followed by a C-terminal mCherry tag for visualization in the cell. Due to DPCK containing an intron the gene was amplified from *P. falciparum* cDNA using the primers listed in **Table 5-3**. This amplicon was then ethanol precipitated and inserted into a plasmid containing a bi-directional Cam/HOP promoter, promoting the expression of the hDHFR drug selection cassette on the other end. This plasmid (Cam Api-*Ec*DPCK-mCherry, described below) also already contained the mCherry sequence, and we were able to generate the C-terminal mCherry tag by digesting the vector with AvrII and BsiWI in the presence of rSAP, ethanol precipitating the plasmid, and then inserting the DPCK gene via In-Fusion cloning methods.

Live cell epifluorescent microscopy

For sample preparation, 100μL of parasite culture with a hematocrit of 1% and a parasitemia between 8-10% was obtained. Parasites were stained with 30nM mitoTracker CMX-Ros (Invitrogen) and 1μg/mL 4', 6-diamidino-2-phenylindole (DAPI), and incubated for 30 minutes at 37°C. Cells were then pelleted via mini-centrifuge (Fischer Scientific) for 10 seconds, and the media was aspirated and the cells were resuspended in 100μL of CMA media and incubated for 5 minutes at 37°C. This was done three times to wash the cells, with the cells being resuspended in 20μL of CMA and then pipetted onto slides and sealed with wax (2 parts paraffin, 1 part Vaseline) for observation on a Zeiss AxioImager M2 microscope. A series of images spanning 5μm were acquired with 0.2μm spacing and images were deconvolved with VOLOCITY software (PerkinElmer) to report a single combined z - stack image.

Confirmation of apicoplast genome loss

The loss of the apicoplast was confirmed via PCR with primers specific for a gene within the nuclear (Lactate Dehydrogenase), apicoplast (SufB), and mitochondrial (Cox1) genomes (**Table 5-4**). Failure to amplify a gene from the apicoplast genome, while amplifying genes from the nuclear and mitochondrial genomes would indicate loss of the organelle (53). To collect samples for PCR, approximately 100μL of a resuspended parasite culture at ~5-10% parasitemia was placed in a 90°C heat block for 2 minutes, and then frozen at -20°C. For the PCR reaction, 1μL of the parasite sample was added to reactions with a 50μL total volume. Reactions were conducted using a Veriti 96 well thermal cycler (Applied Biosystems) and Phusion High-Fidelity DNA polymerase (Thermo Fisher Scientific). PCR products were separated by size on a 1.5% agarose gel stained with ethidium

bromide. The parental PfMev line was always used as a positive control for apicoplast detection.

The PCR reaction volumes were as follows:

Water 34.5μL
5x Phusion HF buffer 10μL
Forward primer (10 μM)1.5μL
Reverse primer (10 μM) 1.5μL
dNTPs (10mM) 1μL
Phusion polymerase 0.5μL
parasite lysate 1μL
Total volume 50μL

The PCR program was as follows:

95°C 3.5 minutes
95°C 30 seconds
63°C 30 seconds
72°C 1 minute
72°C 4 minutes
4°C ∞

(steps 2-4 were repeated 35 times)

Generation of the PfMev *Ec*DPCK complementation lines

The *E. coli* complementation constructs were generated in plasmids containing the Cam/HOP promoter. The hDHFR drug resistance cassette was inserted into the plasmid by being amplified from another plasmid containing the cassette using primers shown in **Table 5-5** (hDHFR F and hDHFR R). The plasmid was cut with BamHI and HindIII in the presence of rSAP, and then ethanol precipitated. The hDHFR gene was then amplified, ethanol precipitated, and then inserted into the cut plasmid using In-Fusion cloning.

The *E. coli* DPCK gene was synthesized and codon optimized for expression in *P. falciparum*. This gene was then inserted into a pLN plasmid containing an mCherry sequence,

which was cut with AvrII and BsiWI in the presence of rSAP and then ethanol precipitated. The *E. coli* DPCK gene was then amplified using the primers in **Table 5-5** (*Ec*DPCK F and *Ec*DPCK R), ethanol precipitated, and inserted into the cut plasmid using In-Fusion cloning to generate a sequence that would encode the *E. coli* DPCK with a C-terminal mCherry protein. This whole sequence was then lifted and inserted into the Cam/HOP plasmid containing the hDHFR drug resistance cassette mentioned above by cutting the plasmid with AvrII and AflII in the presence of rSAP and ethanol precipitating it. The entire *E. coli* DPCK-mCherry gene was then amplified from this plasmid that contained the sequence using the primers in **Table 5-5** (Cam*Ec*DpmCry F and Cam*Ec*DpmCry R), and then ethanol precipitated and inserted into the cut plasmid using In-Fusion cloning.

For the generation of the apicoplast localized *E. coli* DPCK-mCherry protein the aforementioned pLN plasmid containing the *E. coli* DPCK-mCherry gene was cut with AvrII in the presence of rSAP and ethanol precipitated. The N-terminal signal and transit peptide, corresponding to the first 55 amino acids from the *P. falciparum* ACP protein was then amplified from a separate plasmid containing the sequence using the primers in **Table 5-5** (pLN.Api55 F and pLN.Api55 R), ethanol precipitated and then inserted upstream of the *Ec*DPCK-mCherry sequence using infusion cloning. This entire gene sequence, containing the Api55 sequence, *E. coli* DPCK and mCherry was then inserted into the plasmid containing the Cam/HOP promoter and hDHFR sequence as mentioned above. This was done by cutting the plasmid with AvrII and AflII in the presence of rSAP and ethanol precipitating the plasmid. The Api-*Ec*DPCK-mCherry gene was then amplified using the primers in **Table 5-5** (CamAp*Ec*DpmC F and CamAp*Ec*DpmC R)

The previous *Ec*DPCK-mCherry and Api-*Ec*DPCK-mCherry plasmids both contain attP sites for integration into the genome of the a separate PfMev line that was generated,

which contains an attb site at the p230 locus of the parasite genome, generously provided by Dr. Krithika Rajaram (Johns Hopkins Bloomberg School of Public Health). This allowed for integration of these plasmids into the genome of this parasite line using bxb1 integration. In order to generate these lines transfections were conducted using the above-mentioned protocol using the *Ec*DPCK-mCherry or Api-*Ec*DPCK-mCherry plasmids along with the pINT plasmid encoding the bxb1 integrase and selected with 2.5nM WR99210 for 7 days, after which point drug pressure was removed. Infected RBCs were then observed ~20-25 days post transfection, at which point 2.5nM WR99210 was added back, with the parasites maintained in the presence of this drug.

Generation of *P. falciparum* transfection constructs for gene deletion

Homology arms of ~300-600bp for each gene were amplified using the homology arm (HA) 1 and 2 forward and reverse primers corresponding to each gene (**Table 5-6**) from blood-stage *P. falciparum* NF54-attb gDNA. HA1 and HA2 primers were designed to contain ~15bp overhangs for insertion into the cut the pRS(ng) or pL8 plasmid using In-Fusion (Clontech) cloning methods. The pRS(ng) and pL8 plasmids contain the hDHFR drug resistance cassette for selection and contains flanking endonuclease sites for insertion of the homology arms. The pRS(ng) or pL8 plasmid was digested with NotI for insertion of HA1, and with NgoMIV for HA2. Digests with either endonuclease were also treated with recombinant shrimp alkaline phosphatase (rSAP).

The pCasG, pRS, and pL8 plasmids contain a guide RNA (gRNA) expression cassette. Guide RNA sequences were synthesized as oligos (**Table 5-7**), annealed, and inserted into the pCasG, pRS, or pL8 plasmids via In-Fusion cloning after the plasmids were digested with BsaI in the presence of rSAP and ethanol precipitated.

P. falciparum transfections for gene deletion

Transfections were conducted as previously described (31, 57). Briefly, 400μL of red blood cells were washed with 5mL of CytoMix and resuspended in 400μL of CytoMix. The red blood cells were then electroporated with 75μg each of the pUF1-Cas9 and pL8 gene specific knock out plasmids or the pCasG and pRS(ng) gene specific knock out plasmids (32). The electroporated RBCs were then mixed with ~2.5mL PfMev parasites synchronized as schizonts at 1% hematocrit and ~10% parasitemia and given 10mL CMA with 50μM mevalonate. After 48 hours, transfectants were selected with 1.5μM DSM1, 2.5nM WR99210, and 50μM mevalonate for seven days. After seven days, the parasites were switched to media containing only 50μM mevalonate. Infected red blood cells (iRBC) were first observed between 17 and 30 days after beginning drug selection. Once parasites were observed, the medium was switched to 2.5nM WR99210 and 50μM mevalonate.

Confirmation of knockout genotype

In order to screen for integration and successful gene knockout, in addition to the presence of any contaminating residual wild type parasites, a set of six primers were used: 5'F, 3'R, pL8 HA1 R, pL8 HA2F, 5' WT R and 3' WT F (**Table 5-8**). These primers were designed to screen for integration and gene disruption at the 5' and 3' ends (Δ5' and Δ3') in addition to 5' and 3' regions of the WT gene (5' and 3'). The same reactions were also performed on the parental PfMev line concurrently as a control. Samples for PCR were collected when the parasitemia reached been 5-10%, as determined by Giemsa stain. Approximately 100μL of a resuspended parasite culture was placed in a heat block at 90°C

for 2 minutes and stored at -20°C. For the PCR reaction, 1μL of the parasite sample was added to reactions with a 50μL total volume. Reactions were conducted using a Veriti 96 well thermal cycler (Applied Biosystems) and Phusion High-Fidelity DNA polymerase (Thermo Fisher Scientific, cat. #F530L). PCR products were separated on a 1.5% agarose gel stained with ethidium bromide for visualization.

The PCR reaction volumes were as follows:

Water 34.5μL
5x Phusion HF buffer 10μL
Forward primer (10 μM)1.5μL
Reverse primer (10 μM) 1.5μL
dNTPs (10mM) 1μL
Phusion polymerase 0.5μL
parasite lysate 1μL
Total volume 50μL

The PCR program was as follows:

95°C 3.5 minutes
95°C 30 seconds
62°C 1 minute
62°C 4 minutes
4°C ∞

(steps 2 and 3 were repeated 35 times)

Generation of the PfMev CLD-*Ec*DPCK-mCherry-apt parasite line

In order to generate the CLD-*Ec*DPCK-mCherry-apt plasmid, the Cam Api-EcDPCK-mCherry plasmid was used as a starting point. This plasmid was digested with AvrII and BspEI in order to remove the signal and transit peptide sequence from ACP used to target the protein to the apicoplast, and was ethanol precipitated. The conditional localization domain was then amplified from another plasmid that contained this sequence using the primers listed in **Table 5-9** (CLD F and CLD R).

The plasmid (pPB1) used for the generation of the PfMev CLD-*Ec*DPCK-mCherry-apt was graciously provided by Dr. Krithika Rajaram (Johns Hopkins Bloomberg School of Public Health). This plasmid contains a bi-directional Cam/HOP promoter, with one end promoting the expression of the tetR-DOZI system in addition to the BSD drug resistance marker. The other end contained an aptamer array that can be appended to the inserted gene of interest. The above-mentioned CLD-EcDPCK-mCherry gene sequence was amplified using the same CLD F primer along with the EcDPCK CLD R primer (**Table 5-9**), gel purified, and then inserted in to the pPB1 plasmid using In-Fusion cloning. For insertion, the pPB1 plasmid had been previously digested with AvrII and PspOMI in the presence of rSAP and ethanol precipitated. This plasmid also contains an attP site, thus, in order to generate the PfMev CLD-*Ec*DPCK-mCherry-apt the PfMev p230pattb parasites were transfected with this plasmid, along with the pINT plasmid encoding the bxb1 integrase for attb/attP integration. Parasites were transfected following the standard protocol and selected with 2.5ng/mL blasticidin for seven days, after which drug pressure was removed. Parasites were observed via Giemsa stain ~20-25 days later, at which point parasites were again cultured in the presence of 2.5ng/mL blasticidin.

Deletion of DPCK in the PfMev *Ec*DPCK-mCherry, PfMev Api-*Ec*DPCK-mCherry, and PfMev CLD-*Ec*DPCK-mCherry-apt lines

A DPCK specific pL8 plasmid was generated using the above-mentioned protocol. This plasmid contains a hDHFR drug resistance cassette, which was removed by digesting the plasmid with BamHI and HindIII in the presence of rSAP and ethanol precipitating it. The blasticidin deaminase drug resistance cassette was then amplified from a separate plasmid containing the sequence listed in Table 5-3 (pRsBSD F and pRsBSD R). The

amplicon was then ethanol precipitated and inserted into the cut plasmid using In-Fusion cloning.

The PfMev *Ec*DPCK-mCherry and PfMev Api-*Ec*DPCK-mCherry lines were then transfected with pL8-DPCK (BSD) plasmid along with the pUF1-Cas9 plasmid following the standard transfection procedure listed above. The parasites were selected with 2.5ng/mL blasticidin and 1.5μM DSM1 for seven days, also in the presence of 2.5nM WR99210 which selected for the previously integrated drug resistance cassette. After seven days, the 2.5ng/mL blasticidin and 1.5μM DSM1 drug pressure was removed. Infected red blood cells were then typically seen after ~20-25 days. After parasites were observed the cultures were then maintained in the presence of 2.5nM WR99210 and 2.5ng/mL blasticidin.

For deletion of DPCK in the PfMev CLD-*Ec*DPCK-mCherry-apt, since the line was selected for, using 2.5ng/mL blasticidin, due to the presence of the BSD drug selectable marker, the original pL8 plasmid containing the DPCK homology arms flanking the hDHFR drug selectable marker was used. These parasites were transfected with the pL8-DPCK (hDHFR) plasmid along with the pUF1-Cas9 plasmid following the standard transfection procedure listed above. The parasites were selected with 2.5nM WR99210 and 1.5μM DSM1 for seven days, also in the presence of 2.5ng/mL blasticidin which selected for the previously integrated drug resistance cassette. After seven days, the 2.5nM WR99210 and 1.5μM DSM1 drug pressure was removed. Infected red blood cells were then typically seen after ~20-25 days. After parasites were observed the cultures were then maintained in the presence of 2.5nM WR99210 and 2.5ng/mL blasticidin. Parasites were continuously cultured in the presence of 0.5μM aTc from the moment of transfection and onward to allow for protein expression in the permissive state.

Growth curve for the PfMev CLD-*Ec*DPCK-mCherry-apt ΔDPCK line (+aTc/+Shield1)

The PfMev CLD-*Ec*DPCK-mCherry-apt ΔDPCK line was maintained in CMA media with 0.5μM aTc. To begin the growth curve the PfMev CLD-*Ec*DPCK-mCherry-apt ΔDPCK parasite was washed to remove the aTc. This was done by spinning the cells at 1,600rcf, aspirating the media, and adding 10mL of CMA, repeating this four times. These parasites were then used to seed two separate 75cm^2 flasks, each at 1% hematocrit in a 10mL total volume of CMA media, and a starting parasitemia of ~0.5%. One flask was supplemented with 0.5μM aTc, representing the uninduced condition, while the other was treated with 0.5μM Shield1, representing the induced condition. The appropriate media was replaced approximately every 24 hours, at which point a blood-film was made, and the parasitemia was determined via Giemsa stain. On day four of this growth curve the parasitemia was cut 1:10. This experiment was done in singlicate as an initial proof of concept experiment in support of **Figure 5-11**.

Pantothenate titration growth curve

Pantothenate free media was generated, consisting of RPMI 1640 media with L-glutamine, and without pantothenate (USBiological Life Sciences), supplemented with 25mM HEPES, 0.2% sodium bicarbonate, 12.5μg/mL hypoxanthine, 5g/L Albumax II (Life Technologies) and 25μg/ml gentamicin. PfMev parasites were washed to remove the pantothenate. This was done by spinning the cells at 1,600rcf, aspirating the media, and adding 10mL of pantothenate free-media, repeating this four times. Parasites were then seeded in a 24-well plate at 2% hematocrit, a starting parasitemia of 0.5%, and 1mL of pantothenate free media, with the exception of one condition in which parasites were grown

in CMA. Pantothenate was then added back to the wells containing pantothenate-free media at concentrations of 1nM, 10nM, 100nM, or 1μM, with one well receiving no pantothenate. The appropriate media was replaced approximately every 24 hours, at which point a blood-film was made, and the parasitemia was determined via Giemsa stain. On day three of this growth curve the parasitemia was cut 1:10. This experiment was done in singlicate as an initial ranging experiment in support of **Figure 5-11**.

Pantothenate titration for the PfMev CLD-*Ec*DPCK-mCherry-apt ΔDPCK line (+aTc/+Shield1)

The PfMev CLD-*Ec*DPCK-mCherry-apt ΔDPCK line was regularly maintained with media containing 2.5nM WR99210 and 2.5ng/mL blasticidin with 0.5μM aTc. This parasite culture was then washed to remove the pantothenate and aTc from the culture. This was done by spinning the cells at 1,600rcf, aspirating the media, and adding 10mL of pantothenate free-media, repeating this four times. Parasites were then seeded in a 24-well plate at 2% hematocrit, a starting parasitemia of 0.5%, and 1mL of pantothenate free media, with the exception of one condition in which parasites were grown in CMA. Pantothenate was then added back to the wells containing pantothenate-free media at concentrations of 10nM, 25nM, 50nM, or 100nM, with one well receiving no pantothenate. These conditions were set up in duplicate, in order to test permissive and non-permissive conditions at each concentration of pantothenate. Thus, parasites were either supplemented with 0.5μM aTc, representing the permissive condition, or with 0.5μM Shield1, representing the non-permissive condition. The appropriate media was replaced approximately every 24 hours. Every 48 hours a blood-film was made, and the parasitemia was determined via Giemsa

stain. On day four of this growth curve the culture was cut 1:10. This experiment was done in singlicate as an initial ranging experiment in support of **Figure 5-11**.

Growth curve for the PfMev CLD-*Ec*DPCK-mCherry-apt ΔDPCK line (+aTc/+Shield1) under limiting pantothenate concentrations

The PfMev CLD-*Ec*DPCK-mCherry-apt ΔDPCK line was washed with pantothenate free media in order to remove the aTc and pantothenate. This was done by spinning the cells at 1,600rcf, aspirating the media, and adding 10mL of pantothenate free-media, repeating this four times. Parasitemia was determined via Giemsa stain, with that culture then used to seed a 96-well flat bottom cell culture plate (Corning) at a 0.5% starting parasitemia, 2% hematocrit, and a total volume of 250µL per well in quadruplicate. Pantothenate free media was used, as described above, with pantothenate then added back to a concentration of 50nM. Two conditions were tested, with parasites either being supplemented with 0.5µM aTc, representing the permissive condition, or with 0.5µM Shield1, representing the non-permissive condition. The appropriate media was replaced approximately every 24 hours, at which point samples were collected for analysis via flow cytometry as outlined below. On day four of this growth curve the parasitemia was cut 1:10. In order to minimize evaporation and edge effects, the surrounding wells were filled with 250µL of 1mM EDTA. The plates were incubated in a Modular Incubator Chamber gassed with 94% N_2, 3% O_2, 3% CO_2 for 1 minute and 15 seconds, and incubated at 37°C. This experimental setup was also used to generate a growth curve for the apicoplast minus PfMev CLD-*Ec*DPCK-mCherry-apt ΔDPCK parasite line, the only difference being the addition of 50µM mevalonate in both the induced and uninduced conditions.

Inducing apicoplast loss in the PfMev CLD-*Ec*DPCK-mCherry-apt ΔDPCK parasite line

The PfMev CLD-*Ec*DPCK-mCherry-aptamer ΔDPCK line was cultured in media containing 100nM azithromycin in the presence of 50μM mevalonate for 7 days. After 7 days, the parasites were cultured continuously in the presence of 50μM mevalonate. Loss of the apicoplast was confirmed via PCR using the methods described above.

Testing mevalonate dependence in PfMev deletion mutants via growth curve

For each of the PfMev deletion lines, the parasitemia was determined via Gimesa stain, with the appropriate amount of the parental culture removed to seed quadruplicate samples with or without mevalonate. This volume was resuspended in a total of 10mL CMA and centrifuged at 1,600rcf at room temperature (~25°C) for 5 minutes, washed a second time with an additional 10mL CMA, and then resuspended in the appropriate volume of CMA, and then split equally into two tubes. To one of the tubes, the appropriate volume of a 10mM stock of mevalonate was added to bring to final concentration to 50μM mevalonate. Parasites were seeded in a 96-well plate at 0.5% starting parasitemia, 2% hematocrit, and at a total volume of 250μL per well in quadruplicate. Additionally, 150μL of the appropriate media was replaced in each well on days 1, 2, and 3. Parasite samples were collected every 24 hours for four days, and the parasitemia was counted via SYBR green staining and flow-cytometry as outlined below.

Flow cytometry for parasite growth curve determination

Growth curves were generated by staining parasites with SYBR Green and counting parasitemia via flow cytometry. In order to setup the growth curve, the parasitemia of the

starting culture was determined via Giemsa stain. Based on the determined parasitemia the culture was used to seed a 96-well flat bottom cell culture plate (Corning) at a 0.5% starting parasitemia and 2% hematocrit, at a total volume of 250µL in quadruplicate. In order to minimize evaporation and edge effects, the surrounding wells were filled with 250µL of 1mM EDTA. Plates were incubated in chambers gassed with 94% N_2, 3% O_2, 3% CO_2 for 1 minute and 15 seconds, and incubated at 37°C.

Parasite samples were collected immediately after seeding and analyzed via flow cytometry to verify the starting parasitemia and then collected every 24 hours thereafter. Samples collected on days 1-3 were diluted 1:10 in phosphate-buffered saline (PBS) and stored in a 96-well plate (Corning) at 4°C. We have previously verified that storage under these conditions and subsequent staining with SYBR Green reflects accurate parasitemia values.

On day 4 parasites were stained with SYBR Green by transferring 1µL of parasite culture, or 10µL of the 1:10 dilutions (the day 1-3 samples), to a 96-well plate containing 100µL of 1x SYBR Green (Invitrogen) in PBS. The samples were then incubated for 30 minutes on a platform Titramax 101 shaker (Heidolph) at 950rpm while protected from light. Post-incubation, 150µL of PBS was added to each well to dilute unbound SYBR Green dye. A control consisting of uninfected RBCs was also prepared in parallel and treated in the same manner as listed above.

Samples were analyzed with an Attune Nxt Flow Cytometer (Thermo Fisher Scientific). With a 50µL acquisition volume, 250µL total sample volume, and a running speed of 25µL/minute with 10,000 total events were collected within the R2 gate.

For flow cytometer gating, the R1 gate used forward-scatter area by side-scatter area to identify total RBCs from the sample. The R2 gate used forward-scatter height to identify

single cells, and the R3 gate was used to measure parasitemia using fluorescence from the SYBR Green staining of parasite DNA (ratio of SYBR Green positive cells to total cells).

FIGURES

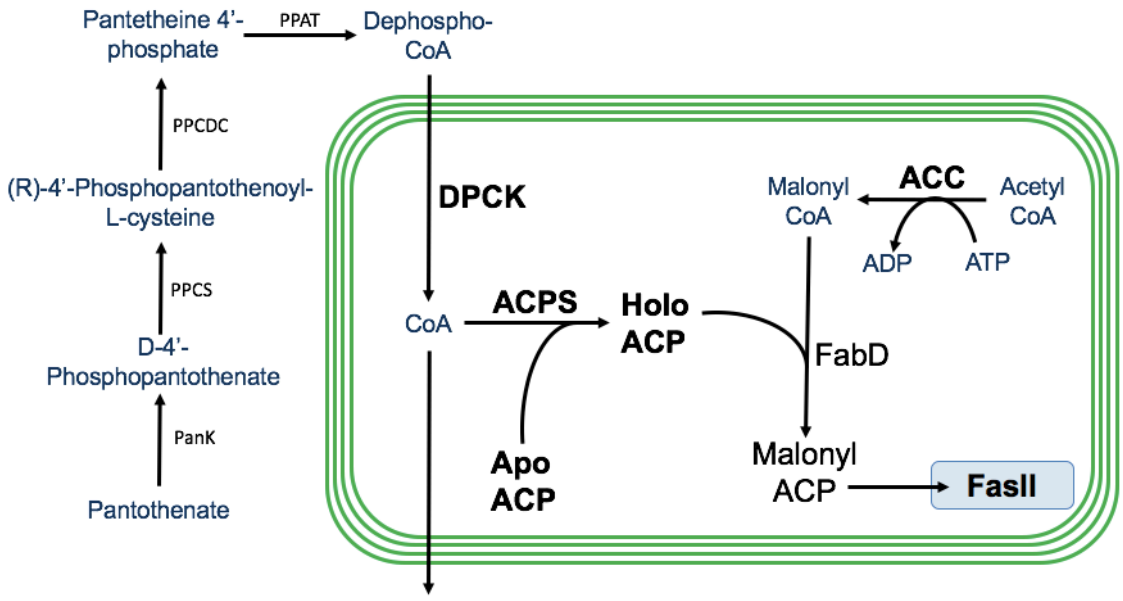

Figure 5-1 Generation of CoA and utilization in the apicoplast

P. falciparum parasites are believed to be reliant on scavenged pantothenate to generate CoA. The generation of CoA occurs through a series of enzymes within the cytosol (PanK, PPCS, PPCDC, and PPAT). The final step involving the conversion of dephospho-CoA to CoA by DPCK is believed to occur within the apicoplast. CoA is utilized within the organelle to modify apo-ACP into holo-ACP, which is involved in the FASII fatty acid biosynthesis pathway. The CoA produced within the apicoplast is also believed to be exported for utilization throughout the cell.

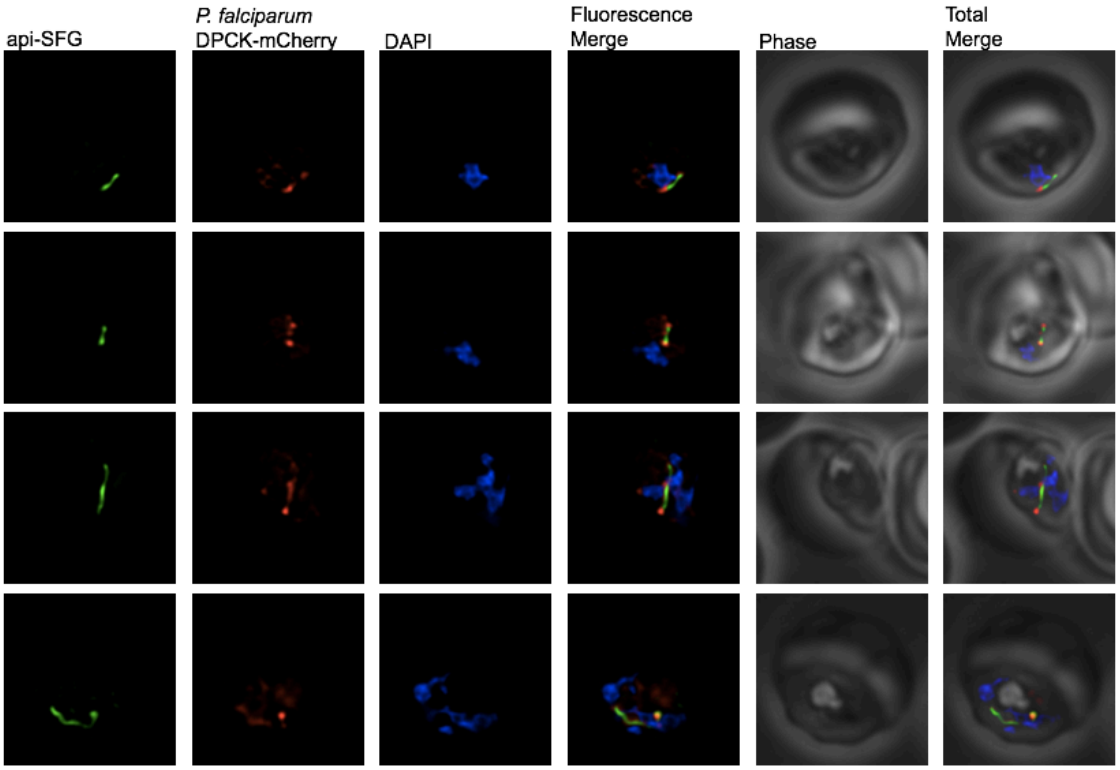

Figure 5-2 Co-localization of DPCK-mCherry with apicoplast marker api-SFG

Live fluorescent microscopy of four different PfMev parasites expressing api-SFG (green), the *P. falciparum* DPCK-mCherry protein (red), and also stained with DAPI (blue). Microscopy images are 10μM long by 10μM wide.

Plasmids	Selection Time	Supplementation	Successful?
pUF1-Cas9/pL8-DPCK-HA1/2+g (31o16)	40 days	50μM mev.	No
pUF1-Cas9/pL8-DPCK-HA1/2+g (8N16)	40 days	50μM mev.	No
pUF1-Cas9/pL8-DPCK-HA1/2+g (16N16)	40 days	50μM mev.	No
pUF1-Cas9/pL8-DPCK-HA1/2+g (28N16)	40 days	50μM mev.	No
pUF1-Cas9/pL8-DPCK-HA1/2+g (5j17)	40 days	50μM mev./5mM CoA	No
pUF1-Cas9/pL8-DPCK-HA1/2+g (24j17)	40 days	50μM mev./5mM CoA	No

Table 5-2 DPCK Transfection Attempts

We attempted to knockout the dephospho-CoA kinase (DPCK) gene in the PfMev parasite line in the presence of 50μM mevalonate. In none of the six independent transfections were we successful in deleting the DPCK gene, even in the two attempts in which the parasites were also supplemented with 5mM CoA.

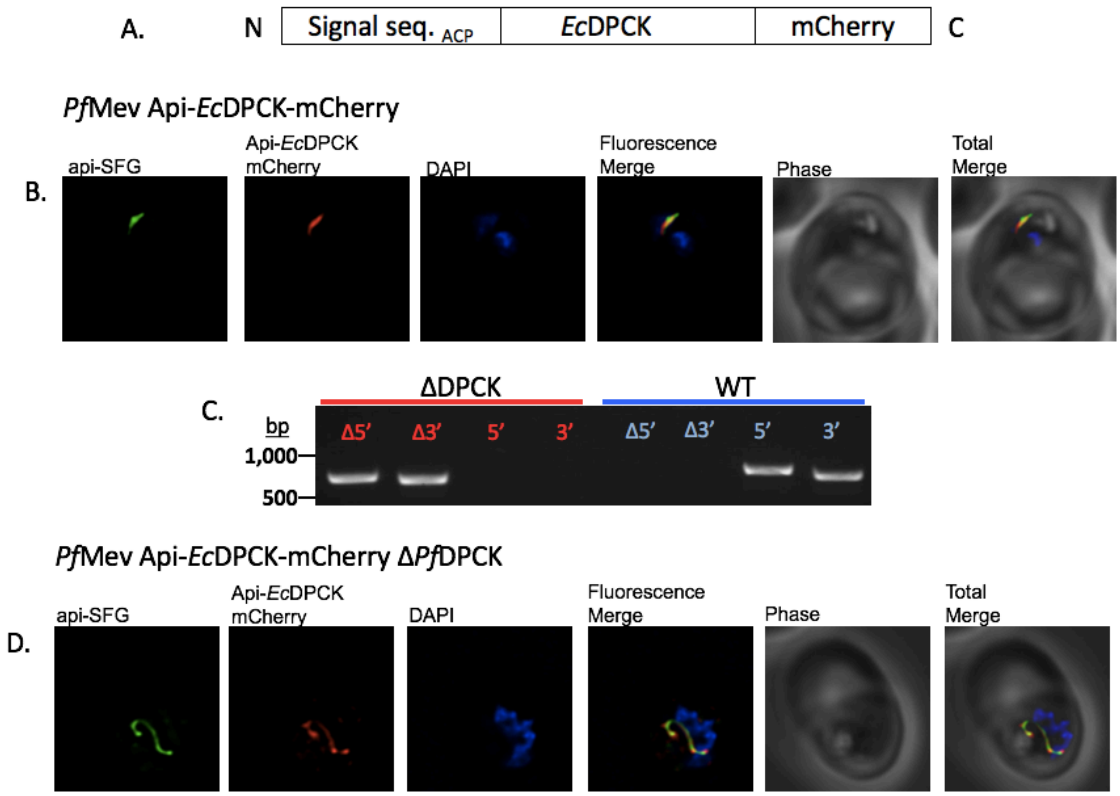

Figure 5-3 *E. coli* DPCK complementation in the apicoplast and deletion of DPCK

A.) Construct used to express *E. coli* DPCK in the apicoplast with an N-terminal signal sequence from ACP, and a C-terminal mCherry tag.

B.) Live epifluorescence microscopy of PfMev parasites expressing api-SFG (green), the Api-*Ec*DPCK-mCherry construct (red), and also stained with DAPI (blue).

C.) Genotyping PCR confirming the deletion of the endogenous DPCK, with amplification demonstrating integration at the Δ5' and Δ3' loci, and lack of wild type parasites due to failure to amplify at the wild type 5' and 3' loci, as compared to the parental control.

D.) Live epifluorescence microscopy of the PfMev Api-*Ec*DPCK-mCherry ΔDPCK parasite line expressing api-SFG (green), the Api-*Ec*DPCK-mCherry construct (red), and also stained with DAPI (blue), with co-localization seen between the api-SFG and Api-*Ec*DPCK-mCherry proteins. Microscopy images are 10μM long by 10μM wide.

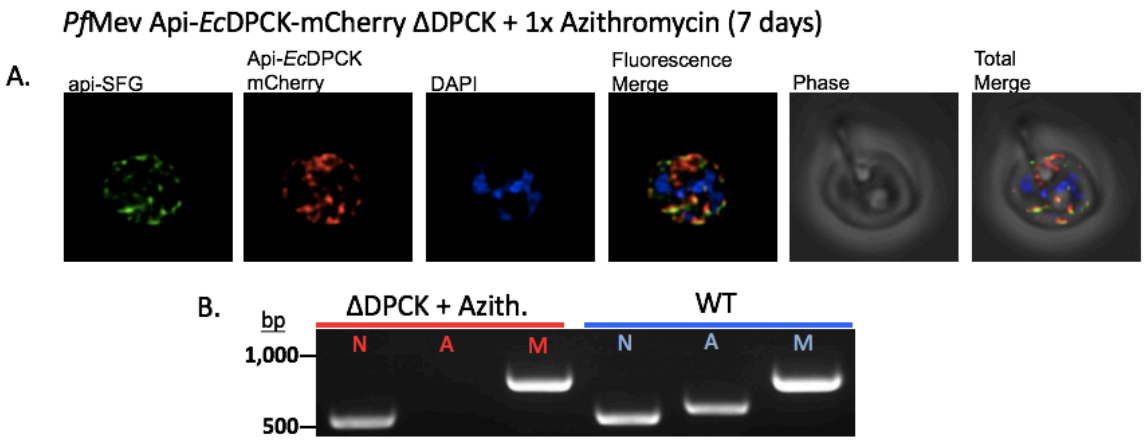

Figure 5-4 Azithromycin treatment of PfMev-asfg Api-*Ec*-DPCK-mCherry ΔDPCK parasites

A.) Live epifluorescence microscopy of the PfMev Api-*Ec*DPCK-mCherry ΔDPCK line treated with 1x azithromycin for 7 days under supplementation with 50μM mevalonate. This parasite line expresses api-SFG (green), the Api-*Ec*DPCK-mCherry construct (red), and is also stained with DAPI (blue). The api-SFG and Api-*Ec*DPCK-mCherry proteins appear to be co-localized in these parasites after apicoplast disruption.

B.) PCR detection of the lactate dehydrogenase, SufB, and Cox1 genes from the nuclear (N), apicoplast (A), and mitochondrial (M) genomes, respectively. We failed to amplify SufB from the *Pf*Mev Api-*Ec*-DPCK-mCherry ΔDPCK parasites, indicating loss of the apicoplast organellar genome.

Microscopy images are 10μM long by 10μM wide.

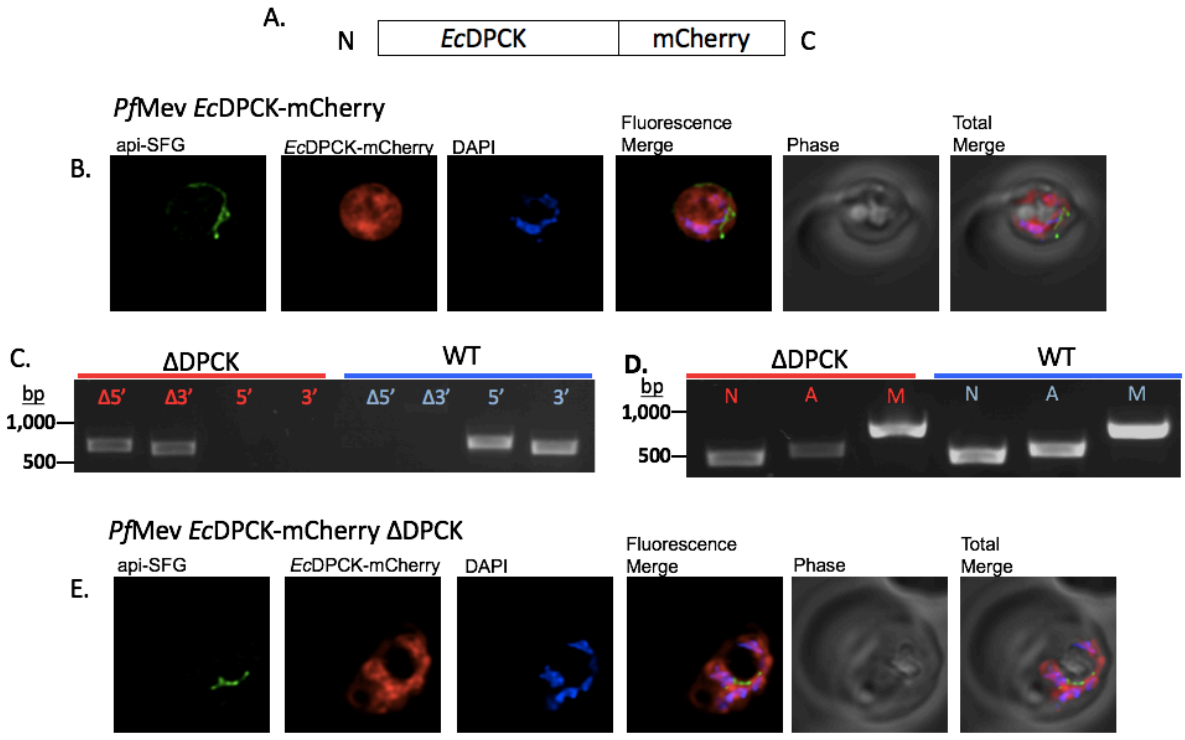

Figure 5-5 *E. coli* DPCK complementation in the cytosol and deletion of DPCK

A.) Construct used to express the *E. coli* DPCK protein with a C-terminal mCherry tag in the cytosol of the PfMev parasite line.

B.) Live epifluorescence microscopy of the PfMev *Ec*DPCK-mCherry line. This parasite line is expressing api-SFG (green), the *Ec*DPCK-mCherry construct (red), and also stained with DAPI (blue).

C.) Genotyping PCR confirming the deletion of the endogenous DPCK, with amplification demonstrating integration at the Δ5' and Δ3' loci, and lack of wild type parasites due to failure to amplify at the wild type 5' and 3' loci, as compared to the parental control.

D.) PCR detection of the lactate dehydrogenase, SufB, and Cox1 genes from the nuclear (N), apicoplast (A), and mitochondrial (M) genomes, respectively. We were successful in amplifying SufB from the *Pf*Mev *Ec*-DPCK-mCherry ΔDPCK parasite line grown under

continuous supplementation with 50μM mevalonate, indicating retention of the apicoplast organelle genome.

E.) Live epifluorescence microscopy of the PfMev api-SFG *Ec*DPCK-mCherry ΔDPCK line. This parasite line expresses api-SFG (green), the *Ec*DPCK-mCherry construct (red), and is also stained with DAPI (blue).

Microscopy images are 10μM long by 10μM wide.

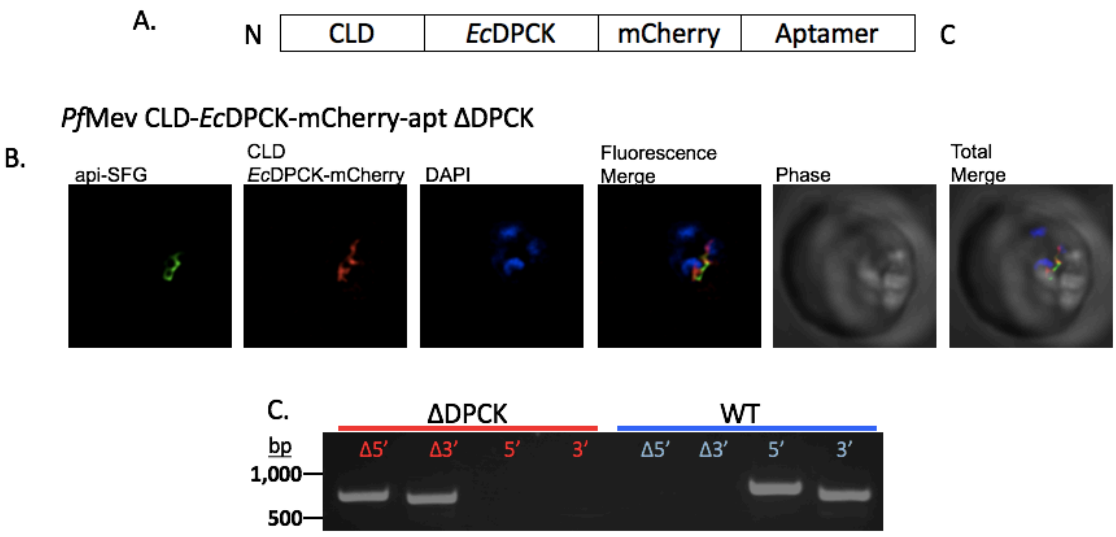

Figure 5-6 Generation of the PfMev CLD-*Ec*DPCK-mCherry-aptamer line and deletion of DPCK

A.) Construct used to generate *Pf*Mev CLD-*Ec*DPCK-mCherry-aptamer parasite line

B.) Live epifluorescence microscopy of the PfMev CLD-*Ec*DPCK-mCherry-aptamer line. This parasite line is expressing api-SFG (green), the CLD-*Ec*DPCK-mCherry protein (red), and also stained with DAPI (blue).

C.) Genotyping PCR confirming the deletion of the endogenous DPCK, with amplification demonstrating integration at the Δ5' and Δ3' loci, and lack of wild type parasites due to failure to amplify at the wild type 5' and 3' loci, as compared to the parental control. Microscopy images are 10μM long by 10μM wide.

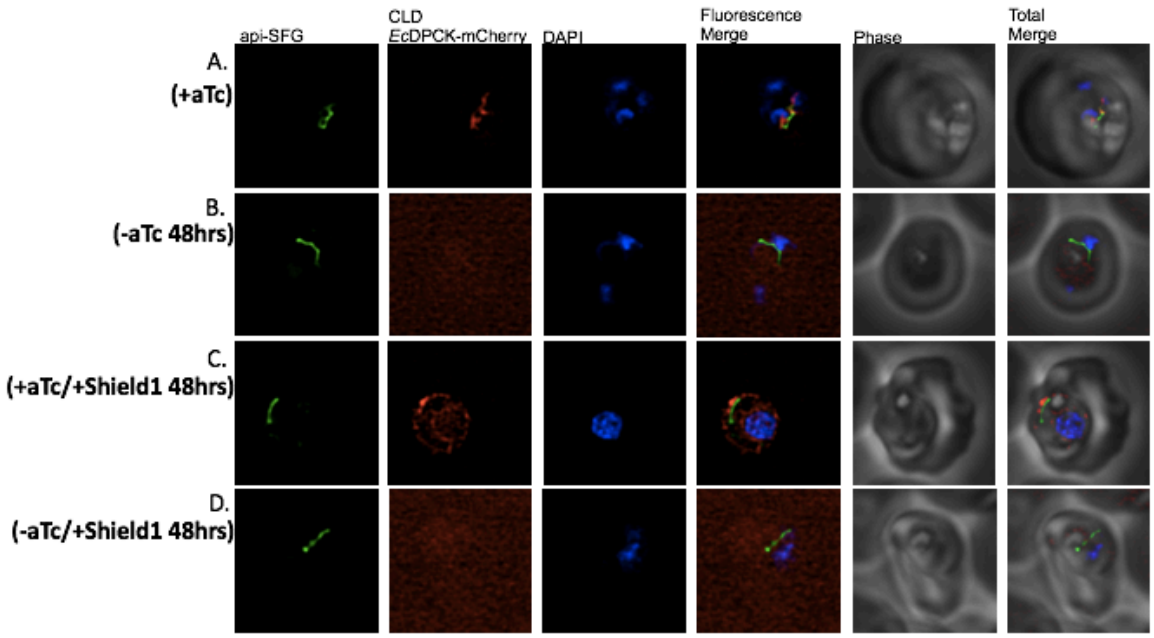

Figure 5-7 Testing protein knockdown and mislocalization in the PfMev CLD-*Ec*DPCK-mCherry-apt parasite line

A.) The PfMev CLD-*Ec*DPCK-mCherry-apt parasite line grown in the presence of 0.5µM aTc.

B.) The PfMev CLD-*Ec*DPCK-mCherry-apt parasite line grown in the absence of aTc for 48 hours.

C.) The PfMev CLD-*Ec*DPCK-mCherry-apt parasite line grown in the presence of 0.5µM aTc, and in the presence of 0.5µM Shield1 for 48 hours.

D.) The PfMev CLD-*Ec*DPCK-mCherry-apt parasite line grown in the absence of aTc, and in the presence of 0.5µM Shield1 for 48 hours.

Microscopy images are 10µM long by 10µM wide.

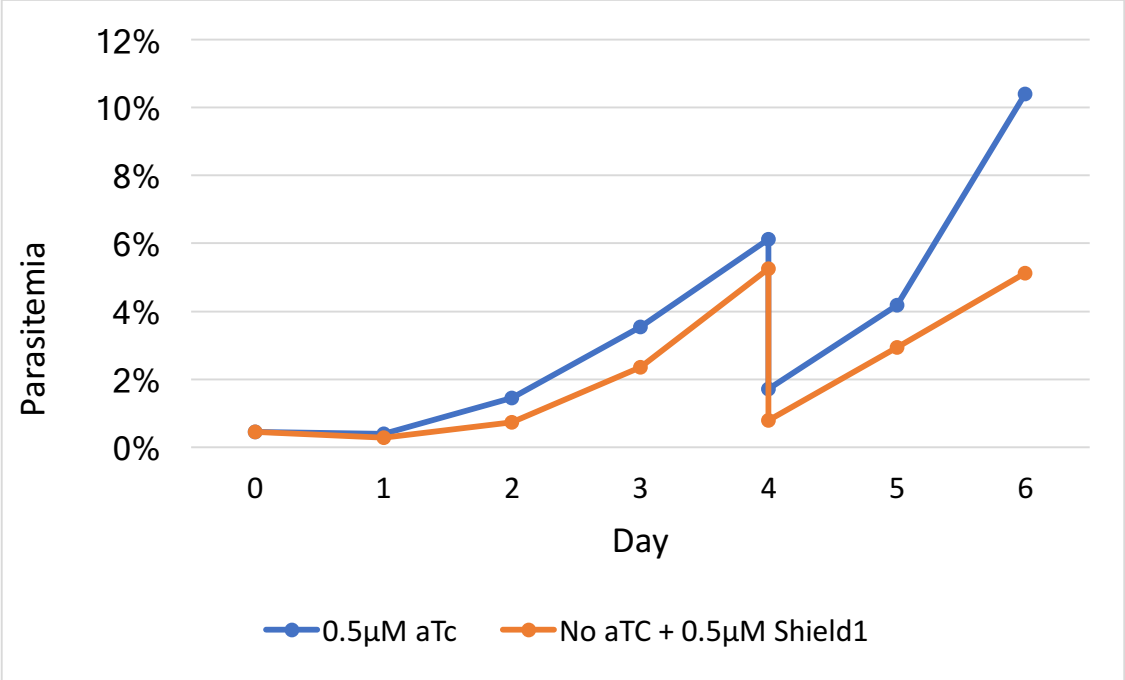

Figure 5-8 Growth of the PfMev CLD-*Ec*DPCK-mCherry-apt ΔDPCK parasite line under permissive and non-permissive conditions

Growth curve of the *Pf*Mev-CLD-*Ec*DPCK-mCherry-aptamer ΔDPCK parasite line grown either in the permissive state (absence of 0.5µM aTc and the presence of 0.5µM Shield1), or the non-permissive state (presence of 0.5µM aTc and the absence 0.5µM Shield1). Parasites were seeded at ~0.5% parasitemia and then cut 1:10 on day 4. Parasites had the media exchanged every 24 hours, at which time a blood film was made, and parasitemia was determined via Giemsa stain. This experiment was done in singlicate as an initial proof of concept experiment in support of the final growth curve shown in **Figure 5-11**.

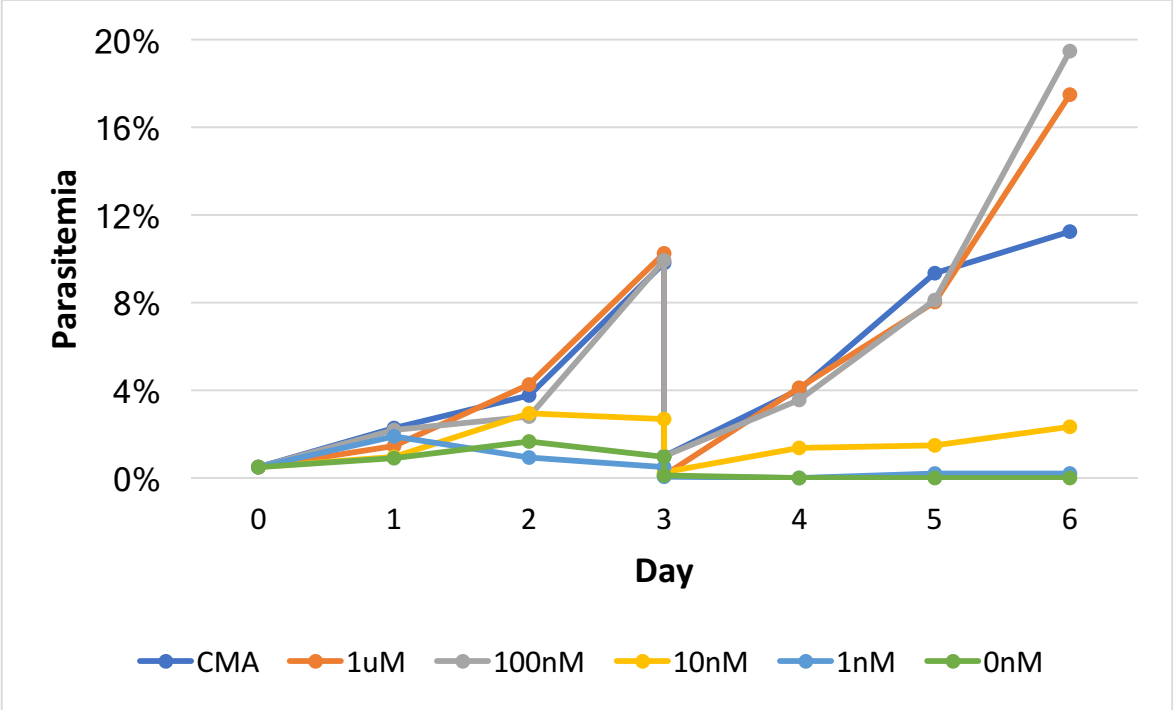

Figure 5-9 Titration of pantothenate affecting the growth of the PfMev parasite line

PfMev parasites were seeded at ~0.5% parasitemia and grown in media containing either 0nM, 1nM, 10nM, 100nM, or 1μM of pantothenate, also with parasites grown in CMA as a control. Parasite media was refreshed every 24 hours, at which time a blood film was made, and parasitemia was determined via Giemsa stain. All parasite cultures were cut 1:10 on day 3. This experiment was done in singlicate as an initial ranging experiment in support of the final growth curve shown in **Figure 5-11**.

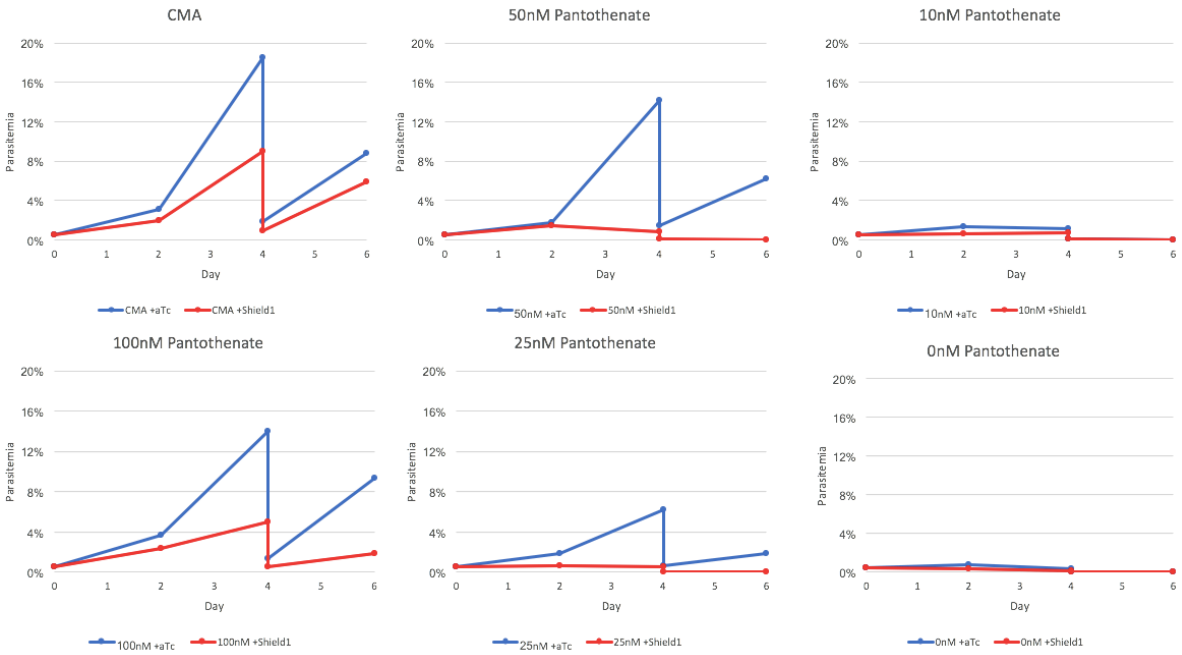

Figure 5-10 Titration of pantothenate affecting the growth of the PfMev CLD-*Ec*DPCK-mCherry-apt ΔDPCK parasite line under permissive and non-permissive conditions

Growth curve of the PfMev CLD-*Ec*DPCK-mCherry-aptamer ΔDPCK parasite line grown either in the presence of 0.5μM aTc and the absence 0.5μM Shield1 (permissive condition, blue), or the absence of 0.5μM aTc and the presence of 0.5μM Shield1 (non-permissive condition, red). Parasites were also grown at varying concentrations of pantothenate, including either 10nM, 25nM, 50nM, 100nM, or grown in 0nM pantothenate as a negative control, and CMA as a positive control. Parasites were seeded at ~0.5% parasitemia, with media exchanged every 24 hours. Every 48 hours a blood film was made, and parasitemia was determined via Giemsa stain. All parasite cultures were cut 1:10 on day 4. These experiments were done in singlicate as an initial ranging experiment in support of the final growth curve shown in **Figure 5-11**.

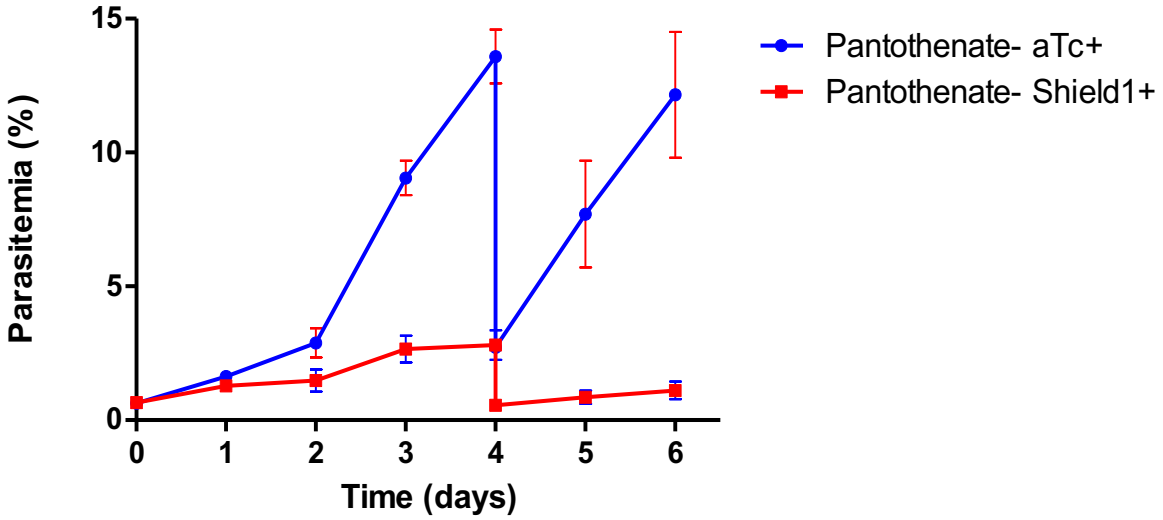

Figure 5-11 Growth curve of PfMev CLD-*Ec*DPCK-mCherry-apt ΔDPCK parasite line under permissive and non-permissive conditions at 50nM pantothenate

Growth curve of the PfMev CLD-*Ec*DPCK-mCherry-apt ΔDPCK parasite line grown either in the presence of 0.5µM aTc and the absence 0.5µM Shield1 (permissive condition, blue), or the absence of 0.5µM aTc and the presence of 0.5µM Shield1 (non-permissive condition, red). All parasite lines were also grown at a concentration of 50nM pantothenate. Parasites were collected during daily media exchanges for determination of parasitemia by flow cytometry. Parasite cultures were cut 1:10 on day 4. Error bars represent the SEM of duplicate experiments, each conducted in quadruplicate.

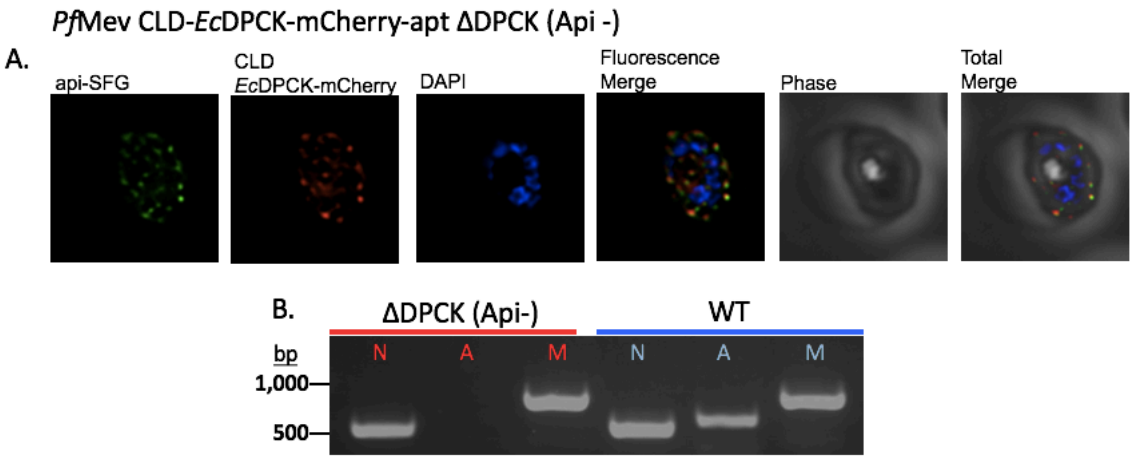

Figure 5-12 Azithromycin treatment of PfMev CLD-*Ec*DPCK-mCherry-apt ΔDPCK parasite line

A.) Live epifluorescence microscopy of the apicoplast negative PfMev CLD-*Ec*DPCK-mCherry-apt ΔDPCK line post treatment with 100nM azithromycin in the presence of 50μM mevalonate. This parasite line expresses Api-SFG (green), the CLD-*Ec*DPCK-mCherry construct (red), and is also stained with DAPI (blue). Images are 10μM long by 10μM wide.

B.) PCR detection of the lactate dehydrogenase, SufB, and Cox1 genes from the nuclear (N), apicoplast (A), and mitochondrial (M) genomes, respectively. We were unsuccessful in amplifying SufB from the PfMev CLD-*Ec*DPCK-mCherry-apt ΔDPCK parasite line after treatment with 100nM azithromycin in the presence of 50μM mevalonate, indicating disruption of the apicoplast organelle.

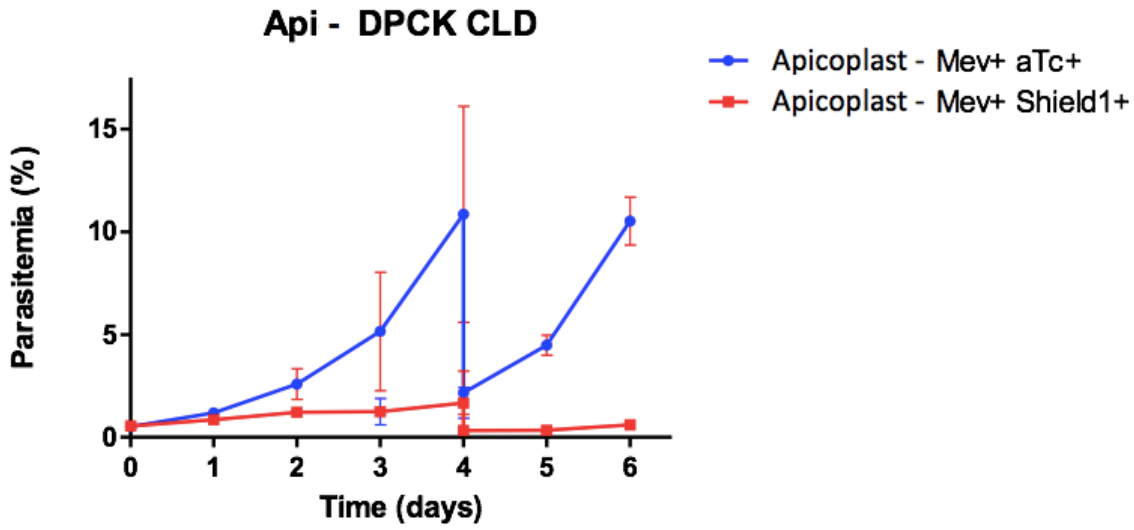

Figure 5-13 Growth curve of the azithromycin-treated PfMev CLD-*Ec*DPCK-mCherry-aptamer ΔDPCK parasite line under permissive and non-permissive conditions at 50nM pantothenate

Growth curve of the *Pf*Mev CLD-*Ec*DPCK-mCherry-aptamer ΔDPCK parasite line containing a disrupted apicoplast, grown either in the presence of 0.5μM aTc and the absence 0.5μM Shield1 (permissive condition, blue), or the absence of 0.5μM aTc and the presence of 0.5μM Shield1 (non-permissive condition, red). All parasite lines were also grown at a concentration of 50nM pantothenate and 50μM mevalonate. Parasites were collected during daily media exchanges for determination of parasitemia by flow cytometry. Parasite cultures were cut 1:10 on day 4. Error bars represent the SEM of duplicate experiments, each conducted in quadruplicate.

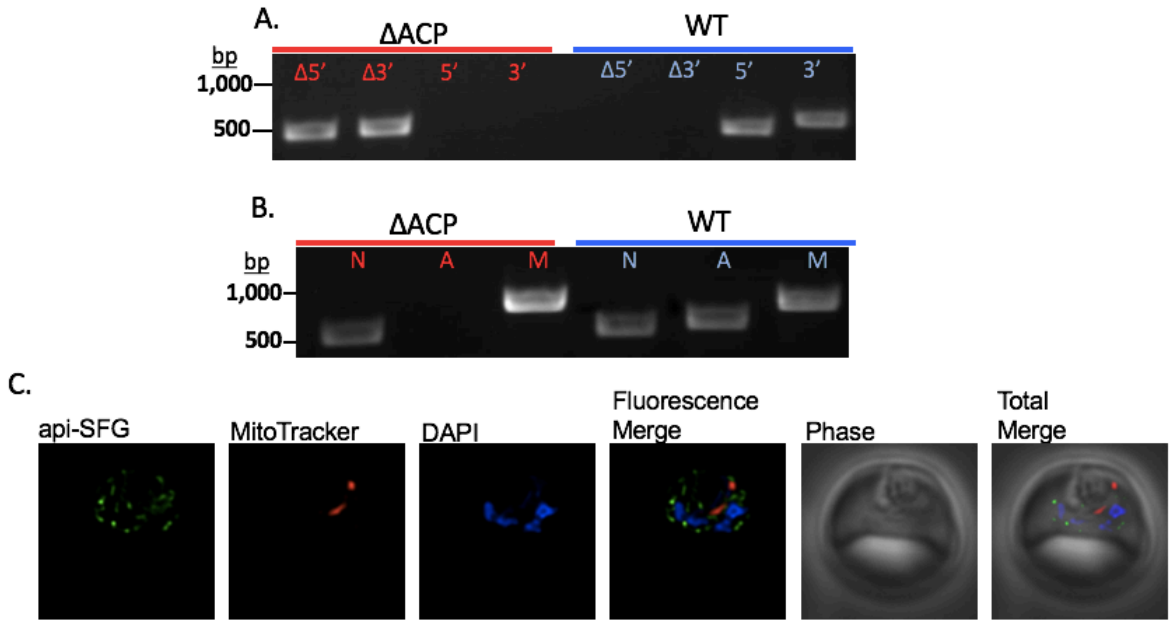

Figure 5-14 Characterization of the PfMev ΔACP parasite line

A.) Genotyping PCR confirming the deletion of ACP, with amplification demonstrating integration at the Δ5' and Δ3' loci, and lack of wild type parasites due to failure to amplify at the wild type 5' and 3' loci, as compared to the parental control.

B.) PCR detection of the lactate dehydrogenase, SufB, and Cox1 genes from the nuclear (N), apicoplast (A), and mitochondrial (M) genomes, respectively. We failed to amplify SufB from the PfMev ΔACP parasite line, indicating loss of the apicoplast organelle genome.

C.) Live fluorescence microscopy of the PfMev ΔACP parasite line. This parasite line is expressing api-SFG (green), and is also stained with MitoTracker (red), and DAPI (blue). Microscopy images are 10 microns long by 10 microns wide.

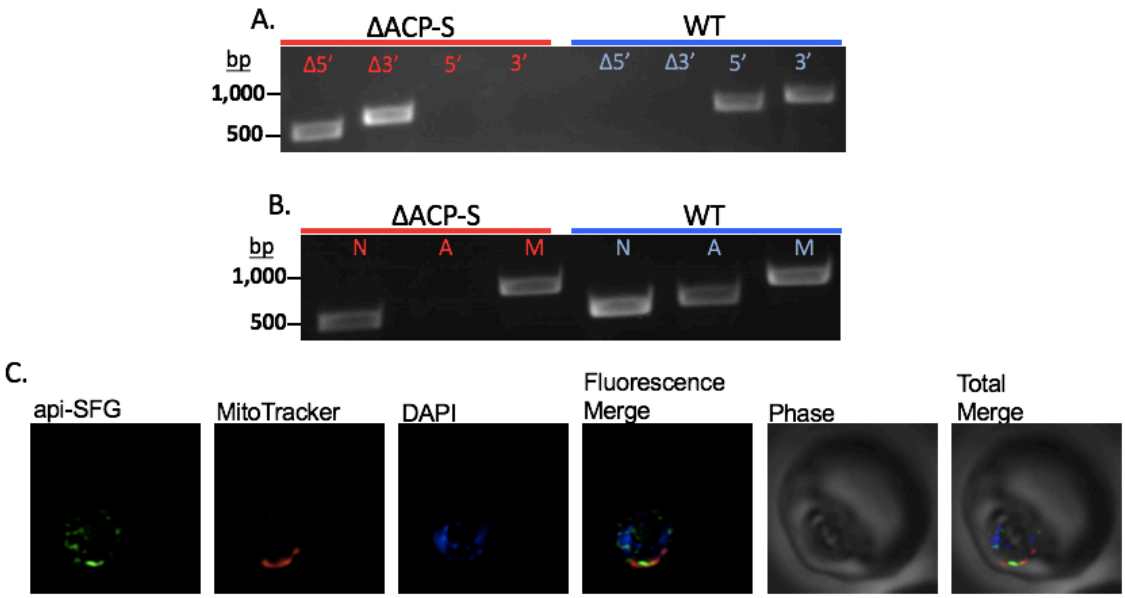

Figure 5-15 Characterization of the PfMev ΔACP-S parasite line

A.) Genotyping PCR confirming the deletion of ACP-S, with amplification demonstrating integration at the Δ5' and Δ3' loci, and lack of wild type parasites due to failure to amplify at the wild type 5' and 3' loci, as compared to the parental control.

B.) PCR detection of the lactate dehydrogenase, SufB, and Cox1 genes from the nuclear (N), apicoplast (A), and mitochondrial (M) genomes, respectively. We failed in attempting to amplify SufB from the PfMev ΔACP-S parasite line, indicating loss of the apicoplast organelle genome.

C.) Live fluorescence microscopy of the PfMev ΔACP-S parasite line. This parasite line is expressing api-SFG (green), and is also stained with MitoTracker (red), and DAPI (blue). Microscopy images are 10 microns long by 10 microns wide.

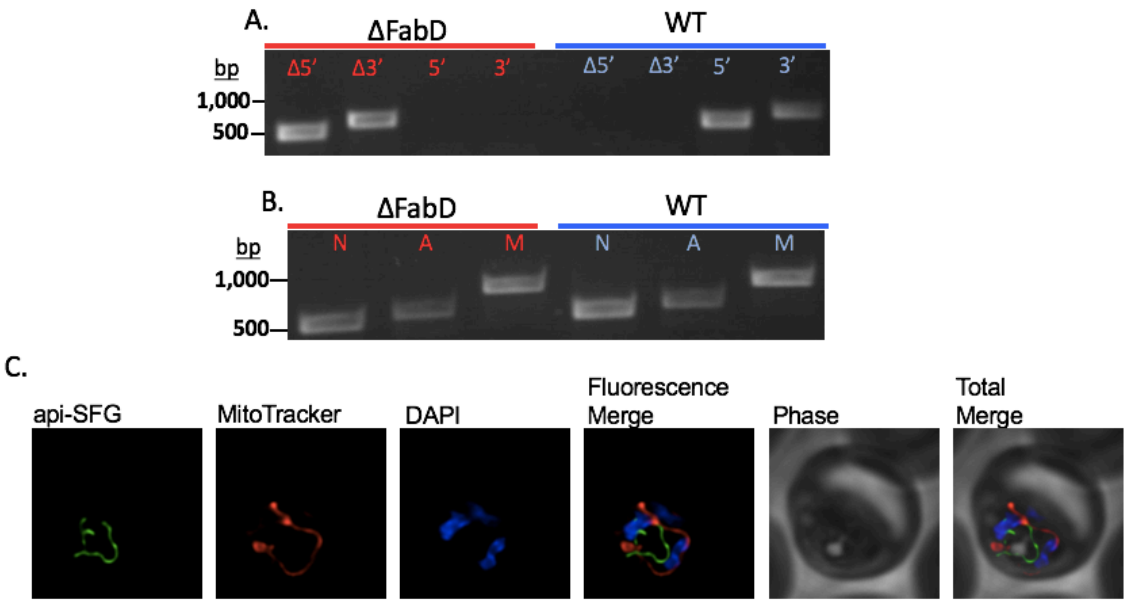

Figure 5-16 Characterization of the PfMev ΔFabD parasite line

A.) Genotyping PCR confirming the deletion of FabD, with amplification demonstrating integration at the Δ5' and Δ3' loci, and lack of wild type parasites due to failure to amplify at the wild type 5' and 3' loci, as compared to the parental control.

B.) PCR detection of the lactate dehydrogenase, SufB, and Cox1 genes from the nuclear (N), apicoplast (A), and mitochondrial (M) genomes, respectively. We were successful in amplifying SufB from the PfMev ΔFabD parasite line, indicating retention of the apicoplast organelle genome.

C.) Live fluorescence microscopy of the PfMev ΔFabD parasite line. This parasite line is expressing api-SFG (green), and is also stained with MitoTracker (red), and DAPI (blue). Microscopy images are 10 microns long by 10 microns wide.

Table 5-3 Primers for the generation of the *P. falciparum* DPCK localization plasmid

Primer Name	Primer Sequence
DPCK.loc.F	TTTAATTTTTTTTACAACCTAGGATGTTTTTAAAATTCTTTCTTGATAAATGTATT
DPCK.loc.R.	CCTCGCCCTTGCTCGTACGGAAGAAAAAGTTTTTTAAATATTTATTATATACCACA

Table 5-4 Primer used for detecting the nuclear and organellar genomes

Primer Name	Primer Sequence
LDH F	GGAGATGTAGTTTTGTTCGATATTG
LDH R	CTTGTAAAGGGATACCACCTACAG
SufB F	CATGTAGCTATAGTAGAAATAATAGTAAAAGATTATGG
SufB R	GACTCTGAAATACTTAAACCACGTTGC
Cox1 F	CTTCATCTTTAAGAATAATTGCACAAGAAAATGTAAATC
Cox1 R	GTACATATGATGTACCCATACTAAGCTTCC

Table 5-5 Primers for the generation of the *E. coli* complementation plasmids

Primer Name	Primer Sequence
hDHFR F	CCTAATAGAAATATATCAGGATCCATGCATGGTTCGCTAAACT
hDHFR R	AATCTATTATTAAATAAGCTTAATCATTCTTCTCATATACTTCA
*Ed*DPCK F	CCTAATAGAAATATATCACCTAGGATGAGGTATATAGTTGCCTTAACGGGAGG
*Ed*DPCK R	CCTCCTCGCCCTTGCTCGTACGCGGTTTTTCCTGTGAGACAAACTGC
Cam*Ed*mCry F	TTTTAATTTTTTTTACAACCTAGGATGAGGTATATAGTTGCCT
Cam*Ed*mCry R	TATATTATATAACTCGACCTTAAGCTCGAGTTACTTGTACAGCTCGTCC
pLN.Api55 F	GAAATATATCACCTAGGATGAAGATCTTATTACTTTGTATAAT
pLN.Api55 R	AACTATATACCTCATCCTAGGATGTGGGTTTTTATTTTTTATC
CamAp*Ed*DpmC F	TTAATTTTTTTTACAACCTAGGATGAAGATCTTATTACTTTGT
CamAp*Ed*DpmC R	TATATTATATAACTCGACCTTAAGCTCGAGTTACTTGTACAGCTCGTCC
pRsBSD F	ACCTAATAGAAATATATCAGGATCCATGGCAAAACCTTTG
pRsBSD R	TCTATTATTAAATAAGCTTATTCCCAAACATAACCAGATG

Table 5-6 Primer sequences used for amplifying homology arms

Primer Name	Primer Sequence
ACP HA1 F	GCCACGAGCGGCCTGAAGTATATATCCACGTCCATAACAG
ACP HA1 R	AAGCGCAGCGGCCCCATCTTTTTGTGTATTTTTAAAAGCT
ACP HA2 F	CGACAGACGCCGGGGTACAAAAAAATAAAATGATACACAA
ACP HA2 R	GGCCACCAGCCGGGGGATACATTTTAACAAAGAAGAAATA
ACP-S HA1 F	GCCACGAGCGGCCCCAGGAGTTCACACACATAATAGATTG
ACP-S HA1 R	AAGCGCAGCGGCCATTCGGCATTTGTTTTTGTATTCAATG
ACP-S HA2 F	CGACAGACGCCGGGAGGGGTCAATAAATTGTTTTCCAATA
ACP-S HA2 R	GGCCACCAGCCGGACCCTCTACCAATAGATTTGACGATAG
FabD HA1 F	GCCACGAGCGGCCACACTCACACTCACACTCACATTATCC
FabD HA1 R	AAGCGCAGCGGCCACGACCCTATCTTATTTGTATTCTCCT
FabD HA2 F	CGACAGACGCCGGGTGGAAAACCAGAATCTATGGATTATC
FabD HA2R	GGCCACCAGCCGGGGTGGTATCATATATATGGAATTGTCC

Table 5-7 Guide RNA oligo sequences

Oligo Name	Oligo Sequence
ACP gRNA F	TAAGTATATAATATTAATGAACTCAAATTTTACCAGTTTTAGAGCTAGAA
ACP gRNA R	TTCTAGCTCTAAAACTGGTAAAATTTGAGTTCATTAATATTATATACTTA
ACP-S gRNA F	TAAGTATATAATATTTAAAATATTGAACCCACGAGGTTTTAGAGCTAGAA
ACP-S gRNA R	TTCTAGCTCTAAAACCTCGTGGGTTCAATATTTTAAATATTATATACTTA
FabD gRNA F	TAAGTATATAATATTGATAGAAAATTTGGTTTATGGTTTTAGAGCTAGAA
FabD gRNA R	TTCTAGCTCTAAAACCATAAACCAAATTTTCTATCAATATTATATACTTA

Table 5-8 Primer sequences used for confirmation of gene deletions

Primer Name	Primer Sequence
pl8insHA1R	TACAAAATGCTTAAGCGCAGCGGCC
pl8insHA2F	CATATTTATTAAATCTAGAATTCGACAGACGCCG
ACP 5' F	CCTATGTTTGTGTACTTTTTTTTTTCCCC
ACP 3'R	CATACATAAATATATGAACATTTTTATAAAGAGGTAAC
ACP 5' WT R	GGTTGCTTCTTTTCTTTTTTAATATTTGTAAG
ACP 3' WT F	CCCATCTAGCTCTTTAAAAAGTACTTTTG
ACP-S 5'F	GTAATATTTGTGGATATATATTTCTTTACATACCTTGC
ACP-S 3'R	CCTAATTGTCTAGCTATTTTTTTTGCTTTG
ACP-S 5'WT R	GTAATATCATTTCTCTTACAAAAAGAAGATAAAATATTC
ACP-S 3' WT F	CAGAACAAGTTGTAATGTTTATGATATTAGTGTTG
FabD 5'F	GAGAAGATATATTAAAAGAGAAATTTTTTTTTTTTTTCG
FabD 3'R	CTTTAAAATATAAAATATACTTTTTTTGTCAATTTGTAAG
FabD 5' WT R	TTCCTTTTATATCTTTATTTACACTAACATTATGTCTAAG
FabD 3' WT F	ACAAAATGAATGATGATATTTTTATTGTTAGTTATATGAC

Table 5-9 Primers used for the generation of the CLD-EcDPCK-mCherry-apt line

Primer Name	Primer Sequence
CLD F	TTAATTTTTTTTACAACCTAGGATGAAGATCTTATTACTTTGTATAATTTTTCT
CLD R	GGCAACTATATACCTTCCGGAACCTTCTAACTTTAGCAATTCTACATC
EcDPCK CLD R	GATAATTTCTAGTGGGCCCTTATGCATAATCAGGTACGTCATAAGGATACTTGTACAGCTCGTCCATGCCG

REFERENCES

1. Geary GT, Divo AA, Bonanni CL, Jensen BJ. 1985. Nutritional requirements of *Plasmodium falciparum* in culture. III. Further observations on essential nutrients and antimetabolites. J Protozool 32:608–613.

2. Saliba KJ, Ferru I, Kirk K. 2005. Provitamin B5 (pantothenol) inhibits growth of the intraerythrocytic malaria parasite. Antimicrob Agents Chemother 49:632–7.

3. Spry C, Saliba JK. 2009. The human malaria parasite *Plasmodium falciparum* is not dependent on host coenzyme A biosynthesis. J Biol Chem 284:24904–24913.

4. Spry C, Kirk K, Saliba JK. 2008. Coenzyme A biosynthesis: an antimicrobial drug target. FEMS Microbiol Rev 32:56–106.

5. Spry C, van Schalkwyk DA, Strauss E, Saliba KJ. 2010. Pantothenate utilization by *Plasmodium* as a target for antimalarial chemotherapy. Infect Disord Drug Targets 10:200–16.

6. Spry C, Chai LCL, Kirk K, Saliba JK. 2005. A class of pantothenic acid analogs inhibits *Plasmodium falciparum* pantothenate kinase and represses the proliferation of malaria parasites. Antimicrob Agents Chemother 49:4649–4657.

7. Spry C, Macuamule C, Lin Z, Virga KG, Lee RE, Strauss E, Saliba KJ. 2013. Pantothenamides Are Potent, On-Target Inhibitors of *Plasmodium falciparum* Growth When Serum Pantetheinase Is Inactivated. PLoS One 8:e54974.

8. Macuamule CJ, Tjhin ET, Jana CE, Barnard L, Koekemoer L, de Villiers M, Saliba KJ, Strauss E. 2015. A Pantetheinase-Resistant Pantothenamide with Potent, On-Target, and Selective Antiplasmodial Activity. Antimicrob Agents Chemother 59:3666–3668.

9. Saliba JK, Horner AH, Kirk K. 1998. Transport and metabolism of the essential vitamin pantothenic acid in human erythrocytes infected with the malaria parasite *Plasmodium falciparum*. J Biol Chem 273:10190–10195.

10. Desai AS, Krogstad JD, McCleskey WE. 1993. A nutrient-permeable channel on the intraerythrocytic malaria parasite. Nature 362:643–646.

11. Augagneur Y, Jaubert L, Schiavoni M, Pachikara N, Garg A, Usmani-Brown S, Wesolowski D, Zeller S, Ghosal A, Cornillot E, Said HM, Kumar P, Altman S, Ben Mamoun C. 2013. Identification and Functional Analysis of the Primary Pantothenate Transporter, PfPAT, of the Human Malaria Parasite *Plasmodium falciparum*. J Biol Chem 288:20558–20567.

12. Hart RJ, Lawres L, Fritzen E, Mamoun C Ben, Aly ASI. 2015. *Plasmodium* yoelii Vitamin B5 Pantothenate Transporter Candidate is Essential for Parasite

Transmission to the Mosquito. Sci Rep 4:5665.

13. Saliba JK, Kirk K. 2001. H+-coupled pantothenate transport in the intracellular malaria parasite. J Biol Chem 276:18115–18121.

14. Ralph SA, van Dooren GG, Waller RF, Crawford MJ, Fraunholz MJ, Foth BJ, Tonkin CJ, Roos DS, McFadden GI. 2004. Tropical infectious diseases: metabolic maps and functions of the *Plasmodium falciparum* apicoplast. Nat Rev Microbiol 2:203–16.

15. Hart JR, Abraham A, Aly IAS. 2017. Genetic Characterization of Coenzyme A Biosynthesis Reveals Essential Distinctive Functions during Malaria Parasite Development in Blood and Mosquito. Front Cell Infect Microbiol 7.

16. Hart RJ, Cornillot E, Abraham A, Molina E, Nation CS, Ben Mamoun C, Aly ASI. 2016. Genetic Characterization of *Plasmodium* Putative Pantothenate Kinase Genes Reveals Their Essential Role in Malaria Parasite Transmission to the Mosquito. Sci Rep 6:33518.

17. Beld J, Lee JD, Burkart DM. 2015. Fatty acid biosynthesis revisited: structure elucidation and metabolic engineering. Mol Biosyst 11:38–59.

18. Shears JM, Botté YC, McFadden IG. 2015. Fatty acid metabolism in the *Plasmodium* apicoplast: Drugs, doubts and knockouts. Mol Biochem Parasitol 199:34–50.

19. Foth JB, Stimmler ML, Handman E, Crabb SB, Hodder NA, McFadden IG. 2005. The malaria parasite *Plasmodium falciparum* has only one pyruvate dehydrogenase complex, which is located in the apicoplast. Mol Microbiol 55:39–53.

20. van Schaijk LBC, Kumar STR, Vos WM, Richman A, van Gemert G-J, Li T, Eappen GA, Williamson CK, Morahan JB, Fishbaugher M, Kennedy M, Camargo N, Khan MS, Janse JC, Sim LK, Hoffman LS, Kappe ISH, Sauerwein WR, Fidock AD, Vaughan MA. 2014. Type II fatty acid biosynthesis is essential for *Plasmodium falciparum* sporozoite development in the midgut of Anopheles mosquitoes. Eukaryot Cell 13:550–559.

21. Yeh E, DeRisi LJ. 2011. Chemical rescue of malaria parasites lacking an apicoplast defines organelle function in blood-stage *Plasmodium falciparum*. PLoS Biol 9.

22. Gisselberg EJ, Dellibovi-Ragheb AT, Matthews AK, Bosch G, Prigge TS. 2013. The suf iron-sulfur cluster synthesis pathway is required for apicoplast maintenance in malaria parasites. PLoS Pathog 9.

23. Wilson RJ, Denny PW, Preiser PR, Rangachari K, Roberts K, Roy A, Whyte A, Strath M, Moore DJ, Moore PW, Williamson DH. 1996. Complete gene map of the plastid-like DNA of the malaria parasite *Plasmodium falciparum*. J Mol Biol 261:155–72.

24. Waller RF, Reed MB, Cowman AF, McFadden GI. 2000. Protein trafficking to the

plastid of *Plasmodium falciparum* is via the secretory pathway. EMBO J 19:1794–802.

25. Stanway RR, Witt T, Zobiak B, Aepfelbacher M, Heussler VT. 2009. GFP-targeting allows visualization of the apicoplast throughout the life cycle of live malaria parasites. Biol Cell 101:415–435.

26. Bouchut A, Geiger JA, DeRocher AE, Parsons M. 2014. Vesicles Bearing *Toxoplasma* Apicoplast Membrane Proteins Persist Following Loss of the Relict Plastid or Golgi Body Disruption. PLoS One 9:e112096.

27. Parsons M, Karnataki A, Feagin JE, DeRocher A. 2007. Protein trafficking to the apicoplast: deciphering the apicomplexan solution to secondary endosymbiosis. Eukaryot Cell 6:1081–8.

28. Chaudhari R, Dey V, Narayan A, Sharma S, Patankar S. 2017. Membrane and luminal proteins reach the apicoplast by different trafficking pathways in the malaria parasite *Plasmodium falciparum*. PeerJ 5:e3128.

29. Waller FR, Reed BM, Cowman FA, McFadden IG. 2000. Protein trafficking to the plastid of *Plasmodium falciparum* is via the secretory pathway. EMBO J 19:1794–1802.

30. Adjalley SH, Lee MCS, Fidock DA. 2010. A method for rapid genetic integration into *Plasmodium falciparum* utilizing mycobacteriophage Bxb1 integrase. Methods Mol Biol 634:87–100.

31. Nkrumah JL, Muhle AR, Moura AP, Ghosh P, Hatfull FG, Jacobs RW, Fidock AD. 2006. Efficient site-specific integration in *Plasmodium falciparum* chromosomes mediated by mycobacteriophage Bxb1 integrase. Nat Methods 3:615–621.

32. Ghorbal M, Gorman M, Macpherson CR, Martins RM, Scherf A, Lopez-Rubio J-J. 2014. Genome editing in the human malaria parasite *Plasmodium falciparum* using the CRISPR-Cas9 system. Nat Biotechnol 32:819–21.

33. Fletcher S, Avery VM. 2014. A novel approach for the discovery of chemically diverse anti-malarial compounds targeting the *Plasmodium falciparum* Coenzyme A synthesis pathway. Malar J 13:343.

34. Fletcher S, Lucantoni L, Sykes ML, Jones AJ, Holleran JP, Saliba KJ, Avery VM. 2016. Biological characterization of chemically diverse compounds targeting the *Plasmodium falciparum* coenzyme A synthesis pathway. Parasit Vectors 9:589.

35. Mishra P k., Park PK, Drueckhammer DG. 2001. Identification of yacE (coaE) as the Structural Gene for Dephosphocoenzyme A Kinase in *Escherichia coli* K-12. J Bacteriol 183:2774–2778.

36. Prigge TS, He X, Gerena L, Waters CN, Reynolds AK. 2003. The initiating steps of a type II fatty acid synthase in *Plasmodium falciparum* are catalyzed by pfACP, pfMCAT, and pfKASIII. Biochemistry 42:1160–1169.

37. Goldfless SJ, Wagner JC, Niles JC. 2014. Versatile control of *Plasmodium falciparum* gene expression with an inducible protein-RNA interaction. Nat Commun 5:5329.

38. Roberts A. 2017. Development and validation of a conditional localization domain to control trafficking of secretory proteins in *Plasmodium falciparum*.

39. Cobbold SA, Vaughan AM, Lewis IA, Painter HJ, Camargo N, Perlman DH, Fishbaugher M, Healer J, Cowman AF, Kappe SHI, Llinás M. 2013. Kinetic flux profiling elucidates two independent acetyl-CoA biosynthetic pathways in *Plasmodium falciparum*. J Biol Chem 288:36338–50.

40. Waters NC, Kopydlowski KM, Guszczynski T, Wei L, Sellers P, Ferlan JT, Lee PJ, Li Z, Woodard CL, Shallom S, Gardner MJ, Prigge ST. 2002. Functional characterization of the acyl carrier protein (PfACP) and beta-ketoacyl ACP synthase III (PfKASIII) from *Plasmodium falciparum*. Mol Biochem Parasitol 123:85–94.

41. Zhang M, Wang C, Otto TD, Oberstaller J, Liao X, Adapa SR, Udenze K, Bronner IF, Casandra D, Mayho M, Brown J, Li S, Swanson J, Rayner JC, Jiang RHY, Adams JH. 2018. Uncovering the essential genes of the human malaria parasite *Plasmodium falciparum* by saturation mutagenesis. Science 360:eaap7847.

42. Schwach F, Bushell E, Gomes AR, Anar B, Girling G, Herd C, Rayner JC, Billker O. 2015. PlasmoGEM, a database supporting a community resource for large-scale experimental genetics in malaria parasites. Nucleic Acids Res 43:D1176-82.

43. Mazumdar J, Striepen B. 2007. Make it or take it: fatty acid metabolism of apicomplexan parasites. Eukaryot Cell 6:1727–1735.

44. Vaughan MA, O'Neill TM, Tarun SA, Camargo N, Phuong MT, Aly IAS, Cowman FA, Kappe ISH. 2009. Type II fatty acid synthesis is essential only for malaria parasite late liver stage development. Cell Microbiol 11:506–520.

45. Yu M, Kumar STR, Nkrumah JL, Coppi A, Retzlaff S, Li DC, Kelly JB, Moura AP, Lakshmanan V, Freundlich SJ, Valderramos J-C, Vilcheze C, Siedner M, Tsai H-CJ, Falkard B, Sidhu SAB, Purcell AL, Gratraud P, Kremer L, Waters PA, Schiehser G, Jacobus PD, Janse JC, Ager A, Jacobs RW, Sacchettini CJ, Heussler V, Sinnis P, Fidock AD. 2008. The fatty acid biosynthesis enzyme FabI plays a key role in the development of liver-stage malarial parasites. Cell Host Microbe 4:567–578.

46. Goodman DC, Mollard V, Louie T, Holloway AG, Watson GK, McFadden IG. 2014. Apicoplast acetyl Co-A carboxylase of the human malaria parasite is not targeted by cyclohexanedione herbicides. Int J Parasitol 44:285–289.

47. Modak R, Sinha S, Surolia N. 2007. Isothermal unfolding studies on the apo and holo forms of *Plasmodium falciparum* acyl carrier protein. Role of the 4'-phosphopantetheine group in the stability of the holo form of *Plasmodium falciparum* acyl carrier protein. FEBS J 274:3313–3326.

48. Misra A, Surolia N, Surolia A. 2009. Catalysis and mechanism of malonyl transferase activity in type II fatty acid biosynthesis acyl carrier proteins. Mol Biosyst 5:651–659.

49. Misra A, Sharma KS, Surolia N, Surolia A. 2007. Self-acylation properties of type II fatty acid biosynthesis acyl carrier protein. Chem Biol 14:775–783.

50. Cai X, Herschap D, Zhu G. 2005. Functional characterization of an evolutionarily distinct phosphopantetheinyl transferase in the apicomplexan *Cryptosporidium parvum*. Eukaryot Cell 4:1211–1220.

51. Van Vranken GJ, Jeong M-Y, Wei P, Chen Y-C, Gygi PS, Winge RD, Rutter J. 2016. The mitochondrial acyl carrier protein (ACP) coordinates mitochondrial fatty acid synthesis with iron-sulfur cluster biogenesis. Elife 5.

52. Boniecki TM, Freibert AS, Mühlenhoff U, Lill R, Cygler M. 2017. Structure and functional dynamics of the mitochondrial Fe/S cluster synthesis complex. Nat Commun 8.

53. Gisselberg JE, Dellibovi-Ragheb T a., Matthews K a., Bosch G, Prigge ST. 2013. The Suf Iron-Sulfur Cluster Synthesis Pathway Is Required for Apicoplast Maintenance in Malaria Parasites. PLoS Pathog 9.

54. Haussig MJ, Matuschewski K, Kooij ATW. 2013. Experimental Genetics of *Plasmodium* berghei NFU in the Apicoplast Iron-Sulfur Cluster Biogenesis Pathway. PLoS One 8.

55. Sato S, Rangachari K, Wilson MRJ. 2003. Targeting GFP to the malarial mitochondrion. Mol Biochem Parasitol 130:155–158.

56. Mazumdar J, H Wilson E, Masek K, A Hunter C, Striepen B. 2006. Apicoplast fatty acid synthesis is essential for organelle biogenesis and parasite survival in *Toxoplasma gondii*. Proc Natl Acad Sci U S A 103:13192–13197.

57. Spalding DM, Allary M, Gallagher RJ, Prigge TS. 2010. Validation of a modified method for Bxb1 mycobacteriophage integrase-mediated recombination in *Plasmodium falciparum* by localization of the H-protein of the glycine cleavage complex to the mitochondrion. Mol Biochem Parasitol 172:156–160.

Chapter 6

Conclusions and Future Directions

Future Applications of the PfMev Line

The creation and utilization of the PfMev apicoplast bypass line was critical to much of the work outlined in this thesis, offering an exceedingly user-friendly platform in which to investigate essential biochemical processes within the apicoplast. This line represents a significant improvement to the previously used IPP chemical bypass system due to the reduced cost, the greater chemical stability of the molecule used for supplementation, in addition to the ability for apicoplast-negative parasites to easily survive cryopreservation and grow at wild-type levels under mevalonate supplementation. The ability to cryopreserve is especially critical, as it allows for the future analysis of lines that are generated either within the lab of origin or throughout the scientific community, in addition to making larger-scale and longer-term experiments more tenable. Furthermore, the method in which the PfMev line was generated did not rely on any of the currently used drug resistance cassettes, allowing for the application of previously established plasmid systems and the ability to conduct experiments that rely on multiple selection cassettes. We hope that these improvements will result in the wide-spread adoption of this line, and help in furthering research into the apicoplast organelle.

We were able to demonstrate that the PfMev line can be used for the facile deletion of essential apicoplast-specific genes, in addition to offering a read-out of the resulting apicoplast phenotype, due to the fluorescent labelling of the organelle. This allows for the determination of which apicoplast-specific genes are essential for parasite survival, in addition to being able to determine which are required for the maintenance of the organelle. As mentioned previously, there have been no published genetic deletions of any essential apicoplast-specific genes since the development of the chemical bypass system, likely due to the difficulties associated with working with that system. However, using the PfMev line we

were successful in deleting multiple apicoplast-specific genes, and were able to determine their requirement for parasite survival and the maintenance of the organelle. While we were able to do this for over 20 genes, this represents a just a small fraction of the over ~400 proteins that are predicted to be trafficked to the organelle that could still be explored [36]–[39].

There are likely to be tens or even hundreds of apicoplast-specific genes that are essential for apicoplast maintenance or replication that are yet to be discovered and characterized. Many of these are likely to be playing essential roles within the apicoplast, critical to processes such as transcription, translation, organelle genome replication, protein trafficking to the organelle, protein import and processing, the import and export of biomolecules, the generation of essential cofactors, and the replication and division of the organelle, among others. However, of the ~400 proteins predicted to be trafficked to the organelle [36]–[39], approximately half are annotated as having no known function, highlighting how much more work there is to be done in investigating this unusual organelle (6). To this end, the PfMev line could help elucidate which apicoplast-specific genes are required for parasite survival and organelle maintenance using a higher-throughput method than targeted gene deletions, such as a forward genetic screen. Forward genetic screens have already been adapted for use in *P. falciparum* including PiggyBac insertional mutagenesis (7) and chemical mutagenesis screens (8).

The PfMev line could also be used for drug target identification and validation, by screening compound libraries against *P. falciparum* parasites and determining which display differential drug activity in the presence or absence of mevalonate supplementation. This would help in better elucidating the mechanism of action of the drug, by determining if the drug is apicoplast-specific. The difference in IC_{50} values determined in the presence or

absence of mevalonate would provide a measure of the apicoplast-specificity of any particular drug. Efforts such as these have been attempted already using the IPP chemical bypass system, in a screen against a limited number of compounds (9). However, the reduced cost of mevalonate and greater ease of usage with the PfMev line would make screening much larger compound libraries more feasible.

Furthermore, the parasite line that we used to generate the PfMev line is not competent in generating infectious gametocytes. Future efforts could introduce this bypass system into a line capable of forming gametocytes. This could allow for the investigation of apicoplast-specific genes in other stages of the parasite lifecycle, including gametocytogenesis, the various mosquito stages, including gamete activation, and formation of the zygote, ookinete, oocyst, or sporozoite, in addition to the liver stage of the parasite.

Iron-sulfur Cluster Biosynthesis, Sulfur Utilization, and tRNA Modification within the Apicoplast

The impetus for this work was originally driven by the finding that the expression of a SufC (K140A) dominant negative mutant resulted in the disruption of the apicoplast under IPP supplementation (10). We wanted to follow up on this by attempting to determine the ultimate mechanism by which the loss of iron-sulfur clusters results in this phenotype by making targeted deletions of the iron-sulfur cluster dependent proteins. However, we determined that none of the iron-sulfur cluster dependent proteins, and that none of the proteins in the SUF iron-sulfur cluster biosynthetic pathway, with the exception of the cysteine desulfurase SufS, are required for the maintenance of the apicoplast. We then attempted to determine why SufS is required for this process, with our results suggesting that

while iron-sulfur clusters are not essential for apicoplast maintenance, the generation of sulfur by SufS, and its utilization by the tRNA modifying enzyme MnmA likely is.

These results obviously contradicted what was previously found, which suggested that iron-sulfur cluster biosynthesis and SufC were required for the maintenance and replication of the apicoplast. While the results of the previous work are not in question, the mechanism by which expression of the SufC (K140A) dominant negative mutant resulted in loss of the organelle is unclear. It was speculated in chapter 3 of this thesis that this may be due to the detrimental effects associated with high concentrations of IPP or through other potential mechanisms. However, in comparison to a dominant negative mutant, the genetic deletion of SufC clearly illustrates that its biochemical activity is not required for the maintenance of the organelle. Furthermore, we were able to demonstrate that iron-sulfur cluster generation in general is not essential for organelle maintenance through the deletion of additional proteins within the SUF pathway. This clarification is likely important to the field, as this paper has been cited over 50 times since it was originally published.

In this work, we targeted all of the predicted iron-sulfur cluster dependent proteins, in addition to all of the nuclear-encoded components of the SUF pathway for deletion in our PfMev line under mevalonate supplementation. We were able to conclusively demonstrate which of these proteins are essential for blood-stage parasite survival, in addition to which are required for organelle maintenance and replication. Through these deletions we were also able to generate important insights into this pathway, more conclusively showing that the SufA and NifU iron-sulfur cluster transfer proteins are functionally redundant as previously hypothesized (11, 12). We additionally were also able to demonstrate that SufE is likely not necessarily required for the cysteine desulfurase activity of SufS, or the transfer of sulfur to downstream enzymes that may rely on it outside of those involved in the SUF pathway.

Our results suggest that the requirement of SufS for organelle maintenance is not driven by its requirement for iron-sulfur cluster biosynthesis, but instead its ability to generate sulfur for another purpose. In general, sulfur generated by cysteine desulfurase enzymes can be utilized by a variety of biochemical pathways, such as the biosynthesis of thiamine, biotin, lipoic acid, molybdopterin, in addition to the sulfur modifications of tRNAs (13). Our bioinformatic analysis and genetic studies indicate that the essentiality of the parasite SufS is most likely driven by its role in generating sulfur for usage by the tRNA modifying enzyme MnmA.

As mentioned previously in this work, MnmA is an extremely conserved gene, present even in the most reduced bacterial genomes (14–17). tRNA modifications in general are ubiquitous throughout life, and play a critical role in protein translation (18–20). The apicoplast of *P. falciparum* is interesting in this regard because it produces all of the required tRNAs needed for translation within the organelle, and is not predicted to import any additional tRNAs (21). Thus, all tRNA modifications are likely to occur within the organelle, making the apicoplast an interesting system in which to study the minimal set of tRNA modifications required for accurate translation *in vivo*. Within the apicoplast the tRNA modifying enzymes MiaA and MiaB are predicted to be present, as described previously (1). MnmA is also predicted to be present within the apicoplast (1). MnmA in many bacterial organisms is part of a larger tRNA modification pathway involving the additional enzymes MnmC, MnmE, and MnmG (22, 23). In addition to MnmA, MnmE and MnmG are also predicted to be present within the *P. falciparum* genome. All three enzymes are predicted to be trafficked to the apicoplast (5), and are also predicted to be essential as determined by a forward genetic screen conducted by Dr. John Adams (7). MnmA and MnmG are also predicted to be essential in *P berghei* as determined by a separate forward genetic screen (24).

Thus, further investigation into these enzymes and the tRNA modifications present within the apicoplast represent an important area of further research.

It should be noted that many of these conclusions are largely speculative due to the fact that the putative *P. falciparum* MnmA (PF3D7_1019800) has not been functionally validated, and its activity as tRNA-specific 2-thiouridylase has not been proven biochemically. In fact, the putative *P. falciparum* MnmA is currently annotated as a tRNA methyltransferase in PlasmoDB. In order to validate the activity of this enzyme, future experiments could express the putative *P. falciparum* MnmA in MnmA deficient *E. coli* and attempt to detect the nucleobases that should be modified by this enzyme using LC-MS (25). Additionally, this protein could be used to complement MnmA deficient *E. coli,* which should rescue their slow-growth phenotype if it is able to compensate for the activity of the deleted endogenous MnmA (25). The *P. falciparum* MnmA also merits further research, due to the potential complexity of the protein. The *E. coli* MnmA is 368 amino acids in length, while the *P. falciparum* MnmA is 1,084 amino acids in length. While there is a domain within putative the *P. falciparum* MnmA that shows homology to other MnmA proteins, this represents just a portion of the overall protein, which may have additional functionality unrelated to its proposed role as a tRNA modifying enzyme that deserves to be investigated.

Lastly, the mechanism by which the absence of MnmA ultimately results in organelle disruption has not been elucidated. In other systems MnmA has been shown to be important for tRNA-ribosome binding (26), wobble codon recognition (27, 28), reading frame maintenance (29), and the reduction of frameshifts and missense errors (30–32). The essential role that it may be playing within the apicoplast, and the mechanism by which its loss results in disruption of the apicoplast are worthwhile topics for future research.

Overall, we have been able to demonstrate that the majority of proteins within the SUF pathway in addition to MnmA are essential for blood-stage parasite survival. These proteins are also closely related to bacterial orthologs (33, 34), and deserve to be studied further to investigate their suitability as drug targets.

Carbon Metabolism, Energy, Reducing Power, and NTP/dNTP Generation within the Apicoplast

To fuel anabolic pathways within the apicoplast, carbon backbones, energy, and reducing power is required. However, there are many gaps in our understanding of how the apicoplast meets these needs.

Several enzymes in the apicoplast require reduced nicotinamide adenine dinucleotides (NADH or NADPH) for enzymatic activity. Our results show that the ferredoxin/ferredoxin reductase system is essential, and it is known from biochemical assays that *P. falciparum* ferredoxin reductase requires NADPH for activity (35). The ferredoxin/ferredoxin reductase system is central to apicoplast metabolism and is predicted to deliver reducing equivalents to LipA, NifU, MiaB, IspG and IspH (1, 36–38). However, the source of reducing power within the apicoplast is unclear. One potential source is the triose phosphate isomerase (TPI) / glyceraldehyde 3-phosphate dehydrogenase (GAPDH) cycle, in which imported DHAP is converted by TPI to form GA3P, which in turn is converted into 1,3-diphosphoglycerate (1,3-DPGA) by GAPDH, reducing NADP+ to NADPH in the process (39, 40). The 1,3-DPGA can then presumably be exchanged for DHAP by the triose phosphate transporters, creating an electron shuttle (39). However, we have been able to demonstrate that TPI is dispensable in blood-stage parasites. In the absence of TPI, it is possible that GAPDH may be able to use GA3P imported directly into

the organelle, but GAPDH has been shown to be localized to the cytosol and is not predicted to be localized to the apicoplast (41). This cycle would provide the only predicted source of NADPH within the apicoplast, but it does not appear to be present or active within the apicoplast (1). Thus, it is predicted that the apicoplast may rely wholly on NADH for reducing power (1). In the apicoplast the only known source of NADH, and thus potentially all reducing power in the organelle is generated by the decarboxylation of pyruvate into acetyl-CoA by the pyruvate dehydrogenase (PDH) complex (42). However, we were successful in deleting the PDH E2 subunit, and previous studies have been successful in deleting the PDH e1α subunit (43). Thus, the source of reducing power within the apicoplast remains unclear, and is deserving of further inquiry. It may be interesting to create a dual deletion of the PDH E2 subunit along with TPI to eliminate all predicted sources of reducing power within the apicoplast in the PfMev line under mevalonate supplementation to determine if together these genes are essential for parasite survival and apicoplast maintenance.

Another outstanding question is the source of energy in the form of ATP in the apicoplast, in addition to the source of all NTPs and dNTPs within the organelle. PyrKII is the only predicted source of ATP within the apicoplast, and no NTP transporters that are predicted to localize to the apicoplast have been identified (1). PyrKII is predicted to be involved in the conversion of PEP and ADP into ATP and pyruvate, with that pyruvate being fed into the FasII and MEP isoprenoid precursor pathways (1, 44). We were successful in deleting PyrKII in our PfMev line under mevalonate supplementation and were able to show that it is essential for the maintenance and replication of the apicoplast. Following up on this, we made deletions in the pathways reliant on pyruvate, but these deletions did not replicate the apicoplast disruption phenotype. These results suggested that the generation or

utilization of pyruvate is not required for organelle maintenance, but that the generation of ATP likely is. Since there is no other known source of NTPs within the organelle, we hypothesized that PyrKII may be capable of generating all NTPs/dNTPs within the apicoplast. This would not be unprecedented as pyruvate kinase enzymes have been previously demonstrated to be active against multiple different NDPs often with very low substrate specificity (45–48). Additionally, in other systems pyruvate kinase enzymes are believed to play an import role in the generation of nucleoside triphosphates, and may function as a competent substitute for nucleoside diphosphate kinase (46). Thus, we tested the enzyme activity of the *P. falciparum* PyrKII and showed that it did not have any strong substrate preferences, indicating that it may be capable of generating all NTPs/dNTPs within the apicoplast. Additionally, were also able to mislocalize PyrKII away from the apicoplast and measure mRNA levels within the organelle as a proxy for NTP levels, and observed a sharp drop in transcript levels, helping to bolster this hypothesis.

While the above results suggest that PyrKII is essential within the apicoplast due to its function in generating NTPs, and may be potentially be responsible for the generation of all NTPs/dNTPs within the cell, the results are not entirely conclusive. We have not tracked the incorporation of NTP products generated by PyrKII into parasite mRNA. Additional experiments could be conducted in order to follow up and confirm the ultimate mechanism by which deletion of PyrKII results in loss of the apicoplast organelle. For example, one could attempt to complement PyrKII with a different pyruvate kinase enzyme that shows a high substrate specificity for a single NDP, helping to demonstrate that the low substrate specificity of the endogenous PyrKII is an essential feature of the enzyme. Additionally, there is the chance that PyrKII is essential for apicoplast maintenance due to some function other than its enzymatic activity. In order to verify this, one could attempt to complement

the parasite with a catalytically dead PyrKII to determine if the apicoplast loss phenotype is replicated.

Based on our results, PyrKII appears to be essential for parasite survival in addition to apicoplast maintenance and replication. Additionally, pyruvate kinase II enzymes are evolutionary distinct, and appear to occur only within Apicomplexans, and thus may represent attractive and viable drug targets (49). To this end, enzymatic assays have already been developed to screen small molecule inhibitors against pyruvate kinase enzymes, with over 100,000 small molecules screened in a single publication (50). Research in other systems have already identified drugs that are active against other pyruvate kinase enzymes that work to clear pathogenic infections (51, 52). These same assays could be applied to the *P. falciparum* PyrKII as well. Additionally, to further drug discovery efforts, the crystal structure of PyrKII could be useful, which is an endeavor that our lab has been pursuing.

The Role of the Apicoplast in CoA Generation and Utilization

CoA was expected to be essential for parasite survival since it was discovered that parasites are reliant on exogenous pantothenate decades ago (53, 54). This hypothesis was supported by studies demonstrating that pantothenate analogs inhibit this pathway and result in parasite death (55–57). Additionally, studies demonstrate that certain enzymes within this pathway are refractory to deletion (58–60). We were able to add to this body of knowledge by more fully demonstrating that the last step of this pathway, mediated by the enzyme dephospho-CoA kinase (DPCK), is essential for parasite survival. We showed that DPCK could only be deleted when the parasites were functionally complemented with the *E. coli* DPCK, and that the subsequent knockdown of DPCK activity resulted in parasites failing to replicate. We were also able to confirm the proposed apicoplast localization of DPCK.

Other than its essentiality, DPCK has remained an interesting enzyme due to its proposed localization to the apicoplast organelle (1). Previous work demonstrated that the apicoplast is dispensable in blood-stage parasites if IPP is supplemented in sufficient quantities (61). The resulting interpretation has been that the essentiality all proteins and pathways within the apicoplast can be bypassed in blood-stage parasites when IPP is provided. However, this is puzzling due to the requirement of CoA for parasite survival, which cannot be bypassed by IPP. The disrupted apicoplast phenotype results in loss of the apicoplast genome and the presence of vesicles within the cell that presumably contain proteins destined for the once present apicoplast (10, 61, 62). Thus, we hypothesized that DPCK remains active in vesicles, and were able to provide evidence for this by demonstrating co-localization of DPCK and apicoplast markers in the vesicles of parasites containing a disrupted apicoplast.

While our results suggest that DPCK is functionally active in the vesicles of parasites containing a disrupted organelle, further research could be done in this area. It is possible that other apicoplast-specific proteins are still present and active in these vesicles and playing essential roles in parasite survival. This work may help to dispel previous assumptions that parasites containing a disrupted apicoplast are 'apicoplast-negative' and that all apicoplast-specific proteins are functionally absent. Further research characterizing these vesicles would also be informative, such as the determination if transporters are present and active on the surface of these vesicles, potentially allowing for the import of substrates and the export of products.

Interestingly, we were also able to demonstrate that CoA is likely required within the apicoplast in blood-stage parasites, due to its predicted use by ACP-S to modify ACP with a 4'-phophopantethine cofactor. This was demonstrated by the deletion of ACP and ACP-S in

PfMev parasites under mevalonate supplementation, which resulted in disruption of the organelle. This was a surprising finding since the only proposed role of ACP and ACP-S is their function within the FASII pathway, which is not essential for blood-stage parasite survival (63). Thus, it is likely that ACP and ACP-S have secondary functions that are essential and required for apicoplast maintenance. Thus, further investigation into the activity of these proteins is merited. Some secondary functionality has already been described, with ACP demonstrating the ability to function as a malonyl-transferase (64) in addition to showing the ability to self-acylate (65), and ACP-S appears to contain a metal-dependent hydrolase domain (66). However, it is yet to be determined if these specific potential secondary functional activities are required for organelle maintenance. In other systems ACP, and specifically the 4'-phosphopantetheine prosthetic group, was shown to play an important role in the generation of sulfur by the cysteine desulfurase enzyme, in addition to the formation of iron-sulfur clusters (67). While we were able to demonstrate that the cysteine desulfurase activity of SufS is essential for apicoplast maintenance, we don't know whether ACP and ACP-S are required for this activity in *P. falciparum*.

Final Remarks

Through this work we have been able to determine the essentiality and role of numerous apicoplast-specific proteins, with these findings summarized in **Figure 6-1** and **Table 6-1**. We hope that the research outlined in this thesis will help contribute to the overall understanding of apicoplast biology in *P. falciparum* parasites, and that these findings will be translated into helping further drug discovery efforts and reduce the burden of infections and deaths caused by *Plasmodium* parasites. Additionally, we hope that the discoveries relating to basic apicoplast biology within *P. falciparum* parasites, as outlined in

this thesis can be translated to other Apicomplexan species and reduce the disease burden associated with those parasitic infections as well, such as *T. gondii* or *Babesia* spp.

FIGURES

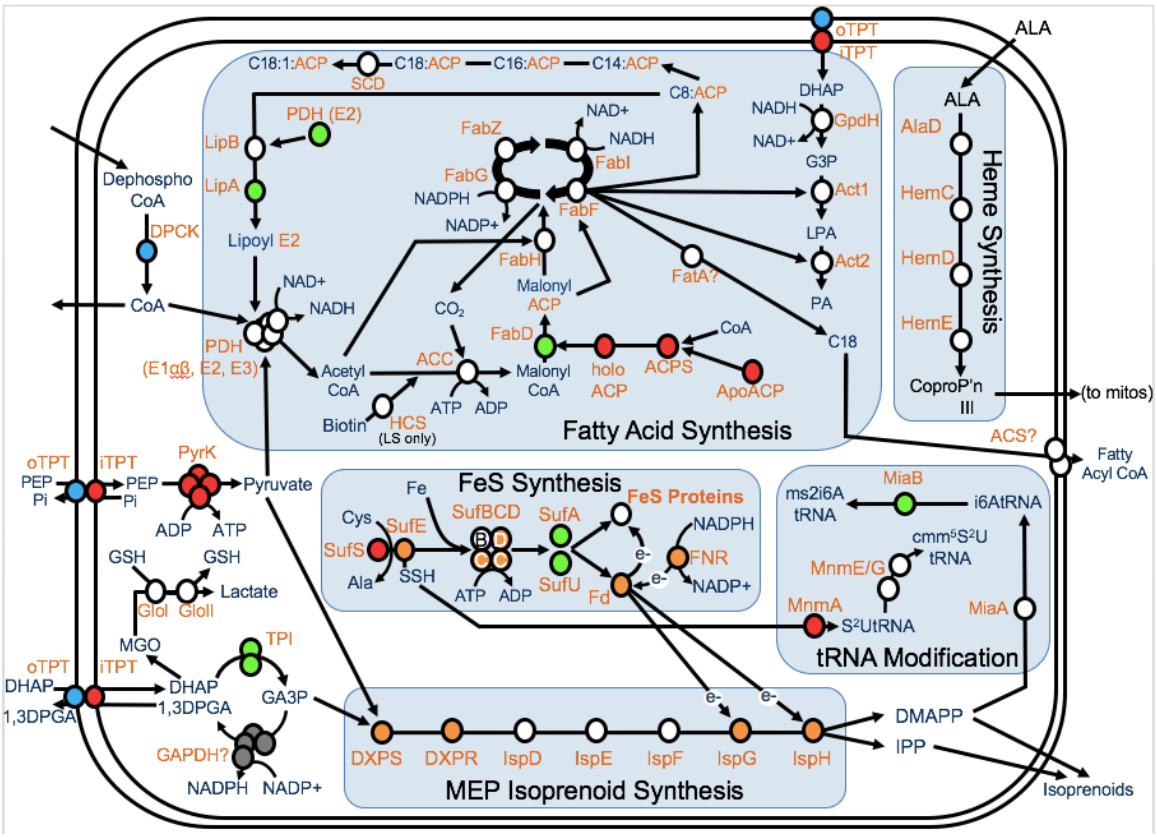

Figure 6-1 Apicoplast metabolic map showing which genes are essential for dispensable, essential, or required for apicoplast maintenance in blood-stage parasites

The resulting phenotypes from the genetic deletions attempted in this work are shown above and color-coded. Genes not required for blood-stage parasite survival are shown in green. Genes that are essential for blood-stage parasite survival, but are not required for organelle maintenance are shown in orange. Genes that are essential for blood-stage survival and are required for apicoplast maintenance are shown in red. Genes that could not be deleted are labeled in blue.

Table 6-2 Resulting apicoplast-specific gene deletion phenotypes

Gene ID	Gene Name	Phenotype
PF3D7_1467300	DXPR	Essential
PF3D7_1344600	LipA	Nonessential
PF3D7_0622200	MiaB	Nonessential
PF3D7_1022800	IspG	Essential
PF3D7_0104400	IspH	Essential
PF3D7_1318100	Ferredoxin (Fd)	Essential
PF3D7_0623200	Ferredoxin reductase (FNR)	Essential
PF3D7_0522700	SufA	Nonessential
PF3D7_0921400	NifU	Nonessential
See above	SufA + NifU	Essential
PF3D7_1103400	SufD	Essential
PF3D7_1413500	SufC	Essential
PF3D7_0206100	SufE	Essential
PF3D7_0716600	SufS	Essential and Maintenance
PF3D7_1019800	MnmA	Essential and Maintenance
PF3D7_1037100	PyrKII	Essential and Maintenance
PF3D7_0530200	iTPT	Essential and Maintenance
PF3D7_0508300	oTPT	Unable to knockout
PF3D7_1020800	PDH E2	Nonessential
PF3D7_1337200	DXS	Essential
PF3D7_0318800	TPI	Nonessential
PF3D7_0208500	ACP	Essential and Maintenance
PF3D7_0420200	ACP-S	Essential and Maintenance
PF3D7_1312000	FabD	Nonessential
PF3D7_1443700	DPCK	Unable to knockout

REFERENCES

1. Ralph SA, van Dooren GG, Waller RF, Crawford MJ, Fraunholz MJ, Foth BJ, Tonkin CJ, Roos DS, McFadden GI. 2004. Tropical infectious diseases: metabolic maps and functions of the *Plasmodium falciparum* apicoplast. Nat Rev Microbiol 2:203–16.

2. Foth JB, Ralph AS, Tonkin JC, Struck SN, Fraunholz M, Roos SD, Cowman FA, McFadden IG. 2003. Dissecting apicoplast targeting in the malaria parasite *Plasmodium falciparum*. Science 299:705–708.

3. Zuegge J, Ralph S, Schmuker M, McFadden GI, Schneider G. 2001. Deciphering apicoplast targeting signals – feature extraction from nuclear-encoded precursors of *Plasmodium falciparum* apicoplast proteins. Gene 280:19–26.

4. Cilingir G, Lau AOT, Broschat SL. 2013. ApicoAMP: The first computational model for identifying apicoplast-targeted transmembrane proteins in Apicomplexa. J Microbiol Methods 95:313–319.

5. Cilingir G, Broschat SL, Lau AOT. 2012. ApicoAP: The First Computational Model for Identifying Apicoplast-Targeted Proteins in Multiple Species of Apicomplexa. PLoS One 7:e36598.

6. Aurrecoechea C, Brestelli J, Brunk BP, Dommer J, Fischer S, Gajria B, Gao X, Gingle A, Grant G, Harb OS, Heiges M, Innamorato F, Iodice J, Kissinger JC, Kraemer E, Li W, Miller JA, Nayak V, Pennington C, Pinney DF, Roos DS, Ross C, Stoeckert CJ, Treatman C, Wang H, Wang H. 2009. PlasmoDB: a functional genomic database for malaria parasites. Nucleic Acids Res 37:D539-43.

7. Zhang M, Wang C, Otto TD, Oberstaller J, Liao X, Adapa SR, Udenze K, Bronner IF, Casandra D, Mayho M, Brown J, Li S, Swanson J, Rayner JC, Jiang RHY, Adams JH. 2018. Uncovering the essential genes of the human malaria parasite *Plasmodium falciparum* by saturation mutagenesis. Science 360:eaap7847.

8. Tang Y, Meister TR, Walczak M, Pulkoski-Gross M, Hari SB, Sauer RT, Amberg-Johnson K, Yeh E. 2018. A mutagenesis screen for essential plastid biogenesis genes in human malaria parasites. bioRxiv 401570.

9. Wu W, Herrera Z, Ebert D, Baska K, Cho HS, DeRisi LJ, Yeh E. 2015. A chemical rescue screen identifies a *Plasmodium falciparum* apicoplast inhibitor targeting MEP isoprenoid precursor biosynthesis. Antimicrob Agents Chemother 59:356–364.

10. Gisselberg EJ, Dellibovi-Ragheb AT, Matthews AK, Bosch G, Prigge TS. 2013. The suf iron-sulfur cluster synthesis pathway is required for apicoplast maintenance in malaria parasites. PLoS Pathog 9.

11. Haussig MJ, Matuschewski K, Kooij ATW. 2014. Identification of vital and dispensable sulfur utilization factors in the *Plasmodium* apicoplast. PLoS One 9.

12. Haussig MJ, Matuschewski K, Kooij ATW. 2013. Experimental Genetics of *Plasmodium berghei* NFU in the Apicoplast Iron-Sulfur Cluster Biogenesis Pathway. PLoS One 8.

13. H. M, N. E. 2002. Bacterial cysteine desulfurases: their function and mechanisms. Appl Microbiol Biotechnol 60:12–23.

14. Grosjean H, Breton M, Sirand-Pugnet P, Tardy F, Thiaucourt F, Citti C, Barré A, Yoshizawa S, Fourmy D, de Crécy-Lagard V, Blanchard A. 2014. Predicting the Minimal Translation Apparatus: Lessons from the Reductive Evolution of Mollicutes. PLoS Genet 10:e1004363.

15. Bjork GR, Ericson JU, Gustafsson CED, Hagervall TG, Jonsson YH, Wikstrom PM. 1987. Transfer RNA Modification. Annu Rev Biochem 56:263–285.

16. McCutcheon JP, Moran NA. 2012. Extreme genome reduction in symbiotic bacteria. Nat Rev Microbiol 10:13–26.

17. Gil R, Peretó J. 2015. Small genomes and the difficulty to define minimal translation and metabolic machineries. Front Ecol Evol 3:123.

18. Diwan GD, Agashe D. 2018. Wobbling Forth and Drifting Back: The Evolutionary History and Impact of Bacterial tRNA Modifications. Mol Biol Evol 35:2046–2059.

19. Tuorto F, Lyko F. 2016. Genome recoding by tRNA modifications. Open Biol 6.

20. Bednářová A, Hanna M, Durham I, VanCleave T, England A, Chaudhuri A, Krishnan N. 2017. Lost in Translation: Defects in Transfer RNA Modifications and Neurological Disorders. Front Mol Neurosci 10:135.

21. Wilson RJ, Denny PW, Preiser PR, Rangachari K, Roberts K, Roy A, Whyte A, Strath M, Moore DJ, Moore PW, Williamson DH. 1996. Complete gene map of the plastid-like DNA of the malaria parasite *Plasmodium falciparum*. J Mol Biol 261:155–72.

22. Moukadiri I, Garzón M-J, Björk GR, Armengod M-E. 2014. The output of the tRNA modification pathways controlled by the *Escherichia coli* MnmEG and MnmC enzymes depends on the growth conditions and the tRNA species. Nucleic Acids Res 42:2602–2623.

23. Armengod ME, Meseguer S, Villarroya M, Prado S, Moukadiri I, Ruiz-Partida R, Garzón MJ, Navarro-González C, Martínez-Zamora A. 2014. Modification of the wobble uridine in bacterial and mitochondrial tRNAs reading NNA/NNG triplets of 2-codon boxes. RNA Biol 11:1495–1507.

24. Schwach F, Bushell E, Gomes AR, Anar B, Girling G, Herd C, Rayner JC, Billker O. 2015. PlasmoGEM, a database supporting a community resource for large-scale experimental genetics in malaria parasites. Nucleic Acids Res 43:D1176-82.

25. Black KA, Dos Santos PC. 2015. Abbreviated Pathway for Biosynthesis of 2-

Thiouridine in *Bacillus subtilis*. J Bacteriol 197:1952–62.

26. ASHRAF SS, SOCHACKA E, CAIN R, GUENTHER R, MALKIEWICZ A, AGRIS PF. 1999. Single atom modification (O → S) of tRNA confers ribosome binding. RNA 5:S1355838299981529.

27. Yarian C, Marszalek M, Sochacka E, Malkiewicz A, Guenther R, Miskiewicz A, Agris PF. 2000. Modified nucleoside dependent Watson-Crick and wobble codon binding by tRNALysUUU species. Biochemistry 39:13390–5.

28. Vendeix FAP, Murphy F V., Cantara WA, Leszczyńska G, Gustilo EM, Sproat B, Malkiewicz A, Agris PF. 2012. Human tRNALys3UUU Is Pre-Structured by Natural Modifications for Cognate and Wobble Codon Binding through Keto–Enol Tautomerism. J Mol Biol 416:467–485.

29. Nilsson K, Lundgren HK, Hagervall TG, Björk GR. 2002. The cysteine desulfurase IscS is required for synthesis of all five thiolated nucleosides present in tRNA from *Salmonella enterica* serovar typhimurium. J Bacteriol 184:6830–5.

30. Urbonavicius J, Qian Q, Durand JM, Hagervall TG, Björk GR. 2001. Improvement of reading frame maintenance is a common function for several tRNA modifications. EMBO J 20:4863–4873.

31. Brégeon D, Colot V, Radman M, Taddei F. 2001. Translational misreading: a tRNA modification counteracts a +2 ribosomal frameshift. Genes Dev 15:2295–306.

32. Nilsson K, Jäger G, Björk GR. 2017. An unmodified wobble uridine in tRNAs specific for Glutamine, Lysine, and Glutamic acid from *Salmonella enterica* Serovar Typhimurium results in nonviability—Due to increased missense errors? PLoS One 12:e0175092.

33. Ayala-Castro C, Saini A, Outten FW. 2008. Fe-S cluster assembly pathways in bacteria. Microbiol Mol Biol Rev 72:110–25, table of contents.

34. Čavužić M, Liu Y. 2017. Biosynthesis of Sulfur-Containing tRNA Modifications: A Comparison of Bacterial, Archaeal, and Eukaryotic Pathways. Biomolecules 7.

35. Röhrich RC, Englert N, Troschke K, Reichenberg A, Hintz M, Seeber F, Balconi E, Aliverti A, Zanetti G, Köhler U, Pfeiffer M, Beck E, Jomaa H, Wiesner J. 2005. Reconstitution of an apicoplast-localised electron transfer pathway involved in the isoprenoid biosynthesis of *Plasmodium falciparum*. FEBS Lett 579:6433–6438.

36. Röhrich CR, Englert N, Troschke K, Reichenberg A, Hintz M, Seeber F, Balconi E, Aliverti A, Zanetti G, Köhler U, Pfeiffer M, Beck E, Jomaa H, Wiesner J. 2005. Reconstitution of an apicoplast-localised electron transfer pathway involved in the isoprenoid biosynthesis of *Plasmodium falciparum*. FEBS Lett 579:6433–6438.

37. Balconi E, Pennati A, Crobu D, Pandini V, Cerutti R, Zanetti G, Aliverti A. 2009.

The ferredoxin-NADP+ reductase/ferredoxin electron transfer system of *Plasmodium falciparum*. FEBS J 276:3825–3836.

38. Vollmer M, Thomsen N, Wiek S, Seeber F. 2001. Apicomplexan parasites possess distinct nuclear-encoded, but apicoplast-localized, plant-type ferredoxin-NADP+ reductase and ferredoxin. J Biol Chem 276:5483–5490.

39. Waller FR, Keeling JP, Donald GR, Striepen B, Handman E, Lang-Unnasch N, Cowman FA, Besra SG, Roos SD, McFadden IG. 1998. Nuclear-encoded proteins target to the plastid in *Toxoplasma gondii* and *Plasmodium falciparum*. Proc Natl Acad Sci U S A 95:12352–12357.

40. Fleige T, Fischer K, Ferguson DJP, Gross U, Bohne W. 2007. Carbohydrate metabolism in the *Toxoplasma gondii* apicoplast: localization of three glycolytic isoenzymes, the single pyruvate dehydrogenase complex, and a plastid phosphate translocator. Eukaryot Cell 6:984–96.

41. Daubenberger CA, Tisdale EJ, Curcic M, Diaz D, Silvie O, Mazier D, Eling W, Bohrmann B, Matile H, Pluschke G. 2003. The N'-Terminal Domain of Glyceraldehyde-3-Phosphate Dehydrogenase of the Apicomplexan *Plasmodium falciparum* Mediates GTPase Rab2-Dependent Recruitment to Membranes. Biol Chem 384:1227–37.

42. Laine LM, Biddau M, Byron O, Müller S. 2015. Biochemical and structural characterization of the apicoplast dihydrolipoamide dehydrogenase of *Plasmodium falciparum*. Biosci Rep 35.

43. Cobbold SA, Vaughan AM, Lewis IA, Painter HJ, Camargo N, Perlman DH, Fishbaugher M, Healer J, Cowman AF, Kappe SHI, Llinás M. 2013. Kinetic flux profiling elucidates two independent acetyl-CoA biosynthetic pathways in *Plasmodium falciparum*. J Biol Chem 288:36338–50.

44. Maeda T, Saito T, Harb SO, Roos SD, Takeo S, Suzuki H, Tsuboi T, Takeuchi T, Asai T. 2009. Pyruvate kinase type-II isozyme in *Plasmodium falciparum* localizes to the apicoplast. Parasitol Int 58:101–105.

45. Boehme C, Bieber F, Linnemann J, Breitling R, Lorkowski S, Reissmann S. 2013. Chemical and enzymatic characterization of recombinant rabbit muscle pyruvate kinase. Biol Chem 394:695–701.

46. Saeki T, Hori M, Umezawa H. 1974. Pyruvate kinase of *Escherichia coli*. Its role in supplying nucleoside triphosphates in cells under anaerobic conditions. J Biochem 76:631–7.

47. Knowles VL, Smith CS, Smith CR, Plaxton WC. 2001. Structural and Regulatory Properties of Pyruvate Kinase from the Cyanobacterium *Synechococcus* PCC 6301 . J Biol Chem 276:20966–20972.

48. Abbe K, Yamada T. 1982. Purification and properties of pyruvate kinase from *Streptococcus mutans*. J Bacteriol 149:299–305.

49. Chan M, Tan DSH, Sim TS. 2007. *Plasmodium falciparum* pyruvate kinase as a novel target for antimalarial drug-screening. Travel Med Infect Dis 5:125–131.

50. Vander Heiden MG, Christofk HR, Schuman E, Subtelny AO, Sharfi H, Harlow EE, Xian J, Cantley LC. 2010. Identification of small molecule inhibitors of pyruvate kinase M2. Biochem Pharmacol 79:1118–24.

51. Zoraghi R, See RH, Axerio-Cilies P, Kumar NS, Gong H, Moreau A, Hsing M, Kaur S, Swayze RD, Worrall L, Amandoron E, Lian T, Jackson L, Jiang J, Thorson L, Labriere C, Foster L, Brunham RC, McMaster WR, Finlay BB, Strynadka NC, Cherkasov A, Young RN, Reiner NE. 2011. Identification of Pyruvate Kinase in Methicillin-Resistant *Staphylococcus aureus* as a Novel Antimicrobial Drug Target. Antimicrob Agents Chemother 55:2042–2053.

52. Zhao B, Fan S, Fan Z, Wang H, Zhang N, Guo X, Yang D, Wu Q, Yu B, Zhou S. 2018. Discovery of Pyruvate Kinase as a Novel Target of New Fungicide Candidate 3-(4-Methyl-1,2,3-thiadiazolyl)-6-trichloromethyl-[1,2,4]-triazolo-[3,4- *b*][1,3,4]-thiadizole. J Agric Food Chem 66:12439–12452.

53. Geary GT, Divo AA, Bonanni CL, Jensen BJ. 1985. Nutritional requirements of *Plasmodium falciparum* in culture. III. Further observations on essential nutrients and antimetabolites. J Protozool 32:608–613.

54. Saliba KJ, Ferru I, Kirk K. 2005. Provitamin B5 (pantothenol) inhibits growth of the intraerythrocytic malaria parasite. Antimicrob Agents Chemother 49:632–7.

55. Spry C, Chai LCL, Kirk K, Saliba JK. 2005. A class of pantothenic acid analogs inhibits *Plasmodium falciparum* pantothenate kinase and represses the proliferation of malaria parasites. Antimicrob Agents Chemother 49:4649–4657.

56. Spry C, Macuamule C, Lin Z, Virga KG, Lee RE, Strauss E, Saliba KJ. 2013. Pantothenamides Are Potent, On-Target Inhibitors of *Plasmodium falciparum* Growth When Serum Pantetheinase Is Inactivated. PLoS One 8:e54974.

57. Macuamule CJ, Tjhin ET, Jana CE, Barnard L, Koekemoer L, de Villiers M, Saliba KJ, Strauss E. 2015. A Pantetheinase-Resistant Pantothenamide with Potent, On-Target, and Selective Antiplasmodial Activity. Antimicrob Agents Chemother 59:3666–3668.

58. Hart JR, Abraham A, Aly IAS. 2017. Genetic Characterization of Coenzyme A Biosynthesis Reveals Essential Distinctive Functions during Malaria Parasite Development in Blood and Mosquito. Front Cell Infect Microbiol 7.

59. Hart RJ, Lawres L, Fritzen E, Mamoun C Ben, Aly ASI. 2015. *Plasmodium yoelii* Vitamin B5 Pantothenate Transporter Candidate is Essential for Parasite

Transmission to the Mosquito. Sci Rep 4:5665.

60. Hart RJ, Cornillot E, Abraham A, Molina E, Nation CS, Ben Mamoun C, Aly ASI. 2016. Genetic Characterization of *Plasmodium* Putative Pantothenate Kinase Genes Reveals Their Essential Role in Malaria Parasite Transmission to the Mosquito. Sci Rep 6:33518.

61. Yeh E, DeRisi LJ. 2011. Chemical rescue of malaria parasites lacking an apicoplast defines organelle function in blood-stage *Plasmodium falciparum*. PLoS Biol 9.

62. Bouchut A, Geiger JA, DeRocher AE, Parsons M. 2014. Vesicles Bearing *Toxoplasma* Apicoplast Membrane Proteins Persist Following Loss of the Relict Plastid or Golgi Body Disruption. PLoS One 9:e112096.

63. Shears JM, Botté YC, McFadden IG. 2015. Fatty acid metabolism in the *Plasmodium* apicoplast: Drugs, doubts and knockouts. Mol Biochem Parasitol 199:34–50.

64. Misra A, Surolia N, Surolia A. 2009. Catalysis and mechanism of malonyl transferase activity in type II fatty acid biosynthesis acyl carrier proteins. Mol Biosyst 5:651–659.

65. Misra A, Sharma KS, Surolia N, Surolia A. 2007. Self-acylation properties of type II fatty acid biosynthesis acyl carrier protein. Chem Biol 14:775–783.

66. Cai X, Herschap D, Zhu G. 2005. Functional characterization of an evolutionarily distinct phosphopantetheinyl transferase in the apicomplexan *Cryptosporidium parvum*. Eukaryot Cell 4:1211–1220.

67. Van Vranken GJ, Jeong M-Y, Wei P, Chen Y-C, Gygi PS, Winge RD, Rutter J. 2016. The mitochondrial acyl carrier protein (ACP) coordinates mitochondrial fatty acid synthesis with iron-sulfur cluster biogenesis. Elife 5.

Appendix I

Introduction of Exogenous Non-Homologous End Joining Machinery in *P. falciparum*

ABSTRACT

When double strand breaks occur in *P. falciparum* parasites they are believed to rely almost exclusively on homology directed repair (HR) mechanisms to repair those breaks. While other eukaryotic organisms can typically use a combination of HR or non-homologous end joining (NHEJ) mechanisms to repair double strand breaks, *P. falciparum* parasites apparently lack the NHEJ pathway. In this brief appendix we outline work conducted attempting to introduce an exogenous non-homologous end joining system into *P. falciparum* parasites. In this work, we generated a vector for the expression of the Ku and LigD proteins from *Mycobacterium tuberculosis* that have been previously validated and shown to function as a two-component NHEJ system that was capable of repairing double strand breaks *in vitro*, in addition to restoring double strand breaks *in vivo* in NHEJ deficient *Saccharomyces cerevisiae,* with indel formation seen in both cases. The motivation for the introduction of this system into *P. falciparum* parasites was to generate a new genetic tool. Presence of an NHEJ system could allow for an easier method to create genetic disruptions within genes that could be scaled up for larger genetic screens. Currently, methods used to create targeted disruption or deletions of specific genes rely on the creation of individual homology directed repair templates, making larger scale genetic investigations using this method difficult.

INTRODUCTION

Double strand breaks of DNA can be highly detrimental to the cell in which it occurs, potentially resulting in chromosomal translocations, damage, or loss, and can induce cell death if not repaired (1). In eukaryotic organisms, double stranded breaks are typically

repaired through one of two repair pathways, homology-directed repair (HR), or non-homologous end joining (NHEJ) (2). In HR, double strand breaks are repaired by using a homologous sequence as a template for accurate repair of the broken region (3). NHEJ is typically more error prone, and does not require a template sequence, but instead joins the broken ends of DNA together, which can result in the insertion or deletion (indel) of nucleotides within the region being repaired (4).

In *P. falciparum,* the overall activity of the HR pathway has been validated, and multiple components of the pathway have been identified and functionally characterized, (5–9). While homology directed repair relies on the presence of a homologous sequence for repair, typically such as a sister chromatid or homologous chromosome (10), *P. falciparum* parasites exist as haploid organisms within the blood-stage of the parasite lifecycle (11). Regardless of this fact, *P. falciparum* parasites have been demonstrated to rely almost exclusively on the HR pathway to repair DSBs within the parasite (12), with this pathway being critical for parasite survival (13). Intriguingly, the NHEJ pathway appears to be absent in *P. falciparum* parasites, with homologues of the proteins that would be typically involved in this process, such as Ku70/80, DNA ligase IV, DNA-PKc, and XRCC4 being seemingly absent from the parasite genome (14). Additionally, induction of DSBs does not result in repair products consistent with the presence of a NHEJ pathway, helping to provide additional evidence that this DNA repair pathway is likely absent in malaria parasites (15).

While the lack of an NHEJ pathway is surprising, it is not entirely unheard of, as other parasites such as *Trichomonas vaginalis* and *Giardia lamblia* appear to be lacking NHEJ machinery as well (16, 17). Surprisingly, the closely related apicomplexan parasite, *T. gondii,* has been shown to possess a functional NHEJ pathway, and the component parts (18),

suggesting that the loss of this pathway in malaria parasites happened relatively recently on an evolutionary timescale.

It should be noted, however, that additional repair pathways appear to be functional and present within the parasite, with studies showing the presence of microhomology-mediated end joining (MMEJ), although occurring at extremely low frequencies (12, 19). Additionally, *P. falciparum* parasites have been shown to be capable of telomere healing, in which DSBs that occur within the distal subtelomeric regions are 'healed' by transforming the broken end of the chromosome into a functional telomere, but losing the broken subtelomeric region in the process (20, 21). While this process can repair DSBs within subtelomeric regions, which typically contain genes used for human infectivity but are largely dispensable for *in vitro* culture, this process is unlikely to be able to repair the conserved and essential genes that reside closer to the center of the chromosome.

While the lack of an NHEJ pathway in *P. falciparum* parasites is interesting, it is also makes certain approaches to genetic experimentation impossible within the parasite. For example, there was a recent study in the Apicomplexan parasite *T. gondii,* in which CRISPR-Cas9 along with a guide RNA (gRNA) library was used to create DSBs throughout the genome with reliance on indel formation to remove or insert bases, resulting in frameshifts and gene disruption used to determine which genes are essential (22). This approach has also been used in other systems as well (23, 24), but these approaches rely on the presence of a functional NHEJ system to work.

One possibility that may make experiments such as this possible would be to introduce a NHEJ system into *P. falciparum* parasites through the expression of proteins involved in this pathway. However, the typical eukaryotic NHEJ pathway consists of multiple proteins, many of which are absent within the *P. falciparum* genome, such as

Ku70/80, DNA ligase IV, DNA-PKc, and XRCC4 (14). However, a reduced end joining pathway is present within prokaryotic organisms. In *Mycobacterium tuberculosis* DNA ligase D (LigD) and Ku alone have been shown to join non-homologous DNA ends *in vitro,* and has been shown to be capable of reconstituting NHEJ in *Saccharomyces cerevisiae* (25). Thus, due to only two proteins being seemingly required for full reconstitution of NHEJ functionality, we attempted to express both of these proteins in *P. falciparum* parasites in order to introduce this pathway into the parasite.

RESULTS

Design of the *Pf*-NHEJ Expression Plasmid and Sequence

The Ku and LigD genes from *M. tuberculosis* were synthesized and harmonized for expression in *P. falciparum* parasites to avoid any issues with translation due to the presence of rare codons (26). Minimal alternations were made to the genes themselves, with both the Ku and LigD genes containing an N-terminal nuclear localization signal in addition to a myc-tag, replicating what had been done in the original work, complementing NHEJ deficient *S. cerevisiae*. The expression of these genes was driven by a bidirectional calmodulin promoter which promoted the expression of LigD, followed by a 2A skip peptide, followed by the Ku protein. The other end of the promoter drove the expression of the blasticidin deaminase drug resistance cassette (27), followed a 2A skip peptide, followed by super folder green (SFG), a green fluorescent protein engineered for rapid folding kinetics and stability (28, 29). Utilization of the 2A skip peptides was critical for the generation of this construct, as it allowed for the expression of multiple proteins within a single expression cassette (**Figure ApI-1**) (15, 30).

Expression of the *Pf*-NHEJ Construct in *P. falciparum* Parasites

The above-mentioned plasmid was integrated into the genome of the NF54-attB *P. falciparum* parasite line using attP/attB integration (31, 32). Integration and expression of the construct was validated through live epifluorescent microscopy to check if the SFG protein was present in the cytosol of the transfected parasites (**Figure ApI-2**). While we were successful in detecting a number of parasites expressing SFG, this was by far not the majority of the parasite population. The estimated percentage of parasites clearly expressing SFG and emitting a fluorescent signal appeared to be between ~1-5% of the total parasite population.

Attempted Generation of Double Strand Breaks and Indel Formation using gRNAs Targeting SFG

The NHEJ line was continuously cultured in the presence of 2.5μg/mL of blasticidin. Once this parasite line was generated, additional transfections were conducted in order to express the Cas9 enzyme along with a gRNA specific for the SFG protein. We attempted transfections with two separate gRNAs, that we are calling SFGg1 and SFGchrm. We were able to generate four and three lines respectively, in which we selected for the plasmids designed to express these gRNAs. We targeted SFG due to it potentially giving a phenotypic readout, with parasites being fluorescent or non-fluorescent, in addition to the gene being not essential for parasite survival, and thus indel formation and gene disruption should be tolerated. Once parasites were transfected with the plasmid containing the Cas9 and gRNA they were continuously cultured in the presence of 1.5μM DSM1 to ensure

retention of the plasmid, and thus, hopefully resulting in constitutive expression of Cas9 and the gRNA to ensure cutting.

Upon the introduction of DSM1, the parasitemia quickly became undetectable by blood film and Giemsa stain, with parasite growth being observed ~20-25 days post transfection. Parasites were grown under continuous treatment with 2.5μg/mL of blasticidin and 1.5μM DSM1. Once the parasites reached a higher parasitemia (>5%), they were allowed to complete multiple growth cycles before samples were taken for analysis. For analysis, primers were used to amplify the region that should have been subject to cutting by the gRNA, containing a potential repair product and indel formation. Sequences were analyzed from the multiple parasite lines that were generated for both of the gRNAs specific to SFG, and while all lines were resistant to DSM1 and blasticidin, none showed any repair products, with all returning wild-type sequences (**Figure ApI-3**).

Attempted Generation of Double Strand Breaks and Indel Formation using gRNAs Targeting FabD

Due to transfection of all constructs expressing the previous gRNAs all returning wild-type sequences, we attempted to create a double strand break in a separate region of the parasite genome, this time targeting the endogenous and dispensable gene FabD of the FASII pathway. We demonstrated previously that FabD is dispensable in chapter 5 of this thesis, and used the same gRNA expressing plasmid for use in this system. To accomplish this, we attempted 4 separate transfections, and saw a different result from what was observed when targeting SFG. While we conducted four transfections, we were only able to generate a single parasite line that survived selection with DSM1. Three transfections did not

result in parasite survival and outgrowth. However, the one line that did survive selection returned a wild-type sequence (**Figure ApI-4**).

CONCLUSIONS AND DISCUSSION

As detailed in this work, we attempted to introduce an exogenous NHEJ pathway into *P. falciparum*. We did this with the hope that this line could be used as a genetic tool that could accelerate genetic investigations into *P. falciparum* parasites. NHEJ parasites could be used for high throughput screening of guide RNA libraries that could cause gene disruption through indel formation, instead of having to rely on current methods that require a homologous repair construct for each gene to be targeted (22–24).

We were able to design and construct a plasmid that allows for expression of the LigD and Ku proteins that comprise the two component NHEJ system in *M. tuberculosis* within *P. falciparum* parasites. We also transfected parasites with this plasmid, and validated that we were able to generate parasites that expressed protein components from this vector. However, when we attempted to induce double stranded breaks in the parasite genome and generate repair products that contained indels due to the error-prone action of the introduced NHEJ system, we were unsuccessful in doing so.

The logic behind our strategy for generating double strand breaks involved introducing a plasmid into the parasite expressing the CRISPR-Cas9 enzyme along with a gRNA specific for the gene of interest, either SFG or FabD. We then selected for parasites that had acquired that plasmid by treating them continuously with 1.5μM DSM1. We hypothesized that parasites that grew out under continuous drug selection must have expressed the Cas9 enzyme along with the gRNA and created a double strand break in the

gene of interest. Since double strand breaks typically result in cell death if not repaired (1), we reasoned that the parasites must have repaired the double strand break, potentially utilizing the introduced NHEJ system, which would result in likely indel formation at the cut site. We reasoned that the cut region should not be able to be repaired back to the original sequence due to the constant selection for the plasmid containing the Cas9 and gRNA. If the sequence was wild-type, or was repaired to the wild-type sequence, the Cas9 and gRNA would continuously cut the region until it was repaired in such a way that the sequence became unrecognizable to the gRNA, favoring this repair product over time.

However, this was not the result that we obtained. While we were able to obtain multiple parasites lines that survived and grew out after drug selection with DSM1, all of the regions in which double strand breaks and indel formation should have occurred, returned wild-type sequences. The reason as to why this occurred is unclear, but it is possible that the introduced NHEJ system simply did not work. However, if the double strand break was actually generated by the gRNA loaded Cas9, and a double strand break was created the sequence would need to be repaired, and if the gRNA loaded Cas9 was constitutively expressed, the sequence would continuously be cut if it remained wild-type and would presumably favor a repair product that resulted in the alteration of the wild-type sequence to avoid targeting and cutting by the gRNA-loaded Cas9.

An alternate hypothesis as to why the parasites survived selection, but returned wild-type sequences is that the expression of the gRNA and Cas9 were somehow repressed or silenced (33). However, the expression of the Cas9 is driven by the same Cam/HOP bidirectional promoter that drives the expression of the yDHOD drug cassette (34). Thus, it is unclear through what mechanism the parasite would be able to silence a single gene on one side of a bidirectional promoter, while the other remains active. One way by which this

may occur though, is if the parasite is able to develop resistance to DSM1 and is able to turn off the entire expression cassette, which may be the case since parasites are capable of developing rapid and high-level resistance to DSM1 (35).

However, when expressing the gRNA specific for FabD, we saw a different result. While we did obtain parasites that survived DSM1 selection, with parasites that returned wild-type sequence results, the other three transfections did not yield parasites. The reasons for this are not clear, and may be due to low transfection efficiency, but this failure could also potentially be attributed to a multitude of other potential reasons. However, it is interesting that all transfections expressing the SFG specific gRNA yielded parasites, while 3 out of four expressing the FabD gRNA did not. One can only speculate as to why this is, but it may be potentially due to more efficient cutting of the FabD gRNA target sequence and failure of the introduced NHEJ system to repair the break. Since there is no homologous template available, the parasite would likely be forced to rely on other repair pathways. If the NHEJ system did not work, the parasites would have to rely on alternative repair pathways that have been demonstrated to operate at a low efficiency. Thus, generation of a double strand break in this scenario may have resulted in parasite death with no significant ability to repair the break.

Future efforts may have better success using an alternative drug resistance cassette in which parasites are unable to develop rapid and high-level resistance (35). While it is purely a hypothesis that repair products were not found due to silencing of the genes involved in generating the double strand break, this may be the case, with formation of resistance being favored over the breakage and repair of the chromosome, which may result in a severe fitness defect, or death if the parasite is unable to repair the break. Thus, in order to truly test if the introduced NHEJ pathway is active, a better way to force the generation of a double

stranded break is needed. This could potentially be done by using a different drug resistance cassette, or expressing an endonuclease, as has been done previously in *P. falciparum* (12).

METHODS

P. falciparum culture and maintenance

Unless otherwise noted, blood-stage *P. falciparum* parasites were cultured in human erythrocytes at 1% hematocrit in a 10mL total volume of CMA (complete medium with albumax) medium containing RPMI 1640 media with L-glutamine (USBiological Life Sciences), supplemented with 25mM HEPES, 0.3% sodium bicarbonate, 12.5μg/ml hypoxanthine, 5g/L Albumax II (Life Technologies) and 25μg/mL gentamicin. Cultures were maintained in gassed flasks (94% N_2, 3% O_2, 3% CO_2) and incubated in sealed 75cm^2 flasks at 37°C.

Generation of the NHEJ construct

The *M. tuberculosis* LigD and Ku proteins containing the N-terminal nuclear localization signal and Myc-tag, separated by a 2A skip peptide were synthesized, and codon harmonized for expression in *P. falciparum* parasites. This cassette was inserted in a plasmid under control of the bidirectional Cam/HOP promoter, with the other side of the plasmid containing the blasticidin deaminase drug resistance cassette, separated by a 2A skip peptide, followed by the green fluorescent protein SFG. The plasmid that these cassettes were inserted into also contained an attP site for integration using the Mycobacteriophage Bxb1 integrase.

P. falciparum transfections to generate the *Pf*-NHEJ line

Transfections were conducted as previously described (31, 36). Briefly, 400µL of red blood cells were washed with 5mL of CytoMix and resuspended in 340µL of CytoMix. The red blood cells were then electroporated with 75µg each of the NHEJ plasmid, along with 75µg of the pINT plasmid expressing the Bxb1 integrase (37). The electroporated RBCS were then mixed with ~2.5mL of the 10mL NF54 attb parasite line synchronized as schizonts at 1% hematocrit and ~10% parasitemia, and given 10mL media. After 48 hours transfectants were selected for with 2.5µg/mL of blasticidin for 7 days, after which, drug selection was removed. Infected RBCs were first observed, ~20-25 days after initiating drug selection.

Generation of *P. falciparum* gRNA expressing constructs

Guide RNA sequences were synthesized as complementary oligos (**Table ApI-1**), annealed, and inserted into the pCasG plasmid via In-Fusion cloning. The pCasG plasmid contains the Cas9 enzyme, in addition to a guide RNA (gRNA) expression cassette. For insertion of the gRNA sequence, the pCasG plasmid was digested with BsaI and also treated with rSAP and then ethanol precipitated before insertion of the gRNA oligo.

P. falciparum transfections to induce double strand breaks

Transfections were conducted as mentioned above, with red blood cells electroporated with 75µg of the gene specific pCasG plasmid (37). The electroporated RBCs were then mixed with ~2.5mL of the 10mL Pf-NHEJ parasite culture synchronized as schizonts at 1% hematocrit and ~10% parasitemia and given 10mL media. After 48 hours transfectants were selected for with 1.5µM DSM1, and kept on DSM1 for the duration that

they were cultured. Infected RBCs were typically first observed, ~25-30 days after beginning drug selection.

Amplification of potential indel sites

In order to screen for potential indel formation we used primers specific for the genetic region in which the gRNA was designed to cut (**Table ApI-2**). Samples for PCR were collected when the parasitemia reached been 5-10%, as determined via Giemsa stain. Approximately 100μL was taken from a resuspended parasite culture and placed in a heat block at 90°C for 2 minutes and stored at -20°C. For the PCR reaction 1μL of the parasite sample was added to reactions with a 50μL total volume. Reactions were conducted using a Veriti 96 well thermal cycler (Applied Biosystems) and Phusion High-Fidelity DNA polymerase (Thermo Fisher Scientific). PCR products were separated on a 1.5% agarose gel stained with ethidium bromide for visualization. The PCR product was then purified via ethanol precipitation and sequenced using the same primers used to amplify the genetic region from the genome of the parasite.

The PCR reaction mix was as follows:

Water 34.5μL
5x Phusion HF buffer 10μL
Forward primer (10 μM)1.5μL
Reverse primer (10 μM) 1.5μL
dNTPs (10mM) 1μL
Phusion polymerase 0.5μL
parasite lysate 1μL
Total volume 50μL

The PCR program was as follows:

95°C 3.5 minutes
95°C 30 seconds
62°C 1 minute

62°C 4 minutes
4°C ∞

(steps 2 and 3 were repeated 35 times)

Live cell epifluorescent microscopy

For sample preparation, 100µL of parasite culture with a hematocrit of 1% and a parasitemia between 8-10% was obtained. Parasites were stained with 30nM MitoTracker CMX-Ros (Invitrogen) and 1µg/mL 4', 6-diamidino-2-phenylindole (DAPI), and incubated for 30 minutes at 37°C. Cells were then pelleted via mini-centrifuge (Fischer Scientific) for 10 seconds, and the media was aspirated and the cells were resuspended in 100µL of CMA media and incubated for 5 minutes at 37°C. This was done three times to wash the cells, with the cells being resuspended in 20µL of CMA and then pipetted onto slides and sealed with wax (2 parts paraffin, 1 part Vaseline) for observation on a Zeiss AxioImager M2 microscope. A series of images spanning 5µm were acquired with 0.2µm spacing and images were deconvolved with VOLOCITY software (PerkinElmer) to report a single combined z - stack image.

FIGURES

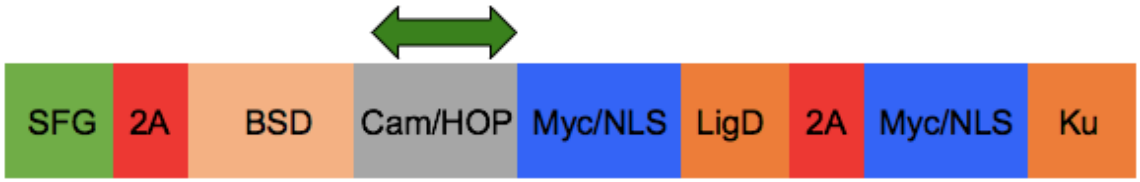

Figure ApI-1 Schematic representation of the *Pf*-NHEJ construct

The synthesized *M. tuberculosis* Ku and LigD genes harmonized for expression in *P. falciparum* were inserted downstream of the Cam/HOP bidirectional promoter, with both containing a N-terminal nuclear localization signal and Myc-tag. The Ku and LigD proteins should be produced as two polypeptides since they are separated by a viral 2A skip peptide. The other end of the promoter helped to drive the expression of the blasticidin deaminase drug resistance cassette as well as the super-folder green protein, separated by a 2A skip peptide.

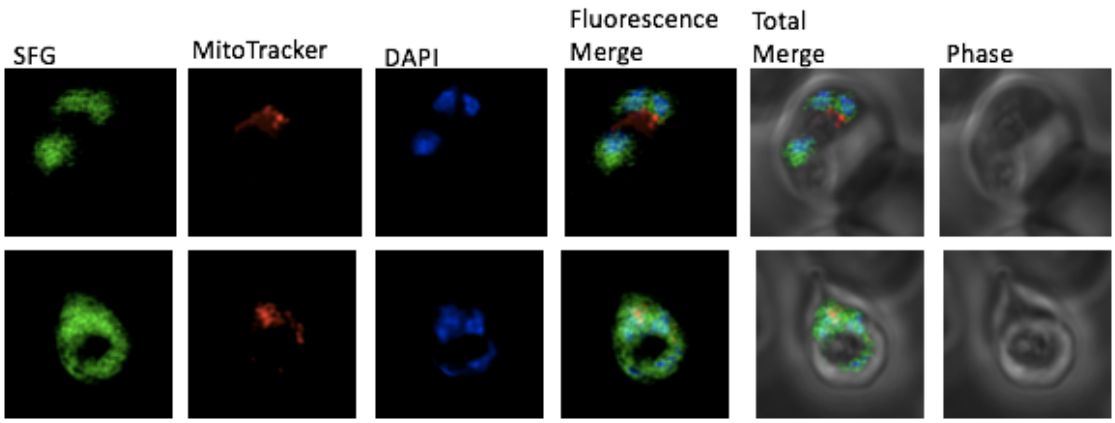

Figure ApI-2 Fluorescence microscopy of the NHEJ lines

Live epifluorescent images of the *Pf*-NHEJ line expressing SFG (green), also stained with mitoTracker (red) and DAPI (blue).

Microscopy images are 10μM long by 10μM wide.

Wild-type genetic region, with gRNA (SFGg1) target sequence highlighted

GATGTGAATGGCCATAAATTTTCTGTACGTGGTGAAGGCGAAGGAGATGCAACAAATGGAAAATTA

Recombinant parasite sequence, with the with gRNA target sequence highlighted

Transfection attempt 1 (3Y17):
GATGTGAATGGCCATAAATTTTCTGTACGTGGTGAAGGCGAAGGAGATGCAACAAATGGAAAATTA

Transfection attempt 2 (16Y17):
GATGTGAATGGCCATAAATTTTCTGTACGTGGTGAAGGCGAAGGAGATGCAACAAATGGAAAATTA

Transfection attempt 3 (24y17):
GATGTGAATGGCCATAAATTTTCTGTACGTGGTGAAGGCGAAGGAGATGCAACAAATGGAAAATTA

Transfection attempt 3 (30y17):
GATGTGAATGGCCATAAATTTTCTGTACGTGGTGAAGGCGAAGGAGATGCAACAAATGGAAAATTA

Wild-type genetic region, with gRNA (SFG chrm) target sequence highlighted

TACCGGTTCCATGGCCAACACTTGTAACGACCTTAACTTACGGAGTACAATGTTTTAGTCGAT

Recombinant parasite sequence, with the with gRNA target sequence highlighted

Transfection attempt 1 (16y17):
TACCGGTTCCATGGCCAACACTTGTAACGACCTTAACTTACGGAGTACAATGTTTTAGTCGAT

Transfection attempt 2 (24Y17):
TACCGGTTCCATGGCCAACACTTGTAACGACCTTAACTTACGGAGTACAATGTTTTAGTCGAT

Transfection attempt 3 (7u17):
TACCGGTTCCATGGCCAACACTTGTAACGACCTTAACTTACGGAGTACAATGTTTTAGTCGAT

Figure ApI-3 Comparison of the wild-type and potential repair products for SFG

Wild-type sequence of the SFG region targeted by the guide RNA, and the genetic sequence of the parasites that survived transfection with the gene-specific gRNA and Cas9 enzyme.

Wild-type genetic region, with gRNA target sequence highlighted

TTATTGTTAGTTATATGACAGATAGAAAATTTGGTTTATGTGGAAAACCAGAATCTATGGATT

Recombinant parasite sequence, with the with gRNA target sequence highlighted

Transfection attempt 1 (25L17):
TTATTGTTAGTTATATGACAGATAGAAAATTTGGTTTATGTGGAAAACCAGAATCTATGGATT

Figure ApI-4 Comparison of the wild-type and potential repair products for FabD

Wild-type sequence of the FabD region targeted by the guide RNA sequence, and the genetic sequence of the parasites that survived trasnfection with the gene-specific gRNA and Cas9 enzyme.

Table ApI-1 Oligonucleotides designed for In-Fusion insertion of gRNA sequences

Name	Oligonucleotide Sequence
SFGg gRNA F	TAAGTATATAATATTTCTGTACGTGGTGAAGGCGAGTTTTAGAGCTAGAA
SFGg gRNA R	TTCTAGCTCTAAAACTCGCCTTCACCACGTACAGAAATATTATATACTTA
SFGchrm gRNA F	TAAGTATATAATATTCTTGTAACGACCTTAACTTAGTTTTAGAGCTAGAA
SFGchrm gRNA R	TTCTAGCTCTAAAACTAAGTTAAGGTCGTTACAAGAATATTATATACTTA
FabD gRNA F	TAAGTATATAATATTGATAGAAAATTTGGTTTATGGTTTTAGAGCTAGAA
FabD gRNA R	TTCTAGCTCTAAAACCATAAACCAAATTTTCTATCAATATTATATACTTA

Table ApI-2 Primer sequences used for amplifying potential indel regions

Primer Name	Primer Sequence
SFG F	GGAAATTTAACTTGTATAGTAGCAATAGGTAACGAAAATC
SFG R	CCTCTACATTATGTCTTATTTTAAAATTAGCTTTAATTCC
FabD F	ACAAAATGAATGATGATATTTTTATTGTTAGTTATATGAC
FabD R	CGACAGACGCCGGGTGGAAAACCAGAATCTATGGATTATC

REFERENCES

1. Kolodner RD, Putnam CD, Myung K. 2002. Maintenance of Genome Stability in *Saccharomyces cerevisiae*. Science (80-) 297:552–557.

2. Cahill D, Connor B, Carney JP. 2006. Mechanisms of eukaryotic DNA double strand break repair. Front Biosci 11:1958–76.

3. Jasin M, Rothstein R. 2013. Repair of strand breaks by homologous recombination. Cold Spring Harb Perspect Biol 5:a012740.

4. Davis AJ, Chen DJ. 2013. DNA double strand break repair via non-homologous end-joining. Transl Cancer Res 2:130–143.

5. Bhattacharyya MK, Kumar N. 2003. Identification and molecular characterisation of DNA damaging agent induced expression of *Plasmodium falciparum* recombination protein PfRad51. Int J Parasitol 33:1385–92.

6. Badugu SB, Nabi SA, Vaidyam P, Laskar S, Bhattacharyya S, Bhattacharyya MK. 2015. Identification of *Plasmodium falciparum* DNA Repair Protein Mre11 with an Evolutionarily Conserved Nuclease Function. PLoS One 10:e0125358.

7. Gopalakrishnan AM, Kumar N. 2013. Opposing Roles for Two Molecular Forms of Replication Protein A in Rad51-Rad54-Mediated DNA Recombination in *Plasmodium falciparum*. MBio 4:e00252-13.

8. Lee AH, Symington LS, Fidock DA. 2014. DNA repair mechanisms and their biological roles in the malaria parasite *Plasmodium falciparum*. Microbiol Mol Biol Rev 78:469–86.

9. Bhattacharyya MK, Bhattacharyya nee Deb S, Jayabalasingham B, Kumar N. 2005. Characterization of kinetics of DNA strand-exchange and ATP hydrolysis activities of recombinant PfRad51, a *Plasmodium falciparum* recombinase. Mol Biochem Parasitol 139:33–39.

10. Li X, Heyer W-D. 2008. Homologous recombination in DNA repair and DNA damage tolerance. Cell Res 18:99–113.

11. Mzilahowa T, McCall PJ, Hastings IM. 2007. "Sexual" population structure and genetics of the malaria agent P. *falciparum*. PLoS One 2:e613.

12. Kirkman LA, Lawrence EA, Deitsch KW. 2014. Malaria parasites utilize both homologous recombination and alternative end joining pathways to maintain genome integrity. Nucleic Acids Res 42:370–379.

13. Roy N, Bhattacharyya S, Chakrabarty S, Laskar S, Babu SM, Bhattacharyya MK. 2014. Dominant negative mutant of *P lasmodium* Rad51 causes reduced parasite burden in host by abrogating DNA double-strand break repair. Mol Microbiol 94:353–366.

14. Gardner MJ, Hall N, Fung E, White O, Berriman M, Hyman RW, Carlton JM, Pain A, Nelson KE, Bowman S, Paulsen IT, James K, Eisen JA, Rutherford K, Salzberg SL, Craig A, Kyes S, Chan M-S, Nene V, Shallom SJ, Suh B, Peterson J, Angiuoli S, Pertea M, Allen J, Selengut J, Haft D, Mather MW, Vaidya AB, Martin DMA, Fairlamb AH, Fraunholz MJ, Roos DS, Ralph SA, McFadden GI, Cummings LM, Subramanian GM, Mungall C, Venter JC, Carucci DJ, Hoffman SL, Newbold C, Davis RW, Fraser CM, Barrell B. 2002. Genome sequence of the human malaria parasite *Plasmodium falciparum*. Nature 419:498–511.

15. Straimer J, Lee MCS, Lee AH, Zeitler B, Williams AE, Pearl JR, Zhang L, Rebar EJ, Gregory PD, Llinás M, Urnov FD, Fidock DA. 2012. Site-specific genome editing in *Plasmodium falciparum* using engineered zinc-finger nucleases. Nat Methods 9:993–998.

16. Manning G, Reiner DS, Lauwaet T, Dacre M, Smith A, Zhai Y, Svard S, Gillin FD. 2011. The minimal kinome of *Giardia lamblia* illuminates early kinase evolution and unique parasite biology. Genome Biol 12:R66.

17. Carlton JM, Hirt RP, Silva JC, Delcher AL, Schatz M, Zhao Q, Wortman JR, Bidwell SL, Alsmark UCM, Besteiro S, Sicheritz-Ponten T, Noel CJ, Dacks JB, Foster PG, Simillion C, Van de Peer Y, Miranda-Saavedra D, Barton GJ, Westrop GD, Muller S, Dessi D, Fiori PL, Ren Q, Paulsen I, Zhang H, Bastida-Corcuera FD, Simoes-Barbosa A, Brown MT, Hayes RD, Mukherjee M, Okumura CY, Schneider R, Smith AJ, Vanacova S, Villalvazo M, Haas BJ, Pertea M, Feldblyum T V., Utterback TR, Shu C-L, Osoegawa K, de Jong PJ, Hrdy I, Horvathova L, Zubacova Z, Dolezal P, Malik S-B, Logsdon JM, Henze K, Gupta A, Wang CC, Dunne RL, Upcroft JA, Upcroft P, White O, Salzberg SL, Tang P, Chiu C-H, Lee Y-S, Embley TM, Coombs GH, Mottram JC, Tachezy J, Fraser-Liggett CM, Johnson PJ. 2007. Draft Genome Sequence of the Sexually Transmitted Pathogen *Trichomonas vaginalis*. Science (80-) 315:207–212.

18. Fox BA, Ristuccia JG, Gigley JP, Bzik DJ. 2009. Efficient Gene Replacements in *Toxoplasma gondii* Strains Deficient for Nonhomologous End Joining. Eukaryot Cell 8:520–529.

19. Singer M, Marshall J, Heiss K, Mair GR, Grimm D, Mueller A-K, Frischknecht F. 2015. Zinc finger nuclease-based double-strand breaks attenuate malaria parasites and reveal rare microhomology-mediated end joining. Genome Biol 16:249.

20. Bottius E, Bakhsis N, Scherf A. 1998. *Plasmodium falciparum* telomerase: *de novo* telomere addition to telomeric and nontelomeric sequences and role in chromosome healing. Mol Cell Biol 18:919–25.

21. Mattei D, Scherf A. 1994. Subtelomeric chromosome instability in *Plasmodium falciparum*: short telomere-like sequence motifs found frequently at healed chromosome breakpoints. Mutat Res 324:115–20.

22. Sidik SM, Huet D, Ganesan SM, Huynh M-H, Wang T, Nasamu AS, Thiru P, Saeij JPJ, Carruthers VB, Niles JC, Lourido S. 2016. A Genome-wide CRISPR Screen in

Toxoplasma Identifies Essential Apicomplexan Genes. Cell 166:1423–1435.e12.

23. Koike-Yusa H, Li Y, Tan E-P, Velasco-Herrera MDC, Yusa K. 2014. Genome-wide recessive genetic screening in mammalian cells with a lentiviral CRISPR-guide RNA library. Nat Biotechnol 32:267–273.

24. Wang T, Wei JJ, Sabatini DM, Lander ES. 2014. Genetic Screens in Human Cells Using the CRISPR-Cas9 System. Science (80-) 343:80–84.

25. Della M, Palmbos PL, Tseng H-M, Tonkin LM, Daley JM, Topper LM, Pitcher RS, Tomkinson AE, Wilson TE, Doherty AJ. 2004. Mycobacterial Ku and ligase proteins constitute a two-component NHEJ repair machine. Science 306:683–5.

26. Angov E, Hillier CJ, Kincaid RL, Lyon JA. 2008. Heterologous protein expression is enhanced by harmonizing the codon usage frequencies of the target gene with those of the expression host. PLoS One 3:e2189.

27. Mamoun CB, Gluzman IY, Goyard S, Beverley SM, Goldberg DE. 1999. A set of independent selectable markers for transfection of the human malaria parasite *Plasmodium falciparum*. Proc Natl Acad Sci U S A 96:8716–20.

28. Pédelacq J-D, Cabantous S, Tran T, Terwilliger CT, Waldo SG. 2005. Engineering and characterization of a superfolder green fluorescent protein. Nat Biotechnol 24.

29. Aronson ED, Costantini ML, Snapp LE. 2011. Superfolder GFP is fluorescent in oxidizing environments when targeted via the Sec translocon. Traffic 12:543–548.

30. Wagner JC, Goldfless SJ, Ganesan SM, Lee MCS, Fidock DA, Niles JC. 2013. An integrated strategy for efficient vector construction and multi-gene expression in *Plasmodium falciparum*. Malar J 12:373.

31. Nkrumah JL, Muhle AR, Moura AP, Ghosh P, Hatfull FG, Jacobs RW, Fidock AD. 2006. Efficient site-specific integration in *Plasmodium falciparum* chromosomes mediated by mycobacteriophage Bxb1 integrase. Nat Methods 3:615–621.

32. Adjalley SH, Lee MCS, Fidock DA. 2010. A method for rapid genetic integration into *Plasmodium falciparum* utilizing mycobacteriophage Bxb1 integrase. Methods Mol Biol 634:87–100.

33. Coleman BI, Duraisingh MT. 2008. Transcriptional control and gene silencing in *Plasmodium falciparum*. Cell Microbiol 10:1935–1946.

34. Ganesan SM, Morrisey JM, Ke H, Painter HJ, Laroiya K, Phillips MA, Rathod PK, Mather MW, Vaidya AB. 2011. Yeast dihydroorotate dehydrogenase as a new selectable marker for *Plasmodium falciparum* transfection. Mol Biochem Parasitol 177:29–34.

35. Siegel S, Rivero A, Kyle D. 2014. Molecular basis of extreme resistance in *Plasmodium falciparum* to atovaquone and other mitochondrial inhibitors. Malar J 13:P81.

36. Spalding DM, Allary M, Gallagher RJ, Prigge TS. 2010. Validation of a modified method for Bxb1 mycobacteriophage integrase-mediated recombination in *Plasmodium falciparum* by localization of the H-protein of the glycine cleavage complex to the mitochondrion. Mol Biochem Parasitol 172:156–160.

37. Ghorbal M, Gorman M, Macpherson CR, Martins RM, Scherf A, Lopez-Rubio J-J. 2014. Genome editing in the human malaria parasite *Plasmodium falciparum* using the CRISPR-Cas9 system. Nat Biotechnol 32:819–21.

Appendix II

P. falciparum Allelic Exchange for *P. vivax* CSP

Attributions:

- Mosquito work for this project was conducted by collaborators at Walter Reed National Military Medical Center under the direction of Dr. Anjali Yadava

ABSTRACT

As outlined in this brief appendix, we attempted to replace the *P. falciparum* CSP protein with the *P. vivax* CSP. We did this with the goal of creating a parasite line that could be used for human trials to measure potential antibody responses to the *P. vivax* CSP protein, with the greater goal of furthering the development of potential vaccine strategies against *P. vivax* infection. While we were successful in creating this allelic exchange parasite line, modified parasites were not able to complete mosquito-stage development and form sporozoites. A small number of sporozoites expressing the *P. vivax* CSP were found, but they appeared to be phenotypically unhealthy. Based on our findings, it appears that the allelic exchange of *P. falciparum* and *P. vivax* CSP results in a fitness defect in the mosquito-stage of the parasite. Additional optimization and troubleshooting would be required in order to generate the sporozoites needed for use in a vaccine challenge model.

INTRODUCTION

Plasmodium vivax represents a significant public health concern, with over 2.5 billion people at risk for infection (1). In order to better develop methods to prevent or treat these parasitic infections, an *in vitro* culture system would help in the screening of potential therapeutic interventions. While continuous *in vitro* culturing of *P. falciparum* was established in the 1970s (2, 3), the development of a similar system for *P. vivax* has remained a challenge, even though some progress has been made in this area (4–7). This is largely due to *P. vivax* parasites having a tropism for reticulocytes which constitute a small percentage of the total RBCs (~1-2%), are difficult to isolate, and mature rather quickly (8). The lack of a robust *in*

vitro culture system makes any sort of experimentation on *P. vivax* extremely difficult, slowing any progress that could be made on drug discovery or vaccine development efforts.

Efforts to create an effective vaccine against *P. falciparum* parasites span many decades, with the most effective methods targeting the sporozoite stage of the parasite. These strategies typically administer attenuated parasites, or administer sporozoites with concomitant chemoprophylaxis (9, 10), and can result in sterilizing immunity (11). The primary target of the protective antibodies that are generated upon administration of sporozoites has been determined to be the circumsporozoite protein (CSP) (12, 13), which is the dominant protein present on the surface of the sporozoite stage parasite (14, 15) involved in adhesion to target cells (16). Targeting *P. falciparum* CSP is the basis of the RTS,S vaccine, which is the only malaria vaccine to have reached phase III clinical trials (17–19).

In order to test how efficacious a vaccine candidate is in protecting against infection from *Plasmodium* parasites, clinical trials using controlled human malaria infection (CHMI) are typically employed (20). While many of these studies have been conducted to test immunization and challenge against infection with *P. falciparum* (20, 21), much less has been done to investigate vaccination against *P. vivax* (22). This is largely due to the technical difficulty in conducting such trials with *P. vivax* since it cannot be cultured *in vitro*, and must rely on having the infected individual and lab strain mosquitos in the same physical proximity. Consequently, the few trials that have occurred have typically taken place in countries like Colombia where *P. vivax* is endemic (23–26). In countries where *P. vivax* is not endemic, such as the United States, this becomes more of a challenge, since infected mosquitos have to be shipped from an endemic country and maintained until challenge (22). The inability to culture *P. vivax* also results in parasite heterogeneity between and even potentially within trials; thus, outcomes may differ based on the genetic backgrounds of the

parasites (27). Additionally, the infectivity of *P. vivax* parasites is also different, in that they are capable of becoming dormant, forming what is termed a hypnozoite phase of the parasite, which can result in relapse of the infection years after the primary infection (28). Thus, primaquine drug administration is typically required post-study to ensure the full clearance of the infection, which can still fail as a result of the genetic background of the individual (29–31), with relapse being seen in the few CHMI studies that have been conducted (22).

Due to these challenges, the progress in developing a vaccine against *P. vivax* has been hindered. Basic understanding of the immunogenicity and efficacy of CSP-based vaccines for *P. vivax* have lagged far behind what is known for *P. falciparum*. Research in this area is likely to be critical, due to the CSP proteins of *P. falciparum* and *P. vivax* being significantly different. For example, while *P. falciparum* has a single allele for CSP, *P. vivax* has two major alleles, termed VK210 and VK247 that differ in the repeat region of the protein when compared to *P. falciparum* and to each other (32), with both alleles occurring throughout the world (33). This is significant because the central repeat region of CSP plays an important role in protective immunity in *P. falciparum* (16).

In order to determine if a *P. vivax* CSP based vaccine can be effective, a greater understanding of the protective efficacy and basic mechanisms of immunity against it is required. Due to the difficulty associated with CHMI trials, and the absence of an easily tractable animal model (34–36), alternative approaches must be taken to speed progress in this area. To achieve this, numerous groups have worked to express the *P. vivax* CSP proteins on the surface of *P. berghei* parasites, which has essentially generated a tractable animal model. These studies resulted in numerous findings that have gone a long way towards characterizing the nature of the immune response mounted against these proteins as

well as their protective efficacy. Experiments demonstrate that prior vaccination with the *P. vivax* CSP is capable of eliciting a high level of cross protection in mice challenged with *P. berghei* parasites expressing *P. vivax* CSP (37–41).

Similar efforts could potentially utilize *P. falciparum* parasites as a vehicle to express the *P. vivax* CSP on the surface in order to analyze immune responses to this protein within human subjects, and may assist in furthering the development of new vaccine strategies against this parasite. This approach may address many of the issues seen with the CHMI studies using *P. vivax*. Namely, this would allow for the *in vitro* culture of clonal parasites which would remove the previous logistical issues that were faced, in addition to eliminating the risk of hypnozoite formation and parasite recrudescence. Additionally, the methodologies that have been previously established for *P. falciparum*, could be easily applied to this line. Thus, in order to generate such a system, we attempted to express the *P. vivax* (Belem) CSP protein on the surface of *P. falciparum* parasites. We attempted to achieve this through a markerless allelic exchange method, removing the entire *P. falciparum* CSP sequence and replacing it with the entire *P. vivax* CSP sequence utilizing CRISPR-Cas9. We were successful in generating this line, but found that this modification prevented the formation of large numbers of viable sporozoites, hindering further progress that could be made with this line.

RESULTS

Construction of the *P. vivax* CSP Allelic Exchange Plasmid

In order to generate *P. falciparum* parasites expressing the *P. vivax* CSP in lieu of the endogenous *P. falciparum* CSP, we designed a construct that would allow us to swap the

endogenous CSP fully with the introduced *P. vivax* CSP using allelic exchange in combination with CRISPR-Cas9 genome editing (42). In order to do this, we designed the plasmid to contain ~260bp from the 5' UTR of the *P. falciparum* CSP gene immediately up to the start codon of the gene, representing the 5' homology arm that would be needed for homology directed repair (HR) and allelic exchange. This sequence was immediately followed by the complete *P. vivax* CSP Belem sequence, beginning with the start codon and ending with the stop codon. This region was then followed by ~380bp from the 3' UTR of the *P. falciparum* CSP beginning immediately after what would have been the endogenous CSP stop codon, with this region representing the 3' homology arm used for HR and allelic exchange (**Figure ApII-1**). The construct was designed as such to prevent perturbation of the gene, keeping the 5' and 3' UTR regions unaltered, while fully replacing the CSP gene.

Allelic Exchange of *P. falciparum* CSP with *P. vivax* CSP

Having generated the repair construct, we made an additional plasmid for the expression of a guide RNA targeting the endogenous CSP, which was co-transfected and selected for along with the repair construct. Selection for both plasmids was maintained for 14 days. Parasites were then observed ~25-30 days post selection and then screened via PCR to look for integration of the *P. vivax* CSP, in addition to screening for the presence of the *P. falciparum* CSP, and thus the presence of any contaminating wild-type parasites. Using this method we were successful in exchanging the *P. falciparum* CSP for the *P. vivax* CSP, and thus generated the desired parasite line (**Figure ApII-2)**.

Passage of *P. falciparum* Parasites Expressing *P. vivax* CSP through the Mosquito-Stage

Having successfully generated the *P. falciparum* line expressing the *P. vivax* CSP, we attempted to passage this line through mosquitos in order to determine if the parasites were competent in completing the mosquito-stage of the parasite lifecycle and were able to generate sporozoites. The parasites did appear to make sporozoites expressing the *P. vivax* CSP, as evidenced by their reactivity against *P. vivax* CSP specific antibodies, but only a very small number were generated and they did not appear to be phenotypically healthy (**Figure ApII-3**). Additionally, when passage through mosquitos was attempted at a later date, the sporozoites that were produced were predominantly those expressing the *P. falciparum* CSP, indicating the presence of a subpopulation of wild-type parasites that were likely selected for over time. This indicated that the line was not clonal, and also suggests that expression of the *P. vivax* CSP in lieu of the *P. falciparum* CSP likely imparts a fitness defect.

CONCLUSIONS AND DISCUSSION

Through this work we were able to demonstrate successful allelic exchange between the *P. falciparum* and *P. vivax* CSP genes. We were also successful in demonstrating that these parasites can successfully complete the mosquito-stage, and express the *P. vivax* CSP protein on the surface of the parasite. Expression of the *P. vivax* CSP on sporozoites was demonstrated by their reactivity against *P. vivax* CSP specific antibodies. However, it appears that the allelic exchange resulted in a fitness defect within the mosquito-stage of the parasite lifecycle, resulting in very few sporozoites being produced, with the few that were identified looking phenotypically unhealthy. The mechanism by which expression of the *P. vivax* CSP results in this fitness defect is unclear. It may be due to difficulty in generating the protein, as the tRNA pools and codon usage bias are different between the two species (43). To address

this issue, the *P. vivax* gene could be recoded and optimized for expression in *P. falciparum* parasites. However, the failure to produce large levels of healthy recombinant parasites could be due to other factors as well, such as the *P. vivax* protein being biologically incompatible, and not being able to complement the function of the endogenous *P. falciparum* CSP. However, overall we believe that this is a viable method for testing the immunogenicity of *P. vivax* CSP in humans and deserves to studied further .

METHODS

P. falciparum culture and maintenance

Blood-stage *P. falciparum* parasites were cultured in human erythrocytes at 1% hematocrit in a 10mL total volume of media containing RPMI 1640 media with *L*-glutamine (USBiological Life Sciences), supplemented with 25mM HEPES, 0.2% sodium bicarbonate, 12.5µg/mL hypoxanthine and 10% human serum. Cultures were maintained in gassed flasks (94% N_2, 3% O_2, 3% CO_2) and incubated in sealed 75cm^2 flasks at 37°C.

Generation of the allelic exchange and gRNA expression plasmids

The homology arms corresponding to the 5' and 3' UTR regions of the *P. falciparum* CSP sequence were synthesized and inserted into the repair template plasmid. Additionally, the full-length *P. vivax* CSP was amplified from the *P. vivax* Belem line, and inserted into the plasmid containing the *P. falciparum* 5' and 3' UTR regions, functioning as homology arms.

For guide RNA (gRNA) expression, the gRNA sequences were synthesized as oligos (**Table ApII-1**), and inserted into the pCasG plasmid containing a guide RNA (gRNA) expression cassette. Guide RNA oligos were annealed, and inserted into the pCasG plasmid

via In-Fusion cloning after being digested with BsaI and also treated with rSAP, and then ethanol precipitated.

P. falciparum transfections for allelic exchange

Transfections were conducted as previously described (44, 45), but briefly 400µL of red blood cells were washed with 5mL of CytoMix and resuspended in 340µL of CytoMix. The red blood cells were then electroporated with 75µg each of the pCasG and allelic exchange repair template plasmids (42). The electroporated RBCS were then mixed with ~2.5mL of 10mL *P. falciparum* parasites synchronized as schizonts at 1% hematocrit and ~10% parasitemia and given 10mL media. After 48 hours transfectants were selected for with 0.75µM DSM1 and 2.5nM WR99210 for 14 days. After 14 days, drug pressure was removed. Infected red blood cells (iRBC) were first observed ~25 and 30 days after beginning drug selection.

Confirmation of allelic exchange

In order to screen for integration and successful allelic exchange, in addition to the potential presence of any contaminating residual wild-type parasites four sets of primers were used, including
PfCSP 5'F, PfCSP 3'R, PfCSP wt 5'R, PfCSP wt 3'F, PvCSP 5'R, and PvCSP 3'F (**Table ApII-2**). These primers were designed to screen for integration at the 5' and 3' ends (Δ5' and Δ3') in addition to 5' and 3' regions of the WT gene (5' and 3'). The same reactions were also performed on the parental parasite line concurrently as a control. Samples for PCR were collected when the parasitemia reached been 5-10%, as determined via Giemsa stain. Approximately 100µL was taken from a resuspended parasite culture and placed in a heat

block at 90°C for 2 minutes and stored at -20°C. For the PCR reaction 1μL of the parasite sample was added to reactions with a 50μL total volume. Reactions were conducted using a Veriti 96 well thermal cycler (Applied Biosystems) and Phusion High-Fidelity DNA polymerase (Thermo Fisher Scientific). PCR products were separated on a 1.5% agarose gel stained with ethidium bromide for visualization.

The PCR reaction mix was as follows:

Water 34.5μL
5x Phusion HF buffer 10μL
Forward primer (10 μM)1.5μL
Reverse primer (10 μM) 1.5μL
dNTPs (10mM) 1μL
Phusion polymerase 0.5μL
parasite lysate 1μL
Total volume 50μL

The PCR program was as follows:

95°C 3.5 minutes
95°C 30 seconds
62°C 1 minute
62°C 4 minutes
4°C ∞

(steps 2 and 3 were repeated 35 times)

FIGURES

tatatacatacactatttttcattataatttttttttttttgtgttttttatatatt
ttggaaatatgtaacgtataaaaaacaagacaaatataatatatactattaataaataa
gatatagttcttgttttaatattaattaaaagaaaatttttgtgaatatataaaaaaaa
aaaaaaaaaaaaagaaaattataaataaatatatatattcgtgtaaaaataagtagaaa
ccacgtatattataaattacaattcATGAAGAACTTCATTCTCTTGGCTGTTTCTTCCA
TCCTGTTGGTGGACTTGTTCCCCACGCACTGCGGGCACAATGTAGATCTGTCCAAGGCC
ATAAATTTAAATGGAGTAAACTTCAATAATGTAGACGCCAGTTCACTTGGCGCGGCACA
CGTAGGACAAAGTGCTAGCCGAGGCAGAGGACTTGGTGAGAACCCAGATGACGAGGAAG
GAGATGCTAAAAAAAAAAAGGATGGAAAGAAAGCAGAACCAAAAAATCCACGTGAAAAT
AAGCTGAAACAACCAGGAGACAGAGCAGATGGACAGCCAGCAGGAGACAGAGCAGATGG
ACAGCCAGCAGGTGATAGAGCAGATGGACAACCAGCAGGAGATAGAGCAGCTGGACAGC
CAGCAGGAGATAGAGCAGATGGACAGCCAGCAGGAGACAGAGCAGATGGACAGCCAGCA
GGAGACAGAGCAGATGGACAGCCAGCAGGAGACAGAGCAGATGGACAGCCAGCAGGTGA
TAGAGCAGCTGGACAACCAGCAGGTGATAGAGCAGCTGGACAGCCAGCAGGCGATAGAG
CAGATGGACAGCCAGCAGGAGATAGAGCAGCTGGACAGCCAGCAGGCGATAGAGCAGAT
GGACAGCCAGCAGGAGATAGAGCAGCTGGACAACCAGCAGGAGATAGAGCAGATGGACA
ACCAGCAGGAGATAGAGCAGCTGGACAGCCAGCAGGAGATAGAGCAGCTGGACAGCCAG
CAGGAGATAGAGCAGCTGGACAGCCAGCAGGAGATAGAGCAGCTGGACAGCCAGCAGGA
AATGGTGCAGGTGGACAGGCAGCAGGAGGAAACGCAGGAGGACAGGGACAAAATAATGA
AGGTGCGAATGCCCCAAATGAAAAGTCTGTGAAAGAATACCTAGATAAAGTTAGAGCTA
CCGTTGGCACCGAATGGACTCCATGCAGTGTAACCTGTGGAGTGGGTGTAAGAGTCAGA
AGAAGAGTTAATGCAGCTAACAAAAAACCAGAGGATCTTACTTTGAATGACCTTGAGAC
TGATGTTTGTACAATGGATAAGTGTGCTGGCATATTTAACGTTGTGAGTAATTCATTAG
GGCTAGTCATATTGTTAGTCCTAGCATTATTtAATTAGataaagaacacatcttagttt
gagttgtacaatatttataaaaatatatactacttttttttcttaattttcatttttctt
tatattttcctatttaatttatttttttgtgaatatttaattacgtttgcgattaattg
tagaaatatatatgtatatactatatttatagaatgtgttattctcaaaaacaacaaca
aaaaaaaaaaaaaaaaaaaaaaaaaaagaaaaaaggattaaaagtaaaatagttataaat
attttcaaaaatatttataacacaaaaaatacttcgaagttcatttaacatttttgttt
atttatttatttatatatttcatttttacgtatttatattataaaatggtgtatcttaa
aaatagtgaa

Figure ApII-1 *P. falciparum/P.vivax* allelic exchange construct

Construct used to generate the Pf/Pv-CSP-allelic exchange line, showing the 5'UTR and 3'UTR from the *P. falciparum* CSP gene (red), flanking the full-length *P. vivax* Belem CSP gene (blue).

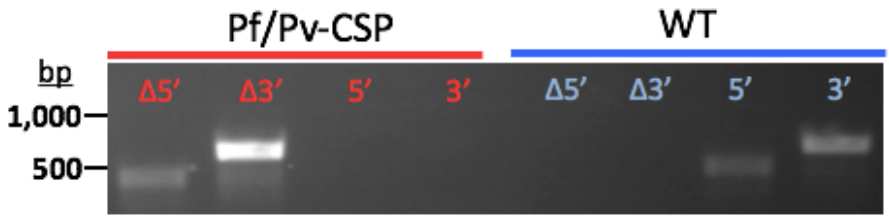

Lane	Primer Combination	Parasite Line
1. Δ5'	PfCSP 5'F, PvCSP 5'R	Pf/Pv CSP Exchange Line
2. Δ3'	PvCSP 3'F, PfCSP 3'R	
3. 5' WT	PfCSP 5'F, PfCSP wt 5'R	
4. 3' WT	PfCSP wt 3'F, PfCSP 3'R	
5. Δ5'	PfCSP 5'F, PvCSP 5'R	Parental Line
6. Δ3'	PvCSP 3'F, PfCSP 3'R	
7. 5' WT	PfCSP 5'F, PfCSP wt 5'R	
8. 3' WT	PfCSP wt 3'F, PfCSP 3'R	

Figure ApII-2 Pf/Pv-CSP-allelic exchange PCR confirmation

PCR confirming the allelic exchange of the *P. vivax* CSP gene, replacing the *P. falciparum* CSP gene, also showing no amplification indicating any residual wild-type population. The line was compared to wild-type parasites, showing amplification of only the recombinant locus. The primers used and the setup of the gel is diagrammed directly below the gel image.

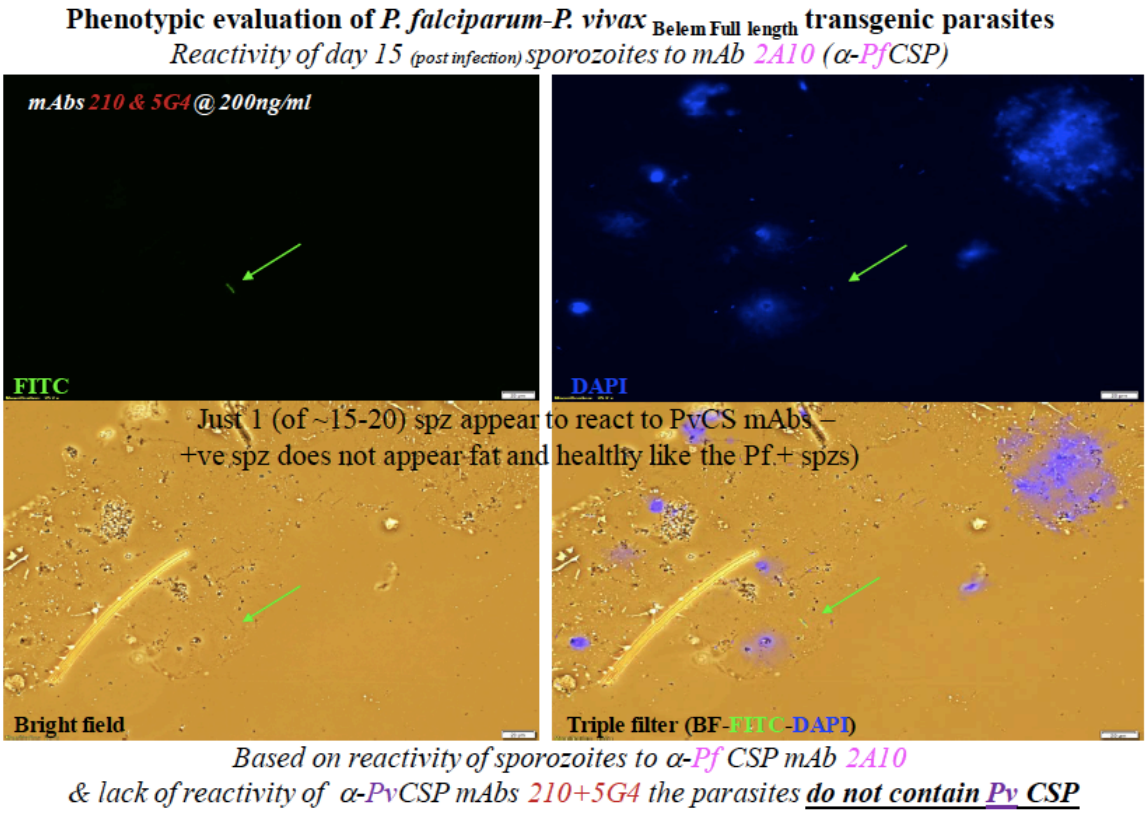

Figure ApII-3 Pf/Pv-CSP allelic exchange mosquito passage and sporozoite formation

Fluorescent microscopy of the Pf/Pv-CSP-allelic exchange line showing reactivity to a *P. vivax* CSP antibody. However, only a very small population of parasites expressing the *P. vivax* CSP protein were able to survive, and did not look phenotypically healthy.

Table ApII-1 Oligonucleotides designed for In-Fusion insertion of gRNA sequences

Oligo Name	Oligo Sequence
PfCSP gRNA F	TAAGTATATAATATTTATCTAATTAAGGAACAAGAGTTTTAGAGCTAGAA
PfCSP gRNA R	TTCTAGCTCTAAAACTCTTGTTCCTTAATTAGATAAATATTATATACTTA

Table ApII-2 Primer sequences used for allelic exchange confirmation

Primer Name	Primer Sequence
PfCSP 5'F	GTAACTTTCTATCATACTTGTCATAAATTCTGAATTATC
PfCSP 3'R	CGTATACGTCTTATGCACAAATATAGTACATTTG
PfCSP wt 5'R	CAACAAATAAAAAGGAAGAAACAGATAAAATAGC
PfCSP wt 3'F	GTTCAATAGGATTAATAATGGTATTATCCTTCTTG
PvCSP 5'R	AGAAACAGCCAAGAGAATGAAGTTCTTC
PvCSP 3'F	GAGTAATTCATTAGGGCTAGTCATATTGTTAGTC

REFERENCES

1. Howes RE, Battle KE, Mendis KN, Smith DL, Cibulskis RE, Baird JK, Hay SI. 2016. Global Epidemiology of *Plasmodium vivax*. Am J Trop Med Hyg 95:15–34.

2. Trager W. 1971. A new method for intraerythrocytic cultivation of malaria parasites (*Plasmodium coatneyi* and P. *falciparum*). J Protozool 18:239–42.

3. Trager W, Jensen JB. 1976. Human malaria parasites in continuous culture. Science 193:673–5.

4. Noulin F, Borlon C, van den Eede P, Boel L, Verfaillie CM, D'Alessandro U, Erhart A. 2012. Cryopreserved Reticulocytes Derived from Hematopoietic Stem Cells Can Be Invaded by Cryopreserved *Plasmodium vivax* Isolates. PLoS One 7:e40798.

5. Mehlotra RK, Blankenship D, Howes RE, Rakotomanga TA, Ramiranirina B, Ramboarina S, Franchard T, Linger MH, Zikursh-Blood M, Ratsimbasoa AC, Zimmerman PA, Grimberg BT. 2017. Long-term in vitro culture of *Plasmodium vivax* isolates from Madagascar maintained in *Saimiri boliviensis* blood. Malar J 16:442.

6. Bermúdez M, Moreno-Pérez DA, Arévalo-Pinzón G, Curtidor H, Patarroyo MA. 2018. *Plasmodium vivax* in vitro continuous culture: the spoke in the wheel. Malar J 17:301.

7. Roobsoong W, Tharinjaroen CS, Rachaphaew N, Chobson P, Schofield L, Cui L, Adams JH, Sattabongkot J. 2015. Improvement of culture conditions for long-term in vitro culture of *Plasmodium vivax*. Malar J 14:297.

8. Moreno-Pérez DA, Ruíz JA, Patarroyo MA. 2013. Reticulocytes: *Plasmodium vivax* target cells. Biol Cell 105:251–260.

9. Khan SM, Janse CJ, Kappe SH, Mikolajczak SA. 2012. Genetic engineering of attenuated malaria parasites for vaccination. Curr Opin Biotechnol 23:908–916.

10. Epstein JE, Richie TL. 2013. The whole parasite, pre-erythrocytic stage approach to malaria vaccine development. Curr Opin Infect Dis 26:1.

11. Hoffman SL, Goh LML, Luke TC, Schneider I, Le TP, Doolan DL, Sacci J, de la Vega P, Dowler M, Paul C, Gordon DM, Stoute JA, Church LWP, Sedegah M, Heppner DG, Ballou WR, Richie TL. 2002. Protection of Humans against Malaria by Immunization with Radiation-Attenuated *Plasmodium falciparum* Sporozoites. J Infect Dis 185:1155–1164.

12. Aikawa M, Yoshida N, Nussenzweig RS, Nussenzweig V. 1981. The protective antigen of malarial sporozoites (*Plasmodium berghei*) is a differentiation antigen. J Immunol 126:2494–5.

13. Nussenzweig V, Nussenzweig RS. 1989. Rationale for the Development of an Engineered Sporozoite Malaria Vaccine. Adv Immunol 45:283–334.

14. Gosling R, von Seidlein L. 2016. The Future of the RTS,S/AS01 Malaria Vaccine: An Alternative Development Plan. PLOS Med 13:e1001994.

15. Nussenzweig RS, Nussenzweig V. Antisporozoite vaccine for malaria: experimental basis and current status. Rev Infect Dis 11 Suppl 3:S579-85.

16. Sinnis P, Nardin E. 2002. Sporozoite antigens: biology and immunology of the circumsporozoite protein and thrombospondin-related anonymous protein. Chem Immunol 80:70–96.

17. RTS,S Clinical Trials Partnership, Agnandji ST, Lell B, Fernandes JF, Abossolo BP, Methogo BGNO, Kabwende AL, Adegnika AA, Mordmüller B, Issifou S, Kremsner PG, Sacarlal J, Aide P, Lanaspa M, Aponte JJ, Machevo S, Acacio S, Bulo H, Sigauque B, Macete E, Alonso P, Abdulla S, Salim N, Minja R, Mpina M, Ahmed S, Ali AM, Mtoro AT, Hamad AS, Mutani P, Tanner M, Tinto H, D'Alessandro U, Sorgho H, Valea I, Bihoun B, Guiraud I, Kaboré B, Sombié O, Guiguemdé RT, Ouédraogo JB, Hamel MJ, Kariuki S, Oneko M, Odero C, Otieno K, Awino N, McMorrow M, Muturi-Kioi V, Laserson KF, Slutsker L, Otieno W, Otieno L, Otsyula N, Gondi S, Otieno A, Owira V, Oguk E, Odongo G, Woods J Ben, Ogutu B, Njuguna P, Chilengi R, Akoo P, Kerubo C, Maingi C, Lang T, Olotu A, Bejon P, Marsh K, Mwambingu G, Owusu-Agyei S, Asante KP, Osei-Kwakye K, Boahen O, Dosoo D, Asante I, Adjei G, Kwara E, Chandramohan D, Greenwood B, Lusingu J, Gesase S, Malabeja A, Abdul O, Mahende C, Liheluka E, Malle L, Lemnge M, Theander TG, Drakeley C, Ansong D, Agbenyega T, Adjei S, Boateng HO, Rettig T, Bawa J, Sylverken J, Sambian D, Sarfo A, Agyekum A, Martinson F, Hoffman I, Mvalo T, Kamthunzi P, Nkomo R, Tembo T, Tegha G, Tsidya M, Kilembe J, Chawinga C, Ballou WR, Cohen J, Guerra Y, Jongert E, Lapierre D, Leach A, Lievens M, Ofori-Anyinam O, Olivier A, Vekemans J, Carter T, Kaslow D, Leboulleux D, Loucq C, Radford A, Savarese B, Schellenberg D, Sillman M, Vansadia P. 2012. A Phase 3 Trial of RTS,S/AS01 Malaria Vaccine in African Infants. N Engl J Med 367:2284–2295.

18. RTS,S Clinical Trials Partnership, Agnandji ST, Lell B, Soulanoudjingar SS, Fernandes JF, Abossolo BP, Conzelmann C, Methogo BGNO, Doucka Y, Flamen A, Mordmüller B, Issifou S, Kremsner PG, Sacarlal J, Aide P, Lanaspa M, Aponte JJ, Nhamuave A, Quelhas D, Bassat Q, Mandjate S, Macete E, Alonso P, Abdulla S, Salim N, Juma O, Shomari M, Shubis K, Machera F, Hamad AS, Minja R, Mtoro A, Sykes A, Ahmed S, Urassa AM, Ali AM, Mwangoka G, Tanner M, Tinto H, D'Alessandro U, Sorgho H, Valea I, Tahita MC, Kaboré W, Ouédraogo S, Sandrine Y, Guiguemdé RT, Ouédraogo JB, Hamel MJ, Kariuki S, Odero C, Oneko M, Otieno K, Awino N, Omoto J, Williamson J, Muturi-Kioi V, Laserson KF, Slutsker L, Otieno W, Otieno L, Nekoye O, Gondi S, Otieno A, Ogutu B, Wasuna R, Owira V, Jones D, Onyango AA, Njuguna P, Chilengi R, Akoo P, Kerubo C, Gitaka J, Maingi C, Lang T, Olotu A, Tsofa B, Bejon P, Peshu N, Marsh K, Owusu-Agyei S, Asante KP, Osei-Kwakye K, Boahen O, Ayamba S, Kayan K, Owusu-Ofori R, Dosoo D, Asante I, Adjei G, Adjei G, Chandramohan D, Greenwood B, Lusingu J, Gesase S, Malabeja A,

Abdul O, Kilavo H, Mahende C, Liheluka E, Lemnge M, Theander T, Drakeley C, Ansong D, Agbenyega T, Adjei S, Boateng HO, Rettig T, Bawa J, Sylverken J, Sambian D, Agyekum A, Owusu L, Martinson F, Hoffman I, Mvalo T, Kamthunzi P, Nkomo R, Msika A, Jumbe A, Chome N, Nyakuipa D, Chintedza J, Ballou WR, Bruls M, Cohen J, Guerra Y, Jongert E, Lapierre D, Leach A, Lievens M, Ofori-Anyinam O, Vekemans J, Carter T, Leboulleux D, Loucq C, Radford A, Savarese B, Schellenberg D, Sillman M, Vansadia P. 2011. First Results of Phase 3 Trial of RTS,S/AS01 Malaria Vaccine in African Children. N Engl J Med 365:1863–1875.

19. Olotu A, Fegan G, Wambua J, Nyangweso G, Leach A, Lievens M, Kaslow DC, Njuguna P, Marsh K, Bejon P. 2016. Seven-Year Efficacy of RTS,S/AS01 Malaria Vaccine among Young African Children. N Engl J Med 374:2519–2529.

20. Stanisic DI, McCarthy JS, Good MF. 2018. Controlled Human Malaria Infection: Applications, Advances, and Challenges. Infect Immun 86:e00479-17.

21. Collins KA, Wang CYT, Adams M, Mitchell H, Rampton M, Elliott S, Reuling IJ, Bousema T, Sauerwein R, Chalon S, Möhrle JJ, McCarthy JS. 2018. A controlled human malaria infection model enabling evaluation of transmission-blocking interventions. J Clin Invest 128:1551–1562.

22. Bennett JW, Yadava A, Tosh D, Sattabongkot J, Komisar J, Ware LA, McCarthy WF, Cowden JJ, Regules J, Spring MD, Paolino K, Hartzell JD, Cummings JF, Richie TL, Lumsden J, Kamau E, Murphy J, Lee C, Parekh F, Birkett A, Cohen J, Ballou WR, Polhemus ME, Vanloubbeeck YF, Vekemans J, Ockenhouse CF. 2016. Phase 1/2a Trial of *Plasmodium vivax* Malaria Vaccine Candidate VMP001/AS01B in Malaria-Naive Adults: Safety, Immunogenicity, and Efficacy. PLoS Negl Trop Dis 10:e0004423.

23. Palacios R, Jordán-Villegas A, Echavarría JF, Richie TL, Herrera S, Solarte Y, Epstein JE, Ramírez Ó, Vélez JD, Rocha L, Arévalo-Herrera M. 2011. Consistent Safety and Infectivity in Sporozoite Challenge Model of *Plasmodium vivax* in Malaria-Naive Human Volunteers. Am J Trop Med Hyg 84:4–11.

24. Palacios R, Chen-Mok M, Epstein JE, Fernández O, Arévalo-Herrera M, Reed ZH, Blanco P, Vergara J, Herrera S, Murrain B, Vélez JD, Manzano MR. 2009. Successful Sporozoite Challenge Model in Human Volunteers with *Plasmodium vivax* Strain Derived from Human Donors. Am J Trop Med Hyg 81:740–746.

25. Arévalo-Herrera M, Vásquez-Jiménez JM, Lopez-Perez M, Vallejo AF, Amado-Garavito AB, Céspedes N, Castellanos A, Molina K, Trejos J, Oñate J, Epstein JE, Richie TL, Herrera S. 2016. Protective Efficacy of *Plasmodium vivax* Radiation-Attenuated Sporozoites in Colombian Volunteers: A Randomized Controlled Trial. PLoS Negl Trop Dis 10:e0005070.

26. Arévalo-Herrera M, Forero-Peña DA, Rubiano K, Gómez-Hincapie J, Martínez NL, Lopez-Perez M, Castellanos A, Céspedes N, Palacios R, Oñate JM, Herrera S. 2014. *Plasmodium vivax* Sporozoite Challenge in Malaria-Naïve and Semi-Immune

Colombian Volunteers. PLoS One 9:e99754.

27. Payne RO, Griffin PM, McCarthy JS, Draper SJ. 2017. *Plasmodium vivax* Controlled Human Malaria Infection – Progress and Prospects. Trends Parasitol 33:141–150.

28. Hulden L, Hulden L. 2011. Activation of the hypnozoite: a part of *Plasmodium vivax* life cycle and survival. Malar J 10:90.

29. Bennett JW, Pybus BS, Yadava A, Tosh D, Sousa JC, McCarthy WF, Deye G, Melendez V, Ockenhouse CF. 2013. Primaquine Failure and Cytochrome P-450 2D6 in *Plasmodium vivax* Malaria. N Engl J Med 369:1381–1382.

30. Thomas D, Tazerouni H, Sundararaj KGS, Cooper JC. 2016. Therapeutic failure of primaquine and need for new medicines in radical cure of *Plasmodium vivax*. Acta Trop 160:35–38.

31. Fernando D, Rodrigo C, Rajapakse S. 2011. Primaquine in *vivax* malaria: an update and review on management issues. Malar J 10:351.

32. González JM, Hurtado S, Arévalo-Herrera M, Herrera S. 2001. Variants of the *Plasmodium vivax* circumsporozoite protein (VK210 and VK247) in Colombian isolates. Mem Inst Oswaldo Cruz 96:709–12.

33. Kain KC, Brown AE, Webster HK, Wirtz RA, Keystone JS, Rodriguez MH, Kinahan J, Rowland M, Lanar DE. 1992. Circumsporozoite genotyping of global isolates of *Plasmodium vivax* from dried blood specimens. J Clin Microbiol 30:1863–6.

34. Craig AG, Grau GE, Janse C, Kazura JW, Milner D, Barnwell JW, Turner G, Langhorne J, Malaria" on behalf of the participants of the HR meeting on "Animal M for R on S. 2012. The Role of Animal Models for Research on Severe Malaria. PLoS Pathog 8:e1002401.

35. Joyner C, Barnwell JW, Galinski MR. 2015. No more monkeying around: primate malaria model systems are key to understanding *Plasmodium vivax* liver-stage biology, hypnozoites, and relapses. Front Microbiol 6:145.

36. Reyes-Sandoval A, Bachmann MF. 2013. *Plasmodium vivax* malaria vaccines: Why are we where we are? Hum Vaccin Immunother 9:2558–2565.

37. Gimenez AM, Lima LC, Françoso KS, Denapoli PMA, Panatieri R, Bargieri DY, Thiberge J-M, Andolina C, Nosten F, Renia L, Nussenzweig RS, Nussenzweig V, Amino R, Rodrigues MM, Soares IS. 2017. Vaccine Containing the Three Allelic Variants of the *Plasmodium vivax* Circumsporozoite Antigen Induces Protection in Mice after Challenge with a Transgenic Rodent Malaria Parasite. Front Immunol 8:1275.

38. Mizutani M, Fukumoto S, Soubeiga AP, Soga A, Iyori M, Yoshida S. 2016. Development of a *Plasmodium berghei* transgenic parasite expressing the full-length

Plasmodium vivax circumsporozoite VK247 protein for testing vaccine efficacy in a murine model. Malar J 15:251.

39. de Camargo TM, de Freitas EO, Gimenez AM, Lima LC, de Almeida Caramico K, Françoso KS, Bruna-Romero O, Andolina C, Nosten F, Rénia L, Ertl HCJ, Nussenzweig RS, Nussenzweig V, Rodrigues MM, Reyes-Sandoval A, Soares IS. 2018. Prime-boost vaccination with recombinant protein and adenovirus-vector expressing *Plasmodium vivax* circumsporozoite protein (CSP) partially protects mice against Pb/Pv sporozoite challenge. Sci Rep 8:1118.

40. Salman AM, Montoya-Díaz E, West H, Lall A, Atcheson E, Lopez-Camacho C, Ramesar J, Bauza K, Collins KA, Brod F, Reis F, Pappas L, González-Cerón L, Janse CJ, Hill AVS, Khan SM, Reyes-Sandoval A. 2017. Rational development of a protective *P. vivax* vaccine evaluated with transgenic rodent parasite challenge models. Sci Rep 7:46482.

41. Atcheson E, Bauza K, Salman AM, Alves E, Blight J, Viveros-Sandoval ME, Janse CJ, Khan SM, Hill AVS, Reyes-Sandoval A. 2018. Tailoring a *Plasmodium vivax* Vaccine To Enhance Efficacy through a Combination of a CSP Virus-Like Particle and TRAP Viral Vectors. Infect Immun 86:e00114-18.

42. Ghorbal M, Gorman M, Macpherson CR, Martins RM, Scherf A, Lopez-Rubio J-J. 2014. Genome editing in the human malaria parasite *Plasmodium falciparum* using the CRISPR-Cas9 system. Nat Biotechnol 32:819–21.

43. Sinha I, Woodrow CJ. 2018. Forces acting on codon bias in malaria parasites. Sci Rep 8:15984.

44. Nkrumah JL, Muhle AR, Moura AP, Ghosh P, Hatfull FG, Jacobs RW, Fidock AD. 2006. Efficient site-specific integration in *Plasmodium falciparum* chromosomes mediated by mycobacteriophage Bxb1 integrase. Nat Methods 3:615–621.

45. Spalding DM, Allary M, Gallagher RJ, Prigge TS. 2010. Validation of a modified method for Bxb1 mycobacteriophage integrase-mediated recombination in *Plasmodium falciparum* by localization of the H-protein of the glycine cleavage complex to the mitochondrion. Mol Biochem Parasitol 172:156–160.

Appendix III

Quantifying the Effect of Fumarate on Central Carbon Metabolism in *Plasmodium falciparum*

Adapted from:

Russell Swift; Shivendra Tewari; Tatsuya Oyama; Krithika Rajaram; Jaques Reifman; Sean T Prigge; Anders Wallqvist. Quantifying the effect of fumarate on central carbon metabolism in *Plasmodium falciparum*. PLOS Computational Biology (Submitted December, 2017)

For all supplemental materials referenced in this chapter, please refer to the published form of this text.

ABSTRACT

The tricarboxylic acid (TCA) cycle is an oxidative pathway in aerobic organisms, producing energy from carbohydrates, fats, and amino acids. The mitochondria of the malarial parasite *Plasmodium falciparum* contain all of the TCA cycle enzymes as the parasite undergoes the intraerythrocytic developmental cycle (IDC). Recent experiments demonstrate that only two sequential TCA enzymes—fumarate hydratase and malate:quinone dehydrogenase—are essential for parasite growth during this period. Herein, we developed a metabolic network method that accounts for parasite transcriptomics and coupled host-pathogen metabolomics to quantify the impact of fumarate, an obligatory side-product recycled through the TCA cycle, on metabolism during different stages of the IDC. At 8hr time intervals during the IDC, we collected metabolomic data from uninfected and parasite-infected erythrocytes as well as transcriptomic data from *P. falciparum*. To predict the metabolic flux profiles of uninfected and parasite-infected erythrocytes, we first developed a method that utilizes metabolomic data, and identified key metabolites that the parasite consumes and secretes during the IDC. Next, we integrated the transcriptomic data with these metabolites to predict the metabolic flux profile of the parasite during the IDC. We then validated this profile by matching independent experimental measurements of DNA synthesis, RNA synthesis, and phospholipid synthesis, and used the validated model to gauge how fumarate levels impact metabolism during the IDC. Overall, we found that an increase in fumarate hydratase flux causes a comparable increase in aspartate aminotransferase activity, consistent with previous studies. Unexpectedly, we also found an equivalent increase in pentose phosphate pathway fluxes (which reduces nicotinamide adenine dinucleotide

phosphate levels). These findings suggest that fumarate, which is an essential side product of the obligatory purine salvage pathway, provides a feedback signal to maintain redox balance in response to changes in the parasite's growth rate.

AUTHOR SUMMARY

Malaria is an ancient disease caused by *Plasmodium* species characterized by a complex life cycle involving both mosquito and mammalian hosts. Recent studies suggest that, in the human-blood stage of the most lethal malarial parasite, *Plasmodium falciparum*, an enzyme in the tricarboxylic acid cycle—fumarate hydratase (fh)—is required for parasite survival. Although both host and parasite have fh, the parasite version is structurally distinct from the human version, and could be an attractive drug target. However, the physiological role of fh in the parasite remains unclear because of the entangled host-pathogen metabolism in infected host cells. Here, we resolve this question computationally by using a coupled host-parasite metabolic network model with multiple -omics datasets to separate the metabolism of the parasite from that of the host. Our findings reveal that the fumarate generated by the parasite's obligatory purine salvage pathway is associated with redox balance, suggesting that inhibiting fh could reduce the parasite's ability to maintain redox balance and proliferate during the blood stage. Importantly, our use of linked transcriptome and metabolomic data with a genome-scale description of the coupled host-pathogen metabolism highlights how a computational biology analysis can reveal detailed mechanistic insights into complex phenomena, otherwise not readily revealed.

INTRODUCTION

Malaria causes about 212 million infections and 429,000 deaths worldwide yearly, of which almost 99% in Africa are caused by *Plasmodium falciparum* (1). The World Health Organization (WHO) recommends using artemisinin and its derivatives to treat uncomplicated *P. falciparum* malaria (2). However, increasing evidence suggests that the efficacy of artemisinin therapy has substantially declined (3). The recent incidents of artemisinin resistance, which are a growing concern in the scientific community given the prior experience with resistance to chloroquine (4), call for the identification of new treatment strategies. One such strategy uses atovaquone (5) to target the mitochondrion of *P. falciparum*, which is highly divergent from that of its host (6) and thus an excellent antimalarial target (7). During the intraerythrocytic developmental cycle (IDC) in which the parasite undergoes proliferation in host blood cells, the mitochondria contain all enzymes of the tricarboxylic acid (TCA) cycle (8)—a terminal oxidative pathway that uses carbohydrates, fatty acids, and amino acids to generate chemical energy in all aerobic organisms.

Recent *in vitro* studies suggest that the TCA cycle of *P. falciparum* plays a limited role during the IDC. For example, although the parasite voraciously consumes glucose, only a very small fraction of it is oxidized to carbon dioxide (9). In fact, each of the TCA cycle enzymes can be individually deleted in IDC except for two enzymes fumarate hydratase (*fh*) and malate:quinone oxidoreductase (*mqo*) (10). These enzymes are apparently required for some function other than the TCA cycle. A study that specifically investigated the fate of fumarate showed that L-aspartate, formed from fumarate through *fh*, is incorporated into uridine monophosphate (UMP), a pyrimidine base, but not into purine nucleotides (11). These results suggest an additional role for fumarate during the IDC, given that UMP is eventually incorporated into the parasite's DNA. However, this is probably not the main

reason why attempts to knock out *fh* have been unsuccessful (10, 12), because *1*) the parasite can synthesize pyrimidine bases *de novo* (13) and *2*) L-aspartate is found in hemoglobin (14), which is amply available to the parasite (15).

To gain a quantitative understanding of the metabolic changes in response to rising fumarate levels during the IDC, we first sought to computationally disentangle erythrocyte metabolism from parasite metabolism—a problem that is difficult to address experimentally when the same host and parasite enzymes are separately involved in the metabolic processes of each organism (i.e., *fh* is active and present in the erythrocytic cytosol (16, 17) as well as in the mitochondria of *P. falciparum* (10, 17)). Therefore, we developed a computational framework that could *1*) isolate the effect of parasite infection on erythrocyte metabolism and *2*) quantify the effect of fumarate on *P. falciparum* metabolism during the three stages of the IDC (i.e., ring, trophozoite, and schizont). To this end, we first collected host metabolomic data from uninfected and parasite-infected erythrocytes and transcriptomic data from parasite-infected erythrocytes during the IDC, and then developed a method that requires only metabolomic data for predicting host metabolic flux profiles of uninfected and parasite-infected erythrocytes. Using this approach, we identified significantly altered host metabolic reactions in parasite-infected erythrocytes, and then used these metabolic fluxes and transcriptomic data in conjunction with a whole-genome metabolic network model of *P. falciparum* to predict its metabolic flux profiles during the IDC. After validating our model results, we computationally perturbed fumarate uptake and quantified the impact of this treatment on *P. falciparum* metabolic fluxes. Our model analysis revealed that increases in fumarate uptake levels leads to an increased flux through oxidative pentose phosphate pathway (PPP) enzymes, which reduces nicotinamide adenine dinucleotide phosphate

($NADP^+$) – a critical component for thioredoxin reductase (18) and glutathione reductase (19) that aid the parasite defend against oxidative damage.

RESULTS

During the IDC, *P. falciparum* metabolism is intertwined with erythrocyte metabolism. Current techniques for predicting parasite metabolism (11, 20, 21) rely on transcriptomic data, which come exclusively from the parasite but do not provide an exact representation of its metabolism at any given time during the IDC (see (22)). By contrast, metabolomic data provide an exact representation of host-parasite metabolism at a specific moment during the IDC, but include contributions from both the parasite and the host cells. To untangle the metabolism of the parasite from that of the host, we aimed to construct a computational framework that uses both metabolomic and transcriptomic data (**Figure ApIII-1**). We first searched the literature for metabolomic data describing extracellular changes in metabolites, to set the uptake and secretion of nutrients by uninfected and parasite-infected erythrocytes (**Figure ApIII-1, Step 1**) (23). We untangled erythrocyte metabolism from parasite metabolism, using erythrocyte-specific metabolomic data to drive metabolic alterations in uninfected and parasite-infected erythrocytes during the IDC (**Figure ApIII-1, Step 2**). Lastly, we used model-predicted interface reactions (**Figure ApIII-1, Step 3a**) and parasite-specific transcriptomic data (**Figure ApIII-1, Step 3b**) to predict the *P. falciparum* metabolic flux profile during the IDC.

Parasite-induced alteration in erythrocyte metabolism

We found 103 metabolic reactions in erythrocytes, in which the flux changed significantly upon parasite infection, as assessed by a paired *t*-test ($p < 0.05$). We also found 145 such reactions in which the time course was altered. We chose the threshold of the correlation coefficient (r) to identify reactions for which the time courses in the infected and uninfected erythrocytes were poorly correlated ($r < 0.25$). In all, parasite invasion altered 33 metabolic reactions in terms of both flux level and time course. **Table ApIII-1** lists some reactions belonging to glycerophospholipid metabolism, glycolysis/gluconeogenesis and ion transport. We have provided a complete list of all metabolic reactions whose flux level and time course were altered in erythrocytes in the Supporting Information (**S1 Table, Sheet 3**). In the column denoted 'fit effect' (**S1 Table**), we have also provided additional information on whether these changes may be due to fitting nutrient secretion or uptake data. In addition, we have listed all metabolic reactions that significantly changed (**Sheet 1**) or were poorly correlated (**Sheet 2**).

Alteration in interface reactions

As an intracellular parasite, *P. falciparum* acquires nutrients from the culture medium indirectly via the erythrocyte. Therefore, we focused on metabolic reactions of the erythrocyte which are known to take part in parasite metabolism during the IDC (henceforth, referred to as the *interface reactions*). We found 86 such reactions. Of these, we incorporated the effects of only those interface reactions that were altered in flux level ($p < 0.05$) or in their time course ($r < 0.25$). Consequently, we integrated 11 reactions with the *P. falciparum* metabolic network. We provide a table containing the estimated values of these interface reactions in the Supporting Information (**S2 Table**). Palmitic and oleic acid transport reactions were among the 11 metabolic reactions. Interestingly, palmitic and oleic

acids, together with lipid-free albumin, are sufficient to support parasite growth during the IDC (27).

Validating predicted values of *P. falciparum* metabolism

We integrated the interface reactions and transcriptomic data to predict the *P. falciparum* metabolic flux profile (**Figure ApIII-1**). As in a previous study (20), we compared the metabolic flux predictions with data from an independent dataset describing DNA (28), RNA (28), and lipid (29) synthesis during the IDC to validate these predictions (see **Figure ApIII-2**). Our model predictions (**Figure ApIII-2**, open circles) of DNA, RNA, and lipid synthesis rates during the IDC showed trends that were generally consistent with the experimental data (**Figure ApIII-2**, solid black bars). We provide a comparison of the current approach and a previous method that only included transcriptomic data (20) in the Supporting Information (**Section A of S1 Text**). Notably, our current approach generally captured the temporal peaks of DNA, RNA, and lipid synthesis, even though the experimental data were independent of those used to obtain the predictions.

Quantifying the effect of fumarate on metabolism in *P. falciparum*

Our perturbation analysis of parasitic fumarate helps us to quantify the enzymatic changes expected to occur within the parasite when fumarate levels increase. As expected, an increase in cytosolic fumarate led to an increase in the activities of *fh*, *mqo*, and aspartate aminotransferase (*aspta*) during the IDC. Specifically, we observed an average increase of 9% during IDC in the activities of *fh*, *mqo*, and *aspta*, respectively. **Table ApIII-2** lists stage-specific changes in the estimated enzyme fluxes of *P. falciparum* in response to a 10% increase

in fumarate production through the obligatory purine salvage pathway. We provide a complete list of estimated enzymatic changes in the Supporting Information (**S1 File**). Our model analysis revealed that an increase in cytosolic fumarate causes a concomitant increase in oxidative PPP enzyme fluxes, i.e., in glucose 6-phosphate dehydrogenase, phosphogluconate dehydrogenase, and 6-phosphogluconate dehydrogenase (*6pgd*). The extent of this increase was equivalent for all three enzymes. (See inset in **Figure ApIII-3** for the observed increase in the flux of *6pgd* in response to 5%–20% increase in cytosolic fumarate production.) Our analysis also suggests that arginine production increases in response to increased production of cytosolic fumarate. Our model captures this through increased argininosuccinate synthase and argininosuccinase enzyme fluxes, which ultimately produce arginine and fumarate. Note that arginine metabolism is important for parasite growth during liver stage (31) and IDC (32).

CONCLUSIONS AND DISCUSSION

Parasite-induced alteration in erythrocyte metabolism

When *P. falciparum* merozoites invade an erythrocyte, they alter its morphology and physiology (24, 33, 34) to facilitate parasite growth. Here, we used erythrocyte-specific metabolomic data to predict alterations in erythrocyte metabolism in response to parasite invasion. Consistent with previous studies, we found that the parasite alters erythrocyte metabolism by *1*) altering Na^+, K^+, Cl^- and HCO_3^- homeostasis within the infected erythrocyte (22, 35); *2*) increasing activity of glycolysis enzymes, such as hexokinase, enolase, and pyruvate kinase (36); *3*) reducing synthesis of 3-phospho-D-glyceroyl phosphate, a

precursor of 2,3-diphosphoglycerate, which declines in infected erythrocytes (36); and *4*) increasing uptake of phospholipids (35).

We found that parasite invasion altered 33 erythrocyte metabolic reactions significantly in terms of both flux level and time course. Most enzyme alterations (26 out of 33) were consistent with the literature (see above paragraph). The five out of the remaining seven reactions do not have direct evidence supporting a decrease or increase in their flux upon parasite invasion. These five reactions are involved in maintenance of pyridine nucleotide pool and hence oxidative stress which is increased in parasite infected erythrocytes (26, 37, 38). Specifically, we predict an increase in flux through glucose-6-phosphate dehydrogenase (*g6pd*) of the infected erythrocyte. Available literature evidence suggests that *g6pd* activity is mandatory for malaria infection (39, 40) but we do not know whether g6pd flux increases in the infected erythrocyte. Our model predictions suggest an increase in galactokinase flux but we did not find any literature evidence either supporting or opposing it.

Impact of fumarate on central carbon metabolism

We found that a 10% increase in cytosolic fumarate production results in a comparable increase in flux through *fh* (**Table ApIII-2**). **Figure ApIII-3** also shows that this increase propagates to malate dehydrogenase (*mdh*) through *mqo* and the oxaloacetate transporter (*oaat*). However, the impact of increasing fumarate on phosphoenolpyruvate carboxykinase (*ppck*) is different at the ring, trophozoite, and schizont stages. Specifically, the *ppck* flux marginally decreases during the ring stage and increases during the trophozoite and schizont stage. This decrease and then increase in *ppck* flux is a result of the interplay between phosphoenolpyruvate carboxylase (*ppc*), aspartate aminotransferase (*aspta*), and *oaat*

fluxes. We believe that the flux through *ppck* decreases during the ring stage because it is an energy-consuming reaction and, hence, it is unimportant during this stage. However, the increase in this flux during the trophozoite and schizont stage suggests improved coupling between fumarate and *ppck*. In contrast, other cytosolic enzymes associated with consuming oxaloacetate show an increase with fumarate (e.g., *mdh* and *aspta*) suggesting better coupling at all stages.

Identifying the link between PPP and fumarate

Our perturbation analysis revealed an increase in oxidative PPP enzyme fluxes with an increase in fumarate production. We investigated the possible mechanism underlying this phenomenon to better understand the relationship between PPP and fumarate. We sought to identify the minimal number of reactions that are sufficient to cause an increase in fumarate production and an increase in oxidative PPP enzyme fluxes (e.g., *6pgd*). We obtained these minimal reactions by iteratively solving the optimization problem shown in Step 3 in **Figure ApIII-1**. Specifically, we sequentially fixed the flux of each individual *P. falciparum* enzyme to its value attained in response to fumarate perturbation (i.e., in v_{pert}; see the Materials and Methods Section for details) and then computed a new solution. After comparing all solutions, we found that OAA transport out of the mitochondria alone was sufficient to cause equivalent increases in fumarate production and oxidative PPP enzyme fluxes. Notably, OAA is a substrate for cytosolic malate dehydrogenase (*mdh*) and plays a role in regulating redox balance in the cytosol of the parasite. Therefore, as a next step, we searched for a possible solution in reactions involving nicotinamide adenine dinucleotide (NAD). Our investigation revealed that an increase in glyceraldehyde-3-phosphate dehydrogenase (*gapd*), a decrease in pyridine nucleotide transhydrogenase (*pnt*), and an

increase in *mdh* fluxes (**Figure ApIII-4**) were sufficient to increase fumarate production and oxidative PPP enzyme fluxes (*6pgd* flux in **Figure ApIII-3**). Our results suggest that fumarate generated via the purine salvage pathway can regulate the oxidative arm of PPP and consequently maintain redox balance in the parasite cytosol. Any alteration in the fumarate-PPP link will lead to a disconnection between purine salvage (which is essential for parasite growth) and redox balance (which is essential to impede oxidative stress).

To verify that the increase in oxidative PPP enzyme fluxes with fumarate did not depend on the strain of parasite or experiment, we also performed similar perturbation analyses by replacing the transcriptomic data for the NF54 strain with those for the HB3 strain (41), and found a similar increase in oxidative PPP enzyme fluxes with increase in fumarate production. We also performed simulations with different increases in fumarate production rates (5%, 10%, 15%, and 20%) and added Gaussian noise (5%, 10%, and 15%) to the transcriptomic data (**S1 and S2 File**). In each case, an increase in cytosolic fumarate production concomitantly increased oxidative PPP enzyme fluxes (**S1 File**). Furthermore, we found that the mechanism identified for the NF54 strain (**Figure ApIII-4**) applied to the HB3 strain as well (**Section B of S1 Text**). A review of the existing literature revealed one study (42) where the authors observed an increase in PPP metabolites by adding fumarate to the culture medium. Although their observations (42) do not validate our findings *per se*, they suggest that an increase in fumarate can lead to an increase in PPP metabolites.

Fumarate: a friend or a foe of *P. falciparum*?

In this article, we aimed to understand the biological consequences of fumarate changes for *P. falciparum* metabolism, using a metabolic network model. Specifically, we addressed this by carefully constructing a framework that integrates metabolomic data from

a culture medium (23), metabolomic data from an erythrocyte (this work), and transcriptomic data from a parasite (this work). After validating our model-predicted metabolic flux profile, we elevated the amount of fumarate in the parasite's cytosol by increasing and fixing the cytosolic fumarate production to a value slightly higher (10%) than that of the control condition in the model. This allowed us to increase the amount of fumarate available inside the parasite's cytosol without perturbing any other enzyme reaction.

In the *P. falciparum* metabolic network model, cytosolic fumarate is produced from the obligatory purine salvage pathway and is recycled by *fh* in the mitochondria, in agreement with the literature (10). A recent systematic study of the role of TCA cycle enzymes in *P. falciparum* (10) found that only two of the eight enzymes (i.e., *fh* and *mqo*) are essential for the parasite during the IDC. The *fh* is considered essential because it generates aspartate, which is a precursor of purine and pyrimidine metabolism (**Figure ApIII-3**). Previously, Bulusu et al. showed in ^{14}C-labeled fumarate experiments (11) that fumarate is only incorporated into UMP (a pyrimidine base) via aspartate. This is probably not the only reason why *fh* is essential for the parasite during the IDC, because sufficient aspartate from hemoglobin degradation should always be available for the parasite (43).

We propose that fumarate accumulation is potentially toxic for the parasite in the absence of *fh* because: *1*) *fh* is the primary mechanism by which the parasite recycles fumarate generated through the obligatory purine salvage pathway (11); *2*) fumarate inhibits adenylosuccinate lyase (an enzyme which cleaves succinyl-adenosine monophosphate to form adenosine monophosphate and fumarate), which is an essential enzyme for synthesizing purines from hypoxanthine (44); *3*) fumarate can modify the function of essential proteins (45-47) and metabolites (48); and, lastly, *4*) recent experiments have

demonstrated that *fh* depletion causes succination of proteins and metabolites, and is toxic for *Mycobacterium tuberculosis* (49).

In summary, we *1*) generated time-dependent gene transcription and metabolite data of synchronized NF54 *P. falciparum* parasites during asexual reproduction in the blood stage, *2*) developed and validated an integrated computational metabolic network model based on these data to disentangling host erythrocyte and parasite metabolism, and *3*) proposed a new role for *fh*, an essential enzyme in the TCA cycle of the parasite, in redox-balance maintenance.

Limitations of the study

In this study, we quantified the effect of fumarate on the metabolic reactions of *P. falciparum* during the ring, trophozoite, and schizont phases. Our model estimates depend on the experimental conditions under which omics data are collected. Specifically, in these experiments the erythrocytes were kept in Roswell Park Memorial Institute (RPMI) 1640 culture medium, which contains nutrients essential for parasite growth in ample quantities. However, these nutrients will be present in variable quantities *in vivo*; for example, the average glucose level in non-diabetic human plasma is about 5.5mmol/L (50), whereas it is about 11mmol/L in RPMI medium. Moreover, because these nutrients vary between individuals *in vivo*, the quantitative effects of fumarate on *P. falciparum* enzymes will vary under *in vivo* conditions.

A recent study by Carey et al. (51) demonstrated that the essentiality of some redox-related genes depends on their location within the parasite (for example, cytosol vs. apicoplast). These results suggest that the link between fumarate and oxidative PPP (identified herein) could arise because of incorrect localization of some metabolic enzymes

within the model. However, fumarate hydratase (10, 52), the key enzyme responsible for fumarate recycling, and glucose-6-phosphate dehydrogenase-6-phosphogluconolactonase (52), the initial bi-functional enzyme of the oxidative PPP, are correctly localized within our model. This suggests that the link between fumarate and oxidative PPP is not due to incorrect localization of these two enzymes.

METHODS

Parasite culture, purification of erythrocytes, and sample collection

P. falciparum NF54 parasites (generously provided by David Fidock, Columbia University) were routinely propagated in human erythrocytes at 2% hematocrit in gassed flasks (94% N_2, 3% O_2, and 3% CO_2) at 37°C. Infected erythrocytes were maintained in RPMI-1640 medium (Gibco, Gaithersburg, MD) supplemented with 25mM HEPES, 12.5μg/mL hypoxanthine, 0.3% sodium bicarbonate, 25μg/mL gentamicin, 0.5μM R-lipoic acid, and 0.5% AlbuMAX II (Life Technologies Inc., Carlsbad, CA).

For white blood cell (WBC) depletion, crudely enriched erythrocytes were overlayed on a 60% Percoll solution and centrifuged at 1,500g for 30 min. After removal of WBCs from the interface, pelleted erythrocytes were carefully collected and washed several times in RPMI-1640 before adjusting the hematocrit to 50%.

To generate synchronized parasites, cultures were magnetically purified by passage through CS MACS columns (Miltenyi Biotec, Auburn, CA). This was done every 44–48hrs for four days prior to the initiation of the experiment. Parasitemia and synchronicity were monitored using Giemsa-stained blood smears and light microscopy. Additionally, immediately prior to sample collection the absence of contaminating mycoplasma was

confirmed by PCR, using primers specific for the gene encoding 16S ribosomal RNA (5'-GGAGCAAACAGGATTAGATACCC, and 5'-CACCATCTGTCACTCTGTTAACC).

Prior to sample collection, 300mL of synchronized parasite culture was passed through a CS column in four 75mL volumes, each of which was eluted with 20mL of culture medium. Eluates were pooled and adjusted to a total culture volume of 300mL at 2% hematocrit and 3% parasitemia levels using Percoll-purified blood, after which the culture was divided into four 75mL replicate flasks. Quadruplicate flasks containing 50mL of media with uninfected Percoll-purified erythrocytes at 2% hematocrit served as the control group for metabolomic analysis. MACS purification resulted in elution of late-stage trophozoites. Cultures were regularly observed by blood smear until 0–2hrs after merozoite invasion of erythrocytes, at which point the culture media from all flasks were replaced with fresh media (time 0 for this experiment). Samples were collected at the following times: 0, 8, 16, 24, 36, 40, and 48hrs.

The amounts of re-suspended parasite culture collected in 15mL conical tubes from test and control flasks were 10.5mL and 7.2mL, respectively. Tubes were centrifuged at 1,500 g for 5 min to pellet the cells. Following aspiration of media, 100μL of test or control cell pellets and 50μL of test pellets were transferred to 1.5mL tubes for metabolomic and transcriptomic analyses, respectively. Tubes were flash-frozen in an ethanol/dry-ice bath and stored at –80°C. Quadruplicate samples were sent to the Johns Hopkins Genomic Analysis and Sequencing Core Facility for microarray analysis using Agilent microarray chip AMADID 037237, and to Metabolon, Inc. (Durham, NC) for metabolite analysis.

Metabolomic profiling

Sample preparation. Following receipt of samples by Metabolon, samples were inventoried and immediately stored at –80°C. To remove protein, dissociate small molecules bound to protein or trapped in the precipitated protein matrix, and recover chemically diverse metabolites, proteins were precipitated with methanol under vigorous shaking for 2 min using a GenoGrinder 2000 (Glen Mills Inc., Clifton, NJ), and then centrifuged. The resulting extract was divided into five fractions: two for analysis by two separate reverse phase (RP) ultrahigh-performance liquid chromatography (UPLC) tandem mass spectrometry (MS/MS) methods with positive ion mode electrospray ionization (ESI), one for analysis by RP/UPLC-MS/MS with negative ion mode ESI, one for analysis by hydrophilic-interaction chromatography (HILIC) UPLC-MS/MS with negative ion mode ESI, and one for use as a backup sample. All methods utilized a Waters ACQUITY UPLC system (Waters Corp., Milford, MA) and a Q-Exactive high resolution/accurate mass spectrometer (Thermo Fisher Scientific, Hampton, NH) interfaced with a heated electrospray ionization (HESI-II) source and Orbitrap mass analyzer operated at 35,000 mass resolution.

Data extraction and compound identification.

Raw data were extracted, peaks were identified, and quality check (QC) was performed using Metabolon's hardware and software. Compounds were identified by comparison to Metabolon's library entries of purified standards or recurrent unknown entities. Biochemical identification was based on three criteria: a retention index (RI) within a narrow RI window of the proposed identification, accurate mass match to the library +/– 10 ppm, and the MS/MS forward and reverse scores between the experimental data and authentic standards. The MS/MS score was based on a comparison of the ions present in

the experimental spectrum to those present in the library spectrum. Although a molecule may resemble another based on one of these factors, the use of all three factors can distinguish and differentiate biochemicals.

Extracellular metabolomic data from the literature

The metabolomic data described thus far originate from the erythrocytes and the parasites. To capture the metabolism of nutrients transported across uninfected and infected erythrocytes accurately, we used extracellular metabolomic data from uninfected and infected erythrocytes provided by Olszewski et al. (23). The experimental conditions they employed closely resemble the culture conditions of our study. The only major difference was the method used to synchronize the parasite culture during the IDC: whereas Olszewski et al. used sorbitol, we used a magnet. We performed student's t-test to compare their intracellular metabolomic data with the corresponding data from our experiments to verify whether the difference in synchronization method greatly altered the metabolomic data. We found that only 10 out of 68 common metabolites were significantly ($p < 0.01$) altered during the IDC, which suggests that the synchronization method has little effect on metabolomic data. We have also provided a direct comparison of the transcriptomic data from Olszewski et al. (23) with those from our experiments (**S1 Text, Section C**).

Microarray methods

RNA quality: For each data point, RNA was extracted from 50 μL of packed erythrocyte culture with Trizol Reagent and the PureLink Mini Kit (Invitrogen/Thermo Fisher Scientific, Carlsbad, CA). Trizol (1mL) was added to each sample, followed by high-speed disruption in tubes containing Lysing Matrix D (MP Biomedical, Santa Ana, CA) in a

FastPrep 120 Instrument at speed 6 for 20 seconds. Homogenates were subsequently processed according to the PureLink Mini Kit manufacturer's (Invitrogen/Thermo Fisher Scientific) protocol, including on-column DNase treatment. Following elution of purified RNA from the PureLink columns with nuclease-free water, quantitation was performed using a NanoDrop spectrophotometer (Thermo Fisher Scientific) and quality assessment determined by RNA ScreenTape analysis on an Agilent TapeStation 2200 (Agilent Technologies, Santa Clara, CA).

Microarray: From 100ng of total RNA, Cyanine 3-labeled cRNA was prepared using the Low Input Quick Amp Labeling Kit One-Color (Agilent Technologies). A mixed stage RNA pool control and the seven time course samples were hybridized (along with the manufacturer's control RNA spike-in samples) according to a standard protocol to the eight sectors of an Agilent 8x15K platform microarray (AMADID 037237) (53, 54), with separate microarray slides used for each biological replicate (in quadruplicate for each condition). Post-hybridization washes were performed, followed by scanning with a G2600D SureScan microarray scanner (Agilent Technologies), using the scan protocol AgilentHD_GX_1color. Scan control software automatically performed autofocus, autogain, and gal file download. Agilent's Feature Extraction Software was used to assign grids, provide raw image files per array, and generate QC metric reports from the microarray scan data. The QC metric reports were used for quality assessment of all hybridizations and scans. Txt files from Agilent's Feature Extraction Software were transferred to Partek Genomics Suite software (v6.6) (Partek Inc., St Louis, MO). Within Partek Genomics Suite, the gene expression workflow was followed for Agilent Feature Extraction files, starting with gProcessingSignal, Quantile Normalization, and Log Transformed base 2.0.

Metabolic network model: We used metabolomic data to further identify metabolites known to exist in parasites but which were not included in our model of *P. falciparum* (55). Specifically, we identified five enzyme reactions not included in the model: *1*) betaine-homocysteine S-methyltransferase; *2*) argininosuccinase; *3*) argininosuccinate synthetase; *4*) aspartate carbamoyltransferase; and *5*) UDP-glucose-6-dehydrogenase. Incorporation of these enzyme reactions resulted in the addition of five new metabolites: *1*) glycine betaine; *2*) dimethylglycine; *3*) L-argininosuccinate; *4*) L-citrulline; and *5*) UDP-glucuronate. We provide details of these metabolic reactions in **Table ApIII-3**, along with the SBML code in the Supporting Information (**S4 File**). The resulting metabolic network model of *P. falciparum* had 1,025 reactions and 923 metabolites. Our erythrocyte metabolic network model was based on the model of Wallqvist et al. (21), which includes different metabolic pathways related to carbohydrates, nucleotides, amino acids, cofactors, and phospholipids. We modified this model to include *interface* reactions that lie at the interface of erythrocyte metabolism and *P. falciparum* metabolism. We also added L-citrulline and L-argininosuccinate to the erythrocyte model, which have been detected in the metabolomic data and which participate in the urea cycle of the erythrocyte (56). The updated erythrocyte model had 407 metabolites and 590 reactions. We have provided a complete list of the reactions added to the erythrocyte model (**S6 Table**). The SBML code is provided in the Supporting Information (**S5 File**). We did not add any other reactions to the erythrocyte model because erythrocytes have a relatively simple metabolism (9) given their primary role as oxygen transporters (57).

Estimating alterations in erythrocyte metabolism after parasite invasion

P. falciparum, like other parasites of the phylum Apicomplexa, needs a host cell as a source of nutrients and to provide protection from host defense mechanisms. During the IDC, *P. falciparum* takes up metabolites from, and secretes them to, the culture medium via the erythrocyte cytosol. Once the parasite invades an erythrocyte, it alters the metabolism of the erythrocyte to make the environment conducive to IDC progression (66, 67). However, owing to experimental difficulties, it is impossible to accurately quantify the changes in erythrocyte metabolism introduced by the parasite. To computationally quantify such changes, we first used metabolomic data that delineate changes in the culture medium during the IDC to constrain the uptake and secretion of metabolites by an erythrocyte (23). Then, we used erythrocyte-specific metabolomic data obtained under uninfected and parasite-infected conditions to predict the metabolic flux profile of the erythrocyte during the IDC. Computationally, we performed the mathematical procedures described in the next three sections.

Estimating uptake and secretion rates of metabolites in the culture medium (Fig 1, Step 1).

Olszewski et al. (23) measured 59 culture medium metabolites at seven time points during the IDC but we were able to calculate uptake/secretion rates for only 22 metabolites whose initial concentrations were known. We calculated uptake/secretion rates at a given hour via linear regression, by plotting relative levels of culture medium metabolites (weighted by their standard deviation) as a function of time for (t, t+2) points, where t is the time point for which the rate is being calculated. Using the initial concentration of the metabolite and the dry weight (gDW) of an erythrocyte, we converted the estimated slopes of the regression lines (uptake/secretion rates) to units of mmol h^{-1} per gDW of erythrocyte. We used these nutrient uptake/secretion rates as constraints when estimating the metabolism of uninfected

and infected erythrocytes during the IDC. Similarly, we estimated the average nutrient uptake/secretion rate during the IDC ($\mathbf{v}_{\text{nut}}$) by performing linear regression on relative levels of culture medium metabolites during the IDC. We used these estimated average rates, shown in **Table ApIII-4**, to estimate the average metabolic state of the erythrocyte during the IDC (see equation 3). **S4 Table** presents the average and time-dependent rates of nutrient uptake/secretion by uninfected and infected erythrocytes during the IDC.

Using metabolomic data to estimate reaction fluxes (Fig ApIII-1, Step 2).

Currently, few methods integrate metabolomic data with large-scale metabolic networks to predict reaction fluxes (68). Here, we used a simple concept to integrate metabolomic data from uninfected and infected erythrocytes with a metabolic network model. We assumed that *1*) flux through an enzyme is proportional to the amount of substrate and *2*) a substrate with the lowest concentration becomes rate-limiting for reactions with multiple substrates. These assumptions hold true for substrates as well as products if a reaction is unidirectional. Specifically, we used the relative metabolite levels of substrates and products to scale *nominal* unidirectional fluxes of the erythrocyte and to predict the time course of erythrocyte metabolism during the IDC. We performed the following optimization scheme:

$$\delta^{\mathrm{t}} = \min\left(\sum_{\mathrm{i}\in R} v_{\mathrm{i}}^{\mathrm{t}} - \alpha_{\mathrm{i}}^{\mathrm{t}} \cdot v_{\mathrm{i,nom}}^{\mathrm{RBC}} + \sum_{\mathrm{j}\in N} v_{\mathrm{j}}^{\mathrm{t}} - v_{\mathrm{j,nut}}^{\mathrm{t}} \right) \tag{1}$$

$$\text{subject to } \mathbf{S}_{\mathrm{RBC}}\mathbf{v} = 0 \text{ and } \mathbf{v}_{\mathrm{lb}} \le \mathbf{v} \le \mathbf{v}_{\mathrm{ub}}$$

$$\min \sum_{i \in M} \left| v_i^t - v_{i,nom}^{RBC} \right| \tag{2}$$

$$\text{subject to } \sum_{i \in R} v_i^t - \alpha_i^t \cdot v_{i,nom}^{RBC} + \sum_{j \in N} v_j^t - v_{j,nut}^t \leq \delta^t$$

$$\mathbf{S}_{RBC}\mathbf{v} = 0$$

$$\mathbf{v}_{lb} \leq \mathbf{v} \leq \mathbf{v}_{ub}$$

Here, $\mathbf{S}_{RBC}$ is the stoichiometric matrix and α^t is a column vector with each element containing the minimum value of a substrate and product metabolite relative to its median during the IDC at a given time t. We focused on only those metabolites that are part of erythrocyte metabolism and not part of *P. falciparum* metabolism. We provide a list of these metabolites and associated reactions in the Supporting Information (**S5 Table**). '*R*' is a set of unidirectional reactions, '*N*' is the set of reactions associated with nutrient uptake/secretion, and '*M*' is the set of all metabolic reactions in the erythrocyte. $\mathbf{v}_{lb}$ and $\mathbf{v}_{ub}$ are vectors representing the lower and upper bounds, respectively, of the metabolic reactions of the erythrocyte. We determined the directionality of the reactions by identifying their thermodynamic feasibility, which is equivalent to analyzing flux variability without any closed loop in the metabolic network (69, 70). The relative value of a given metabolite is equal to the area under the curve (AUC) of the metabolite normalized by the Bradford protein concentration (71) of each sample and the median value of the AUC over the IDC. To simulate infected erythrocytes, we normalized the AUC of the metabolites by the median value of the AUC of the metabolites over the IDC from the uninfected sample.

$\mathbf{v}_{nut}^t = \left\{ v_{j,nut}^t : j \in N \right\}$ is a set containing the estimated rates of metabolite uptake/secretion by

uninfected or infected erythrocytes over the IDC. These uptake and secretion rates were multiplied by a factor of 2 to account for differences in hematocrit level in the culture media of Olszewski et al. (23) and our experiments. $\mathbf{v}_{\text{nom}}^{\text{RBC}} = \left\{ v_{\text{i,nom}}^{\text{RBC}} : \text{i} \in M \right\}$ is the nominal flux vector of the erythrocyte obtained by solving the following optimization problem:

$$\max v_{\text{NaK}} \tag{3}$$

$$\text{subject to } \mathbf{S}_{\text{RBC}}\mathbf{v} = 0$$

$$\mathbf{v}_{\text{lb}} \le \mathbf{v} \le \mathbf{v}_{\text{ub}}$$

$$\sum_{\text{j}\in N} \left| v_{\text{j}} - v_{\text{j,nut}} \right| \le \varepsilon$$

$$v_{\text{lb}}^{\text{NaK}} \ge \mu$$

Here, $\mathbf{v}_{\text{nut}}$ is a vector representing the average rate of metabolites secreted or consumed by an erythrocyte from the RPMI-1640 medium. These values are the slopes of the regression lines obtained by performing a linear regression of the extracellular metabolites measured by Olszewski et al. (23) over the entire IDC from uninfected or infected erythrocytes. When simulating uninfected erythrocytes, we set μ to be 35% of the maximum attainable sodium pump (*NaK*) flux in the erythrocyte model because *NaK* controls the membrane potential, which is greatly reduced in an uninfected erythrocyte (24). On the other hand, when simulating parasite-infected erythrocytes, we maximized *NaK* activity while keeping the metabolite consumption/secretion at its average value, because the membrane potential of an infected erythrocyte is much larger than that of an uninfected erythrocyte (72).

Identifying interface reactions and integration with *P. falciparum* metabolism (Fig ApIII-1, Step 3).

We identified reactions that form the interface of erythrocyte metabolism and *P. falciparum* metabolism (i.e., *interface reactions*), based on *1*) statistical significance and *2*) changes in directionality and time course. We employed paired *t*-tests to identify statistically significant ($p < 0.05$) differences in metabolic fluxes of uninfected and infected erythrocytes. We performed correlation tests to identify reactions with altered directionality by a negative correlation ($r < 0$) and those with altered time course by a low correlation ($| r | < 0.25$). Note that although these interface reactions are in units of mmol h^{-1} per gDW of erythrocyte, metabolic reactions within the parasite model are in units of mmol h^{-1} per gDW of parasite. As the parasite mass changes throughout the IDC, conversion of gDW of erythrocyte into gDW of parasite is not straightforward. However, the parasite mass within the erythrocyte at the beginning of the IDC is minimal and increases during the IDC. Therefore, when obtaining nominal fluxes of the parasite (as described in the next section), we used the median flux of each interface reaction as the minimum of that reaction. On the other hand, when estimating parasite metabolism during the IDC, we normalized each interface reaction by its median value during the IDC to obtain unitless temporal profiles of interface reactions. Before solving the optimization problem, the temporal profile of each normalized interface reaction was multiplied by its nominal value to realize the units of mmol h^{-1} per gDW of parasite.

We first solved the following optimization problem, using interface reactions to obtain nominal fluxes ($v_{\text{nom}}^{\text{Pf}}$):

$$\min \sum_{i \notin B} |v_i| \tag{4}$$

$$\text{subject to } v_{\text{growth}} = \gamma$$

$$v_{\text{int}} \leq v_j \forall\ j \in I$$

$$\mathbf{S}_{\text{Pf}} \mathbf{v} = 0 \text{ and } \mathbf{v}_{\text{lb}} \leq \mathbf{v} \leq \mathbf{v}_{\text{ub}}$$

Here, *B* is the set of reactions that contribute to the parasite's growth *in silico*. Following the original work of Fang et al. (20), we set the nominal growth rate (γ) to be 0.48 g h^{-1} per gDW of the original merozoite, as this is indicative of the average growth rate of the parasite during the IDC. v_{int} is the median value of the estimated interface reaction flux during the IDC, *I* is the set of all interface reactions, and $\mathbf{S}_{\text{Pf}}$ is the stoichiometric matrix. We integrated these nominal fluxes and transcriptomic data with the *P. falciparum* metabolic model to predict the metabolic fluxes during the IDC. Briefly, we solved the following optimization problem:

$$\min \left\| v^t - v_{\text{nom}}^{\text{Pf}} \right\| \tag{5}$$

$$\text{subject to } \sum_{j \in G} \left| v_j^t - r_j^t \cdot v_{\text{nom}}^{\text{Pf}} \right| \leq J^t$$

(6)

$$v^t{}_{\text{int}} \leq v_j{}^t \forall\ j \in \text{interface reactions}$$

$$\mathbf{S}_{\text{Pf}} \mathbf{v}^t = 0 \text{ and } \mathbf{v}_{\text{lb}} \leq \mathbf{v}^t \leq \mathbf{v}_{\text{ub}}$$

where *G* is a set containing all unidirectional intracellular fluxes of *P. falciparum*. Here, $r_j^t = \varphi\left(g_j^t\right)$, where g_j^t is the temporal gene-expression profile of a reaction 'j', and $v^t{}_{int}$ is the normalized temporal profile of each interface reaction 'j' times the nominal value of this reaction obtained by solving equation (4). Following the original work of Fang et al. (20), we obtain J^t, shown in equation (6), by solving the following:

$$\min J^t = \sum_{j \in G} \left| v_j^t - r_j^t \cdot v_{nom}^{Pf} \right|$$

(7)

$$\text{subject to } \mathbf{S}_{Pf} \mathbf{v}^t = \mathbf{0}$$

$$v^t{}_{int} \leq v_j \forall\ j \in \text{interface reactions}$$

$$\mathbf{v}_{lb} \leq \mathbf{v}^t \leq \mathbf{v}_{ub}$$

Note that, while simulating the NF54 strain, we computationally suppressed the expression of four genes involved in DNA synthesis (PlasmoDB ID: PF3D7_1015800, PF3D7_1405600, PF3D7_1437200, PF3D7_0923800) and four genes involved in lipid synthesis (PlasmoDB ID: PF3D7_0922900, PF3D7_0211400, PF3D7_0615100, PF3D7_1232200) to achieve minimal DNA and lipid synthesis during the first 15 h of the IDC. Specifically, we achieved this by modifying the transcriptional delays of these genes, which were previously set to 11hrs —the median gene-protein delay (20, 22). In **Table ApIII-5**, we have provided the transcriptional delays estimated for the DNA and lipid synthesis genes mentioned above.

Validation of model simulations.

We validated our model simulations of parasite-infected erythrocyte metabolism and *P. falciparum* metabolism by comparing their outputs with the corresponding experimental

data from parasite-infected erythrocytes and parasites during the IDC. Specifically, we validated parasite-infected erythrocyte simulations by comparing their outputs with observed alterations in glycolytic enzymes (25), ion homeostasis (22, 35), uptake of phospholipids (35), synthesis of 2,3-diphosphoglycerate (36), and uptake of arginine (56) (**Table ApIII-1**). Following Fang *et al.* (10), we validated model simulations of parasite metabolism by comparing their outputs with experimental data on DNA (28), RNA (28), and lipid synthesis (29) during the IDC (Fig 2).

Quantifying the impact of fumarate on parasite metabolism.

We used our validated *P. falciparum* metabolic fluxes as baseline data and perturbed cytosolic fumarate production to identify the most fumarate-sensitive reactions. Specifically, we computed the following metric: $\varrho_{\text{stage}} = \text{median}(\Delta v^{t})$ where, t ∈ ring, trophozoite, or schizont stage and $\Delta v = v_{\text{pert}}/v_{\text{ctrl}}$, where both v_{ctrl} and v_{pert} belong to the space $\{S : \Re^n \rightarrow \phi\}$. Here, S is the stoichiometry matrix of the parasite model, $\Re^n$ is an n-dimensional real coordinate space, and ϕ is the kernel of the linear transformation S. v_{ctrl} and v_{pert} are obtained by solving equations (4) and (5); however, while solving for v_{pert}, the fumarate boundary flux is increased by a small quantity 'δ' to simulate an increase in fumarate inside the parasite's cytosol. Specifically, we increased the fumarate exchange flux by 5%, 10%, 15%, or 20% of its estimated value under normal conditions.

FIGURES

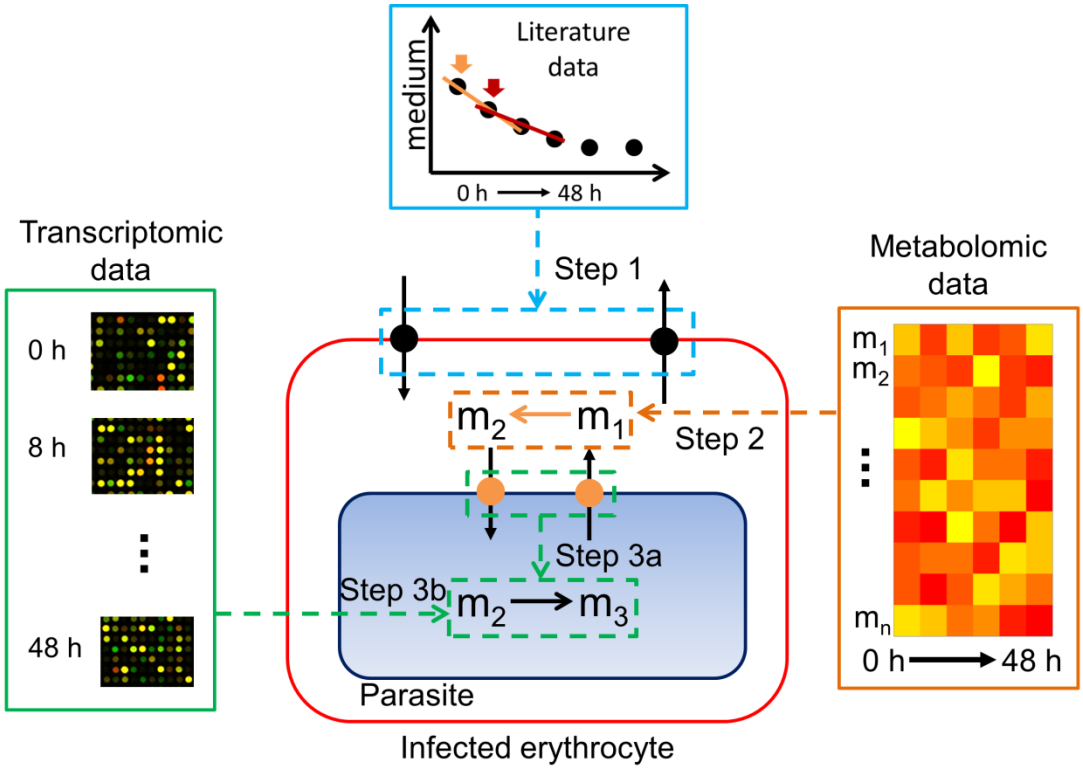

Figure ApIII-1 Schematic of our computational approach for predicting *P. falciparum* metabolic fluxes during the intraerythrocytic developmental cycle (IDC)

There are three major steps: *1*) compute the rates at which nutrients are transported across the membrane of an uninfected or parasite-infected erythrocyte during the IDC (light blue dotted lines); *2*) integrate host metabolomic data obtained from uninfected or parasite-infected erythrocytes with the erythrocyte metabolic network model to predict the metabolic flux profile of the corresponding erythrocyte during the IDC (orange dotted lines); and *3*) integrate the *a*) nutrient consumption or secretion rate of the parasite during the IDC estimated from Step 2, and the *b*) transcriptomic data obtained from the same biological

sample as that used to acquire the metabolomic data, with the *P. falciparum* metabolic network model to predict its metabolic flux profile during IDC (green dotted lines).

Table ApIII-1 Erythrocyte metabolic reactions altered by parasite invasion

Name	Catalyzed reaction‡	Pathway	Effect*	Reference
Bicarbonate transport exchange)	Chloride + Bicarbonate (medium) ⇌ Bicarbonate + Chloride (medium)	Ion homeostasis	Backward flux increased	(24)
Hexokinase	ATP + D-glucose ⇌ ADP + glucose-6-phosphate + H	Glycolysis	Forward flux increased	(25)
K^+–Cl^- coupled transport	Chloride (medium) + Potassium (medium) ⇌ Chloride + Potassium	Ion homeostasis	Backward flux increased	(24)
Malic enzyme	L-malate + nadp ⇌ CO2 + nadph + pyruvate	Pyruvate metabolism	Forward flux increased	(26)¶
D-sorbitol reductase	D-glucose + H + nadph ⇌ nadp + D-sorbitol	Fructose metabolism	Forward flux increased	(26)¶
Glucose 6-phosphate dehydrogenase	D-glucose-6-phosphate + nadp ⇌ 6-phospho-D-glucono-1,5-lactone + nadph	Pentose phosphate pathway	Forward flux increased	(26)¶

‡A forward reaction is read from left to right.

*A metabolic reaction flux is said to increase (or decrease) upon parasite invasion if its median value (taken over the IDC) is greater (or smaller) than its median value under uninfected conditions.

¶The parasite-infected erythrocyte is exposed to increased oxidative stress, which requires increased cycling of reducing agents (nadp and nadph)

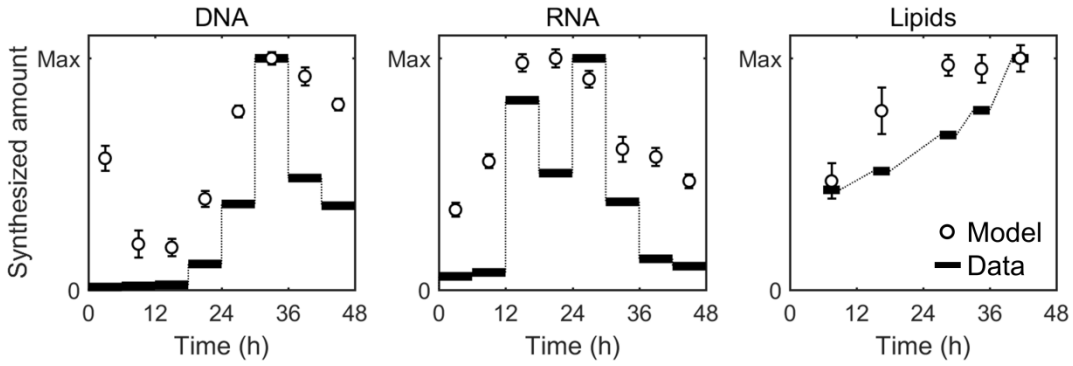

Figure ApIII-2 Model predictions of DNA, RNA, and lipid synthesis during the intraerythrocytic developmental cycle (IDC)

Flux predictions (open circles with error bars) and the experimental data (solid black bars) for DNA, RNA, and phospholipid synthesis are normalized by their respective maximum values during the IDC. The error bars show mean ± standard error computed from 20 random simulations performed after adding 5% Gaussian noise to the transcriptomic data. The predictions capture the temporal peaks of DNA and RNA synthesis reasonably well. Furthermore, they reproduce the increase in phospholipid synthesis satisfactorily. Overall, the predictions made with the current approach are at the least equally well as compared to our earlier approach (20) (see Fig A in S1 Text for a direct comparison).

Table ApIII-2 Average estimated deviation in *P. falciparum* enzymatic fluxes expressed relative to a 10% increase in fumarate[‡]

Reaction name	PlasmoDB ID	Estimated increase/decrease (% of fumarate perturbation)			Pathway
		Ring	Trophozoite	Schizont	
Oxaloacetate transporter	See footnote[†]	+9.3±0.2	+8.9±0.4	+9.3±0.3	Mitochondrial transporter
6-Phosphogluconate dehydrogenase	PF3D7_1453800	+8.8±0.1	+8.2±0.1	+8.4±0.1	Pentose phosphate pathway
Aspartate transaminase	PF3D7_0204500	+9.7±0.2	+9.5±0.3	+7.4±0.4	Pyruvate metabolism
Malate dehydrogenase (cytosol)	PF3D7_0618500	+5.1±0.0	+5.3±0.2	+5.0±0.0	Pyruvate metabolism
Phosphoenolpyruvate carboxykinase	PF3D7_1342800.1	–0.5±3.5	+2.2±4.4	+5.1±6.2	Pyruvate metabolism
Phosphoenolpyruvate carboxylase	PF3D7_1426700	+1.4±0.7	–15.1±8.8	+0.3±0.3	Pyruvate metabolism
Fumarate hydratase	PF3D7_0927300	+9.8±0.1	+8.6±0.4	+9.0±0.2	TCA cycle
Malate:quinone oxidoreductase	PF3D7_0204500	+9.6±0.1	+8.7±0.4	+9.3±0.1	TCA cycle
Citrate synthase	PF3D7_1022500	+4.6±0.1	+4.3±0.1	+4.5±0.0	TCA cycle
Oxoglutarate dehydrogenase	PF3D7_0820700	+0.7±0.2	–1.3±1.3	+4.2±0.5	TCA cycle
Succinate dehydrogenase (ubiquinone)	PF3D7_1034400	+0.1±0.1	–50.0±15.8	–3.6±2.6	TCA cycle

[†]Transport is shown to occur *in vitro*, but the gene specific to this transporter has not been identified (18, 30).

[‡] Values represent mean ± one standard error of 20 random simulations after adding 5% Gaussian noise to the transcriptomic data.

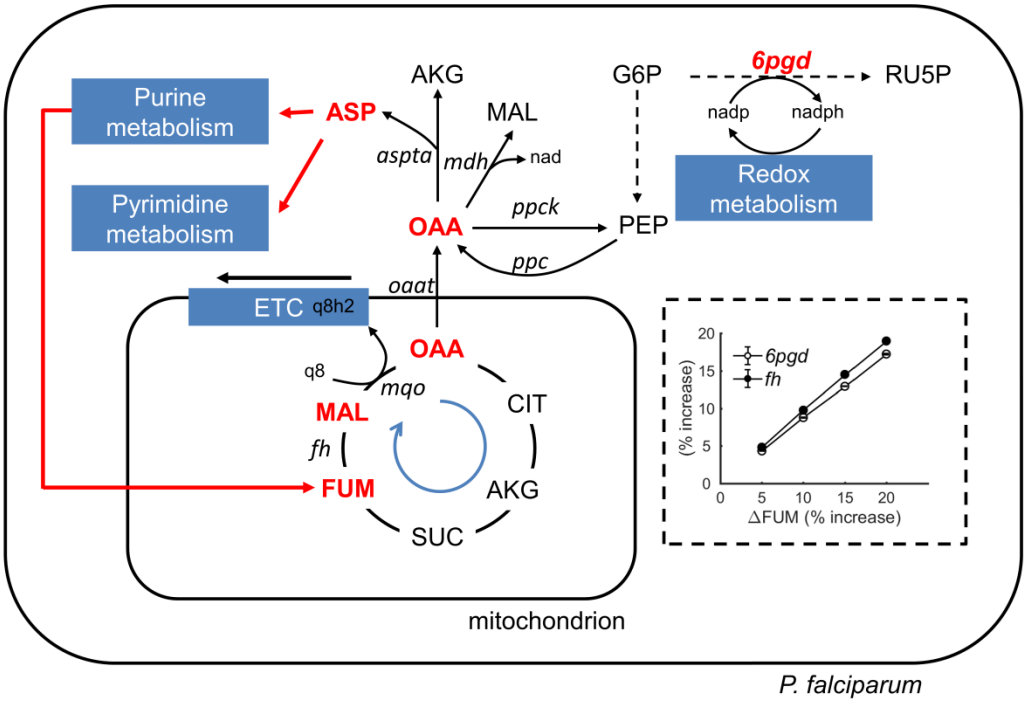

Figure ApIII-3 Fate of fumarate based on perturbation analysis

Arrows and metabolites highlighted in red indicate the flow of fumarate (FUM) entering the tricarboxylic acid cycle. Recycling of FUM in the mitochondrion starts with its conversion into malate (MAL), which is then converted into oxaloacetate (OAA) by malate:quinone oxidoreductase (*mqo*). In this process, *mqo* reduces ubiquinone (q8) to ubiquinol (q8h2), which feeds into the electron transport chain (ETC). Cytosolic OAA reacts with phosphoenolpyruvate carboxykinase (*ppck*) to yield phosphoenolpyruvate (PEP). It also reacts with aspartate aminotransferase (*aspta*) to yield aspartate (ASP), which is a precursor of pyrimidine. ASP is also a precursor of cytosolic FUM in purine metabolism, which completes the FUM recycling process. Our analysis reveals that oxidative pentose phosphate pathway enzyme fluxes, which reduce nicotinamide adenine dinucleotide phosphate ($NADP^+$), increase in proportion to an increase in FUM production. Inset shows a

comparison between the estimated increases in 6-phosphogluconate dehydrogenase (*6pgd*) and fumarate hydratase (*fh*) fluxes during the ring stage in response to a 5%–20% increase in cytosolic FUM production. Values are means ± standard errors computed over 20 simulations after adding 5% Gaussian noise to the transcriptomic data. Note that the error bars in the inset are eclipsed by the markers. Abbreviations: AKG, alpha-ketoglutatare; *aspta*, aspartate transaminase; G6P, glucose-6-phosphate; *mdh*, malate dehydrogenase; *oaat*, oxaloacetate transporter; *ppc*, phosphoenolpyruvate carboxylase; RU5P, ribulose-5-phosphate.

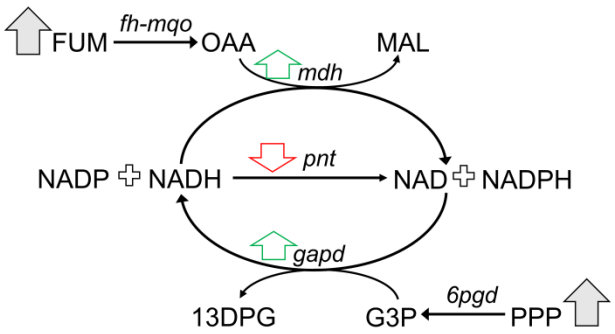

Figure ApIII-4 Proposed mechanism responsible for an increase in oxidative pentose phosphate pathway (PPP) enzyme fluxes in response to an increase in cytosolic fumarate (FUM)

An increase in cytosolic FUM production increases oxaloacetate (OAA) via fumarate hydratase (*fh*) and malate:quinone oxidoreductase (*mqo*). An increase in OAA increases malate dehydrogenase (*mdh*) flux, and hence, creates a demand for reduced nicotinamide adenine dinucleotide (NADH). This demand is met by an increase in glyceraldehyde-3-phosphate dehydrogenase (*gapd*). An increase in *mdh* also decreases pyridine nucleotide transhydrogenase (*pnt*) flux, possibly because of overflow of nicotinamide adenine dinucleotide (NAD) from *mdh*. Abbreviations: 13DPG, D-glycerate 1,3-bisphosphate; *6pgd*, 6-phosphogluconate dehydrogenase; G3P, glyceraldehyde-3-phosphate dehydrogenase; MAL, malate; NADP, nicotinamide adenine dinucleotide phosphate; NADPH, reduced NADP.

Table ApIII-3 Metabolites and reactions added to the models based on intracellular metabolomic data

Metabolite	Reaction	EC number	KEGG ID	Reference†
P. falciparum metabolism model‡				
dimethylglycine	L-homocysteine + glycine betaine ⇌ L-methionine + dimethylglycine	2.1.1.5	C01026	(58, 59)
glycine betaine	L-homocysteine + glycine betaine ⇌ L-methionine + dimethylglycine	2.1.1.5	C00719	(60)
L-argininosuccinate	L-argininosuccinate ⇌ L-arginine + fumarate	4.3.2.1	C03406	(56, 60)
L-citrulline	L-aspartate + L-citrulline + ATP ⇌ L-argininosuccinate + AMP + diphosphate + H	6.3.4.5	C00327	(23, 56, 58, 60)
UDP-glucuronate	UDP-glucose + 2NAD + H_20 ⇌ UDP-glucuronate + 2NADH + 3H	1.1.1.22	C00167	(60, 61)
Erythrocyte metabolism model¶				
L-argininosuccinate	ATP + L-citrulline + L-aspartate ⇌ AMP + PPi + L-argininosuccinate	6.3.4.5	C03406	(56)
L-argininosuccinate	L-argininosuccinate ⇌ L-arginine + fumarate	4.3.2.1	C03406	(56)
L-citrulline	L-ornithine + carbamoyl phosphate ⇌ L-citrulline + Pi + H	2.1.3.3	C00327	(56, 62)

‡All metabolic reactions are as provided at biocyc.org (63) for *P. falciparum*

¶All metabolic reactions are as provided at ExPASy (64) and KEGG (65).

†Studies/databases that also detected these metabolites in *P. falciparum* and erythrocyte

Table ApIII-4 Average rates of uptake/secretion of 10 nutrient by uninfected and infected erythrocytes during the IDC[†]

Nutrient	Estimated rate (mmol h^{-1} per gDW of erythrocyte)	
	Uninfected erythrocytes	Infected erythrocytes
D-glucose	-1.94×10^{-2}	$+1.09 \times 10^{0}$
Hypoxanthine	-7.44×10^{-4}	$+3.42 \times 10^{-3}$
Inositol	-9.06×10^{-4}	-4.19×10^{-5}
L-aspartate	-5.10×10^{-4}	$+1.38 \times 10^{-3}$
L-glutamate	-1.43×10^{-2}	-3.68×10^{-2}
L-valine	-4.73×10^{-2}	-1.09×10^{-1}
Nicotinamide	-5.48×10^{-4}	$+9.52 \times 10^{-4}$
Pyridoxine	$+2.27 \times 10^{-4}$	$+1.67 \times 10^{-4}$
Riboflavin	-5.17×10^{-5}	-3.10×10^{-5}
Thiamine	-2.33×10^{-4}	-5.75×10^{-4}

[†]A positive sign indicates uptake, whereas a negative sign indicates secretion.

Table ApIII-5 Gene transcription delays for DNA and lipid synthesis genes

PlasmoDB ID	Number of reactions transcribed	Estimated delay (h)	Metabolic pathways
PF3D7_1015800	4	+3	Nucleotide, Redox
PF3D7_1405600	4	+3	Nucleotide, Redox
PF3D7_1437200	4	+3	Nucleotide, Redox
PF3D7_0923800	2	+3	Nucleotide, Redox
PF3D7_0922900	20	+5	Lipid
PF3D7_0211400	21	+5	Lipid
PF3D7_0615100	12	+25	Lipid
PF3D7_1232200	6	+25	Amino Acid, Carbohydrate, Lipid

REFERENCES

1. WHO. World Malaria Report 2015. Geneva: World Health Organization; 2016.

2. WHO. WHO Policy Recommendation: Seasonal Malaria Chemoprevention (SMC) for *Plasmodium falciparum* malaria control in highly seasonal transmission areas of the Sahel sub-region in Africa. World Health Organization; 2012.

3. Phyo AP, Ashley EA, Anderson TJ, Bozdech Z, Carrara VI, Sriprawat K, et al. Declining efficacy of artemisinin combination therapy against *P. falciparum* malaria on the Thai–Myanmar border (2003–2013): the role of parasite genetic factors. Clin Infect Dis. 2016;63(6):784-91. doi: 10.1093/cid/ciw388. pmid: 27313266.

4. Awasthi G, Das A. Genetics of chloroquine-resistant malaria: a haplotypic view. Mem Inst Oswaldo Cruz. 2013;108(8):947-61. doi: 10.1590/0074-0276130274. pmid: 24402147.

5. Nixon GL, Moss DM, Shone AE, Lalloo DG, Fisher N, O'Neill PM, et al. Antimalarial pharmacology and therapeutics of atovaquone. J Antimicrob Chemother. 2013;68(5):977-85. doi: 10.1093/jac/dks504. pmid: 23292347.

6. Vaidya AB, Mather MW. Mitochondrial evolution and functions in malaria parasites. Annu Rev Microbiol. 2009;63:249-67. doi: 10.1146/annurev.micro.091208.073424. pmid: 19575561.

7. Goodman CD, Buchanan HD, McFadden GI. Is the mitochondrion a good malaria drug target? Trends Parasitol. 2017;33(3):185-93. doi: 10.1016/j.pt.2016.10.002. pmid: 27789127.

8. Gardner MJ, Hall N, Fung E, White O, Berriman M, Hyman RW, et al. Genome sequence of the human malaria parasite *Plasmodium falciparum*. Nature. 2002;419(6906):498-511. doi: 10.1038/nature01097. pmid: 12368864.

9. Olszewski KL, Llinas M. Central carbon metabolism of *Plasmodium* parasites. Mol Biochem Parasitol. 2011;175(2):95-103. doi: 10.1016/j.molbiopara.2010.09.001. pmid: 20849882.

10. Ke H, Lewis IA, Morrisey JM, McLean KJ, Ganesan SM, Painter HJ, et al. Genetic investigation of tricarboxylic acid metabolism during the *Plasmodium falciparum* life cycle. Cell Rep. 2015;11(1):164-74. doi: 10.1016/j.celrep.2015.03.011. pmid: 25843709.

11. Bulusu V, Jayaraman V, Balaram H. Metabolic fate of fumarate, a side product of the purine salvage pathway in the intraerythrocytic stages of *Plasmodium falciparum*. J Biol Chem. 2011;286(11):9236-45. doi: 10.1074/jbc.M110.173328. pmid: 21209090.

12. Jayaraman V, Suryavanshi A, Kalale P, Kunala J, Balaram H. Biochemical characterization and essentiality of *Plasmodium* fumarate hydratase. bioRxiv. 2017:158956. doi: 10.1101/158956.

13. Gero AM, Brown GV, O'Sullivan WJ. Pyrimidine de novo synthesis during the life cycle of the intraerythrocytic stage of *Plasmodium falciparum*. J Parasitol. 1984;70(4):536-41. pmid: 6150076.

14. Hill RJ, Konigsberg W, Guidotti G, Craig LC. The structure of human hemoglobin. I. The separation of the alpha and beta chains and their amino acid composition. J Biol Chem. 1962;237:1549-54. pmid: 13907376.

15. Goldberg DE, Slater AF, Cerami A, Henderson GB. Hemoglobin degradation in the malaria parasite *Plasmodium falciparum*: an ordered process in a unique organelle. Proc Natl Acad Sci U S A. 1990;87(8):2931-5. pmid: 2183218.

16. Tanaka KR, Valentine WN. Fumarase activity of human leukocytes and erythrocytes. Blood. 1961;17:328-33. pmid: 13775141.

17. Storm J, Sethia S, Blackburn GJ, Chokkathukalam A, Watson DG, Breitling R, et al. Phosphoenolpyruvate carboxylase identified as a key enzyme in erythrocytic *Plasmodium falciparum* carbon metabolism. PLOS Path. 2014;10(1):e1003876. doi: 10.1371/journal.ppat.1003876. pmid: 24453970.

18. Pannala VR, Dash RK. Mechanistic characterization of the thioredoxin system in the removal of hydrogen peroxide. Free Radic Biol Med. 2015;78:42-55. doi: 10.1016/j.freeradbiomed.2014.10.508. pmid: 25451645.

19. Pannala VR, Bazil JN, Camara AK, Dash RK. A biophysically based mathematical model for the catalytic mechanism of glutathione reductase. Free Radic Biol Med. 2013;65:1385-97. doi: 10.1016/j.freeradbiomed.2013.10.001. pmid: 24120751.

20. Fang X, Reifman J, Wallqvist A. Modeling metabolism and stage-specific growth of *Plasmodium falciparum* HB3 during the intraerythrocytic developmental cycle. Mol Biosyst. 2014;10(10):2526-37. doi: 10.1039/c4mb00115j. pmid: 25001103.

21. Wallqvist A, Fang X, Tewari SG, Ye P, Reifman J. Metabolic host responses to malarial infection during the intraerythrocytic developmental cycle. BMC Syst Biol. 2016;10(1):58. doi: 10.1186/s12918-016-0291-2. pmid: 27502771.

22. Foth BJ, Zhang N, Chaal BK, Sze SK, Preiser PR, Bozdech Z. Quantitative time-course profiling of parasite and host cell proteins in the human malaria parasite *Plasmodium falciparum*. Mol Cell Proteomics. 2011;10(8):M110 006411. doi: 10.1074/mcp.M110.006411. pmid: 21558492.

23. Olszewski KL, Morrisey JM, Wilinski D, Burns JM, Vaidya AB, Rabinowitz JD, et al. Host-parasite interactions revealed by *Plasmodium falciparum* metabolomics. Cell Host Microbe. 2009;5(2):191-9. doi: 10.1016/j.chom.2009.01.004. pmid: 19218089.

24. Kirk K. Ion regulation in the malaria parasite. Annu Rev Microbiol. 2015;69:341-59. doi: 10.1146/annurev-micro-091014-104506. pmid: 26488277.

25. Roth EF, Jr., Calvin MC, Max-Audit I, Rosa J, Rosa R. The enzymes of the glycolytic pathway in erythrocytes infected with Plasmodium falciparum malaria parasites. Blood. 1988;72(6):1922-5. pmid: 3058230.

26. Becker K, Tilley L, Vennerstrom JL, Roberts D, Rogerson S, Ginsburg H. Oxidative stress in malaria parasite-infected erythrocytes: host-parasite interactions. Int J Parasitol. 2004;34(2):163-89. doi: 10.1016/j.ijpara.2003.09.011. pmid: 15037104.

27. Mi-Ichi F, Kita K, Mitamura T. Intraerythrocytic *Plasmodium falciparum* utilize a broad range of serum-derived fatty acids with limited modification for their growth. Parasitology. 2006;133(Pt 4):399-410. doi: 10.1017/S0031182006000540. pmid: 16780611.

28. Gritzmacher CA, Reese RT. Protein and nucleic acid synthesis during synchronized growth of *Plasmodium falciparum*. J Bacteriol. 1984;160(3):1165-7. pmid: 6389509.

29. Vial HJ, Thuet MJ, Philippot JR. Phospholipid biosynthesis in synchronous *Plasmodium falciparum* cultures. J Protozool. 1982;29(2):258-63. pmid: 7047730.

30. Nozawa A, Fujimoto R, Matsuoka H, Tsuboi T, Tozawa Y. Cell-free synthesis, reconstitution, and characterization of a mitochondrial dicarboxylate–tricarboxylate carrier of *Plasmodium falciparum*. Biochem Biophys Res Commun. 2011;414(3):612-7. doi: 10.1016/j.bbrc.2011.09.130. pmid: 21986531.

31. Meireles P, Mendes AM, Aroeira RI, Mounce BC, Vignuzzi M, Staines HM, et al. Uptake and metabolism of arginine impact Plasmodium development in the liver. Sci Rep. 2017;7(1):4072. doi: 10.1038/s41598-017-04424-y. pmid: 28642498.

32. Awasthi V, Chauhan R, Chattopadhyay D, Das J. Effect of L-arginine on the growth of *Plasmodium falciparum* and immune modulation of host cells. J Vector Borne Dis. 2017;54(2):139-45. pmid: 28748834.

33. Mohandas N, An X. Malaria and human red blood cells. Med Microbiol Immunol. 2012;201(4):593-8. doi: 10.1007/s00430-012-0272-z. pmid: 22965173.

34. Kirk K. Membrane transport in the malaria-infected erythrocyte. Physiol Rev. 2001;81(2):495-537. pmid: 11274338.

35. Ginsburg H. Transport pathways in the malaria-infected erythrocyte. Their characterization and their use as potential targets for chemotherapy. Biochem Pharmacol. 1994;48(10):1847-56. pmid: 7986195.

36. Roth E, Jr. *Plasmodium falciparum* carbohydrate metabolism: a connection between host cell and parasite. Blood Cells. 1990;16(2-3):453-60; discussion 61-6. pmid: 2257322.

37. Mishra NC, Kabilan L, Sharma A. Oxidative stress and malaria-infected erythrocytes. Indian J Malariol. 1994;31(2):77-87. pmid: 7713262.

38. Hunt NH, Stocker R. Oxidative stress and the redox status of malaria-infected erythrocytes. Blood Cells. 1990;16(2-3):499-526; discussion 7-30. pmid: 2257324.

39. Peters AL, Van Noorden CJ. Glucose-6-phosphate dehydrogenase deficiency and malaria: cytochemical detection of heterozygous G6PD deficiency in women. J Histochem Cytochem. 2009;57(11):1003-11. doi: 10.1369/jhc.2009.953828. pmid: 19546473.

40. Mbanefo EC, Ahmed AM, Titouna A, Elmaraezy A, Trang NT, Phuoc Long N, et al. Association of glucose-6-phosphate dehydrogenase deficiency and malaria: a systematic review and meta-analysis. Sci Rep. 2017;7:45963. doi: 10.1038/srep45963. pmid: 28382932.

41. Llinas M, Bozdech Z, Wong ED, Adai AT, DeRisi JL. Comparative whole genome transcriptome analysis of three *Plasmodium falciparum* strains. Nucleic Acids Res. 2006;34(4):1166-73. doi: 10.1093/nar/gkj517. pmid: 16493140.

42. Storm J, Sethia S, Blackburn GJ, Chokkathukalam A, Watson DG, Breitling R, et al. Phosphoenolpyruvate carboxylase identified as a key enzyme in erythrocytic *Plasmodium falciparum* carbon metabolism. PLOS Pathog. 2014;10(1):e1003876. doi: 10.1371/journal.ppat.1003876. pmid: 24453970.

43. Liu J, Istvan ES, Gluzman IY, Gross J, Goldberg DE. *Plasmodium falciparum* ensures its amino acid supply with multiple acquisition pathways and redundant proteolytic enzyme systems. Proc Natl Acad Sci U S A. 2006;103(23):8840-5. doi: 10.1073/pnas.0601876103. pmid: 16731623.

44. Bulusu V, Srinivasan B, Bopanna MP, Balaram H. Elucidation of the substrate specificity, kinetic and catalytic mechanism of adenylosuccinate lyase from *Plasmodium falciparum*. Biochim Biophys Acta. 2009;1794(4):642-54. doi: 10.1016/j.bbapap.2008.11.021. pmid: 19111634.

45. Alderson NL, Wang Y, Blatnik M, Frizzell N, Walla MD, Lyons TJ, et al. S-(2-Succinyl)cysteine: a novel chemical modification of tissue proteins by a Krebs cycle intermediate. Arch Biochem Biophys. 2006;450(1):1-8. doi: 10.1016/j.abb.2006.03.005. pmid: 16624247.

46. Blatnik M, Frizzell N, Thorpe SR, Baynes JW. Inactivation of glyceraldehyde-3-phosphate dehydrogenase by fumarate in diabetes. Diabetes. 2008;57(1):41-9. pmid: 17934141.

47. Piroli GG, Manuel AM, Clapper AC, Walla MD, Baatz JE, Palmiter RD, et al. Succination is increased on select proteins in the brainstem of the NADH dehydrogenase (ubiquinone) Fe-S protein 4 (Ndufs4) knockout mouse, a model of leigh

syndrome. Mol Cell Proteomics. 2016;15(2):445-61. doi: 10.1074/mcp.M115.051516. pmid: 26450614.

48. Zheng L, Cardaci S, Jerby L, MacKenzie ED, Sciacovelli M, Johnson TI, et al. Fumarate induces redox-dependent senescence by modifying glutathione metabolism. Nat Commun. 2015;6:6001. doi: 10.1038/ncomms7001. pmid: 25613188.

49. Ruecker N, Jansen R, Trujillo C, Puckett S, Jayachandran P, Piroli GG, et al. Fumarase deficiency causes protein and metabolite auccination and intoxicates *Mycobacterium tuberculosis*. Cell Chem Biol. 2017;24(3):306-15. doi: 10.1016/j.chembiol.2017.01.005. pmid: 28219662.

50. Kim HY, Lee SY, Suh S, Kim JH, Lee MK, Park HD. The relationship between estimated average glucose and fasting plasma glucose. Clin Chem Lab Med. 2013;51(11):2195-200. doi: 10.1515/cclm-2013-0045. pmid: 24057595.

51. Carey MA, Papin JA, Guler JL. Novel *Plasmodium falciparum* metabolic network reconstruction identifies shifts associated with clinical antimalarial resistance. BMC Genomics. 2017;18(1):543. doi: 10.1186/s12864-017-3905-1. pmid: 28724354.

52. Ginsburg H, Abdel-Haleem AM. Malaria Parasite Metabolic Pathways (MPMP) Upgraded with Targeted Chemical Compounds. Trends Parasitol. 2016;32(1):7-9. doi: 10.1016/j.pt.2015.10.003. pmid: 26530861.

53. Kafsack BF, Painter HJ, Llinas M. New Agilent platform DNA microarrays for transcriptome analysis of *Plasmodium falciparum* and *Plasmodium berghei* for the malaria research community. Malar J. 2012;11:187. doi: 10.1186/1475-2875-11-187. pmid: 22681930.

54. Painter HJ, Altenhofen LM, Kafsack BF, Llinas M. Whole-genome analysis of *Plasmodium* spp. Utilizing a new agilent technologies DNA microarray platform. Methods Mol Biol. 2013;923:213-9. doi: 10.1007/978-1-62703-026-7_14. pmid: 22990780.

55. Tewari SG, Prigge ST, Reifman J, Wallqvist A. Using a genome-scale metabolic network model to elucidate the mechanism of chloroquine action in *Plasmodium falciparum*. Int J Parasitol Drugs Drug Resist. 2017;7(2):138-46. doi: 10.1016/j.ijpddr.2017.03.004. pmid: 28355531.

56. Cobbold SA, Llinas M, Kirk K. Sequestration and metabolism of host cell arginine by the intraerythrocytic malaria parasite *Plasmodium falciparum*. Cell Microbiol. 2016;18(6):820-30. doi: 10.1111/cmi.12552. pmid: 26633083.

57. Brown KA. Erythrocyte Metabolism and Enzyme Defects. Lab Med. 2015;27(5):329-33.

58. Carey MA, Covelli V, Brown A, Medlock GL, Haaren M, Cooper JG, et al. Influential Parameters for the Analysis of Intracellular Parasite Metabolomics. mSphere. 2018;3(2). doi: 10.1128/mSphere.00097-18. pmid: 29669882.

59. Nzila A, Ward SA, Marsh K, Sims PF, Hyde JE. Comparative folate metabolism in humans and malaria parasites (part II): activities as yet untargeted or specific to Plasmodium. Trends Parasitol. 2005;21(7):334-9. doi: 10.1016/j.pt.2005.05.008. pmid: 15936248.

60. Siddiqui G, Srivastava A, Russell AS, Creek DJ. Multi-omics Based Identification of Specific Biochemical Changes Associated With PfKelch13-Mutant Artemisinin-Resistant *Plasmodium falciparum*. J Infect Dis. 2017;215(9):1435-44. doi: 10.1093/infdis/jix156. pmid: 28368494.

61. Aurrecoechea C, Brestelli J, Brunk BP, Dommer J, Fischer S, Gajria B, et al. PlasmoDB: a functional genomic database for malaria parasites. Nucleic Acids Res. 2009;37(Database issue):D539-43. doi: 10.1093/nar/gkn814. pmid: 18957442.

62. Nishibe H. Urea cycle enzymes in human erythrocytes. Clin Chim Acta. 1974;50(3):305-10.

63. Caspi R, Altman T, Dreher K, Fulcher CA, Subhraveti P, Keseler IM, et al. The MetaCyc database of metabolic pathways and enzymes and the BioCyc collection of pathway/genome databases. Nucleic Acids Res. 2012;40(Database issue):D742-53. doi: 10.1093/nar/gkr1014. pmid: 22102576.

64. Artimo P, Jonnalagedda M, Arnold K, Baratin D, Csardi G, de Castro E, et al. ExPASy: SIB bioinformatics resource portal. Nucleic Acids Res. 2012;40(Web Server issue):W597-603. doi: 10.1093/nar/gks400. pmid: 22661580.

65. Tanabe M, Kanehisa M. Using the KEGG database resource. Curr Protoc Bioinformatics. 2012;Chapter 1:Unit1 12. doi: 10.1002/0471250953.bi0112s38. pmid: 22700311.

66. Cowman AF, Crabb BS. Invasion of red blood cells by malaria parasites. Cell. 2006;124(4):755-66. doi: 10.1016/j.cell.2006.02.006. pmid: 16497586.

67. Cowman AF, Healer J, Marapana D, Marsh K. Malaria: biology and disease. Cell. 2016;167(3):610-24. doi: 10.1016/j.cell.2016.07.055. pmid: 27768886.

68. Topfer N, Kleessen S, Nikoloski Z. Integration of metabolomics data into metabolic networks. Front Plant Sci. 2015;6:49. doi: 10.3389/fpls.2015.00049. pmid: 25741348.

69. Schellenberger J, Lewis NE, Palsson BO. Elimination of thermodynamically infeasible loops in steady-state metabolic models. Biophys J. 2011;100(3):544-53. doi: 10.1016/j.bpj.2010.12.3707. pmid: 21281568.

70. Yang F, Qian H, Beard DA. Ab initio prediction of thermodynamically feasible reaction directions from biochemical network stoichiometry. Metab Eng. 2005;7(4):251-9. doi: 10.1016/j.ymben.2005.03.002. pmid: 16140239.

71. Bradford MM. A rapid and sensitive method for the quantitation of microgram quantities of protein utilizing the principle of protein-dye binding. Anal Biochem. 1976;72(1-2):248-54. pmid: 942051.

72. Mikkelsen RB, Tanabe K, Wallach DF. Membrane potential of *Plasmodium*-infected erythrocytes. J Cell Biol. 1982;93(3):685-9. pmid: 6288730.

Curriculum Vitae

RUSSELL P. SWIFT

Address: Department of Molecular Microbiology and Immunology
Johns Hopkins Bloomberg School of Public Health
615 N. Wolfe Street, Room E4410
Baltimore MD, 21205
Telephone: 443-287-6695
Cell: 805-766-2126
Email: rswift3@jhu.edu

Academic History

Dept. of Molecular Microbiology and Immunology, Johns Hopkins University School of Public Health
PhD Candidate – Project: Elucidation of Essential Apicoplast Metabolic Pathways in *Plasmodium falciparum*
Advisor – Dr. Sean Prigge

2013-Present

The Evergreen State College. Olympia, WA
Bachelors of Science and Bachelors of Arts

2008-2012

Ventura Community College, Ventura CA.
General education

2005-2007

Research Experience

Graduate Research, Johns Hopkins Bloomberg School of Public Health. Baltimore, MD.
Research Advisor: Dr. Sean Prigge.
Project: Elucidating the essentiality and role of multiple metabolic pathways of the apicoplast organelle in *P. falciparum* parasites.

2013-Present

Postbaccalaureate Fellow, National Institute of Allergy and Infectious Diseases, Rocky Mountain Labs, National Institute of Health. Hamilton, MT.
Research Advisor: Dr. Jean Celli
Project: Determining the cytotoxicity of *Brucella abortus* secreted proteins, investigating the role of the flagella in protein secretion, and determining the role of human host trafficking proteins in the intracellular replication of *B. abortus*.

2012-2013

Undergraduate Research, Evergreen State College. Olympia, WA.
Research Advisor: Dr. Benjamin Simon

Project: Developing *Yersinia ruckeri* as a bacterial vector to deliver functional mRNA to eukaryotic cells, functioning as a gene delivery system to vaccinate salmonid fish against infectious hematopoietic necrosis virus.

2011-2012

Academic Awards, Scholarships, and Fellowships

2009 Scholastic Achievement Scholarship
2009 Evergreen Foundation Scholarship
2010 Ed Kelly Memorial Scholarship
2011 Ed Kelly Memorial Scholarship
2011 Evergreen Alumni Scholarship
2012-2013 National Institute of Allergy and Infectious Diseases Post-baccalaureate Fellow
2014 Keerti V. Shah Fund
2015 Dr. Harry J. Lawler Award for academic excellence and research potential in molecular microbiology and immunology
2016 Frederik B. Bang Award
2017 Emergent Biosolutions Centennial Scholarship
2017 Johns Hopkins Bloomberg School of Public Health Conference Travel Award
2018 Jane Welsh Russell Fellowship
2018 Gordis Teaching Fellowship

Publications

Russell Swift, Hans Liu, Krithika Rajaram, Bobby Kwan, Sean Prigge. Dephospho-CoA kinase is essential and active in disrupted apicoplast vesicles (In preparation).

Russell Swift, Cyrianne Keutcha, Hans Liu, Sean Prigge. The NTP generating activity of PyrKII is required for apicoplast maintenance in *P. falciparum* parasites (In preparation).

Russell Swift, Hans Liu, Sean Prigge. Sulfur modifications of tRNAs are essential for apicoplast maintenance (In preparation).

Russell Swift, Krithika Rajaram, Hans Liu, Sean Prigge. Iron-sulfur cluster formation is not required for apicoplast maintenance (In preparation).

Russell Swift, Hans Liu, Krithika Rajaram, Aleah Roberts, Krista Matthews, Hugo Jhun, Sean Prigge. Generation of an alternative genetically-encoded apicoplast metabolic bypass system (In preparation).

Russell Swift, Shivendra Tewari, Tatsuya Oyama, Krithika Rajaram, Jaques Reifman, Sean T Prigge, Anders Wallqvist. The fumarate recycling in *Plasmodium falciparum* promotes maintenance of redox metabolism during the asexual cycle. Nature Scientific Reports (Submitted December, 2018).

Shivendra G. Tewari, Krithika Rajaram, Patric Schyman, **Russell Swift**, Jaques Reifman, Sean T. Prigge, Anders Wallqvist. Short-term metabolic adjustments in *Plasmodium falciparum* counter

hypoxanthine deprivation at the expense of long-term viability. Malaria Journal (Submitted December, 2018).

Afanador GA, Guerra AJ, **Swift RP**, Rodriguez RE, Bartee D, Matthews KA, Schön A, Freire E, Freel Meyers CL, Prigge ST. A novel lipoate attachment enzyme is shared by *Plasmodium* and *Chlamydia* species. Mol Microbiol. 2017 Aug 24. doi: 10.1111/mmi.13776. PubMed PMID: 28836704.

Talks

Pyruvate Kinase II is Required for Apicoplast Maintenance. Gordon Research Conference invited talk. June 13th, 2018. Salve Regina University, Newport, RI.

Elucidation of Essential Apicoplast Proteins in *Plasmodium falciparum*. Johns Hopkins Malaria Research Institute invited talk. 2017, June 16th: Baltimore, MD.

Lipoylation of *Plasmodium falciparum* mitochondrial substrates. Johns Hopkins School of Public Health, Biochemistry, Cell and Molecular Biology departmental talk. 2015, February 26: Baltimore, MD.

Functional mRNA delivery using *Yersinia ruckeri* for vaccination against IHNV in salmonid fish. NIAID Rocky Mountain Laboratories, post-baccalaureate fellow job talk. 2012, July 13: Hamilton, MT.

Posters

Pyruvate Kinase II is Required for Apicoplast Maintenance. Gordon Research Conference. June 13th, 2018. Salve Regina University, Newport, RI.

Iron-Sulfur Cluster Formation is Required for Apicoplast Maintenance. American Society of Tropical Medicine and Hygiene Annual Meeting. November 8th, 2017. Baltimore, MD.

Iron-Sulfur Cluster Formation is Required For Apicoplast Maintenance. Johns Hopkins School of Public Health, Molecular Microbiology and Immunology Departmental Retreat. 2017, September 13th: Baltimore, MD.

Teaching Experience

Preparing Future Faculty Teaching Academy Certificate of Completion
I took part in a year-long training program with the aim of preparing graduate students for future teaching positions. The program consisted of three phases, with phase I covering various didactic methods such as Phase II consisted of training in instructional material development, in which I developed the curriculum for a class I would like to teach. The program culminated in phase III, in

which I assisted in teaching the class Introduction to Biomedical Sciences under the direction of Dr. Gundula Bosch, my faculty mentor.

Johns Hopkins University, Baltimore MD

Instructor for Genetics and Public Health, a class offered to upper level undergraduate public health majors at the Johns Hopkins University. I was awarded the Gordis Teaching Fellowship and developed curriculum and taught a 13-week semester long course, meeting twice a week for 75 minutes. The class focused on the intersection of genetics and public health using interactive and hands-on learning techniques.

Fall 2018

Johns Hopkins Bloomberg School of Public Health, Baltimore MD

Guest lecturer for the Introduction to the Biomedical Sciences course. I developed material and delivered lectures on hematology, immunology, endocrinology, and reproductive biology.
Summer 2016, 2017, and 2018

Teachers Assistant for the Public Health Biology course. I acted as the student faculty liaison, online discussion facilitator, and performed general teachers assistant duties.

Spring 2016 and Summer 2015

Teachers Assistant for the Biology of Parasitism course. I assisted in running the hands-on laboratory portion of the course.

Fall 2015

Professional Memberships

2013-present Member, American Society of Microbiology
2017-present Member, American Society for Biochemistry and Molecular Biology

Extracurricular Experience

2009-2012 Left Foot Organics: board secretary
2007-2009 Emma Goldman Youth and Homeless Outreach Project: board member